UNIVERSITY OF OKLAHOMA

GRADUATE COLLEGE

LATERAL DEFORMATION OF BRIDGE EMBANKMENTS SUPPORTED ON SOFT SOILS

A DISSERTATION

SUBMITTED TO THE GRADUATE FACULTY

in partial fulfillment of the requirements for the

degree of

DOCTOR OF PHILOSPHY

By

TOMMY DALE BOUNDS
Norman, Oklahoma
2020

LATERAL DEFORMATION OF BRIDGE EMBANKMENTS
SUPPORTED ON SOFT SOILS

A DISSERTATION APPROVED FOR THE
SCHOOL OF CIVIL ENGINEERING AND ENVIRONMENTAL SCIENCE

BY THE COMMITTEE CONSISTING OF

Dr. Gerald Miller, Co-Chair

Dr. Kanthasamy Muraleetharan, Co-Chair

Dr. James Baldwin

Dr. Amy Cerato

Dr. Royce Floyd

Dedicated to My Mother and Father

Acknowledgements

I would like to express my sincere gratitude to Professors Dr. Gerald A. Miller and Dr. Kanthasamy K. Muraleetharan for being my advisors and providing guidance and support during this research.

I would also like to thank Professors Dr. Amy B. Cerato, Dr. Royce W. Floyd, and Dr. James D. Baldwin for participating on my committee and providing feedback and suggestions on this dissertation.

I would also like to thank my wife, Claudia, for always believing in me and providing her full support to me.

Table of Contents

Table of Tables

List of Figures

Abstract

Excessive bridge embankment deformation, namely in the lateral direction, continues to damage bridges leading to costly repairs or early replacement. The lateral deformation of bridge embankments is often overlooked in routine analysis due the complex nature of the deformation. Unlike vertical deformation, or settlement, which has established methods used to calculate it, lateral deformation is by nature non-linear and can currently only be estimated through the use of a finite element program. Lateral deformation of bridge embankments is further complicated due to the unknown and changing drainage conditions in the foundation soil below the embankment. The study outlined in this dissertation is an important step in expanding the knowledge base for lateral deformation of bridge abutments founded on soft soils. The goal of this study was to develop relationships between embankment and foundation soil variables such as geometry and strength and the lateral deformation the embankment experiences. Such a method would be very useful for a practicing engineer.

To support this research an advanced constitutive model, the Bounding Surface Plasticity model for isotropic cohesive soils developed by Dafalias and Herrmann (1986), was implemented into the commercial finite element software PLAXIS 2D. The advanced constitutive model allowed for the realistic estimation of bridge embankment lateral and vertical deformations. The abilities of the advanced constitutive model, as implemented in PLAXIS 2D, were displayed by modeling four instrumented test embankments from the literature. In general, the model was able to accurately predict the lateral and vertical deformation of embankments. The study was then expanded to incorporate the influence of bridge piles, this was achieved by modeling a local bridge embankment, SH 3 over BNSF Railroad in Ada, OK, which had experienced damage apparently as the result of excessive lateral deformation of the bridge embankment. An in-situ and lab testing

program was carried out for the SH 3 over BNSF Railroad bridge to provide necessary subsurface soil geometries as well as constitutive model parameters. The results from the SH 3 over BNSF Railroad bridge agreed well with field observations. Following the SH 3 over BNSF Railroad analysis a parametric study was performed on a fairly standard bridge embankment. The parametric study varied the embankment foreslope (slope facing the bridge), embankment height, foundation soil thickness, foundation soil strength, and the foundation soil permeability. The parametric study was performed to find relationships between the various parameters and the lateral deformation the bridge embankment experienced.

The major contributions of this research include: 1) The Bounding Surface Plasticity model was implemented into PLAXIS 2D. The implemented soil model is stored as a Dynamic Link Library and can be distributed for use by other practitioners. 2) The foundation soil for the four test embankments has been calibrated for the Bounding Surface Model. The calibrated soils can now be used by researchers to further study the behavior of the four test embankments. 3) The influence of bridge piling on the lateral deformation behavior was studied in a limited capacity. 4) Finite element modeling was completed on a case study, SH 3 over BNSF Railroad. The modeling further validates the original hypothesis regarding the initial source of the distress experienced by the bridge. 5) A parametric study was completed on a trial embankment. The results of the parametric study can be used to find additional relationships regarding the lateral or vertical deformation behavior of piled bridge abutments. 6) Relationships from the parametric study were analyzed and summarized. 7) An empirical equation was developed to estimate the magnitude of lateral deformation of piled bridge abutments. 8) Recommendations for the potential of lateral deformation of piled bridge abutments for the practicing engineer were developed.

1.0 INTRODUCTION

1.1 Overview

Roadway embankment deformation continues to be an area of concern and interest for transportation departments. Numerous failures have occurred as a result of excessive embankment deformation (e.g., Crawford, 1994). The deformation can range from catastrophic slope and bearing capacity failures to minor settlement problems with the approach slab or as it is commonly known, the bump at the end of the bridge. The deformation can also cause additional stresses on the bridge, Muraleetharan et al. (2018) observed closed expansion joints, tilted roller bearings, sheared anchor bolts and abutment back wall cracking at a twin five span bridge in Ada, Oklahoma that had experienced apparent horizontal embankment deformation. Meade and Allen (1988) reported that in Kentucky, bridge approach embankments have been reconstructed due to excessive continuous movements; they also reported that one bridge was lengthened due to the severity of settlement and movement of the abutment. In general, deformation of one form or another to some degree will occur for all earthen embankments. If the magnitude of deformation, whether vertical or horizontal, is known in advance, soil remediation efforts or improvement methods can be considered to ensure a resilient embankment bridge system. For example, if excessive vertical displacement or settlement is expected, the embankment can be allowed extra settlement time during construction so that the settlement once the bridge is constructed is minimized. If excessive horizontal deformation is expected, the bridge foundation elements can be designed to resist the anticipated forces or the embankment foundation can be reinforced through one of many available methods, such as geogrid reinforcement, to decrease the likelihood of excessive lateral deformation.

When designing and analyzing a bridge embankment it would be ideal to have a good estimate of the anticipated vertical and lateral deformation. Vertical deformation or settlement is generally estimated using an analytical approach with reasonable results when high quality lab data is available. Lateral deformation, on the other hand, can be more complicated to estimate and numerical modeling is generally required to provide reasonable estimates, although the estimated lateral deformation and the observed lateral deformation can be quite different even when numerical modeling is employed (Poulos, 1972; Shen et al., 2005; Huang et al. 2006; Oliveria and Lemos, 2011; Karstunen et al. 2005). There are methods to estimate the magnitude of lateral deformation when correlated with the vertical deformation. Methods are also available to estimate the factor of safety against excessive lateral deformation; however, as will be discussed in this dissertation the methods still need additional research and are largely based on observations. Some of the shortcomings of the current methods are related to the complexity of soil behavior, soil drainage conditions, embankment geometry and construction sequence (Poulos, 1972; Qu et al. 2009).

This research focuses on the lateral deformation, also known as horizontal movement, lateral spreading, and lateral squeeze, of piled bridge embankments. The research has largely been accomplished through numerical and analytical modeling using data previously gathered and available in the literature. Field data and samples have also been collected at a bridge embankment thought to be experiencing horizontal movement that is currently being monitored by the University of Oklahoma. The ultimate goal of this research is not to develop methods to predict catastrophic embankment failure as a large amount of research has already been conducted on that topic and slope stability analysis has a decent predictability record. Rather the goal of this research is to quantify the anticipated lateral movement and its impact on bridge elements as a result of

embankment construction so that transportation departments can have an additional tool to assist in design and decision making. If the anticipated movement could be reasonably estimated then transportation departments could determine if remedial measures or alternative design methods are necessary prior to construction.

1.2 Objectives

The main objective of this research is to develop a method for determining the magnitude of lateral movement a piled bridge embankment will experience. A method such as this would assist with decision making about remedial measures for bridge embankments prior to the onset of distress and damage. A robust method would also allow for the determination of bending moments that piles would experience to ensure capacity is not exceeded, it could also allow for the consideration of different pile types based on more than just axial capacity and familiarity with one or two different pile shapes. To support the main objective the following tasks have been completed:

1. Implement Bounding Surface Plasticity Model as proposed by Dafalias and Herrmann (1986) into the commercial software PLAXIS 2-D.
2. Model four instrumented test embankments with Bounding Surface Plasticity Model in two-dimensions and compare results to the measured data. It should be noted that many of the test embankments in the literature are for embankments that are constructed without the influence of piles or a bridge.
3. Perform laboratory testing on soil samples collected from the SH-3 Bridge over the BNSF Railroad in Ada, Oklahoma to calibrate the Bounding Surface Plasticity Model. Model the embankment in PLAXIS and compare the predicted and observed behavior. The embankment will also be modeled using commercially available soil models in PLAXIS

to compare the Bounding Surface Plasticity Model to those already available. This embankment served as a controlled study into the effects of a piled bridge abutment on lateral movement of embankments on soft soil and determine the efficacy of the Bounding Surface Plasticity Model to predict this behavior.

4. Develop a trial embankment for a parametric study in PLAXIS, similar to the benchmark embankment modeled by Karstunen et al. (2006), to systematically find relationships through a parametric study between the embankment geometry and soil conditions to develop design recommendations and guidance that can be used by practicing engineers.

1.3 Layout of Dissertation

This dissertation is organized into eight chapters. Chapter 2 provides a literature review to familiarize the reader with the work that has been completed thus far on the lateral deformation of piled bridge abutments as well as supporting background information. Chapter 3 presents an overview of the Bounding Surface Plasticity Model for Isotropic soils. The overview, while relatively brief is intended to familiarize the reader with the general scheme the model uses to predict soil behavior. Chapter 4 presents an overview of the implementation of the Bounding Surface Plasticity Model into PLAXIS along with several verification measures that were taken to ensure the model was working properly. Chapter 5, presents the results of 5 test embankments that were modeled using the Bounding Surface Plasticity Model in PLAXIS, this chapter serves to demonstrate the capability of the model to accurately model a wide range of soils when subjected to embankment loading. Chapter 6 presents the analyses and results of the SH-3 over BNSF bridge in Ada, Oklahoma, which was modeled in PLAXIS using the Bounding Surface Plasticity model. The SH-3 bridge is founded on piles, unlike the test embankments modeled in Chapter 5, allowing for the influence of piles to be studied. Chapter 7 presents the analyses and results from a trial

embankment developed as part of this dissertation. The trial embankment was developed to assist in finding key factors that contribute to the lateral deformation of bridge embankments. Chapter 8 provides the conclusion as well as recommendations for future research on this topic. The terminology used in this dissertation follows that used by the Oklahoma Department of Transportation (ODOT), for reference, key components are labeled in Figure 1.

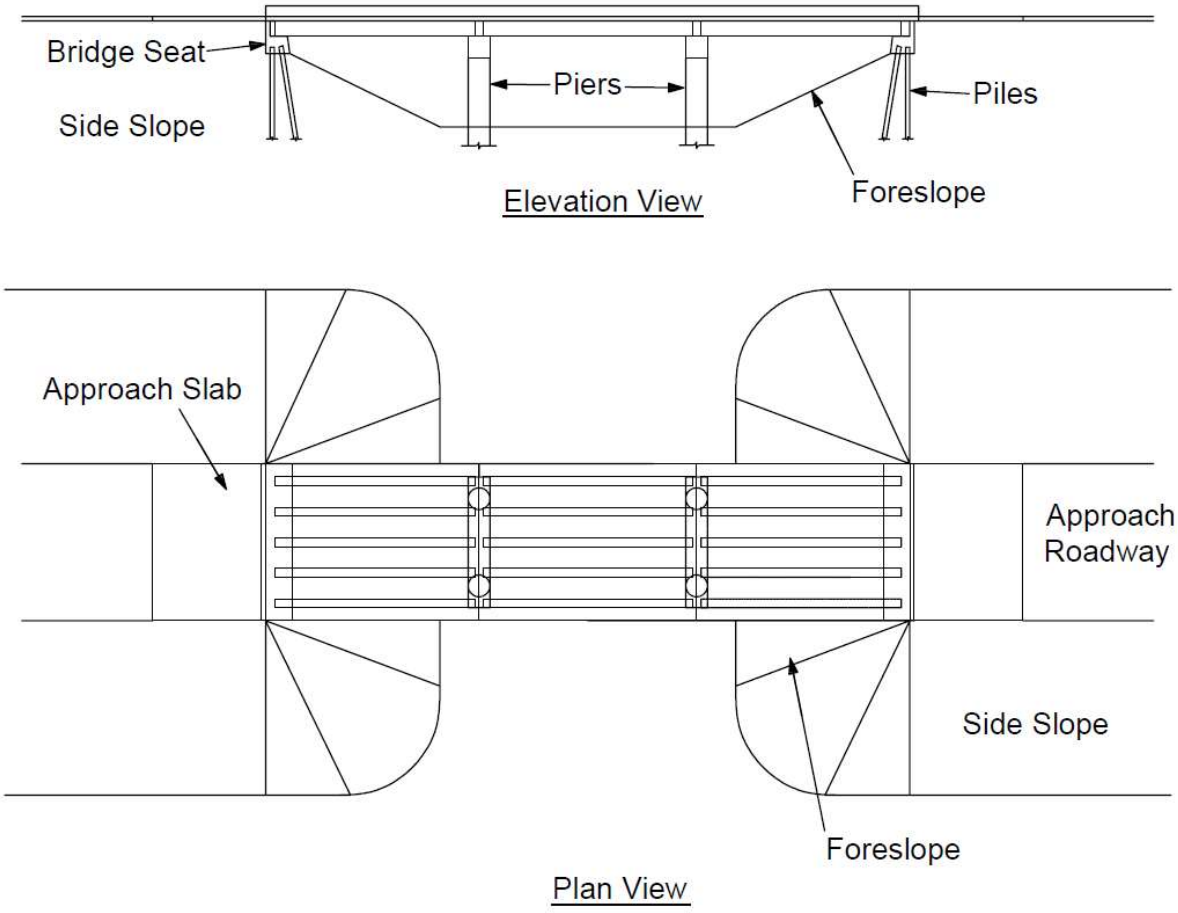

Figure 1. Bridge Plan and Elevation View

2.0 LITERATURE REVIEW

2.1 Organization of This Literature Review

This literature review will begin with the deformation behavior of embankments to establish the anticipated deformations and how embankment foundation deformations differ from other types of foundation soil. The second section will present soil behavior as it pertains to the drainage condition. The third section will present case studies involving lateral deformation of bridge embankments. The fourth section will present currently available analytical methods to estimate the potential for and magnitude of lateral deformation of bridge embankments. The next section will present examples of numerical modeling attempts at quantifying the magnitude of lateral deformation, and the following section will present the influence and response of abutment piles to the lateral deformation of bridge embankments. The final section presents a summary of the critical findings of the literature review and the knowledge gaps that this dissertation addresses are presented.

2.2 Deformation Behavior of Bridge Embankments

When bridge embankments are constructed, vertical and lateral deformations within the embankment soil and foundation soil can be expected. It is generally accepted practice to ignore internal embankment deformation and focus solely on foundation soil settlements. However, Miller et al. (2013), when conducting an analysis of bridge approach settlement problems recommended that settlement analysis also be carried out for the compacted embankment material. The magnitude of settlement in the embankment foundation soil can be estimated using high quality one-dimensional consolidation test results and analytical equations. Tavenas et al. (1979)

found for approximately 20 case studies, that the coefficient of correlation was approximately 0.98 between calculated and observed vertical deformations for bridge embankments.

The preconsolidation pressure, or maximum past pressure, of the embankment foundation soil is critical to the magnitude of settlement the foundation experiences. Soil can be said to have "memory" due to the irreversible plastic strains it experiences during loading. If in the past the soil experienced a higher state of vertical stress than what is now present the soil is considered overconsolidated. An overconsolidated soil will experience less vertical deformation than an identical normally consolidated soil under the same loading conditions. Tavenas et al. (1979) suggested that all natural soil deposits become overconsolidated even if only by a small degree; they suggested that since basically all soil deposits will experience aging, water table variations, or snow loads. This is important for embankment foundations because the rate of deformation will also depend on the past stress state of the foundation soil.

Lateral deformation tends to be more complicated and there are not well established methods for determining the magnitude of deformation. Poulos (1972) indicated five reasons why horizontal stress and horizontal movement is difficult to predict, they are as follows:

1. Difficulty in estimating Poisson's ratio of the soil
2. Anisotropy of the soil
3. Nonlinear stress-strain behavior of the soil
4. Inhomogeneity of the soil
5. Neglect of specific case factors such as embankment stiffness and foundation roughness, or the adhesion of the embankment to the foundation soil.

Poulos (1972) further pointed out that incorrect assumptions made regarding stresses applied to the soil by the embankment lead to difficulties in estimating lateral displacement. In his analysis

he noted that some of the horizontal movements were overpredicted by 10 to 20 times the measured magnitude highlighting the difficulties in determining the magnitude of lateral deformation under bridge embankments.

The problem can become more complex due to the non-uniform loading caused by embankments as a result of their varying shape in three dimensions. The varying shape of embankments in three dimensions is one of the characteristics that set them apart from other types of foundations, such as shallow footings. Bridge embankments are typically increasing in height as the embankment nears the bridge which adds a varying load on the soil parallel to the roadway that rapidly declines once the bridge abutment is met. The gradual increase in loading on the soil followed by a rapid decline in loading parallel to the roadway could be one factor in bridge abutment movement in the direction of the bridge. Abutment movement into the bridge as a result of suspected embankment movement has been noted by researchers, for example Bozozuk (1978) and Muraleetharan et al. (2018).

The side slope of the embankment can also have an impact on the lateral movement the foundation experiences. Meade and Allen (1988) used the finite element program ISBILD, developed by Ozawa and Duncan (1973), to analyze six bridge embankments in Kentucky and found that the maximum lateral strain measured at the mid-slope or toe of the embankment decreased by approximately 30 percent when the side slope of the embankment was changed from a 2H:1V to a 2.5H:1V. Furthermore, they found that the lateral strain decreased by approximately 50 percent when going from a 2H:1V to a 3H:1V side slope.

2.3 Drainage of Bridge Embankment Foundation Soil

To properly quantify the magnitude of lateral movement in an embankment a distinction must be made about the drainage conditions of the soil. Since soil is a three-phase porous media (solid skeleton, fluid, gas), or four if you include the contractile skin as proposed by Fredlund and Rahardjo (1993), the drainage of the gas and fluid (air and water in general for natural soils) will play a crucial role in the behavior of the soil. Traditionally soil is treated as fully saturated meaning it can be thought of as a two-phase porous media (solid skeleton and water), this assumption or condition simplifies calculations, but has large implications for the drainage condition of the soil during loading.

Initially when a load is placed on a saturated low permeable soil (clay) the increase in stress will be transferred to pore water within the soil. This transfer of stress will cause the pore water pressure to increase. The pore water pressure will remain at this increased or excess pore water pressure until the soil structure begins draining the excess pressure. When the soil starts to drain, the stress will begin transferring from the pore water to the soil skeleton. During this transfer of stress, the soil will be in a partially drained state since it is not able to drain uniformly at once, that is the middle of the soil layer will still have more excess pore water pressure while the edges of the layer where drainage is permitted will have less pressure. The drainage of excess pore water pressure is represented as primary consolidation settlement for the vertical component of embankment displacement or settlement. The complete drainage of excess pore water pressure can take many years depending on the permeability of the soil, which suggests that horizontal deformations, like vertical deformation, should be anticipated to occur for many years after the embankment is constructed.

During the undrained portion of loading (immediately following the placement of the load for a saturated soil) any vertical deformations the soil experiences must be accompanied by horizontal deformations to satisfy the constant volume assumption. Since water and the soil skeleton are both considered incompressible, when the load is applied, no volume change can take place without the removal of water or soil; this behavior is known as undrained shear distortion. Ellis and Springman (1999) conducted centrifuge testing and finite element modeling on a full height bridge abutment founded on soft clay. They observed a ratio of 1H:1V for displacements during the undrained loading period, however, once the soil began to drain the ratio of vertical to horizontal deformation varied. For the full height embankment, they observed that the horizontal deformation was approximately 0.2 to 0.3 times the magnitude of the vertical deformation. Similarly, Leroueil et al. (1990) proposed using a ratio of 1H:1V for the undrained displacements and 0.12H:1V for the drained displacements. This suggests that the damaging effects of long term lateral deformation on the bridge can be reduced by allowing excess pore water pressure to dissipate before constructing the bridge. However, as will be discussed later, there are situations when the excessive lateral movements continued for years after embankment construction, sometimes in the absence of excessive vertical deformation.

The state of drainage becomes more complicated if the soil is not initially saturated, as is the case in many arid regions of the world. The surface foundation soils are typically prepared for embankment construction by being compacted to a percentage of the maximum dry density and a range of the optimum moisture content. It should be noted that soils at the optimum moisture content are not fully saturated. Since the soils are not fully saturated they behave as a 3 phase media and are partially drained from the beginning of embankment construction. The partial drainage is permitted since air can travel through soil faster than water; if the embankment load is

large enough at some point, the foundation soil would become fully saturated due to the escaping of air and the reduction in void space within the soil matrix. In addition, any deeper foundation soils above the water table are also unsaturated. Tavenas et al. (1979) suggested that initially sufficient drainage will occur in overconsolidated soil foundations; however, this initial consolidation will cause the soil to become partly or entirely normally consolidated and saturated in which case the soil will behave as undrained until sufficient time has passed to once again allow the soil to drain. The total and effective stress paths of foundation soil under an embankment have been presented by Tavenas et al. (1979) and are included in Figure 2.

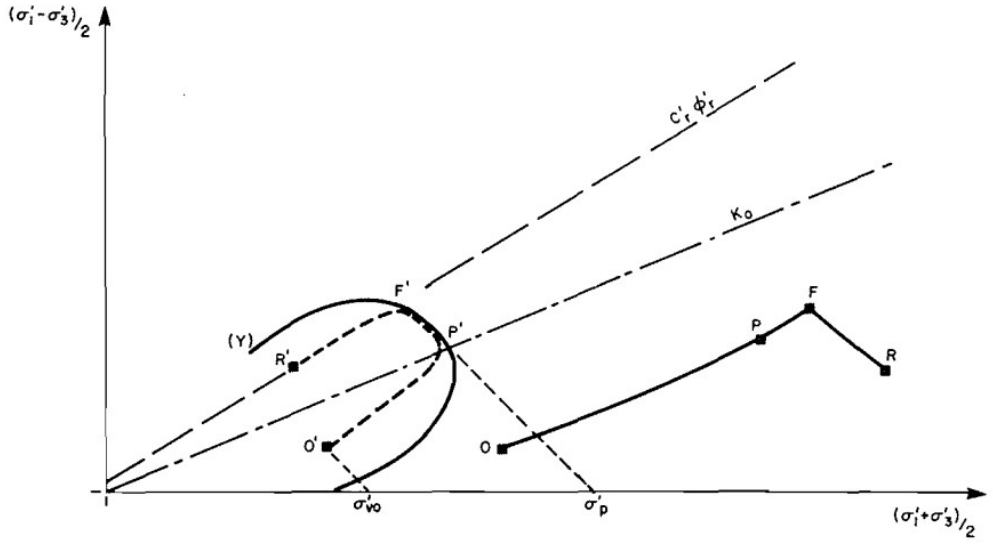

Figure 2. Total and effective stress paths under an embankment during construction, from Tavenas et al. (1979)

From O' to P' the soil is within the limit state surface, the soil behaves as overconsolidated, and deformations will be small. Since this portion of the stress path is partially drained the magnitude of horizontal movement will be less than the magnitude of vertical movement, i.e. Poisson's ratio will be much less than 0.5. From P' to F' the soil follows the limit state surface of a normally consolidated soil, and the deformations should be greater than what they were from O' to P'. Since this portion of the stress path is undrained it is expected that the vertical and horizontal

deformations will be roughly equal, or Poisson's ratio will be approximately 0.5. At F' local failure will begin and strain softening will develop as the soil approaches the critical state at R'. Tavenas et al. (1979) points out that this stress path is not replicated by standard laboratory tests. This makes it improbable to draw conclusions about the deformations the embankment will experience from standard lab testing methods.

2.4 Case Studies

There have been a number of case studies on lateral movement associated with bridge embankments. Smadi (2001) completed a rather comprehensive study on lateral squeeze, or movement, of embankments. He reviewed 180 case studies throughout the world lamenting the magnitude of research on a problem that continues to evade traditional civil engineering practices. Furthermore, Bozozuk (1978) circulated a survey in the United States and Canada and received approximately 90 cases of vertical and horizontal movements for bridge abutments located on piers and end bearing piles. The horizontal movements ranged from no movement to 1.8 feet while the vertical movement ranged from no movement to 3.6 feet. In approximately 60% of the reported cases the experienced movement was deemed not tolerable. A few case studies that are relevant to the problem this dissertation is attempting to address are presented below.

Turan et al. (2013) presented a case study of a highway approach embankment located on Leda Clay in Ontario, Canada. The embankment was constructed in 1961. Following construction, the embankment experienced excessive vertical settlement, approximately 1.02 meters. The bridge abutment also pulled away from the bridge, arguably as a result of the lateral movement of the piles toward the bridge at a lower depth within the foundation soils. The researchers attempted to validate the movements using PLAXIS 2-D, modeling the embankment using plane strain conditions. The interface between the piles and soil was fully bonded meaning

slippage at the interface was restricted. The Soft Soil Model available in PLAXIS 2-D was used to model the Leda Clay. The researchers found good agreement between the model and the observed field data where field data was available. The researchers noted that Terzaghi's one-dimensional consolidation theory underestimated the settlement by approximately 0.3 meters suggesting that soil yielding was occurring in the Leda Clay.

Jones et al. (2008) presented a case study over the Surtees Bridge constructed in the late 1970's in the United Kingdom that started showing signs of distress prior to being opened to traffic. The area is underlain by soft to firm clay. Excessive settlement was suspected to occur at the site of the bridge so one of the two embankments was constructed approximately 2 years in advance to allow for some of the settlement to occur, according to the authors there is no information as to why both embankments were not allowed to settle prior to construction. Since the distress in the embankment built at the time of bridge construction was visible and occurred very quickly the site was monitored and instrumented in the years following its opening. Inclinometers placed at the edge of the embankment showed movements up to 14 cm laterally up to a depth of 4 meters. The distress continued well into 2004, so much distress occurred that in 2000 one of the bridge piers was noted as out of plumb. The authors did not perform rigorous numerical modeling to verify the lateral deformation rather they used some simpler equations based on pile deflection. While the method they used overestimated the magnitude of observed movement by a factor of 2 the authors reasoned that it still proved the source of the movement was from the embankment foundation lateral deformation.

Allen et al. (1985) presented a case study of a bridge in Campbell County, Kentucky on Interstate 471 that experienced excessive vertical and horizontal deformation. The site of the bridge embankments was underlain by a 10 to 15 feet thick layer of soft clay. The report also

mentioned that potentially a farm pond had once been in the area of the now bridge embankment. The site was instrumented with settlement gauges and horizontal and vertical inclinometers. A horizontal inclinometer was used to measure the settlement trough under the embankment perpendicular to the roadway alignment. During the simultaneous construction of the north and south embankments, when the elevation difference was 33 feet between the two embankments, the south embankment foundation began moving laterally. The lateral movement of the foundation soil caused the tilting of recently completed bridge piers near the south end causing the piers to be approximately 8 inches out of plum. This movement suggests the north embankment was causing the soft foundation soil to move to the south laterally, it also highlights the magnitude of potential damage that can be caused by lateral foundation soil movement. Remedial efforts were made and the bridge was eventually completed. Data from the inclinometers indicated that once completed the south abutment began moving north. The authors did not present the magnitude of lateral movement due to difficulties in analyzing the inclinometer data collected. However, they did mention that it appears as though the soil was flowing through the bridge piers located at the toe of the embankments.

Crawford et al. (1994) presented the deformation behavior of two test embankments that ultimately experienced slope stability failure along Highway 97, west of Vernon, British Columbia, Canada. The embankments were located over a soft to firm silty clay, the soil had a stiffer layer at a depth of 2 meters underlain by an additional 18 meters of soft clay. The test embankments were constructed to determine if remedial measures would be needed for the roadway embankment construction. The test embankments were instrumented with settlement plates and inclinometers. The construction of the embankments was initially very slow to allow excess pore water pressures to dissipate and then construction speed was increased before one of

the embankments ultimately failed. Data on the lateral behavior was last collected before the increase in construction speed was approved. The last lateral deformation measurements indicated a movement of 6 mm toward the embankment at a depth of 4 meters and a movement of 10 mm away from the embankment at a depth of 12 meters. The sinusoidal deformation with depth suggests that the stiff layer was impacting the distribution of lateral movement of the soil layer. Tavenas et al. (1979) suggested that the distribution of lateral movement within a soil layer can be represented by a cubic polynomial in which all the movement was in one direction.

Meade and Allen (1988) reported on the lateral and horizontal movements of an embankment on Interstate 64 over Bull Fork Creek in Kentucky. The interstate crossed the creek on twin bridges that were completed in 1968. Little to no information is presented on the site geology in the report. The abutments were instrumented with settlement gauges, piezometers, and a single slope inclinometer in the eastern embankment slope. The slope inclinometer was installed approximately 3 years after the completion of the bridge embankment. It is reported that the western and eastern embankments settled 10 and 17 inches, respectively, but the settlement occurred by the time the embankment construction was complete and predated the installation of the slope inclinometer. The embankments continued to settle after construction and long term settlement of the eastern approach (the side with the slope inclinometer) was 4.9 inches in 3.1 years. Significant lateral movement of the embankment was revealed with the slope inclinometer, lateral movement near the top of the embankment was approximately 7 inches. The lateral movement increased to approximately 10 inches at a depth of 2 to 4 feet.

2.5 Analytical Methods to Estimate Lateral Deformations of Embankments

Efforts have been made to estimate the magnitude of lateral deformation and estimate the potential for lateral deformation. The Federal Highway Administration (FHWA) Soil and

Foundations – Volume 1 (Samtani and Nowatzki, 2006) publication presents methods to calculate the factor of safety against lateral deformation, FS_{sq}, or squeezing as it is referred to in that publication. The method is based on work completed by Silvestri (1983). The equation is presented below:

$$FS_{SQ} = \left[\frac{2S_u}{\gamma D_s tan\theta}\right] + \left[\frac{4.14 s_u}{\gamma H}\right] \quad (1)$$

θ = angle of slope

γ = unit weight of the fill

D_s = depth of soft soil beneath the toe of the end slope or side slope of the fill

H = height of the fill

S_u = undrained shear strength of soft soil beneath the fill

The geometry of the problem with applicable terminology is included below.

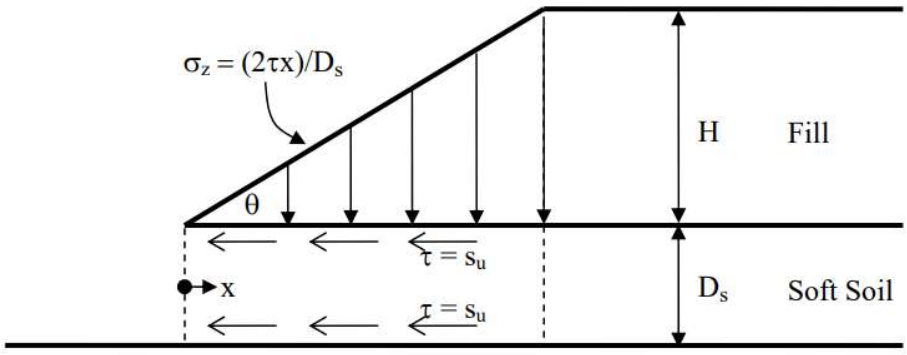

Figure 3. Definitions for calculating safety factor against lateral squeeze (after Silvestri, 1983), from Samtani and Nowatzki, 2006

Samtani and Nowatzki (2006) suggest that when $FS_{SQ} < 2$ the embankment will need to have a rigorous slope stability analysis and possibly advanced finite element modeling to ensure the

stability of the embankment. They also suggested that general slope stability will govern when the base width of the end slope is less than the depth of the soft layer.

A simpler approach to determine if an embankment will undergo lateral spreading has been presented in different ways by several authors. The most common method found during this literature review is presented in the FHWA Design and Construction of Driven Pile Foundations – Volume 1 (Hannigan et al, 2016). According to that publication lateral deformation and possibly abutment tilting can occur when:

$$\gamma_f h_f > 3S_u \tag{2}$$

γ_f = unit weight of fill

h_f = height of fill

S_u = undrained shear strength of soft cohesive soil

A similar relationship was recommended by Tschebotarioff (1973), he suggested that shear deformation began when the vertical stress increase exceeded 3 times the undrained shear strength and that the movement became harmful when the vertical stress exceeded 5.14 times the undrained shear strength. However, Hong and Lee (2009) suggested the upper bound criteria for acceptable lateral movement to be 8.3 times the undrained shear strength. Peck (1969) proposed an equation very similar to equation 2, he used a stability number defined as:

$$N = \frac{\gamma H}{S_u} \tag{3}$$

γ = unit weight of soil

H = height of soil fill

Su = undrained shear strength of foundation soil

Peck (1969) suggested that no significant deformation would occur if N is less than 3.14, between N equal to 3.14 and 6 deformation will occur in increasing severity as N approaches 6, and beyond N equal to 6 large deformations will occur with the possibility of failure.

The FHWA publication by Hannigan et al. (2016) recommends estimating the magnitude of lateral deformation based on the estimated settlement using the following equation.

$$S_h = 0.25 S_v \tag{4}$$

S_h = horizontal abutment movement (inches)

S_v = vertical fill settlement (inches)

The relationship in Equation 4 is similar to what was observed by Ellis and Springman (1999) and Leroueil et al. (1990). It should also be noted that construction sequence can have a big impact on the reliability of the prediction methods above. If the abutment is built shortly after embankment construction, when the relationship between S_h and S_v is closer to 1, then equation 4 could largely underestimate the magnitude of anticipated lateral movement.

Hong and Lee (2009) developed a chart based on the undrained shear strength of the foundation soil and the surcharge pressure or increase in vertical stress. The design chart was developed from field monitoring data of 43 bridge abutments in Korea. The chart, shown in Figure 4, is further divided into zones based on allowable horizontal deformation criteria similar to what was proposed by Bozozuk (1978).

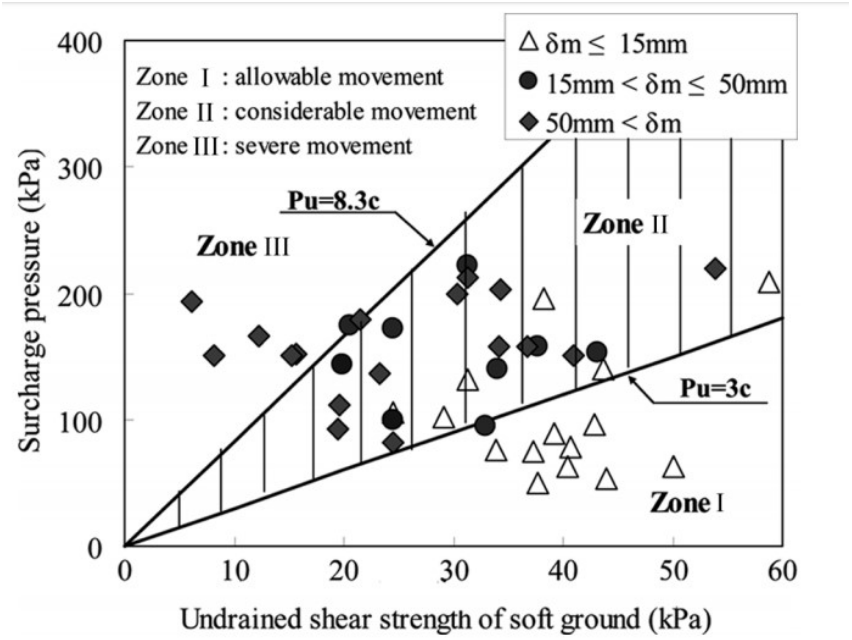

Figure 4. Relationship between the surcharge pressure behind abutments and undrained shear strength of soft ground, from Hong and Lee (2009)

Hong and Lee (2009) also plotted their data with respect to the stability number as proposed by Peck (1969) and presented in equation 3, however the authors choose to use bounds of N = 3 for the lower limit and N = 8.3 for the upper limit as opposed to 3.14 and 6.0 as proposed by Peck (1969). The relationship between the measured lateral displacement and the stability number is shown in Figure 5.

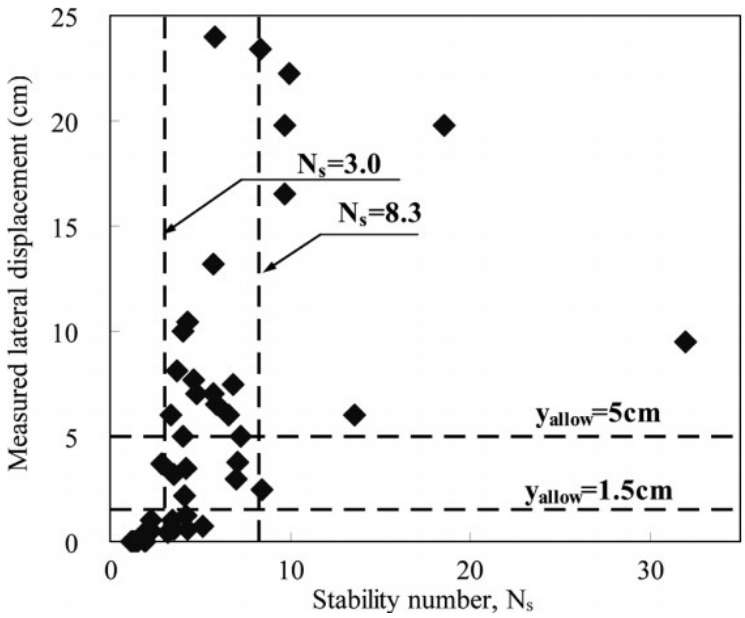

Figure 5. Relationship between the measured lateral displacement of abutments and the stability number, from Hong and Lee (2009)

Figure 5 shows that the stability number proposed by Peck (1969) does indicate that a stability number less than three will have small lateral displacements, but beyond a stability number of three there appears to not be a direct relationship. For example, Hong and Lee (2009) found largely different lateral displacements for the same stability number. Similarly, the same magnitude of movement was realized for different stability numbers.

The distribution of lateral spreading with depth through the foundation layer has been investigated by Tavenas et al. (1979) based on work completed by Bourges and Mieussens (1979). The general form of lateral displacement, *Y*, under an embankment with respect to depth can be expressed by Equation 5 (Tavenas et al., 1979).

$$Y = \left[1.78\left(\frac{z}{d}\right)^3 - 4.7\left(\frac{z}{d}\right)^2 + 2.21\left(\frac{z}{d}\right) + 0.71 \right] \times y_m \quad (5)$$

y_m = maximum lateral displacement anticipated

z = depth within the clay layer

d = layer thickness

Equation 5 is based on an elastic solution for a normally consolidated soil, which is what is anticipated at the end of construction in a saturated soil profile; the coefficients are based on data from 20 monitored embankments. Tavenas et al. (1979) noted that if the soil is partially drained then the distribution presented in Equation 5 will change. They also noted there were standard deviations ranging between 0.14 and 0.25 when choosing the coefficients which means Equation 5 could result in error of approximately 30 to 40 percent based on the data used to develop the equation.

There are analytical methods to estimate a factor of safety against lateral movement under embankments, estimate the magnitude of lateral movement based on the vertical deformation, and to estimate the distribution of lateral deformation. However, the present methods to estimate the magnitude of lateral movement are largely based on observations and they often do not accurately estimate the amount of lateral movement. As was shown by Hong and Lee (2009) a stability number of 8.3 corresponded to approximately 3 cm of lateral displacement in one embankment and 23 cm of lateral displacement in another embankment in the study. The discrepancy between estimated, or calculated, lateral movement and observed lateral movement has been noted by many. In the study by Tavenas et al. (1979) the coefficient of determination for estimated and observed lateral displacement was 0.25 suggesting the current methods based on observations need improvement if they are to be used widespread.

2.6 Numerical Methods to Estimate Lateral Spreading

Due to the complex issues referenced in the proceeding sections, the Finite Element Method (FEM) has been an attractive solution for lateral deformation problems. The FEM is capable of calculating vertical and horizontal displacements in soil, however, the estimation ability is largely impacted by the constitutive soil model used and the model parameters, which can often be difficult to estimate. Furthermore, the FEM relies heavily on user experience, making it unpractical for routine geotechnical analysis of bridge embankments. The FEM can, however, be useful in modeling lateral spreading to understand the fundamental displacement mechanisms and to establish relationships between lateral movement and soil properties or behavior. There are numerous examples of embankments modeled using the FEM in the literature with various soil constitutive models. Some, not all, of the available constitutive models are presented in this section followed by several case studies that employed the various models to show their applicability to the lateral behavior of bridge embankments.

2.6.1 Relevant Soil Constitutive Models

2.6.1.1 Modified Cam Clay Model

Roscoe and Burland (1968) developed the Modified Cam Clay (MCC) Model. The MCC Model is based on the original Cam Clay Model developed by Roscoe et al. (1963) based on a concept they called the Critical State Soil Mechanics. The original Cam Clay Model was the first mathematical model for predicting the mechanical behavior of 'wet' (normally and lightly overconsolidated saturated) clay that was entirely self-consistent. The MCC model has been widely used as the constitutive driver in Finite Element Programs for many case studies involving lateral deformation of embankments. The model was developed in order to extend results gathered in a conventional triaxial test on 'wet' clay to generalized stress and strain conditions. The model

relies on five soil parameters, which are M, λ, κ, ν, and e_{int}. The soil parameters can be determined from one dimensional consolidation tests and triaxial compression tests on the soil since this model does not distinguish between triaxial compression and extension behavior.

The relative ease of determining input parameters and the availability of the model in commercial modeling software such as PLAXIS (PLAXIS, 2019a) make the MCC Model an attractive option for modeling lateral movement of embankments. However, the model tends to over-predict the range of elastic soil behavior (PLAXIS, 2019a). The model may also allow for unrealistically high shear stresses and cannot be used in overconsolidated soil since high shear stresses will be prevalent as the soil crosses the critical state line as overconsolidated soils do, which could also lead to soil softening in the model (PLAXIS, 2019a).

2.6.1.2 Bounding Surface Plasticity Model

Dafalias and Herrmann (1986) developed the Bounding Surface Plasticity Model utilizing a projection center for radial mapping, which is different than the stress origin as had been proposed previously. Dafalias and Herrmann (1986) suggested using a projection center to considerably improve the prediction capability for large over consolidation ratios. The model was developed within the critical state soil mechanics framework. They also, for the first time, proposed analytical expressions for calibration of some of the model constants for particular loading histories such as K_o consolidation, undrained loading at OCR=1, and specific drained loading. The model can effectively handle monotonic loading conditions for different OCRs and cyclic loading conditions, see Figure 6, which previously wasn't possible (Dafalias and Herrmann, 1986). The model requires 18 model parameters (κ, ν or G, λ, M_c, M_e, P_L, P_{atm}, R_c, R_e, A_c, A_e, T, C, s, m, h_c, h_e and h_2) that can be identified using triaxial compression and extension tests or default values can be used. Dafalias and Herrmann (1986) suggested that although the model requires 18

parameters, more if visco effects are considered, the parameters have a well understood and distinctive role in soil response.

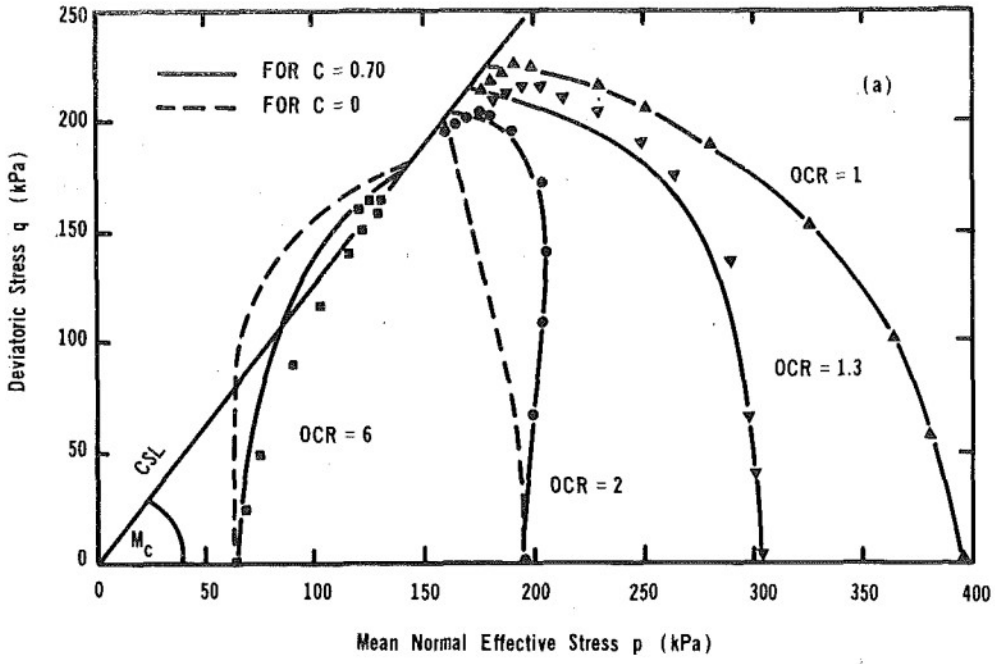

Figure 6. Comparison of Experimental Data (solid circles) with Model Simulation, from Dafalias and Herrmann (1986) (C is the projection center parameter; C = 0 implies that the projection center is at the origin)

The large number of input parameters as well as the non-routine laboratory testing needed to accurately define the parameters, (i.e., triaxial extension and triaxial drained compression) have likely been a factor in the limited adoption of the bounding surface plasticity model in commercial software despite the prediction capabilities as can be observed in Figure 6.

MIT – E3 Model for Overconsolidated Clays

Whittle and Kavvadas (1994) developed the MIT-E3 Model for overconsolidated (OCRs up to 8.0) clays. The model was developed primarily to study how offshore friction piles behave when supporting tension leg platforms (Whittle 1987). The model is limited to saturated clays obeying normalized behavior and that are rate independent. Normalized clays are described by Leroueil and Vaughn (1990) as clays which are not highly structured. The model incorporates

small strain nonlinearity, hysteretic stress strain response, volumetric and shear deformation coupling, and transitional yielding as the soil approaches the normally consolidated stress state (as the soil reaches the preconsolidation pressure) (Whittle and Kavvadas, 1994). In a companion paper, Whittle et. al. (1994) evaluated the predictive capabilities as well as the limitations of the MIT-E3 model using Boston Blue Clay (a low-plasticity marine clay of moderate sensitivity) data. The model and lab comparison for simple shear tests are presented in Figure 7.

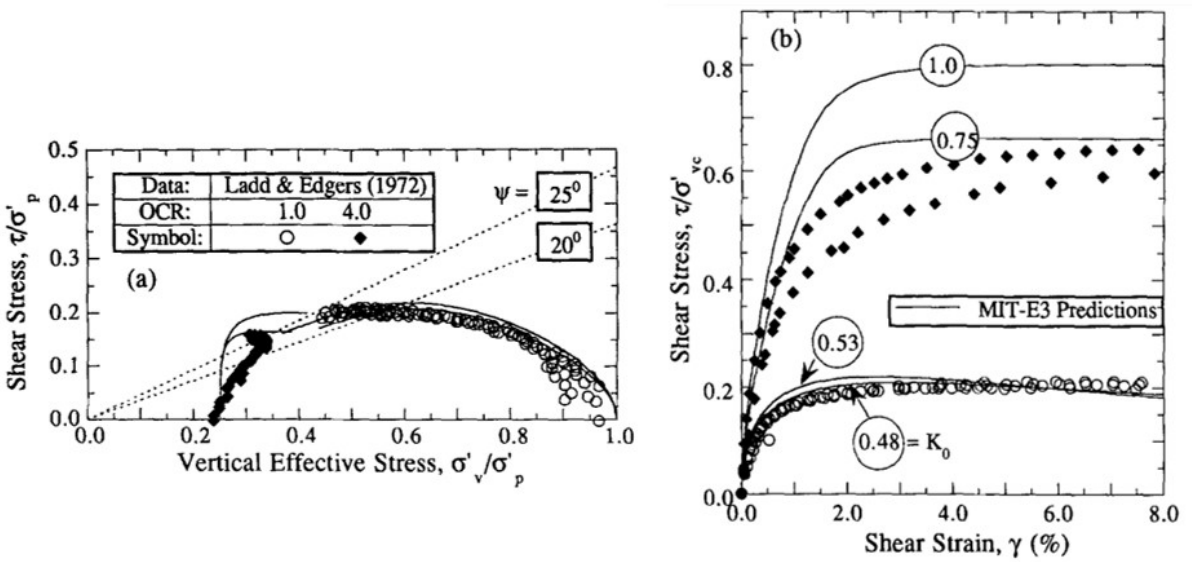

Figure 7. Comparison of MIT-E3 Predictions and Measured Data for Undrained Direct Simple Shear Tests on Ko-Consolidated Boston Blue Clay: (a) Effective Stress Paths and (b) Shear Stress-Strain Response, from Whittle and et al. (1994)

Whittle et al. (1994) noted that for an OCR of 1.0 the model appears to predict the behavior quite well but at the higher OCR of 4.0 the model tends to overestimate the undrained shear strength. Another pitfall of the model is the large number of parameters required as input, 15, which can only be gathered through multiple lab tests. Whittle and Kavvadas (1994) developed a table, see Table 1, identifying the different parameters and the laboratory tests required to get the parameters.

Table 1. Input Parameters for MIT-E3 Model, Recreated from Whittle and Kavvadas (1994)

Test Type	OCR	Test Details and Measurements	Input Parameters	
			Direct	Indirect
Oedometer or CRS	-	measure void ratio, e_0	e_0, λ	-
Oedometer or CRS	-	swelling at two stress levels	-	C, n
Oedometer or CRS	-	include two unload-reload cycles	-	h
K_0 - Oedometer or K_0-Triaxial	1 - 4	measure effective stress path during consolidation and swelling	K_{ONC}, 2G/K	-
Undrained shear test	1.0,2.0	two tests in different modes at OCR = 1 (e.g., CK_0UC, CK_0UE)	ϕ'_{TC}, ϕ'_{TE}	S_t, c
Undrained shear test	1.0,2.0	one CK_0UC test at OCR = 2.0	-	ω, γ
Resonant Column or in-situ crosshole	-	direct measurement of G_{max} from elastic shear wave velocity	K_o	-
special tests	1	drained triaxial stain path test	-	ψ_o

While the MIT-E3 soil model has been used in the investigation of lateral spreading, for example Oliveria and Lemos (2011), the large number of parameters and overestimation of undrained shear strength at high OCRs make widespread adoption of this model unlikely.

2.6.1.3 S-CLAY 1 Model

Wheeler et al. (2003) developed the S-CLAY 1 model, an anisotropic elastoplastic model for soft clay. The model is based on the critical state soil mechanics and represents plastic behavior and anisotropy through an inclined yield surface. To model the development or loss of fabric anisotropy during plastic straining the model uses a rotational component of hardening. The model is intended for normally and lightly overconsolidated soils that are likely to predominantly exhibit plastic deformations. The model uses the same input parameters from the MCC Model (*M, λ,* and *κ)* plus two additional parameters (β and μ) as well as an initial value for the inclination of the yield surface, α. The parameter β is used to define how the plastic shear and volumetric strains rotate

the yield surface and can be determined through a relationship with the normally consolidated value of K_0; however Wheeler et al. (2003) noted that β is sensitive to other assumed values needed for calculation from K_0. The value of μ is used to control the rate toward the specified inclination of the yield curve, the authors suggest there is no convenient way to attain μ but rather suggest conducting numerous simulations and varying μ to determine the most appropriate value.

Since the model was developed to require the least amount of input parameters the nonlinearity of small strain stiffness is not addressed as it is in the model by Dafalias and Herrmann (1986) with the use of bounding surfaces. Furthermore, the model was developed around the simplified triaxial space; the authors present a method to bring the model into generalized stress space but do not discuss generalized stress space in detail. The authors point out that in general the model performs better than the MCC Model; however model simulations when compared with test data show the volumetric strain to be underpredicted during loading by 27 to 37%, see Figure 8.

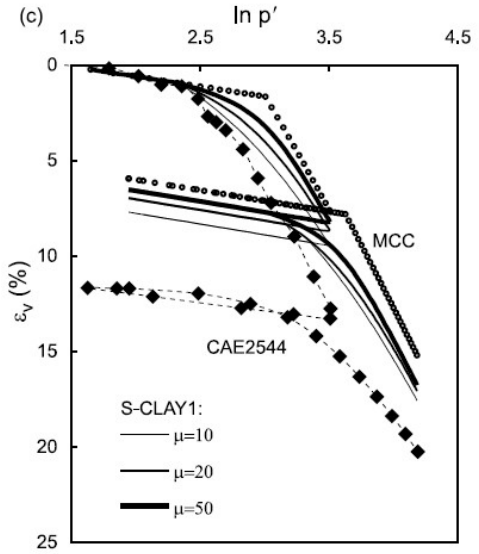

Figure 8. Model Simulations with S-CLAY 1 and MCC: test CAE2544, from Wheeler et al. (2003)

2.6.2 Case Studies with Numerical Models

McCarron and Chen (1987) modeled the MIT test embankment in the finite element program NFAP developed by Chang (1980). The researchers used the Bounding Surface Plasticity model proposed by Dafalias and Herrmann (1986). The embankment is approximately 35 feet tall and is located over medium to soft clay. The embankment was instrumented and has been well documented and studied (McCarron and Chen, 1987). The authors calibrated the model for Boston Blue Clay before performing the analysis using finite elements. The vertical and lateral displacements that were predicted using the bounding surface model matched reasonably well to those measured, see Figure 9 for the lateral displacement comparison.

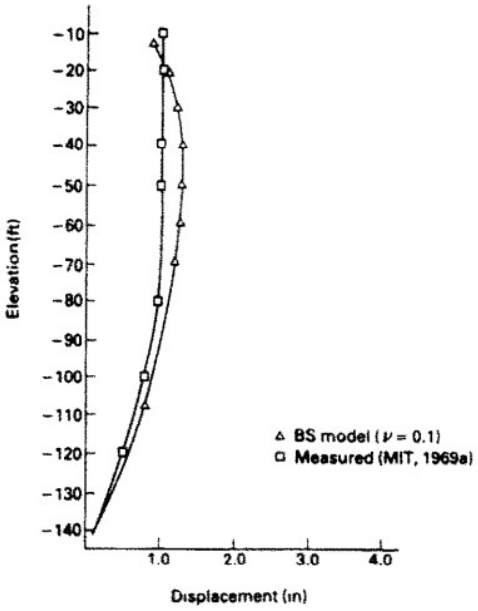

Figure 9. Lateral deformation for MIT test embankment, from McCarron and Chen (1987)

The lateral deformation shown in Figure 9 was measured 160 feet from the centerline of the embankment, 56 feet from the toe of the embankment, while the calculated values correspond to a distance of 170 feet from the centerline of the embankment. The authors noted that in areas of high excess pore water pressure, such as beneath the centerline of the embankment, the lateral

displacement predictions are too large. The authors also noted that the Bounding Surface Plasticity model overpredicted excess porewater pressures exaggerating the amount of lateral displacement.

Mead and Allen (1988) modeled six bridge embankments in Kentucky and performed FEM for each site. They modeled the bridge embankments in the finite element program ISBILD developed by Ozawa and Duncan (1973) which is a nonlinear hyperbolic finite element code. Mead and Allen (1988) did not address lateral movement of the simulated embankments; however they mentioned that ISBILD overpredicted the vertical settlement in four of the simulated embankments. ISBILD was also used to analyze several hypothetical models which varied the dimensions of the embankment and the thickness of the foundation soils while keeping the strength parameters of the soil constant. In general, they found that lateral spreading or squeeze increases with thicker foundation layers, embankment height, or steeper side slopes. They also suggested that the maximum lateral movement occurred at the toe of the embankment.

Chai et al. (1994) modeled a Malaysian test embankment constructed over soft clay soil that was rapidly constructed to failure. The test embankment was instrumented with piezometers, inclinometers, and settlement plates. The construction of the embankment progressed at a rate of 0.4 meters in height per week with lifts of 0.2 meters thick (Chai et al. 1994). The embankment was modeled using the MCC model for the foundation soil and the hyperbolic nonlinear elastic model for the compacted fill, which consisted of decomposed granite. The magnitude of surface settlement matched relatively well and the distribution of surface settlement and was also relatively well captured by the modeling, however the magnitude of maximum lateral displacement was overestimated, see Figure 10.

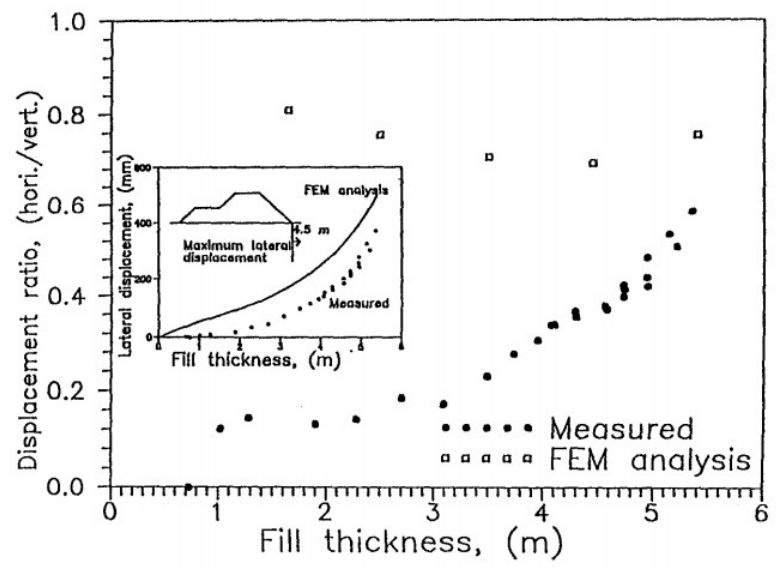

Figure 10. Comparing the measured and calculated foundation deformation ratio, from Chai et al. (1994)

Inset within Figure 10 is the measured lateral displacement versus fill thickness plotted against the predicted. The predicted displacements have a similar trend, but they do not match the measurements. The Malaysian test embankment was constructed rapidly to failure meaning that undrained soil behavior should have controlled, if the site is assumed to be saturated. If the soil was truly behaving undrained, i.e. no volume change, then the displacement ratio should be approximately 1.0, however the ratio starts out around 0.2 and increases to approximately 0.6 suggesting the soil was behaving as drained initially but tending to an undrained state as suggested by Tavenas et al. (1979) for embankments built on natural soils. Chai et al. (1994) noted the inability of the MCC model to predict the lateral displacement within the foundation soil and suggested that if the foundation soil was treated as drained initially that the lateral displacement prediction could be improved at the expense of the vertical displacement prediction.

Karstunen et al. (2005) studied the influence of anisotropy and destructuration when modeling embankments on soft clays. The modeled embankment, known as the Murro Test

Embankment, is located near Murro in Finland. The foundation soils at the site include approximately 23 meters of soft silty clay (S_u = 10 to 30 kPa) overlain by a relatively thin unsaturated zone near the surface. The embankment was constructed in 1993 over the course of 2 days. The embankment has a base width of 30 meters, a crest width of 10 meters, and 2H:1V side slope. Instrumentation at the site includes settlement plates, inclinometers, pore pressure probes, and an extensometer (Koskinen et al. 2002). Karstunen et al. (2005) modeled the soil using 3 constitutive models, S-CLAY1S, S-CLAY1, and MCC. The S-CLAY1S model includes interparticle bonding and degradation of bonds whereas the S-CLAY1 model does not. To reduce discrepancies that arise during implementation, the authors implemented the S-CLAY1S model in the commercial finite element software SAGE CRISP and modified parameters so that the S-CLAY1S model would reduce back to the S-CLAY1 model which could further be reduced to the MCC model. Reducing the most complicated model, S-CLAY1S, to the other models is possible since they were initially based on the MCC and expanded to incorporate additional features such as anisotropy, bonding, and degradation of bonds. As has been found by many other researchers, the vertical settlement predictions and measured data agree quite well. The horizontal displacements agree quite well immediately after construction following a period of undrained loading, but tend to overpredict horizontal displacements after 8 years, see Figure 11.

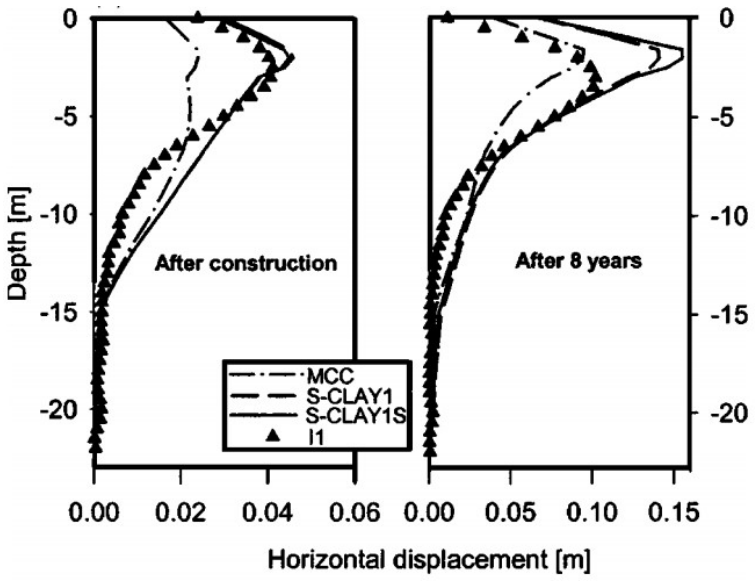

Figure 11. Horizontal displacements underneath crest of embankment slope, from Karstunen et al. (2005)

The S-CLAY1 and S-CLAY1S models do a better job of capturing the undrained behavior of the embankment, however it can be seen from the 8 year figure that the MCC model is closer to the measured values for horizontal displacement.

Shen et al. (2005) studied the influence of Prefabricated Vertical Drains (PVDs) on embankment deformation. PVDs are often used to shorten the consolidation time associated with low permeable soils such as clay. The study involved two test embankments, one with PVDs and one without, in the same area near Shaoxing in Eastern China. The embankments were placed on a 0.5 meter sand mat located over approximately 20 meters of soft to very soft mucky clay which was instrumented with inclinometers, piezometers, and surface settlement gauges. The embankment for the unimproved soil was 4.66 meters tall and the PVD improved soil embankment was 5.88 meters tall. The soft clay soil was modeled using the MCC Model and the sand mat and decomposed granite fill was modeled assuming linear elastic behavior. The settlement behavior of the foundation soil was captured relatively well for both the unimproved and PVD improved foundation soil when modeled with the MCC Model. As has been realized by many other authors

(ex. Chai et al. 1994) the MCC Model overestimated the magnitude of lateral displacement, however for this test embankment the distribution of lateral movement was effectively captured, see Figure 12.

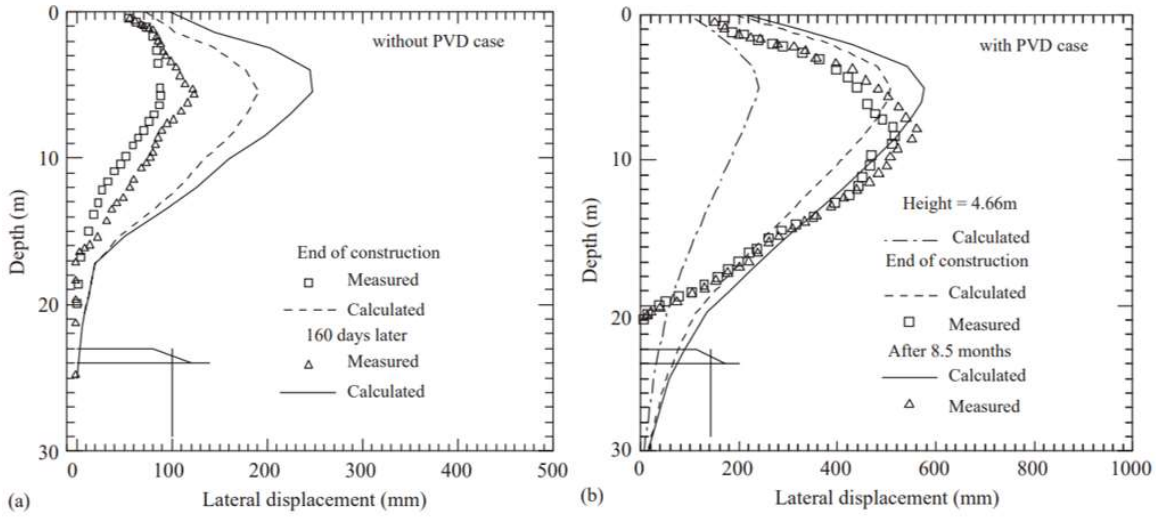

Figure 12. Measured and calculated lateral displacement: (a) without PVD; (b) with PVD, from Shen et al. (2005)

The MCC Model is overestimating the magnitude of lateral displacement by more than a factor of 2 when the ground is unimproved. It is interesting to notice that when the foundation is improved with PVDs the MCC Model predicts the magnitude of movement quite well. The effect of the PVDs was included in the model by modifying the hydraulic conductivity of the soil. The varying magnitude in lateral displacement between the unimproved and PVD improved foundation soil can be partly attributed to the different embankment heights and the spatial variability of the foundation soil (Shen et al. 2005).

Huang et al. (2006) studied the horizontal and vertical movement of a trial embankment constructed in New South Wales, Australia on soft clay. The trial embankments were constructed to better understand the behavior of multiple embankments to be built in the same area as part of a large construction project. The trial embankments were instrumented with settlement plates,

vertical settlement profilers, vibrating wire piezometers, and horizontal profilers. Standard laboratory testing was also conducted on the foundation and embankment soils. The researchers used the commercial finite element program ABAQUS and modeled the soil behavior with the MCC model. The MCC model was chosen due to the relative ease in selecting parameters and the general ability to model soil. The embankment was modeled as two-dimensional plane strain with symmetry applied about the centerline of the embankment. In general the MCC model overpredicted the magnitude of lateral movement and didn't capture the distribution of lateral movement within the soil profile as shown in Figure 13.

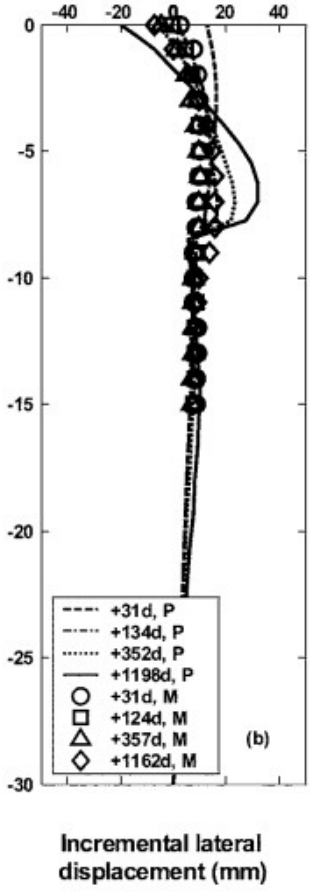

Figure 13. Measured (M) and Predicted (P) lateral displacement, from Huang et al. (2006)

Huang et al. (2006) suggested that the toe of the embankment initially moved outward and then inward due to the bending caused by differential settlement over the embankment, this can be observed in the predicted data in Figure 13, however it is less obvious in the measured data. The authors found the vertical settlement between the model, measured data, and one-dimensional analytical calculations to match quite well.

Karstunen et al. (2006) studied the horizontal movement prediction differences between isotropic constitutive models and anisotropic constitutive models. Two isotropic models were chosen, the MCC model and the Soft-Soil model. The researchers chose three anisotropic models, the S-CLAY1, S-CLAY1S, and the Multilaminate Model for Clay (MMC). The S-CLAY1S model accounts for bonding and destruction, whereas the S-CLAY1 model does not. The MMC handles soil anisotropy using a multilaminate framework (Karstunen et al., 2006). The embankment modeled, the 'benchmark' embankment, had a base of 28 meters, a crest of 16 meters, and a height of 2 meters making the slope 3H:1V. The soil foundation was a lightly overconsolidated soft clay known as Porvoo-Koskenkylä, or POKO, clay which is found near Porvoo in Finland. The various soil constitutive models were implemented in PLAXIS 2D version 8.2. The models calculated vertical settlement varying from 0.8 meters for the MCC model to 1.2 meters for the S-CLAY1S model, since in this study the embankment was only simulated there is no actual measured data for validating the models, rather the research serves as a comparison between the models. The MCC, S-CLAY1, and S-CLAY1S models all predicted a similar maximum horizontal movement of approximately 0.06 meters. The MMC model and soft soil model predicted the most horizontal movement to be approximately 0.08 meters. Since the S-CLAY1 and S-CLAY1S model had similar horizontal predictions it seems that the effects of bonding and destructuration are less pronounced than the effects of anisotropy (Karstunen et al., 2006). The authors also suggested,

based on the benchmark embankment, that when considering long term behavior of embankments anisotropic models will predict less horizontal movement.

Oliveria and Lemos (2011) investigated the behavior of an embankment constructed on soft clay using two anisotropic elastoplastic models. The two models used were the MIT-E3 Model and the Melanie model associated with Mohr Coulomb Criterion (MEL/MC). The MEL/MC model is a simpler model than the MIT-E3 model, but considers a non-associative flow rule which was developed using experimental results (Oliveria and Lemos, 2011). Initially the authors investigated each model's ability to replicate triaxial compression and extension results, they found the MIT-E3 model to be more suitable stating that it includes important behavior characteristics. The authors then modeled a test embankment built over Boston Blue Clay and found the MIT-E3 model predicted the vertical and horizontal deformation better, Figure 14 shows a comparison between the measured horizontal movement data and the predicted data from the MEL/MC and the MIT-E3 model. The MIT-E3 model overpredicted the vertical settlement slightly whereas the MEL/MC model underpredicted the vertical settlement by approximately 40%.

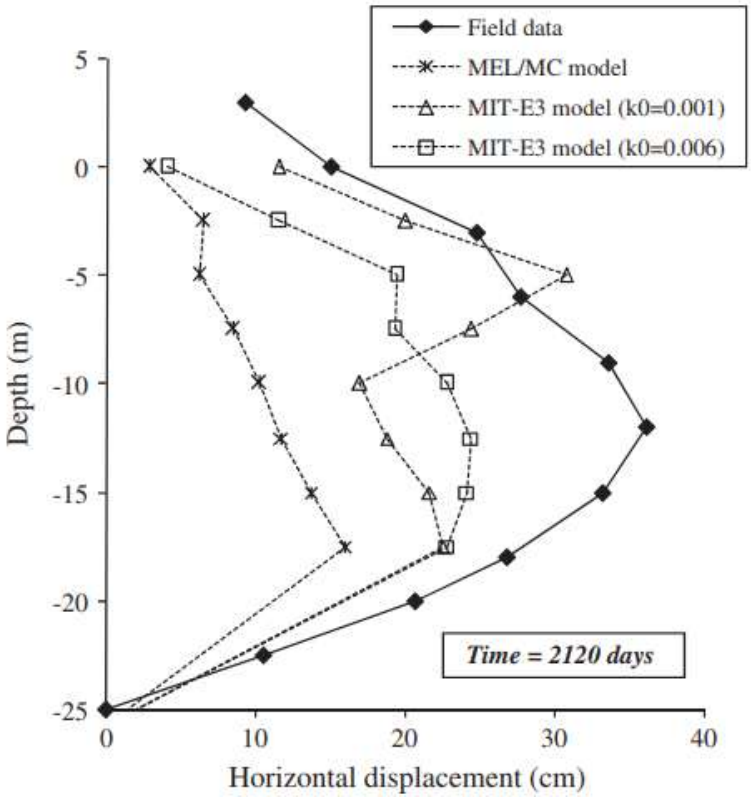

Figure 14. Observed and computed horizontal displacements at 2120 days, from Oliveira and Lemos (2011)

The MIT-E3 Model predicted the horizontal displacement considerably better than the MEL/MC Model; however neither model was able to match the magnitude of observed horizontal displacement. The k0 value in the MIT-E3 model corresponds to the initial slope of the swelling line in e-ln p' space; it appears that when k0 is equal to 0.006 the distribution of horizontal movement is modeled relatively well but the maximum displacement is captured better when k0 is equal to 0.001.

Poulos (1979) summarized several embankment modeling projects and found poor agreement between measured and predicted horizontal movement. He developed a summary table, see Table 2, with key relationships found in using finite elements to model embankments. The table, while a little dated, provides insight into some of the effects of the basic considerations for modeling lateral displacement in embankments.

Table 2. Summary of Effect on Various Factors, Recreated from Poulos (1979)

Factor	Effect on Vertical Displacement	Effect on Horizontal Displacement	Remarks
Poisson's ratio of soil, υ	Increases as υ decreases	Increases as υ decreases	Effect on horizontal displacement much greater than effect on vertical displacement
Anisotropy of soil (cross-anisotropy) E_h/E_v[a]	Increases as E_h/E_v decreases	Increases as E_h/E_v decreases	Effects most pronounced for horizontal displacement when $E_h/E_v < 1$
υ_{VH}[b]	Very significant increase as υ_{VH} decreases (for $E_h/E_v = 2$)	Very significant increase as υ_{VH} decreases	Effect on horizontal displacement greater than effect on vertical displacement
υ_H[c]	Little effect for $E_h/E_v = 2$	increase as υ_H decreases	Effect on horizontal displacement greater than effect on vertical displacement
Nonlinear stress strain soil behavior	Local yield causes increases	Local yielding causes increase and changes distribution with depth	Effect on horizontal displacement greater than effect on vertical displacement
Embankment stiffness	Very little effect	Little effect	Effect on horizontal displacement greater than effect on vertical displacement, but is probably negligible
Foundation roughness	Small reduction for full adhesion when compared with no adhesion	Very significant reduction for full adhesion, compared with no adhesion	Effect on horizontal displacement greater than effect on vertical displacement

[a] E_h/E_v = Young's moduli in horizontal and vertical directions, respectively
[b] υ_{VH} = Poisson's ratio for effect of horizontal strain on vertical strain
[c] υ_H = Poisson's ratio for effect of horizontal strain on complementary horizontal strain

While numerical modeling has its advantages for modeling lateral spreading there is still room for improvement. A common observation from this literature review is the near exclusive use of the MCC model due to the ease of parameter determination and the availability of this model in commercial finite element programs despite the known shortcomings of the soil model and the

advances in constitutive models that have followed the development of the MCC model. Some of the other soil models presented in the previous section can improve the prediction abilities of finite element programs if wider use can be achieved.

2.7 Influence and Response of Abutment Piles on Lateral Deformation

Typically bridge abutments are supported by a series of piles; the piles can be designed as friction piles or they can extended to bedrock, or other hard strata, and be treated as end bearing piles. Since the piles supporting the abutment are driven through the embankment and foundation soil, lateral movement of the soil around and near the piles will have an influence on the capacity and performance of the piles. Similarly, the abutment piles can also somewhat restrict the lateral movement of the embankment. This effect is called the pile pinning effect. In the absence of lateral forces from the soil, abutment piles are typically designed as active piles. Active piles are piles that are horizontally loaded from the pile top whereas passive piles are horizontally loaded adjacent to the pile (De Beer, 1977) such as from lateral movement of foundation soils. There is a need to design abutment piles as passive piles when lateral movement of the abutment or foundation is expected, several techniques have been suggested and will be presented below.

Goh et al. (1997) developed a chart to assist with preliminary estimates of the maximum bending moment of piles subjected to horizontal movement. The chart was developed by completing parametric studies using a finite element program utilizing linear elastic springs along the pile with the pile top fixed. Goh et al. (1997) also modeled 4 case studies using a finite element program and had mixed results; the calculated horizontal displacement was less than the measured leading to lower calculated bending moments. The under prediction of horizontal displacement and bending moments is likely the result of the soil being modeled as linear elastic. The chart developed by Goh et al. (1997) is shown in Figure 15.

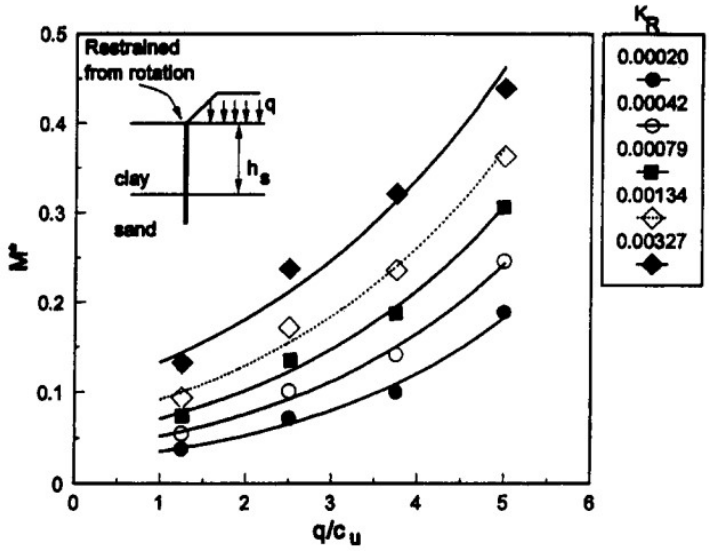

Figure 15. Nondimensionalized Plot of M* versus q/cu, from Goh et al. (1997)

In Figure 15, q is the applied embankment pressure, c_u is the undrained shear strength of the soil, M* is the nondimensionalized bending moment defined in Equation 6 and K_R is the relative pile-soil stiffness ratio proposed by Poulos (1973) defined in Equation 7.

$$M^* = \frac{M_{max}}{C_u d h_s^2} \tag{6}$$

M_{max} = pile maximum bending moment

c_u = soil undrained shear strength

d = pile width

h_s = thickness of soft clay layer

$$K_R = \frac{E_P I_P}{E_{50} h_s^4} \tag{7}$$

E_pI_p = pile flexural stiffness

E_{50} = soil undrained secant modulus at half ultimate load

It should also be noted that the chart in Figure 15 was developed for a pile located at the toe of the embankment which may be applicable to piles supporting bridge piers but, as mentioned previously, the abutment piles are located within the embankment not at the toe of the embankment.

Stewart et al. (1994) also developed an analytical technique to estimate the maximum bending moment and deflection in piles subjected to embankment loading. The equations Stewart et al. (1994) developed utilized empirical design charts and curve fitting techniques to determine some of the parameters. The design charts, shown in Figure 16, were developed using 2 sets of centrifuge data as well as 1 set of field measurements. The equations, similar to Goh et al. (1997), require the relative pile-soil stiffness ratio, K_R, proposed by Poulos (1972). The equations relating maximum bending moment and maximum deflection and the necessary design charts are shown below.

$$\left(\frac{M_{max}}{s_u d L_{eq}^{\ 2}}\right) = a_1 \left(\frac{q}{s_u}\right)^{b_1} \tag{8}$$

$$\left(\frac{y E_p I_p}{s_u d L_{eq}^{\ 2}}\right) = a_2 \left(\frac{q}{s_u}\right)^{b_2} \tag{9}$$

M_{max} = maximum bending moment

d = diameter of pile

L_{eq} = equivalent length of pile between points of fixity

Stewart et al. (1994) suggested

(a) rotation prevented $L_{eq} = L$

(b) pinned $L_{eq} = 0.6L$

(c) free $L_{eq} = 1.3L$

L = length of pile

a_1, a_2, b_1, b_2 = curve fitting parameters determined from Figure 16, shown below.

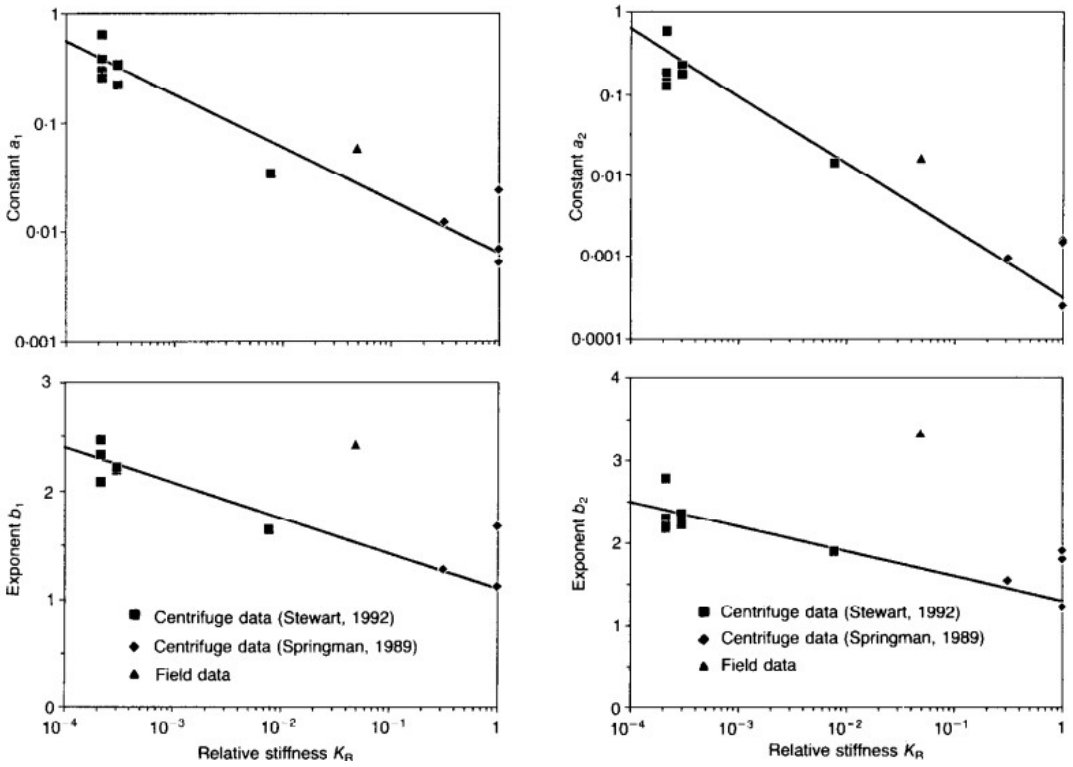

Figure 16. Variation of curve-fitting parameters for maximum pile bending moment and deflection, from Stewart et al. (1994)

The method proposed by Goh et al. (1997) can be used with information typically already available from soil investigations and material properties. Several other methods have been proposed that show good agreement between measured and predicted bending moments; however, they typically need a lateral movement profile before calculation of the bending moments can be achieved. Essentially the methods decouple the pile-soil system and propose analyzing each one independently, which assumes that the piles will have minimal effects on the embankment system. One of the early efforts using this method was completed by Chen and Poulos (1997). They used a simplified boundary-element analysis along with user specified free-field soil movement to predict the bending moments in piles. Chen and Poulos (1997) also incorporated a maximum lateral pile-soil stress to allow for failure in the soil to occur so some of the non-linear effects of

soil could be captured. They developed a series of charts (see Chen and Poulos 1997), based on elastic solutions for constant and tapered piles; however they note that the charts provide an upper bound to the solution highlighting the effects the soil nonlinearity have on the system. In conclusion, Chen and Poulos (1997) suggested that the proposed boundary-element program could provide satisfactory predictions if the lateral movement of the soil, Young's modulus of the soil, and limiting pile-soil contact pressure could be accurately assessed.

More recently additional methods have been developed to determine pile bending moments that require the free field displacement of the soil profile. One such method was proposed by Kelesoglu and Cinicioglu (2010). Their method involved capturing the soil degradation curves from full scale test and then using that data along with a corresponding degradation stiffness matrix to solve for pile bending moments. The authors then compared their results against the soft soil creep model commercially available in PLAXIS and noted the good agreement after minor corrections were made within the PLAXIS software. Kelesoglu and Cinicioglu (2010) suggested the new method as an alternative to traditional modeling that provided good results; they acknowledged that to use the method, a full-scale embankment would first have to be built on site and monitored prior to performing analysis of the bending moments in the piles. Similar methods have been proposed by others (see Martin and Chen, 2004) and has been included in the commercially available software LPILE, which has an option to input free field displacement and then analyze pile response (Ensoft, 2019). Free field displacement is, however, difficult to accurately determine, introducing an obstacle when using these methods. Furthermore, free field displacement methods ignore the interaction between the embankment and the bridge piling.

2.8 Summary of Knowledge Gaps and Contributions of Current Research

The literature review reveals that while there has been a large amount of research on the topic of embankment lateral displacement, mostly for embankments without piling, there is still not a firm understanding of the problem and guidance for negating the displacements is scarce. Many of the recommendations on dealing with lateral displacements of bridge embankments follow general rules of thumb or lean heavily on the engineer's previous experience. Research completed as part of this dissertation contributes to the knowledge base in the following ways:

1. The Bounding Surface Plasticity model was implemented into PLAXIS 2D.
2. The influence of bridge piling on the lateral deformation behavior was studied in a limited capacity.
3. Finite element modeling was completed on a case study, SH 3 over BNSF Railroad.
4. Relationships from a parametric study relating bridge embankment deformation with embankment geometry and soil conditions were analyzed and summarized. Key relationships are discussed.
5. An empirical equation was developed to estimate the magnitude of lateral deformation of piled bridge abutments.
6. Recommendations regarding the design of piled bridge abutments with respect to lateral deformation for the practicing engineer were developed.

3.0 BOUNDING SURFACE PLASTICITY MODEL FOR ISOTROPIC COHESIVE SOILS

The bounding surface plasticity model implemented into PLAXIS and used in this dissertation was developed by Dafalias and Herrmann (1986). The model was developed within the framework provided by critical state soil mechanics and is for isotropic time independent soils. The advantage of the bounding surface plasticity model over classical models is the allowance of plastic strains within the bounding surface during loading; when unloading the behavior is elastic but plastic strains are allowed once reloading starts. The implemented Bounding Surface Plasticity model has two forms, one with a bounding surface defined by a single ellipse and one with a bounding surface defined by two ellipses and a hyperbola portion. Both forms of the Bounding Surface model were implemented but this dissertation will utilize the form consisting of two ellipses and a hyperbola portion, unless otherwise stated. A schematic of the bounding surface model with the radial mapping rule used is shown in Figure 17, where F is the bounding surface function in the stress invariant space defined by I and J.

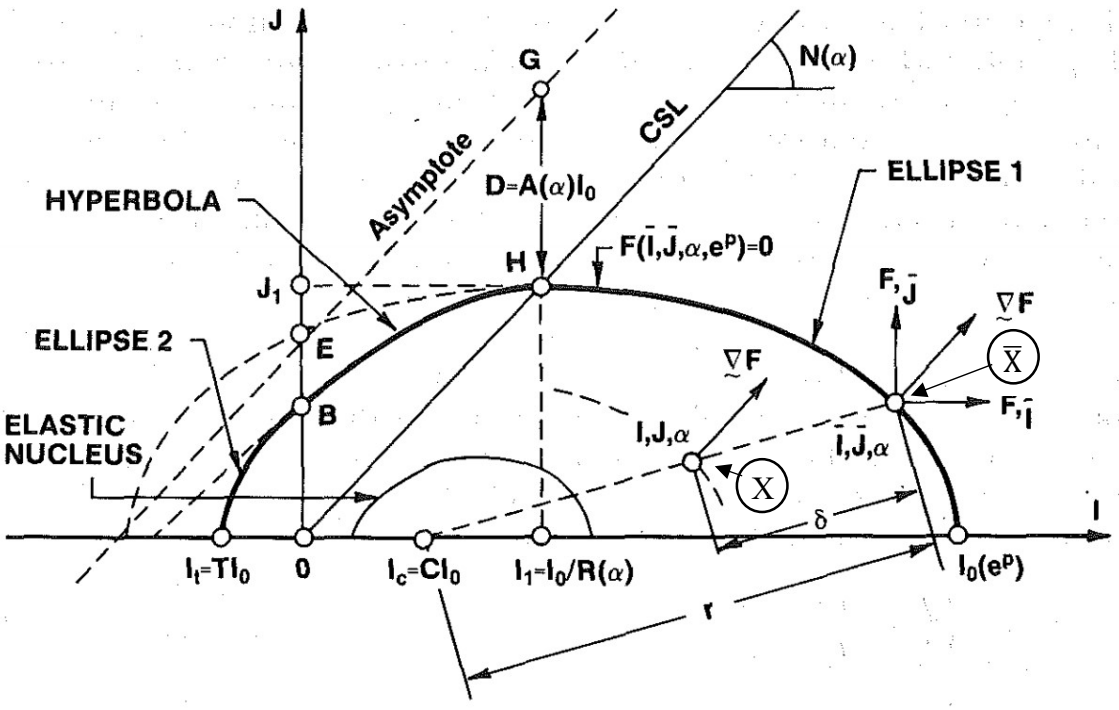

Figure 17. Schematic illustration of bounding surface and radial mapping rule in stress invariant space, from Dafalias and Herrmann (1986)

The equations describing the bounding surface, defined by Dafalias and Herrmann (1986), are as follows:

Ellipse 1

$$F = \left(\bar{I} - I_0\right)\left(\bar{I} + \frac{R-2}{R} I_0\right) + \left(R-1\right)^2 \left(\frac{\bar{J}}{N}\right)^2 = 0 \tag{10}$$

Hyperbola

$$F = \left(\bar{I} - \frac{I_0}{R}\right)^2 - \left(\frac{\bar{J}}{N} - \frac{I_0}{R}\right)\left[\frac{\bar{J}}{N} - \frac{I_0}{R}\left(1 + 2\frac{RA}{N}\right)\right] = 0 \tag{11}$$

Ellipse 2

$$F = \left(\bar{I} - TI_0\right)\left[\bar{I} - \left(T + 2\zeta\right) I_0\right] + \rho \bar{J}^2 = 0 \tag{12}$$

$$\zeta = -\frac{T\left(Z + TF'\right)}{Z + 2TF'}; \quad \rho = \frac{T^2}{Z\left(Z + 2TF'\right)} \tag{13}$$

$$y = \frac{RA}{N}; \quad F' = \frac{N}{\sqrt{1+y^2}}; \quad Z = \frac{N}{R}\left(1 + y - \sqrt{1+y^2}\right) \tag{14}$$

where:

I = first stress invariant

J = second stress invariant

model parameters:

R = defines ratio of the major to minor axis of ellipse 1

N = slope of the critical state line

A = controls shape of hyperbolic portion

T = defines ellipse 2 (i.e., tensile zone of soil)

In Figure 17, and the equations describing the bounding surface, a bar over the stress invariant signifies that the stress is the image or projection of the current stress state onto the bounding surface. The image of a stress state (in Figure 17) is determined using a simple 'radial' rule, using the intersection of a straight line connecting the project center defined by a parameter C (I_c in Figure 17) and the current stress state (X in Figure 17) with the bounding surface.

In the following equations the standard indicial notation convention is utilized. That is free indices vary over 1, 2 and 3 and repeated indices indicate summation over 1, 2, and 3. Furthermore, compressive stress and stains are considered positive. The first and second stress invariants I and J are defined as:

$$I = \sigma_{ii} \tag{15}$$

$$J = \left(\frac{1}{2} s_{ij} s_{ij} \right)^{\frac{1}{2}} \tag{16}$$

where:

$$s_{ij} = \sigma_{ij} - \frac{I}{3}\delta_{ij} \tag{17}$$

σ_{ij} = total stress tensor

δ_{ij} = Kronecker delta, defined as

$$\delta_{ij} = \begin{cases} 0 \text{ if } i \neq j \\ 1 \text{ if } i = j \end{cases} \tag{18}$$

Initially the size of the bounding surface is related to the initial stress state and the over consolidation ratio (OCR), as the bounding surface evolves the size is related to the plastic void ratio, denoted as e^p and defined as:

$$e^p = -\left(1 - e_0\right)\varepsilon^p{}_{ij} \tag{19}$$

e_0 = initial void ratio

$\varepsilon^p{}_{ij}$ = plastic strain tensor

The slope of the critical state line, denoted by N, is a function of the lode angle (α) which is defined as:

$$-\frac{\pi}{6} \leq \alpha = \frac{1}{3}\sin^{-1}\left[\frac{3\sqrt{3}}{2}\left(\frac{S}{J}\right)^3\right] \leq \frac{\pi}{6} \tag{20}$$

where:

$$S = \left(\frac{1}{3}s_{ij}s_{jk}s_{ki}\right)^{\frac{1}{3}} \tag{21}$$

The direction of plastic strains are given by ∇F, the normal to the bounding surface. The magnitude of the plastic potential is a function of the location of the current stress state relative to the bounding surface, the distance is denoted as δ. As δ decreases the plastic potential increases until the current stress state reaches the bounding surface at which time δ approaches zero and then the stress state will remain on the bounding surface as loading continues and detach if unloading

occurs. If a zone of purely elastic behavior is needed the model includes an elastic nucleus within which only elastic behavior is permitted that can be defined using the model parameter S.

The model also includes a shape hardening function, , which relates the plastic modulus, K_p, with the bounding plastic modulus, ; which can be fully specified in terms of the state variables I, J, α, and $I_0(e^p)$. The shape hardening function defines the shape of the stress-strain curves for points within the bounding surface (i.e. for overconsolidated soils). The shape hardening function is defined as:

$$\hat{H} = \frac{1+e_0}{\lambda-\kappa} g^{*2} p_a \left[z^m h(\alpha) + \left(1 - z^m\right) h_0 \right] \tag{22}$$

where:

$$z = \frac{J}{J_1} = \frac{JR}{NI_0} \text{ ;see Figure 17} \tag{23}$$

$$g^* = \left(9F^2{}_{,\bar{I}} + \frac{1}{3} F^2{}_{,\bar{J}} \right)^{\frac{1}{2}} \tag{24}$$

$$h_0 = \frac{\left(h_c + h_e\right)}{2} \tag{25}$$

$$h = \frac{2\left(\frac{h_e}{h_c}\right)}{1 + \left(\frac{h_e}{h_c}\right) - \left[1 - \left(\frac{h_e}{h_c}\right)\right] \sin 3\alpha} h_c \tag{26}$$

F, = I coordinate of bounding surface

F, = J coordinate of bounding surface

For a closed-form analytical expression for F, and F, see Dafalias and Herrmann (1986).

model parameters:

m = positive material constant

h_c = shape hardening parameter in triaxial compression

h_e = shape hardening parameter in triaxial extension

All the parameters necessary for the model can be determined from laboratory testing, namely one-dimensional consolidation tests, triaxial compression tests and triaxial extension tests following guidelines from Kaliakin et al. (1987). Furthermore, typical values as well as a range of values has been compiled by Kaliakin et al. (1987) and are included in Table 3.

Table 3. Typical Values for Model Parameters Associated with the Elastoplastic Bounding Surface Model, from Kaliakin et al. (1987)

Traditional Model Parameters	Typical Value	Range of Values
Slope of isotropic consolidation line in e – ln p' plot, λ	0.20	0.10 – 0.20
Slope of elastic rebound line in e – ln p' plot, κ	0.05	0.02 – 0.08
Slope of critical state line in q – p' space (compression), M_c	1.00	0.80 – 1.40
Slope of critical state line in q – p' space (extension), M_e	0.80	0.65 -1.00
Shear modulus, G	3000 psi	1000 – 10000 psi
Poisson's ratio, v	0.25	0.15 – 0.30
Transitional stress, P_L	$P_a/3$	$P_a/3$

Surface Configuration Parameters	Typical Value	Range of Values
Value of parameter defining ellipse 1 in compression, R_c	2.30	2.00 – 3.00
Value of parameter defining ellipse 1 in extension, R_e	2.30	1.70 – 2.70
Value of parameter defining the hyperbolic portion in compression, A_c	0.10	0.02 – 0.20
Value of parameter defining the hyperbolic portion in extension, A_e	0.10	0.01 – 0.40
Value of parameter defining ellipse 2 (purely tensile zone), T	0.10	0.05 – 0.15
Projection center parameter, C	0.30	0.0 – 0.50
Elastic zone parameter, S	1.20	1.00 – 2.00

Hardening Parameters	Typical Value	Range of Values
Positive material constant, m	.020	0.020
Shape hardening parameter in triaxial compression, h_c	10	5-50
Shape hardening parameter in triaxial extension, h_e	10	2-100
Shape hardening parameter for states near I-axis, h_2	$(h_c+h_e)/2$	-

4.0 IMPLEMENTATION OF THE BOUNDING SURFACE MODEL IN PLAXIS

4.1 Overview of Implementation

PLAXIS 2020 includes seven soil models in the introductory subscription and an additional four models in the VIP edition. In general, the models included in the introductory subscription would be sufficient for routine geotechnical analysis; however, when more complex analysis is sought, such as in this dissertation, a more sophisticated constitutive model needs to be implemented within the PLAXIS finite element framework. To implement a new model a user defined soil model (UDSM) option is used within PLAXIS. Essentially the model can be written in any programing language; FORTRAN 77 was used during this implementation, and then compiled into a Dynamic Link Library (DLL), which was then added to a subfolder within the PLAXIS program directory (PLAXIS, 2019a). The model parameters can then be specified within PLAXIS and the model can be assigned to soil elements. During the calculation phase PLAXIS will call the DLL for every integration point within the finite element mesh for each iteration of each time step. During the call, PLAXIS will provide information to the UDSM about the previous stresses, previous state variables, strain increments, and time increments. The UDSM will then provide the current stresses and state variables back to PLAXIS (PLAXIS, 2019a).

The code for the Bounding Surface Model was previously utilized in a single element code called EVAL (not commercially available), and presented in Kaliakin and Herrmann (1991). EVAL essentially allows the user to characterize the soil using the Bounding Surface Plasticity model, describe the initial stress state and then specify the loading on the soil element as well as the number of steps that the load is applied over. The code was written in a modular fashion making use of subroutines to make implementation easier. The model code also included a local iteration

scheme to improve prediction capability as well as a radial return routine to return the stress state back to the bounding surface in the event it fell outside of the surface.

For this implementation, the code was written in terms of effective stress, meaning PLAXIS handles the pore water pressures within the main finite element program. PLAXIS uses Biot's theory for coupled analysis assuming the soil skeleton behaves elastic; Darcy's law is used for fluid flow (PLAXIS, 2019b). PLAXIS does allow for the user to provide a bulk modulus value to be applied to the pore water during undrained loading or consolidation analysis. In keeping with previous implementations of this model, the bulk modulus value for pore water can be assigned by the user as a material parameter.

4.2 Implementation Process

The PLAXIS UDSM uses a series of tasks to retrieve information from the soil constitutive model. The tasks used are:

- Initialization of state variables
- Calculation of constitutive stresses
- Effective material stiffness matrix
- Elastic material stiffness matrix
- Matrix attributes
- Number of state variables

With the exception of the initialization of the state variables PLAXIS can call on the task in any order so any dependencies between tasks must be dealt with. The last two tasks listed, matrix attributes and number of state variables, are only called on one time during the calculation process for a given time step since they will not vary with the iterations.

The code used during the implementation was already written in a modular form by Kaliakin and Herrmann (1991) so the intent of this portion of the research was to ensure that PLAXIS and the soil model were communicating properly. To accomplish this task, three subroutine template sets provided by PLAXIS via their website were utilized. Only two of these sets were modified. One of the subroutine sets, USRADDDF.for, was used to get the model information and parameter names, this group of subroutines essentially interacted with the graphical user interface for PLAXIS allowing the parameter names to be displayed within the input boxes used to describe soil properties. In addition to the model parameter names, the names of the state variables could be entered within this subroutine set. PLAXIS output program allows the user to view the values of state parameters for each step of the calculation, for example the size of the bounding surface, I_0, can be monitored as it expands or shrinks with the calculation steps. The other subroutine template set, User_Mod.for, used in this implementation interacts with the calculation phases of PLAXIS and is called on by PLAXIS for each integration point. The remaining subroutine set that was not explicitly modified was a library of operations that were available for programing soil constitutive models. The file, LIBRARY.for, was still compiled with the other source files due to dependencies of LIBRARY.for with USRADDDF.for and User_Mod.for.

PLAXIS treats tension stresses and forces as positive and compressive stresses and forces as negative. The Bounding Surface Plasticity model was written using the opposite sign convention with compression taken as positive as is common for geotechnical formulations. In general, the stresses and strains were multiplied by -1 when being provided to the soil model and then were again multiplied by -1 once the calculations were completed, but before being handed back to PLAXIS. Typically for non-linear models, such as the Bounding Surface Plasticity model,

iterations have to be performed in order to converge on a solution. In addition to iterations the calculation phases are completed in steps both within the soil model and within PLAXIS. To differentiate between the soil model and PLAXIS, local will be analogous to the soil model and global will refer to PLAXIS.

PLAXIS passes many variables to the soil model, many of these variables, however, are not used by the Bounding Surface Model. Therefore, the following discussion will only focus on the variables that are used within the Bounding Surface model. At the start of the calculation phase, PLAXIS will initialize the model. During this time the state variables necessary for the model will be calculated, typically the state variables would be passed from iteration to iteration for each integration point but, the initial values must be calculated at the start of the calculation process. The Bounding Surface Plasticity model only has 2 state variables: the size of the bounding surface, I_0, and the size of the sub-steps used for internal iterations. The equation for the initial size of the bounding surface is as follows:

$$I_0 = (\sigma_{ii}^{'} \times OCR) \times (-1) \tag{27}$$

where:

$\sigma_{ii}^{'}$ = 3 times effective mean stress

OCR = overconsolidation ratio

-1 = accounts for coordinate system differences

The other state parameter, size of sub-steps, is initially set to 1.0. The sub-step size is reduced by half for each internal sub-step as needed to ensure convergence of the sub-step. The sub-stepping routine was originally added to reduce the number of global iterations that would be necessary thereby reducing the computing costs. As the calculation progresses global step to global

step the size of the bounding surface and sub-step size for each integration point is passed back to PLAXIS and stored for the next global step.

In addition to the two state variables the following information is passed to the constitutive model:

- Bounding surface type - single ellipse or two ellipse and a hyperbola
- Drainage conditions
- Soil parameters
- Strain increments and previous total strains for the current stress point in the current step - $\Delta\varepsilon_{xx}$, $\Delta\varepsilon_{yy}$, $\Delta\varepsilon_{zz}$, $\Delta\gamma_{xy}$, ε^{0}_{xx}, ε^{0}_{yy}, ε^{0}_{zz}, γ^{0}_{xy}
- Previous effective stress components for the current stress point in the current step – σ'^{0}_{xx}, σ'^{0}_{yy}, σ'^{0}_{zz}, σ'^{0}_{xy}
- Effective material stiffness matrix for the current stress point in the previous step

while the following are received from the constitutive model:

- Effective material stiffness matrix for the current stress point for the current step
- Resulting constitutive stresses for the current stress point - σ'_{xx}, σ'_{yy}, σ'_{zz}, σ'_{xy}

Since the constitutive stresses and the effective material matrix are linked, the calls for those two tasks were combined into a nested subroutine. This means that if either the constitutive stresses or effective material matrix are requested by PLAXIS then both will be calculated. There are some computational costs associated with nesting the two tasks together, but problems were encountered when attempts were made to separate the two. Furthermore, with modern computing the computation costs are not very high.

The matrix attributes are provided to PLAXIS to ensure the resulting matrix is calculated correctly. For the Bounding Surface Plasticity model, the following attributes were provided to PLAXIS:

- Non-symmetric matrix – PLAXIS will store and calculate full matrix
- Stress dependent matrix – PLAXIS will create and decompose the matrix for each calculation step based on the actual stress state (modified Newton-Raphson procedure)
- Not time dependent matrix
- Tangent Matrix – PLAXIS will create and decompose the matrix for each iteration based on the stress state (full Newton-Raphson procedure); must be used in combination with a stress dependent matrix

4.3 Verification of Implementation

Non-linear numerical models are difficult to verify due to the complexity associated with non-linearity. Since the Bounding Surface Plasticity model had previously been implemented into a single element program (EVAL) as well as a legacy research finite element code, SAC2 (Herrmann and Mish, 1983), an easy method to verify a correct implementation is to model a single element and a simplified boundary value problem in PLAXIS and to compare the results with those of EVAL and SAC2. It should be noted that SAC2 is a 32-bit program which cannot run on modern computers. In addition, SAC2 does not contain beam elements so embankments with piling cannot be analyzed which is why the Bounding Surface Plasticity model was implemented in PLAXIS.

The results from the single element program, EVAL, were compared to the results gathered in the Soil Test module within PLAXIS. The Soil Test module is a subprogram of PLAXIS and can be used to model standard lab tests such as triaxial, cyclical triaxial, oedometer, constant rate of strain, direct simple shear and cyclic direct simple shear tests. Soil Test also includes a general

stress space option which is essentially a single element program. For the general stress state option, the initial stresses in the three coordinate directions are entered as well as the boundary conditions, loading duration and number of steps. The options within Soil Test are similar to what is available in EVAL allowing it to be effectively used to make comparisons between the two. When a user defined model is used in the Soil Test subprogram, the calculation process is the same as it would be for a full boundary value problem, that is the implemented model is called by PLAXIS in the same manner for both the main program and the Soil Test subprogram. Before moving onto more complicated comparisons an exact match was found between PLAXIS and EVAL for the single element condition under simulated triaxial tests for multiple OCRs.

Next a one-dimensional problem was modeled in PLAXIS and SAC2. The model consisted of a single layer of soil that was 1 meter in height and 3 meters long. The model was allowed to drain at the top and bottom with the sides allowed to move in the vertical direction, but not in the horizontal direction and the bottom boundary was fixed. Along the top of the model a 20 kN/m/m line load was applied over 1 day. The soil was then allowed to consolidate for 480 days. Both models were ran as a fully coupled analysis meaning that pore water pressures and soil deformations were calculated simultaneously.

Efforts were made to keep the mesh for each program as close as possible to reduce variations in the comparison. PLAXIS automatically determines the mesh allowing for some user input and influence, while SAC2 requires the mesh to be described by the user node by node. Furthermore, PLAXIS uses 6 node triangular elements and SAC2 uses square 4 node quadrilateral elements. To limit these differences the PLAXIS model was broken up into 10 layers that corresponded to the element height used in the SAC2 mesh. The meshes used are shown below in Figure 18 and 19.

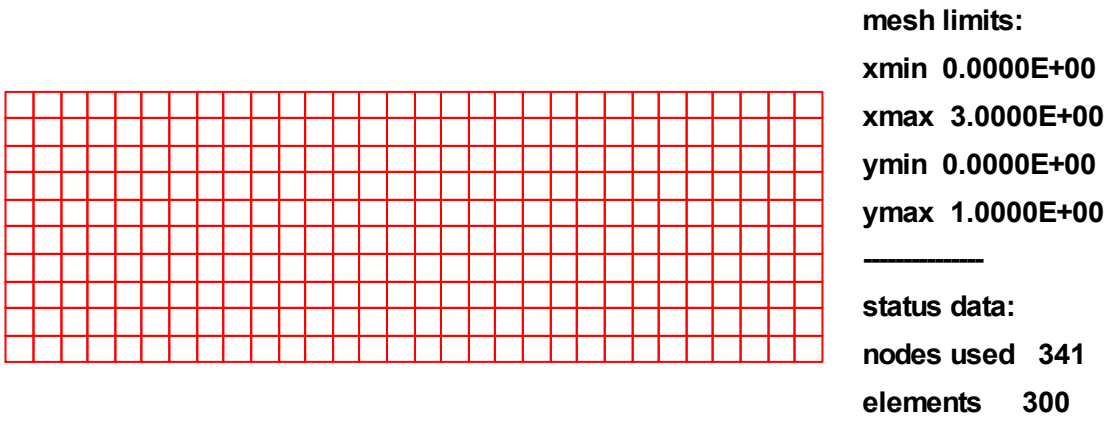

Figure 18. SAC2 One-Dimensional Consolidation Mesh

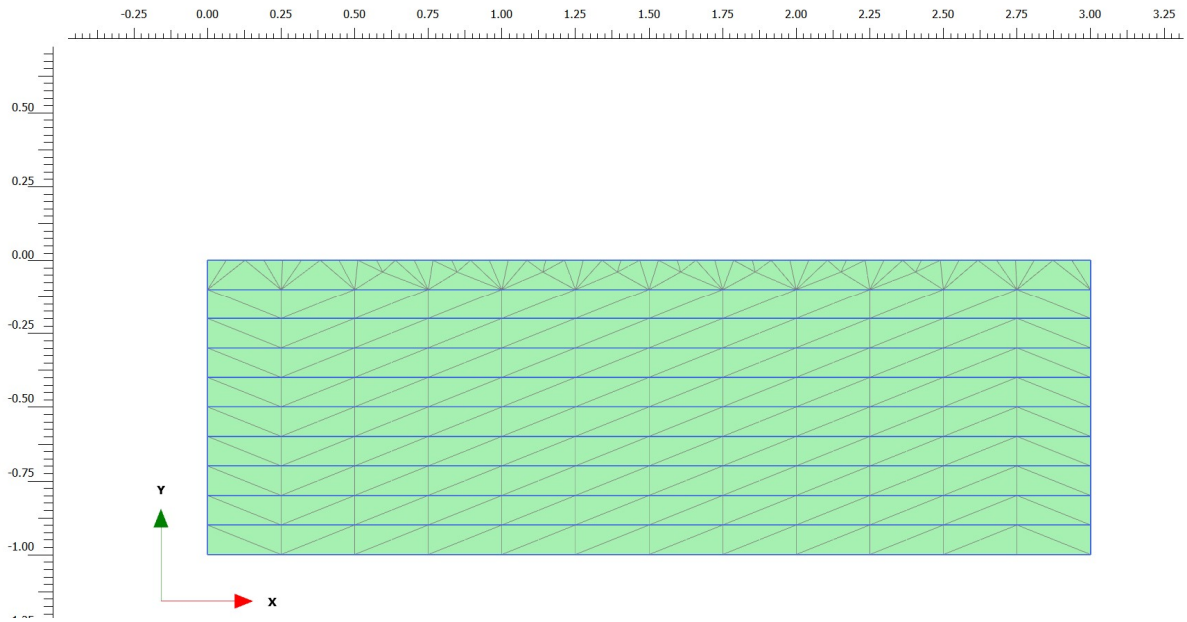

Figure 19. PLAXIS One-Dimensional Consolidation Mesh

Since the model only experienced one-dimensional loading, the settlement with time as well as the pore water pressure dissipation with time are good metrics to compare. Comparison graphs are shown below.

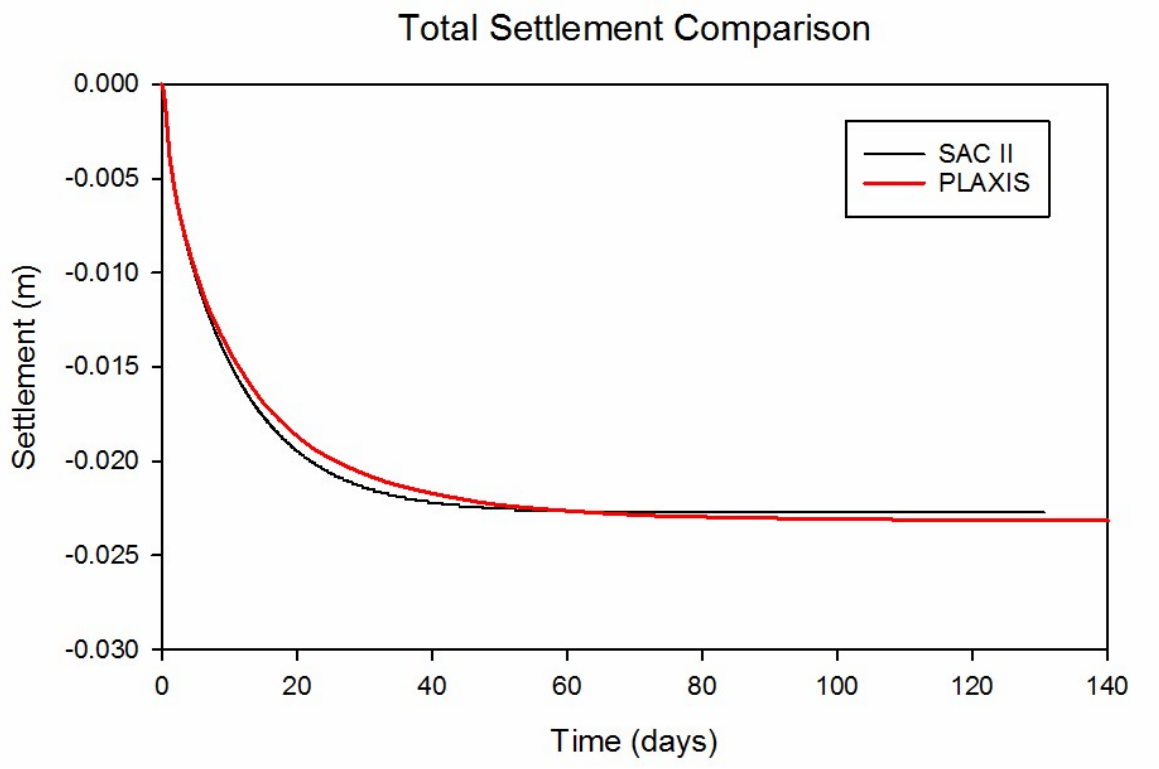

Figure 20. Comparison of PLAXIS and SAC2 Settlement - Time Curves

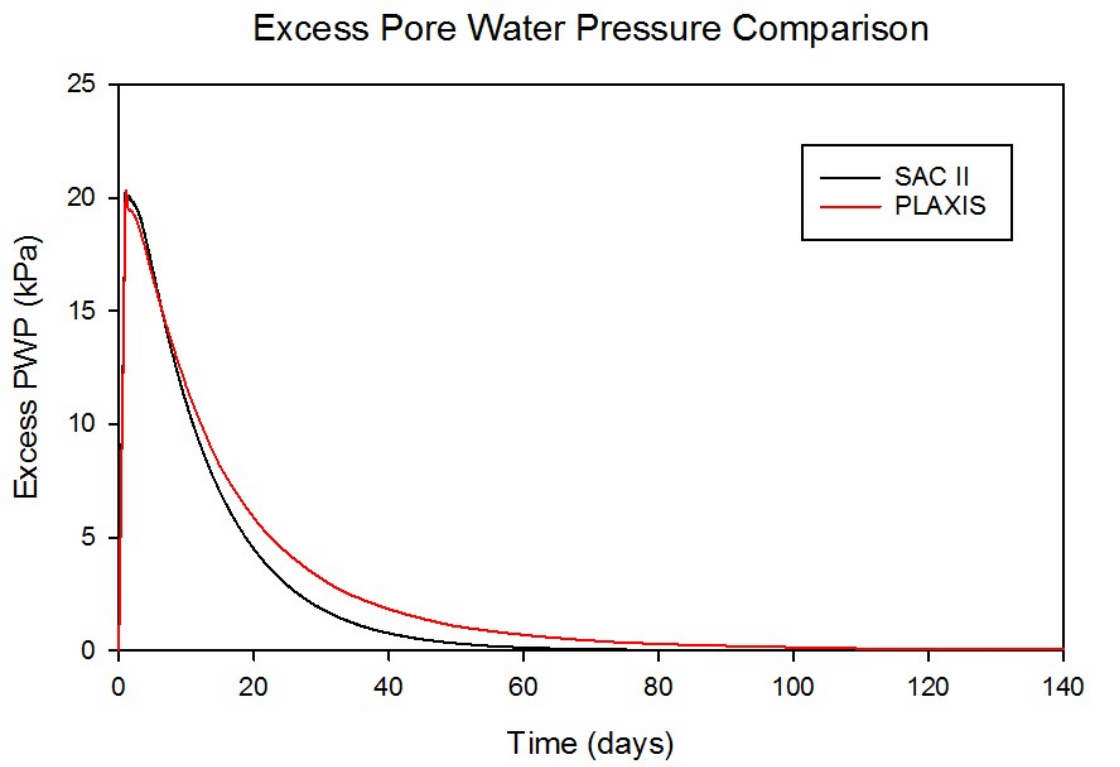

Figure 21. Comparison of PLAXIS and SAC2 Excess Pore Water Pressure – Time Curves

Figure 20 and 21 show that, based on this analysis, the Bounding Surface plasticity model was successfully implemented into PLAXIS. There are some slight differences, but that can be attributed to the differences in element shapes and integration points as well as the stepping procedures used; the automatic stepping feature was used in PLAXIS while uniform steps were taken in SAC2.

An additional check on the implementation is to check whether the pore water pressure dissipation is behaving according to Terzaghi's one-dimensional consolidation theory. Traditional critical state model parameters, utilized in the Bounding Surface plasticity model, can be related to traditional soil mechanics parameters that are used in settlement calculations and in Terzaghi's one-dimensional consolidation theory. The model parameters λ and κ are related to the recompression index, C_r, and the compression index, C_c, as follows:

$$C_r = 2.303 \times \kappa \tag{28}$$

$$C_c = 2.303 \times \lambda \tag{29}$$

The compression index along with the initial void ratio, e_0, and the soil permeability in the vertical direction, k_y, and the average of the initial and final stresses, σ_{va}, can be used to calculate the coefficient of consolidation, C_v, using the following relationships:

$$C_v = \frac{k_y}{\gamma_w m_v} \tag{30}$$

$$m_v = \frac{0.435 C_c}{(1+e_0)\sigma_{va}} \tag{31}$$

The coefficient of consolidation can then be used with Terzaghi's one-dimensional consolidation theory to calculate the excess pore water pressure isochrones for a given time and loading. A

comparison was made utilizing the same one-dimensional consolidation problem described previously. The comparisons are shown below.

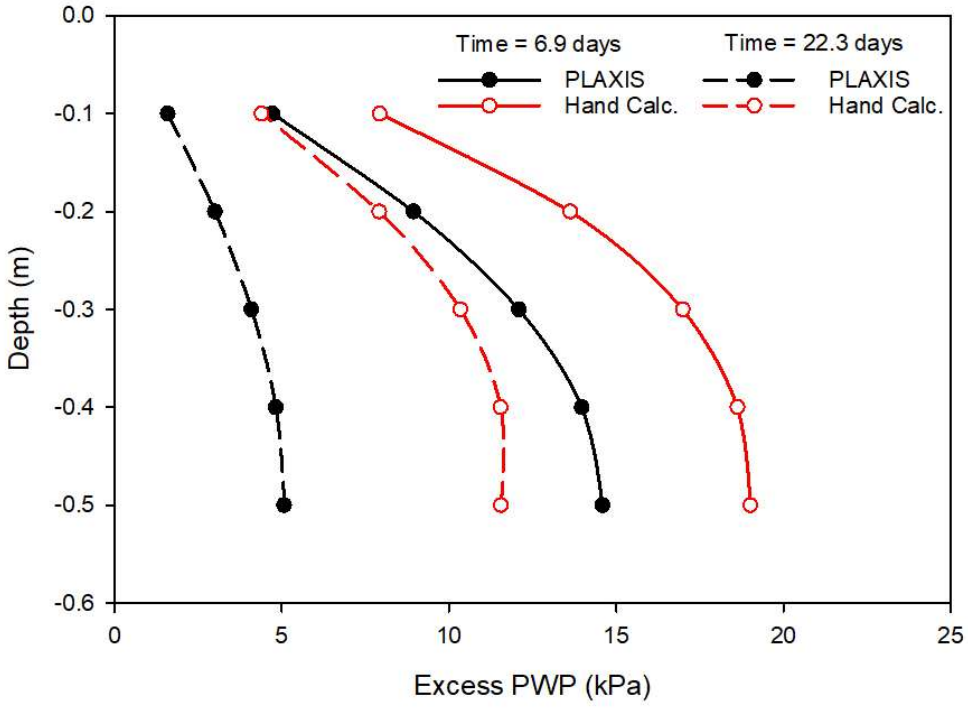

Figure 22. Comparison of Results from PLAXIS and Terzaghi's 1-D Consolidation Theory

One of the reasons for the discrepancies shown in Figure 22 could be that PLAXIS continuously updates variables that are assumed unchanging average values (e.g., mv) in Terzaghi's theory.

5.0 MODELING OF INSTRUMENTED TEST EMBANKMENTS

To demonstrate the Bounding Surface Plasticity model's ability to predict full scale boundary value problems, four test embankments from the literature were selected and analyzed. The selected embankments were chosen due to instrumentation and availability of modeling parameters or lab tests results that were used to calibrate the model. In instances where insufficient data was available to calibrate the model, typical values as presented in Chapter 3 were used. The test embankments, in general, were constructed by transportation agencies to provide a better understanding of the behavior of embankments on soft soils. The embankments span several continents and were located on a range of soils with and without wick drains. All of the embankments were modeled using plane strain conditions with 6 node triangular elements. The analysis was treated as a fully coupled analysis meaning that pore water pressures and soil deformations were handled simultaneously.

5.1 Ballina Test Embankment - New South Wales, Australia

The Ballina test embankment was constructed as part of Australia's first National Field Testing Facility. The need for such a program arose from the construction of the Australian Pacific Highway Upgrade project between Sydney and the border with Queensland. During the project inaccurate predictions of embankment foundation behavior resulted in unnecessary costs and time delays (Kelly et al. 2017).

The embankment had a total height of 2.4 m above the working platform (Kelly et al. 2017). The working platform was 80 m in length and 15 m wide and 0.6 m thick. Following placement of the working platform, instrumentation was installed. The instrumentation included vibrating wire piezometers, settlement plates, inclinometers, piezometers and a hydrostatic profile gauge that extended the width of the embankment to capture the deformed shape at the base of the

embankment. The first layer of the embankment, 0.4 m thick, was then placed next Prefabricated Vertical Drains (PVDs) were installed from the top of the embankment layer in a 1.5 m square pattern. The final layer of the embankment, 2 m thick, was placed and then allowed to consolidate for approximately 3 years while data was collected. A plan and elevation view of the embankment with instrumentation is shown in Figure 23.

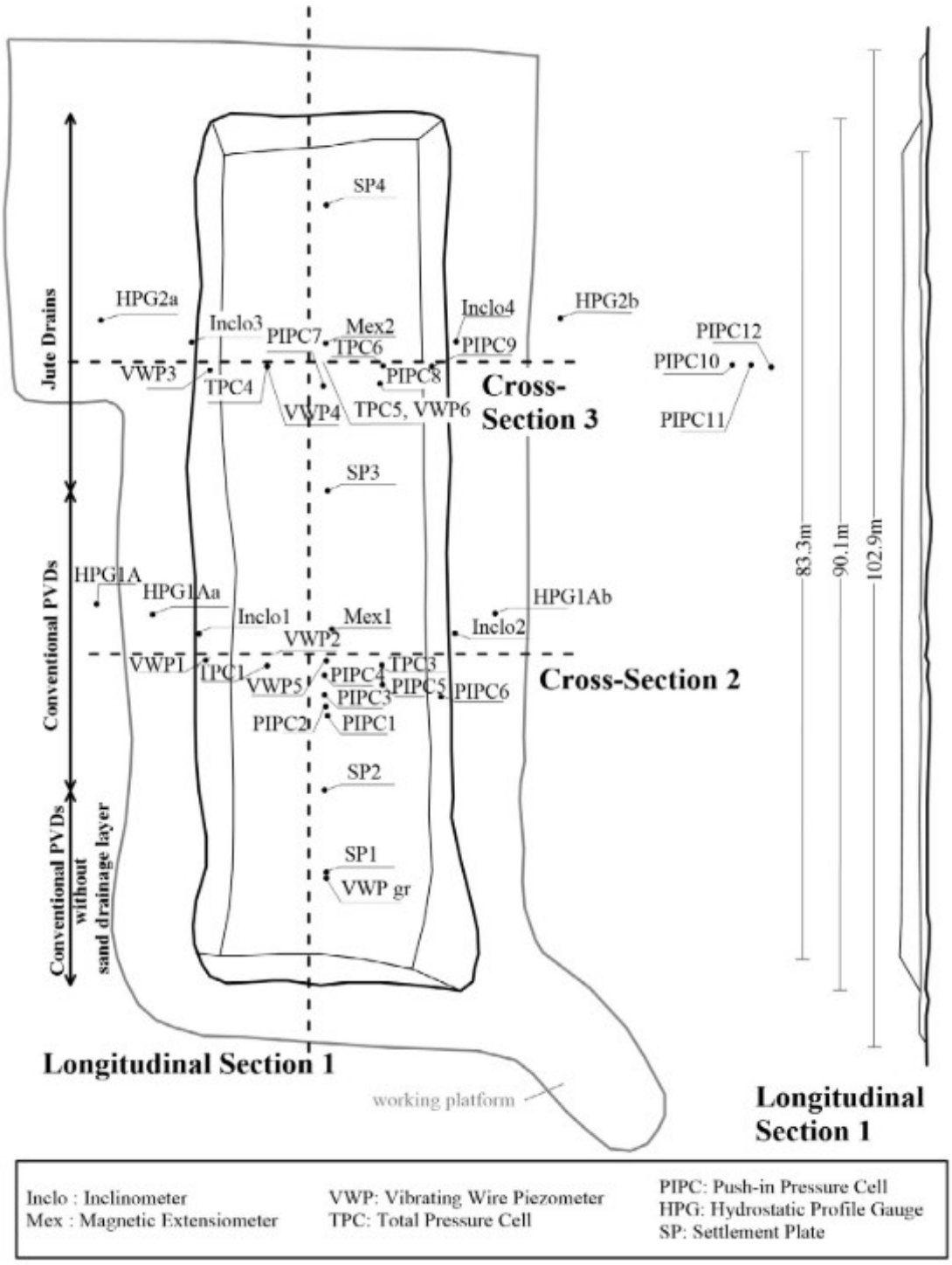

Figure 23. Ballina Test Embankment Plan and Elevation, from Kelly et al. (2018)

The subsurface soils have been idealized as 6 layers. The top and bottom layers are sandy soils and the embankment fill material were modeled using the Mohr-Coulomb model available in

PLAXIS, while the remaining layers were modeled using the Bounding Surface Plasticity Model. The Mohr-Coulomb model was chosen for the embankment fill material due to the lack of information presented on the embankment fill material. Triaxial compression and extension along with one dimensional consolidation tests were used to calibrate the Bounding Surface Plasticity model. The triaxial test results presented by Doherty et al. (2018) were performed using k_0 consolidation meaning the initial stresses on the sample were anisotropic and k_0 generally ranged between 0.4 and 0.8. Despite the anisotropic initial stresses, the Bounding Surface Plasticity model was able to capture the behavior of the soil reasonably well. The adopted material parameters are presented in Table 4. Once the parameters were adopted, six triaxial compression tests were simulated, the comparison is shown in Figure 24. The axis values in Figure 24, mean effective stress (p') and deviatoric stress (q), are based on the Cambridge definition and are defined as:

$$p' = \frac{\left(\sigma'_1 + 2\sigma'_3\right)}{3} \tag{32}$$

$$q = \left(\sigma'_1 - \sigma'_3\right) \tag{33}$$

σ'_1 = major principal effective stress

σ'_3 = minor principal effective stress

Table 4. Ballina Embankment Model Parameters

Depth (m)	Emb.	0 – 0.9	0.9 – 2.1	2.1 – 4.0	4.0 – 10.9	10.9 -13.6	13.6 – 17.8
E (kPa)	20,000	11,000	-	-	-	-	11,000
cohesion, c' (kPa)	5	5	-	-	-	-	5
friction angle, φ (°)	30	30	-	-	-	-	30
dilatancy angle, ψ (°)	5	5	-	-	-	-	5
λ	-	-	0.13	0.61	1.30	1.04	-
κ	-	-	0.003	0.04	0.05	0.04	-
M_c	-	-	1.29	1.09	1.88	1.4	-
M_e/M_c	-	-	0.76	0.76	0.67	0.76	-
v	0.3	0.3	0.2	0.2	0.2	0.2	0.3
R_c	-	-	2.55	2.0	2.0	2.0	-
A_c	-	-	0.2	0.1	0.1	0.1	-
T	-	-	0.1	0.1	0.1	0.1	-
R_e /R_c	-	-	0.8	1.0	1.0	1.0	-
A_e /A_c	-	-	1.0	1.0	1.0	1.0	-
C	-	-	0.4	0.25	0.15	0.6	-
S	-	-	1.0	1.0	1.1	1.0	-
m	-	-	0.02	0.02	0.02	0.02	-
h_c	-	-	10	35	45	50	-
h_e /h_c	-	-	1	1	1	1	-
h_2	-	-	10	35	45	50	-

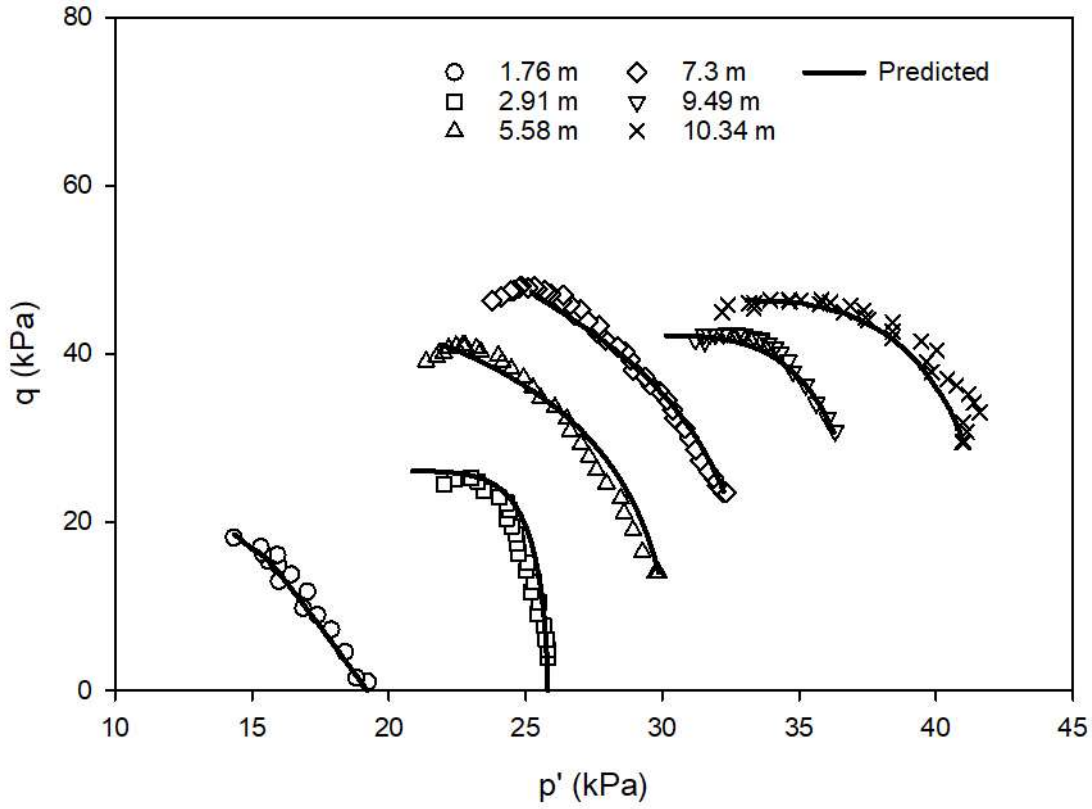

Figure 24. Ballina Embankment Subsurface Soil Triaxial Compression Simulated Results

Since the embankment had PVDs installed, special consideration had to be given to the coefficient of permeability used. PLAXIS allows for one-dimensional elements to be used for drains that essentially provide an exit location for the excess pore water pressure, but it was found that using the drainage elements disrupted the mesh. To model the drains properly each drain would need to be modeled in 3-D with a prohibitively fine mesh rendering this method impractical (Amirebrahimi and Herrmann, 1993). While methods have been proposed to convert the 3-D behavior to an equivalent 2-D model (Indrarantna and Redana, 1997) there are many unknowns with PVDs such as the smear zone around the drains and the long term performance of the drains. The smear zone is an area surrounding the drain that is disturbed during instillation of the drains, the extent of the smear zone and its impact on the soil permeability is difficult to determine. Furthermore, Chai and Carter (2011) suggested that PVDs only operate effectively for half a year

meaning there is likely some non-linear behavior associated with the drain behavior. Chai et al. (2001) suggested an alternative method which is used to determine an equivalent vertical permeability for the soil layers that considers the contributions the PVDs provide. Using the equivalent method allows for the finite element mesh to remain relatively uniform. The equations for the equivalent hydraulic conductivity method proposed by Chai et al. (2001) are presented below:

$$k_{ve} = \left(1 + \frac{2.5l^2}{\mu D_e^2}\frac{k_h}{k_v}\right)k_v \tag{34}$$

where:

l = drainage length

D_e = drain spacing (unit cell diameter)

k_h = horizontal permeability

k_v = vertical permeability

And the parameter μ can be determined from the following equation (Hansbo, 1981):

$$\mu = \ln\frac{n}{s} + \frac{k_h}{k_s}\ln(s) - \frac{3}{4} + \pi\frac{2l^2 k_h}{3q_w} \tag{35}$$

where:

$n = D_e/d_w$

d_w = drain diameter

$s = d_s/d_w$

d_s = diameter of smear zone

k_s = hydraulic conductivity of smear zone

q_w = drainage capacity of PVD when installed

Using the equivalent hydraulic conductivity method only the vertical permeability is changed and the horizontal permeability will remain the same, leading to an anisotropic permeability for the soil layers. The permeabilities used in the analysis in the PVD improved zone are presented in Table 5, the permeabilities listed are based on the results presented in Pineda et al. (2016). In that paper a range of permeabilities are provided for the soil layers as measured during constant rate of strain tests when the soil was under in-situ and at yield conditions. The fairly large range for the permeabilities required some judgment; but in general, the yield permeability was taken to represent the smear zone permeability and the in-situ permeability was used for the horizontal and vertical permeability in Equation 27.

Table 5. Ballina Embankment Adopted Subsurface Soil Permeabilities

Depth (m)	k_v (m/day)	k_h (m/day)
0 – 0.9	1.2*10-1	1.2*10-1
0.9 – 2.1	6.4*10-3	4.03*10-3
2.1 – 4.0	4.7*10-3	4.09*10-3
4.0 – 10.9	5.0*10-4	2.6*10-4
10.9 – 13.6	4.0*10-3	4.0*10-3

The analysis was completed in phases to mimic the construction sequence in the field, the construction sequence was as follows:

- Working platform constructed (10 days)
- Installation of instruments (10 days)
- Placement of first embankment layer (5 days)
- PVD installation (22 days)
- Placement of second embankment layer (15 days)

The above sequence was then followed by null phases to allow the embankment to consolidate, the total analysis time was 1100 days. The mesh used in the analysis is shown in Figure 25, all units are in meters. It is common practice to only model half of an embankment due to symmetry, however the entire Ballina test embankment was modeled due to the sloping clay layer beneath the embankment.

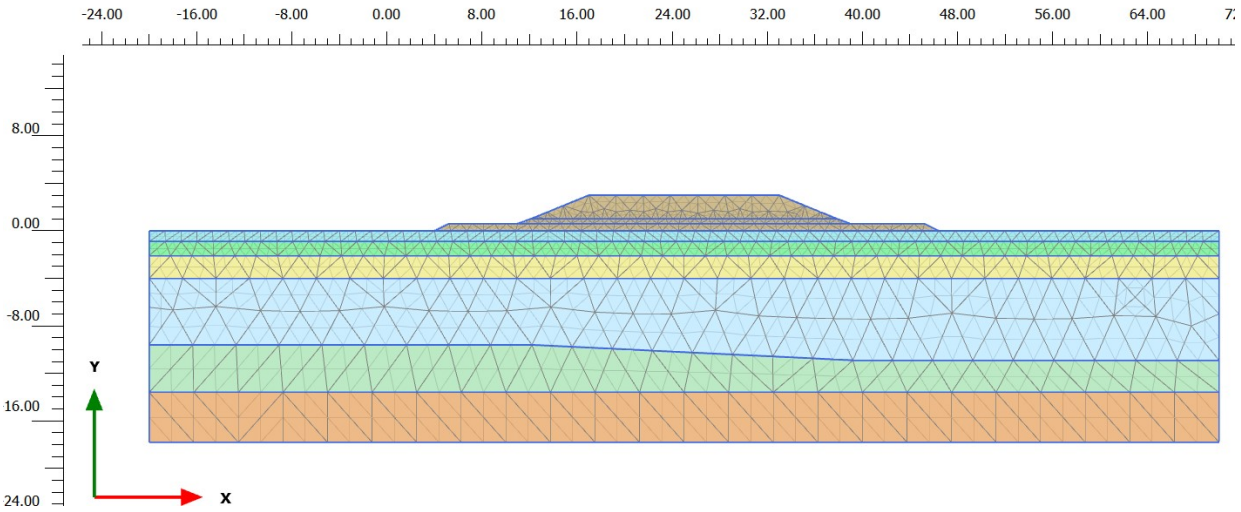

Figure 25. Ballina Embankment Geometry and Mesh

The settlement at three locations beneath the center of the embankment, the lateral displacement profile at the toe of the embankment and the pore water pressure at 3 locations were used as metrics for comparison. The comparison graphs followed by a brief discussion are presented in Figures 26-28.

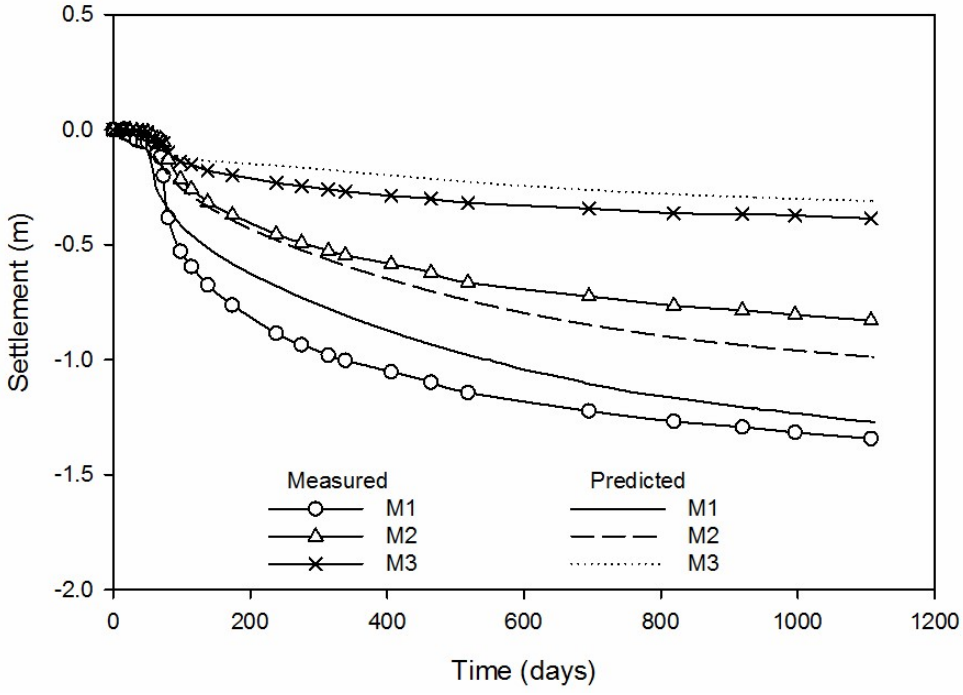

Figure 26. Ballina Embankment Settlement Comparison

The settlement plates M1, M2, and M3 were located beneath the center of the embankment at depths of 1.1 m, 4.1 m and 7.1 m, respectively. In general, the settlement is captured reasonably well by the Bounding Surface Plasticity model as shown in Figure 26. The settlement of the embankment, best visualized by settlement plate M1, was underpredicted by about 70 mm, which is about 6% of the actual settlement. Some of the discrepancy in the settlement simulation can be attributed to the time independent nature of the soil model; the necessity of considering creep behavior when modeling soft soils has been noted by many researchers (eg. Karstunen and Yin, 2010; Yin et. al, 2015; and Rezania et al. 2017).

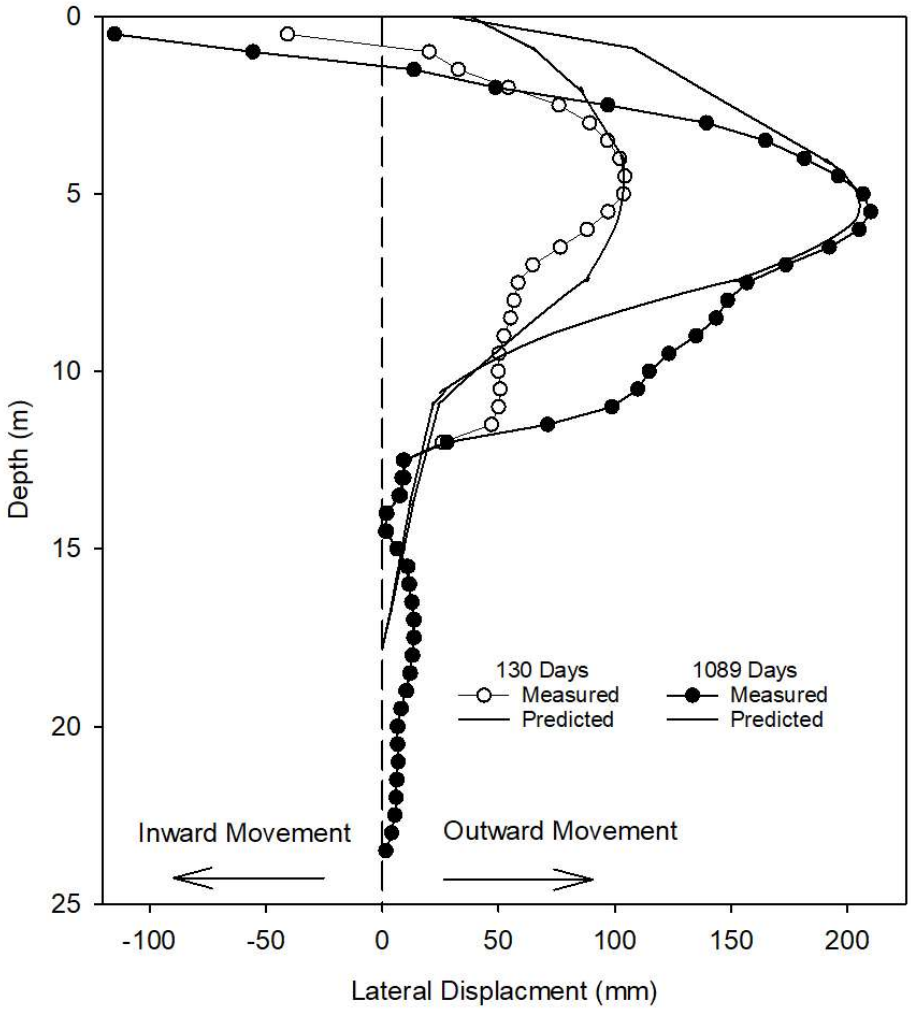

Figure 27. Ballina Embankment Lateral Displacement Profile Comparison

The predicted lateral displacement profile, taken near the toe of the embankment, matches well with inclinometer 2 as shown in Figure 27. Two times were compared for the lateral profile to determine the creep effects, if any, on the lateral behavior of the soil. For both times the maximum amount of lateral displacement and the location of the maximum were captured well, but the profile on either side of the maximum deviates. Near the top of the profile the inclinometer data shows that the soil moved inward. This inward movement is the result of the concave deformation of the embankment, as the embankment's vertical settlement increases the top soil layers are pulled in toward the embankment. This behavior was not captured in the simulation at the location of inclinometer 2.

The pore water pressure was monitored in the field using vibrating wire piezometers at several depths and locations. The comparisons in Figure 28 are for depths of 1.6 m, 5.6 m and 9.6 m. The piezometers were located near the centerline of the embankment in the vicinity of inclinometer 2.

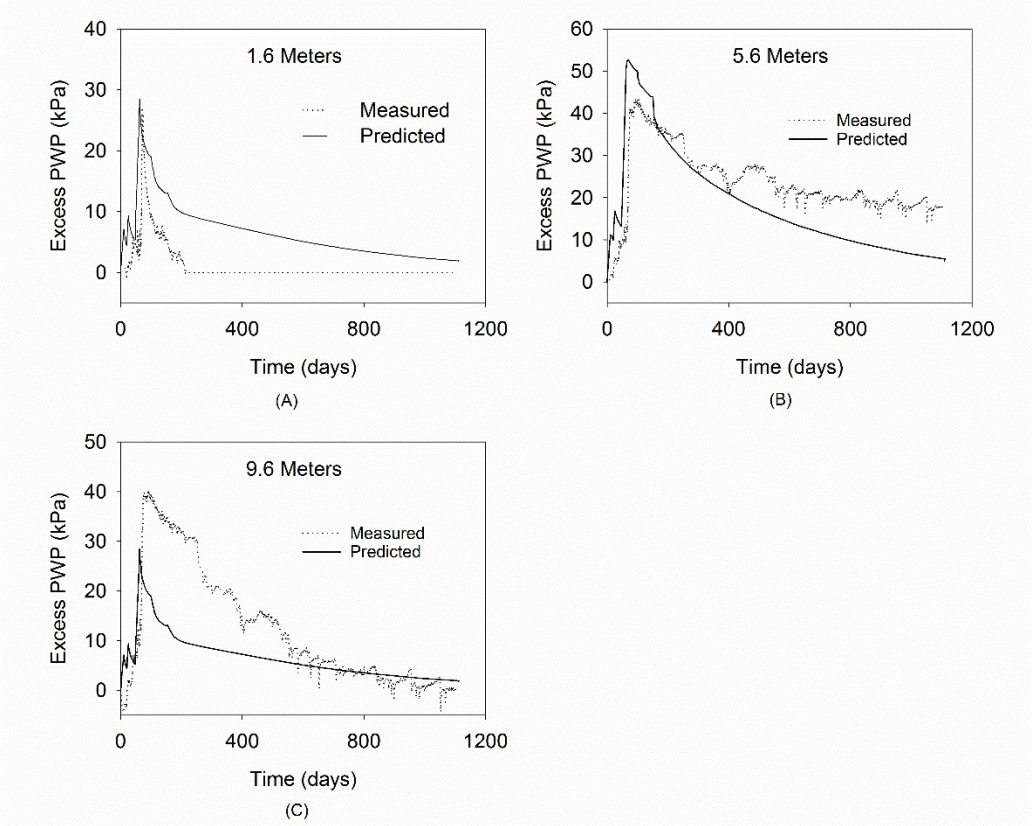

Figure 28. Ballina Embankment Excess PWP Comparisons

Considering the uncertanty involved with predicting excess pore water pressures when PVDs are present, the simulation was able to capture the maximum pore water pressure at 1.6 m and 5.6 m reasonably well and the dissipation of excess pore water pressure at 5.6 m. The maximum excess pore water pressure at 9.6 m was not matched as well, but this depth is near the interface with the layer below and is likely being influenced by that layer. The layer beginning at 10.9 m didn't have much permeability data available and thus is largly based on just a few test results, whereas the other layers had many test results available.

5.2 Shaoxing Test Embankment – Zheijiang Province, China

During the construction of the 145 km Hangzhou-Ningbo Expressway twelve test embankments were constructed to better understand the behavior of embankments on the soft soils

present in the area (Shen et al. 2005). The following analysis and comparisons are based on one of the twelve test embankments. The details of the test embankment and measured data were not locatable from the original source, Transportation Planning Institute of Zhejiang (TPIZ), so the following analysis is based on the embankment details, model parameters, and field measurements reported by Shen et al. (2005). A plan and elevation of the Shaoxing test embankment is shown in Figure 29.

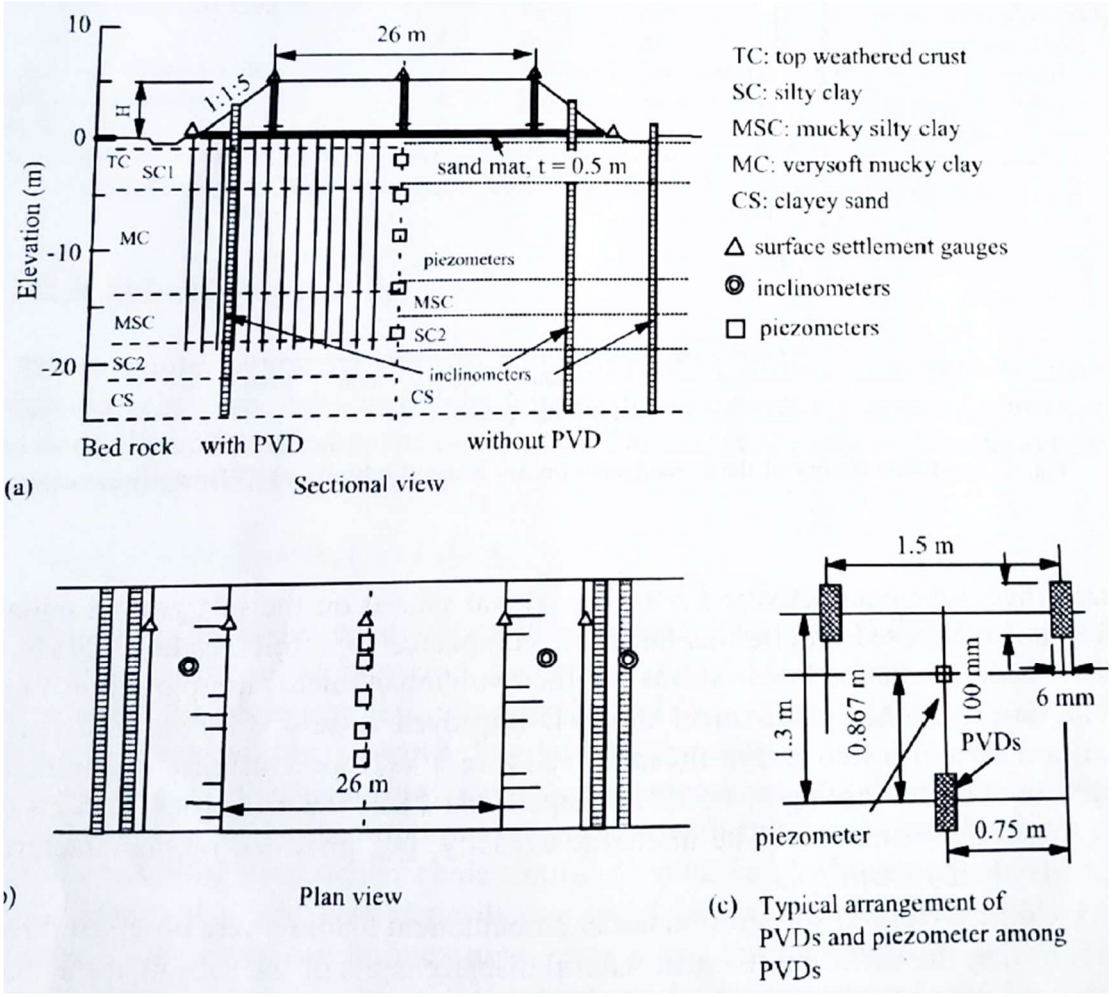

Figure 29. Shaoxing Test Embankment Plan and Elevation, from Shen et al. (2005)

The subsurface soils at the Shaoxing test embankment site consists of silty clay, very soft clay, mucky silty clay and clayey sand. The subsurface soils have been idealized as 5 layers not including a sand mat that is 0.5 m in thickness directly below the embankment. Unlike the Ballina

test embankment, the Shaoxing test embankment did not have soil test results available for a proper calibration of the Bounding Surface Plasticity model. The traditional model parameters were available in Shen et al. (2005) and the remaining surface configuration and hardening parameters were taken as the typical values proposed by Kaliakin et al. (1987) as presented in Table 3. The parameters and permeabilities adopted for this analysis are shown in Table 6.

Table 6. Shaoxing Embankment Model Parameters

Depth (m)	0 – 0.5	0.5 – 5.0	5.0 – 13.0	13.0 – 17.0	17.0 -19.2	19.2 – 23.0
Soil	sand mat	silty clay	very soft clay	mucky silty clay	silty clay	clayey sand
E (kPa)	11,000	-	-	-	-	11,000
λ	-	0.16	0.28	0.18	0.10	-
κ	-	0.016	0.028	0.018	0.01	-
M_c	-	1.0	0.8	0.8	1.0	-
M_e/M_c	-	0.8	1.0	1.0	0.8	-
v	0.25	0.35	0.35	0.35	0.30	0.25
R_c	-	2.3	2.3	2.3	2.3	-
A_c	-	0.10	0.10	0.10	0.10	-
T	-	0.10	0.10	0.10	0.10	-
R_e/R_c	-	1.0	1.0	1.0	1.0	-
A_e/A_c	-	1.0	1.0	1.0	1.0	-
C	-	0.3	0.3	0.3	0.3	-
S	-	1.2	1.2	1.2	1.2	-
m	-	0.02	0.02	0.02	0.02	-
h_c	-	10	10	10	10	-
h_e/h_c	-	1	1	1	1	-
h_2	-	10	10	10	10	-
k_x (m/day)	0.6	5.6*10-4	2.54*10-3	2.0*10-3	3.9*10-4	.025
k_y (m/day)	0.6	2.2*10-4	1.69*10-3	1.0*10-3	1.8*10-4	.025

The embankment was constructed in lifts spanning 130 days. To simplify the modeling of the embankment, the construction was considered to have occurred uniformly with the load of the embankment being increased linearly over the 130 day time span. Following the embankment construction, the model was allowed to consolidate for approximately 3 years making the total time of the analysis 1300 days. The model geometry and mesh are shown in Figure 30, all units

are in meters. Unlike the Ballina embankment, only half of the Shaoxing embankment was modeled to take advantage of the model symmetry reported by Shen et al. (2005).

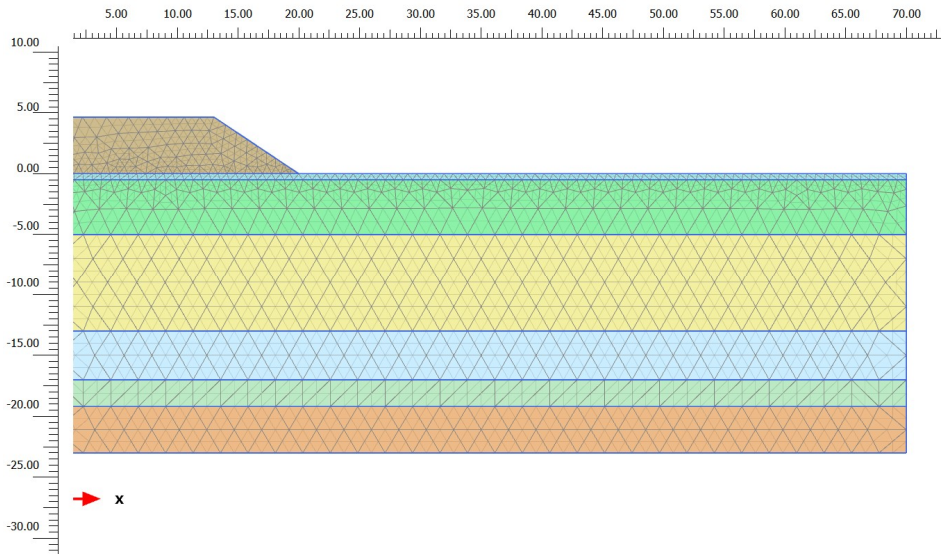

Figure 30. Shaoxing Embankment Geometry and Mesh

The settlement was recorded from the top of the embankment near the center. In addition to the settlement, the lateral deformation of the subsurface soil was recorded under the side slopes of the embankment and the pore water pressure was measured using piezometers at 3 depths: 2.5 m, 10.4 m and 16.5 m. The comparison graphs followed by a discussion are presented in Figures 31-33.

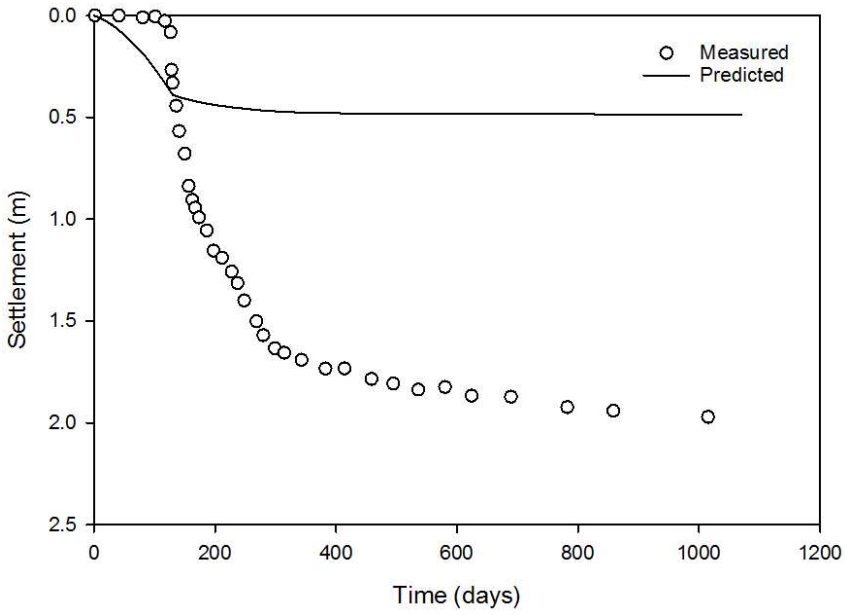

Figure 31. Shaoxing Embankment Settlement Comparison

The simulation underpredicted the total settlement by approximately 1.5 m. The underprediction could partially be the result of inadequate calibration data for the soils or could be partly attributed to creep effects. The simulation suggests that the embankment finished settling relatively quickly when the measured data shows the settlement to occur over a long period of time possibly continuing beyond the analysis period. The excess pore water pressure plots, Figure 32, also show this discrepancy, after 800 days the excess pore water pressure has only reduced by 50% or less in the depths of 10.4 and 16.5 m. The initial predicted settlement also doesn't match well which is likely due to the construction sequencing not being accurate. Based on the settlement that was measured, it appears that the embankment construction started or accelerated some time after what was taken as the starting point for the analysis.

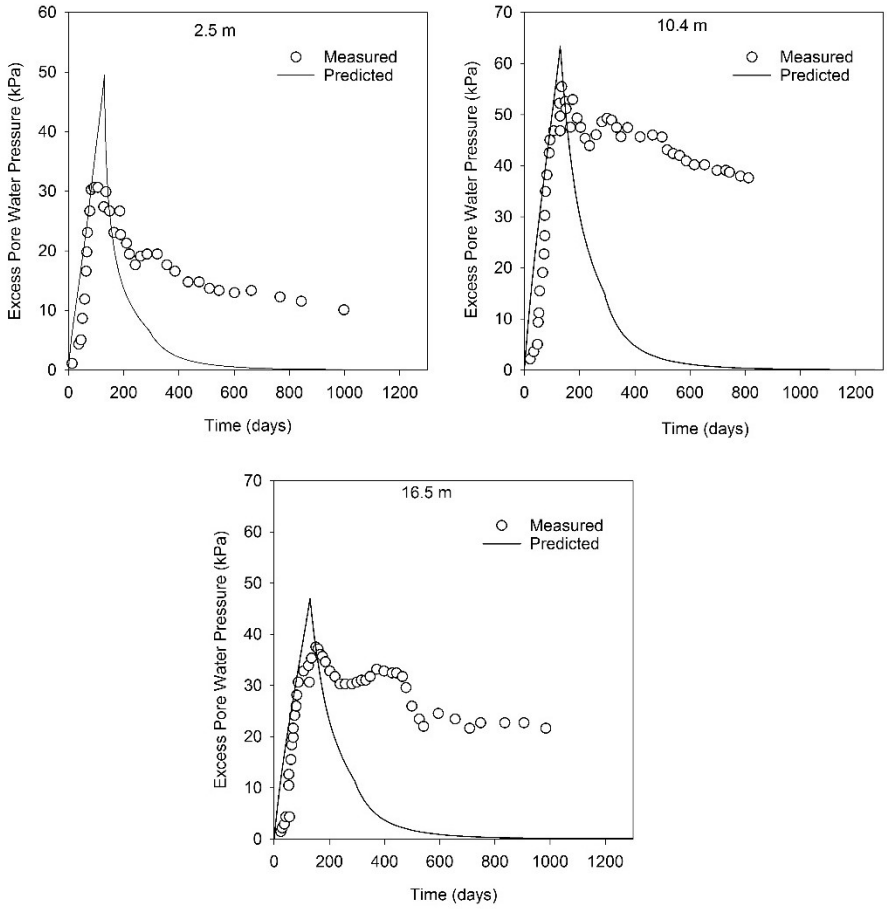

Figure 32. Shaoxing Embankment Excess Pore Water Pressure Comparisons

Much like the settlements, the excess pore water pressure dissipation was not captured well. From the rate of dissipation in the plots it appears as though incorrect permeabilities were adopted in the analysis. The maximum excess pore water pressure was matched reasonably well at 10.4 and 16.5 m giving some confidence to the permeabilities used since a higher permeability will result in less excess pore water pressure being developed and vice versa for a lower permeability up to a certain point. The maximum excess pore water pressure matching while the dissipation rate is apparently different suggest there could have been some issues in the pore water pressure measurements. Shen et al. (2005) found similar results during their simulation and suggested that the piezometers used for these measurements became clogged with fine particles

effectively “locking in” the excess pore water pressures. Similar behavior has been reported by other researchers for different embankments (eg. Hird et al., 1995 and Indraratna et al., 1994). Attempts were made to reduce the permeabilities used in the analysis but the result was higher maximum excess pore water pressures and the dissipation rate still exceeded that measured in the field.

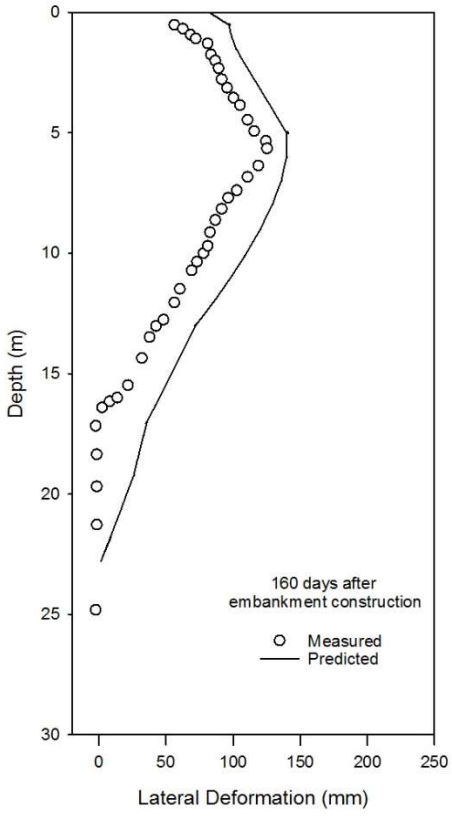

Figure 33. Shaoxing Embankment Lateral Deformation Comparison

Unlike the large disparities found between the simulation and field measurements for settlement and excess pore water pressures, the lateral deformation 160 days after construction was predicted relatively well. The lateral deformation profile is overpredicted a little, but the shape of the profile is nearly identical. Given the number of layers involved in the analysis and the uncertainty in the model calibration, it is interesting that such a close prediction was achieved.

Previous researchers have suggested that the ratio of lateral deformation to settlement is partly attributed to the drainage condition (eg. Leroueil et al., 1990). With the ratio initially starting out as 1:1 and decreasing from there as the soil tends toward a drained condition. Based on the piezometer data, the soil is still behaving predominately undrained at the time the lateral displacement profile was taken. If the soil behaves as Leroueil et al. (1990) suggested then the settlement and lateral deformation would be approximately equal at the time of the profile since the soil is undrained per the piezometer data. However the settlement exceeds the lateral deformation at this point by approximately 1.6 meters with a ratio of approximately 0.08:1. In general, all the data gathered in the field does not seem to agree suggesting there may have been some issues with the instruments or data collection.

5.3 Murro Test Embankment – Murro, Finland

The Murro test embankment was constructed by the Finnish Road Administration near Murro, Seinäjoki in 1993. The embankment was constructed to better understand the behavior of embankments on soft soils to assist in the design and renovations of road projects in Finland (Koskinen et al., 2002). Measurements of installed instruments were recorded for 8 years following the embankment construction. A plan and elevation view of the instrumented embankment is shown in Figure 34.

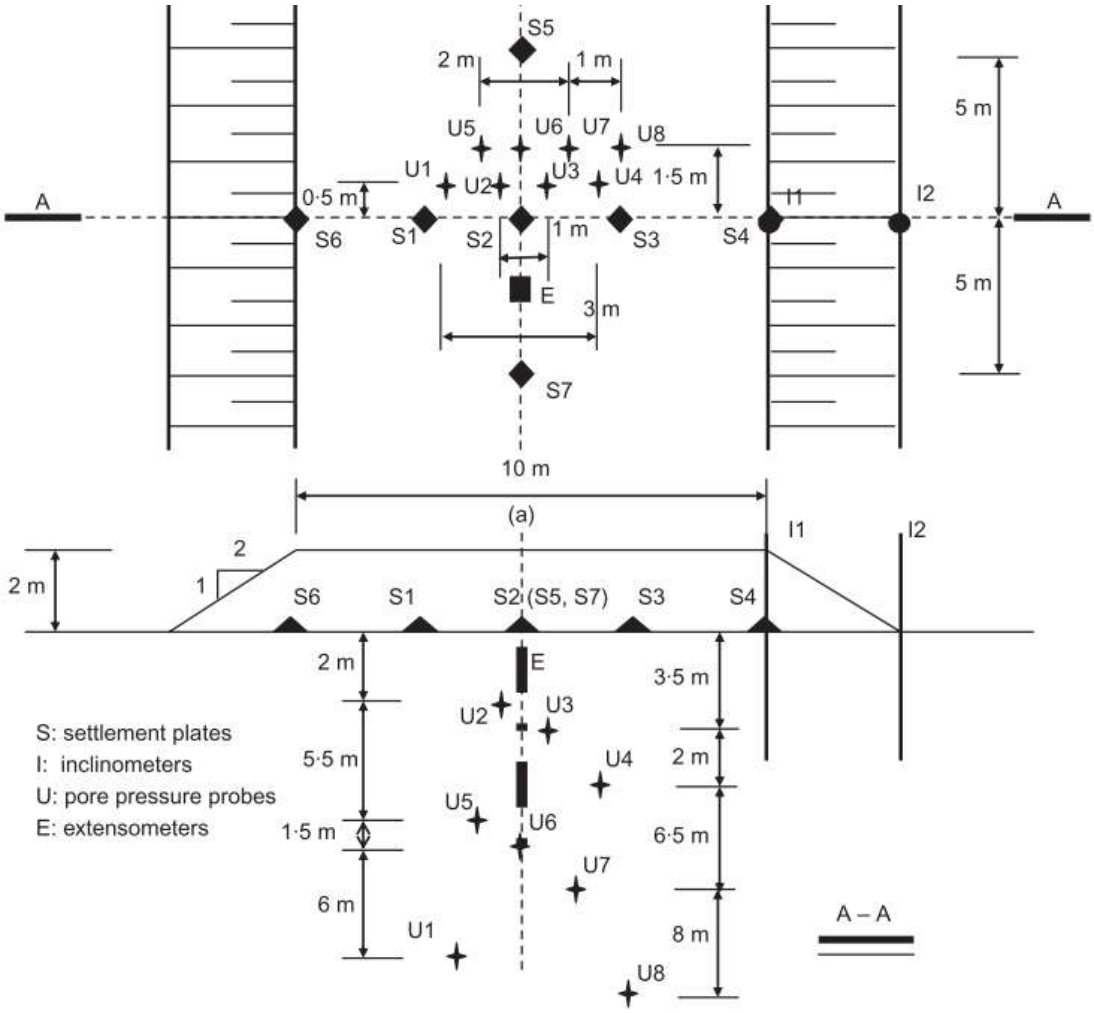

Figure 34. Murro Test Embankment Layout, from Karstunen et al. (2010)

The subsurface soils of the Murro test embankment consists of soft silty clay overlain by a thin dry crust, the deposit is approximately 23 m thick (Karstunen et al. 2005). The deposits are geologically young and considered to be normally consolidated. The lab test results for the soil were not available excluding index properties, hence a full calibration of the Bounding Surface Plasticity model could not be completed for these subsurface soils. Koskinen et al. (2002) and Karstunen et al. (2005) have presented the traditional model parameters and have chosen very similar values with a few exceptions. In general, the model parameters presented by Koskinen et

al. (2002) were adopted for this study and were based on well established relationships with lab test results for the subsurface soils. The non-traditional parameters were chosen based on typical values and judgment. The soil profile has been separated into 6 layers. The top dry crust has been modeled using the Mohr-Coulomb model available in PLAXIS and the remaining 5 layers have been modeled using the Bounding Surface Plasticity model. The layer thicknesses and adopted model parameters are shown in Table 7.

Table 7. Murro Embankment Model Parameters

Depth (m)	0 – 1.6	1.6 – 3.0	3.0 – 6.7	6.7 – 10.0	10.0 -15.0	15.0 – 23.0
Soil	dry crust	Murro clay	Murro clay	Murro clay	Murro clay	Murro clay
E (kPa)	11,300	-	-	-	-	-
λ	-	0.4	0.5	0.38	0.38	0.14
κ	-	0.03	0.036	0.0338	0.0338	0.0039
M_c	-	1.6	1.6	1.6	1.6	1.6
M_e/M_c	-	0.7	0.7	0.7	0.7	0.7
v	0.35	0.35	0.1	0.15	0.15	0.15
R_c	-	2.3	2.3	2.3	2.3	2.3
A_c	-	0.10	0.10	0.10	0.10	0.10
T	-	0.10	0.10	0.10	0.10	0.10
R_e/R_c	-	1.0	1.0	1.0	1.0	1.0
A_e/A_c	-	1.0	1.0	1.0	1.0	1.0
C	-	0.3	0.3	0.3	0.3	0.3
S	-	1.2	1.2	1.2	1.2	1.2
m	-	0.02	0.02	0.02	0.02	0.02
h_c	-	10	10	10	10	10
h_e/h_c	-	1	1	1	1	1
h_2	-	10	10	10	10	10
void ratio		1.8	2.5	2.1	1.8	1.6
k_x (m/day)	6.2e-4	2.1*10-4	1.7*10-4	1.1*10-4	6.85*10-5	1.04*10-4
k_y (m/day)	4.7e-4	1.6*10-4	1.3*10-4	9.07*10-5	5.48*10-5	8.22*10-5

The embankment was constructed relatively quickly consisting of 2 lifts placed over 2 days. Following embankment construction, the site was allowed to consolidate for 8 years. The PLAXIS model followed the same loading and consolidation procedure as was used in the field. The subsurface layers at the site were idealized as perfectly horizontal layers so the simulation has

taken advantage of symmetry and only half of the embankment has been modeled. The mesh used during the simulation is shown in Figure 35.

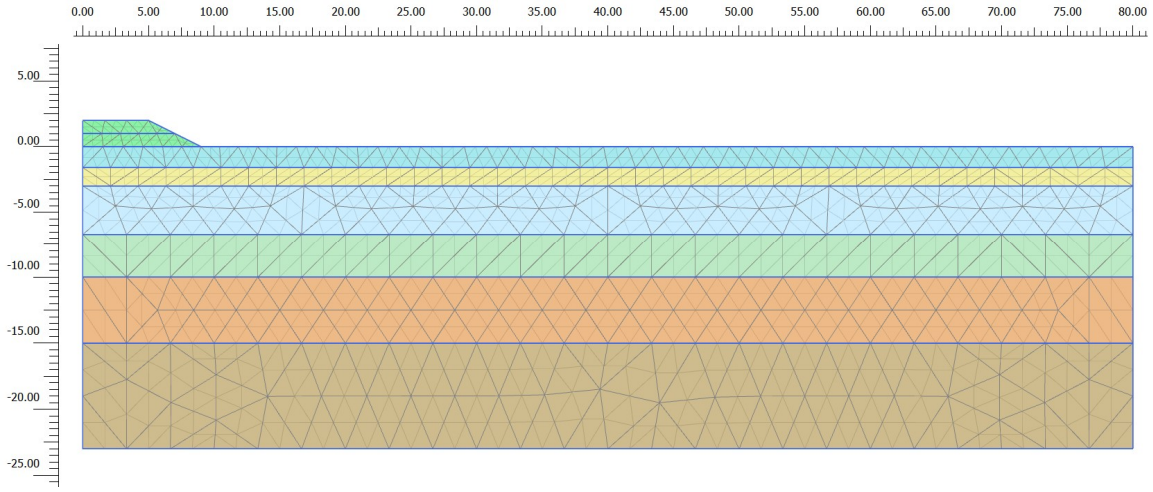

Figure 35. Murro Embankment Geometry and Mesh

The modeled subsurface soils extend quite far considering the size of the embankment, but due to the low reported permeabilities, the embankment loading has a large influence zone for excess pore water pressure. For example, the excess pore water pressure immediately following the placement of the second embankment layer is shown in Figure 36.

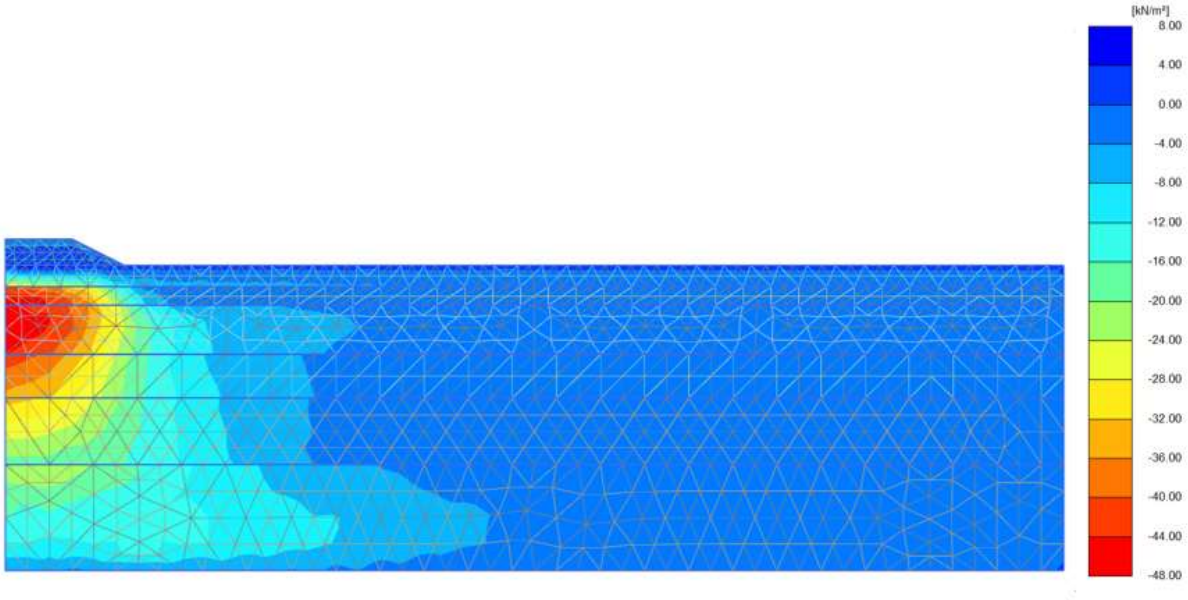

Figure 36. Murro Embankment Excess PWP Right After End of Loading

The settlement was recorded at the middle of the embankment at the ground surface (at the interface of the embankment and ground surface). Lateral deformation was measured through use of an inclinometer placed at the toe of the embankment. Excess pore water pressure was recorded at 7 depths; however as will be further discussed later many of the depths showed erroneous data and were not used in this comparison. The comparison graphs are presented in Figures 37-39 followed by a discussion.

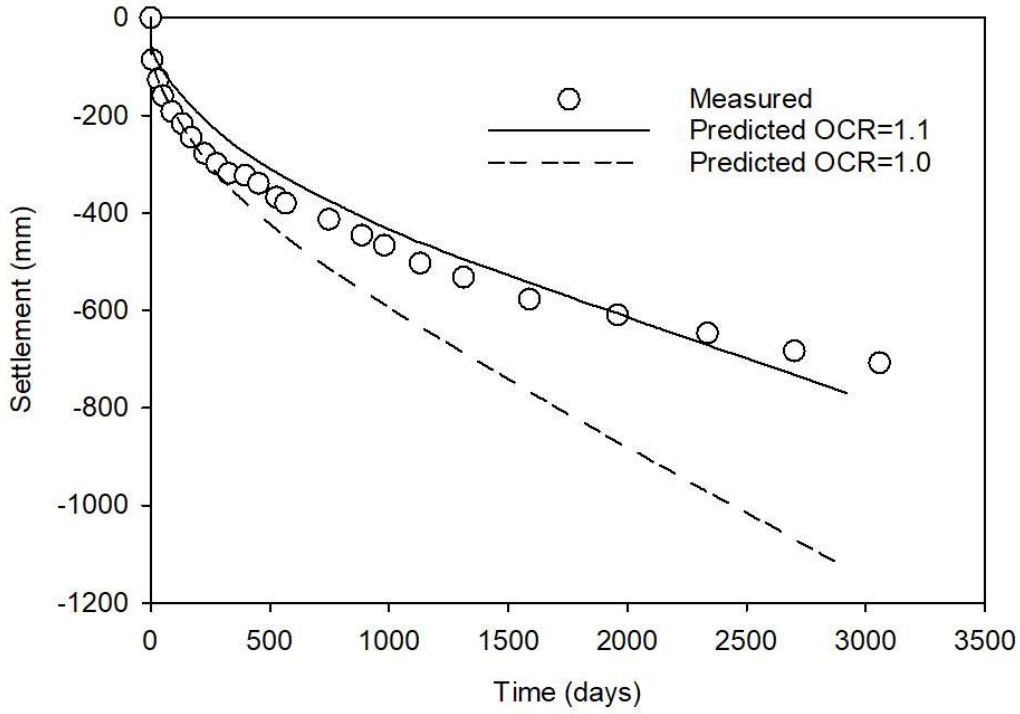

Figure 37. Murro Embankment Settlement Comparison

The simulation was able to capture the settlement behavior of the embankment very well when the soil OCR = 1.1. The subsurface soils are reported to be normally consolidated but a better match was found when the soils were slightly overconsolidated (OCR = 1.10) as found through back analysis. After approximately 2000 days, the simulation starts to exceed the measured behavior and would likely continue to deviate if more data was available.

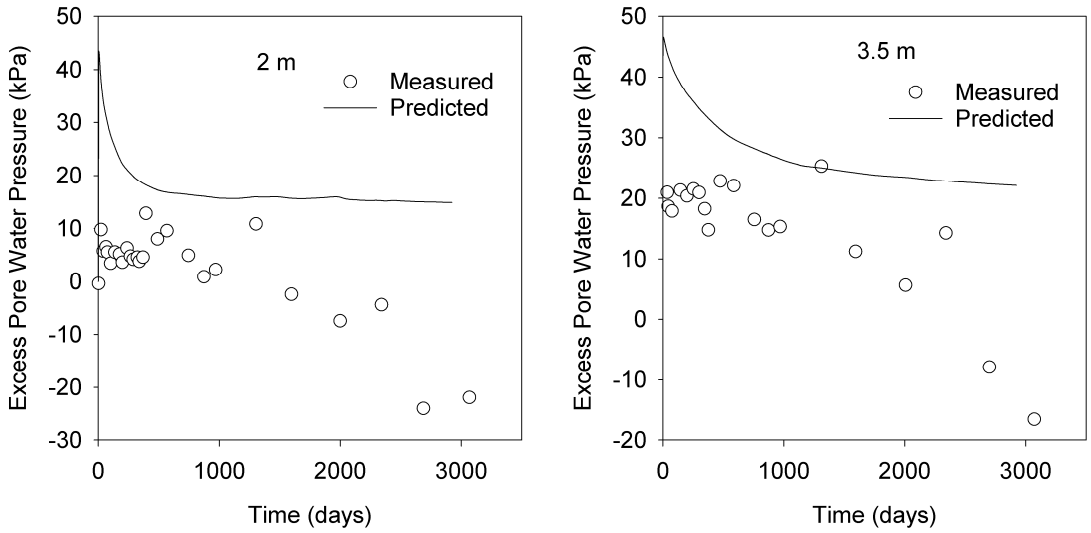

Figure 38. Murro Embankment Excess PWP Comparisons

The excess pore water pressure increase and dissipation was not well captured at depths of 2 and 3.4 m. In total the pore water pressure was recorded for 7 depths but many of the depths showed erratic and erroneous data suggesting the sensors were not functioning properly so comparisons for excess pore water pressure are limited. The results for 2 and 3.5 m appear to be influenced by a fluctuating water table, the water table was located at a depth of 0.8 m for the entire analysis based on the reported water table depth by Karstunen et al. (2005). It is unlikely that the water table remained constant for 8 years but in lieu of available data on the water table elevation it was kept constant for the simulation.

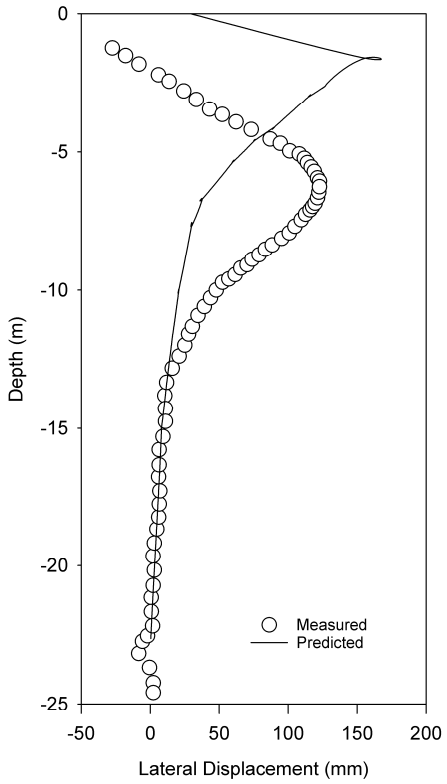

Figure 39. Murro Embankment Lateral Deformation Comparison

The magnitude of lateral displacement was relatively close but the location was approximately 5 m from what was measured in the field. The simulated location of the maximum lateral displacement is at the interface of the top dry crust and the first layer of the Murro clay. Similar results were also obtained by Karstunen et al. (2005) when using the Modified Cam Clay model, S-CLAY1 and S-CLAY1S models. The lateral displacement results calculated by Karstunen et al. (2005) are presented in Figure 11 (Chapter 2). Karstunen et al. (2005) suggested that the amount of lateral displacement indicated that the embankment was slipping on the dry crust. Another possibility could be that the test results which the material parameters are based on are not representative of the subsurface soils.

The Bounding Surface Plasticity model was able to capture the measured results for the Murro test embankment as good or better than the available soil models in PLAXIS (see Figure 11). The results were achievable despite inadequate test results for a proper calibration of the subsurface and embankment soils.

5.4 Muar Test Embankment – Muar, Malaysia

The Muar test embankment was constructed by the Malaysian Highway Authority to further investigate the behavior of Muar clay deposits to assist in the design of the Malaysian North-South Expressway across the Muar Plain (Indraratna et al. 1992). The Muar Plain is home to 10 to 20 m thick deposits of low strength clay soils with high water contents. Instability as well as settlement were major concerns for embankments constructed in the planned route of the North-South Expressway. Unlike the other test embankments included in this chapter, the Muar test embankment was rapidly constructed to failure. A plan and elevation view of the Muar test embankment in shown in Figure 40.

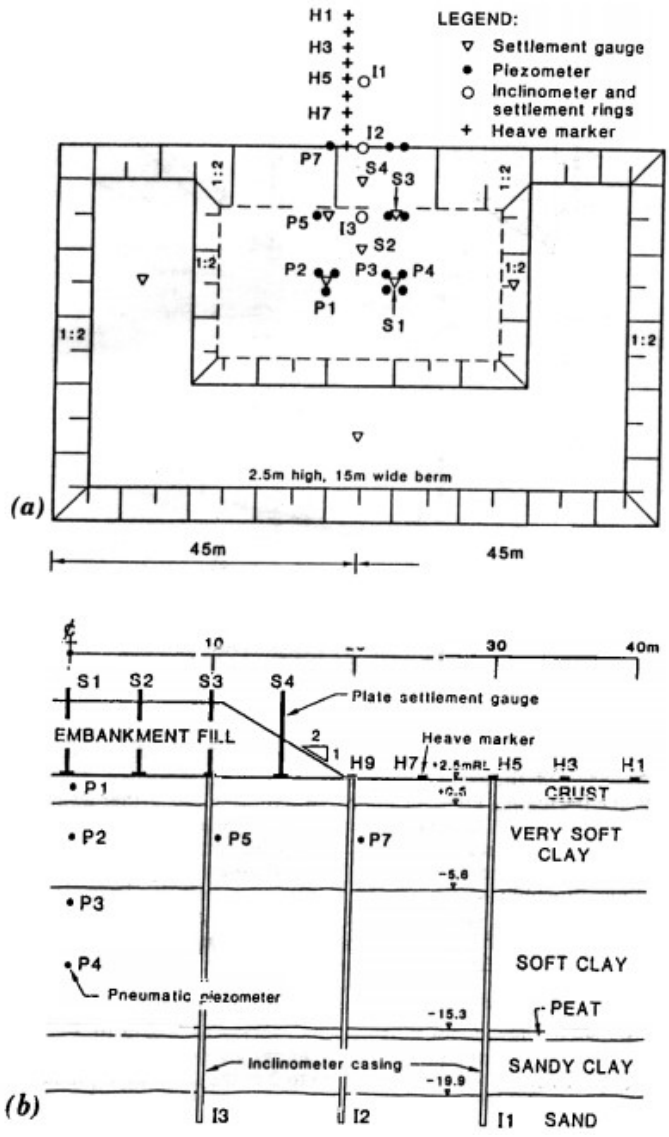

Figure 40. Muar Test Embankment Plan and Elevation, from Indraratna et al. (1992)

The subsurface soils at the site of the test embankment consisted of a hard crust underlain by soft clay transitioning to sandy clay and then sand. The original report with the test results from 1989 is written in Japanese so the traditional model parameters determined through laboratory tests and presented by Chai et al. (1994) have been adopted for this analysis. The remaining parameters were chosen based on typical values presented by Kaliakin et al. (1987). The values of permeability

were based on reported values by Chai et al. (1994). The adopted material parameters for the analysis are presented in Table 8.

Table 8. Muar Embankment Model Parameters

Depth (m)	0 – 2.0	2.0 – 7.0	7.0 – 12.0	12.0 – 18.0	18.0 -22.0
Soil	crust	Muar clay	Muar clay	Muar clay	Sand
E (kPa)	-	-	-	-	11,000
λ	0.35	0.61	0.28	0.22	-
κ	0.06	0.1	0.06	0.04	-
M_c	1.2	1.2	1.2	1.2	-
M_e/M_c	0.75	0.75	0.75	0.75	-
v	0.2	0.25	0.25	0.25	0.35
R_c	2.3	2.3	2.3	2.3	-
A_c	0.10	0.10	0.10	0.10	-
T	0.10	0.10	0.10	0.10	-
R_e/R_c	1.0	1.0	1.0	1.0	-
A_e/A_c	1.0	1.0	1.0	1.0	-
C	0.3	0.3	0.3	0.3	-
S	1.2	1.2	1.2	1.2	-
m	0.02	0.02	0.02	0.02	-
h_c	10	10	10	10	-
h_e/h_c	1	1	1	1	-
h_2	10	10	10	10	-
void ratio	0.8	1.4	0.64	0.5	0.5
k_x (m/day)	2.4*10-3	1.2*10-3	9*10-4	6.4*10-4	12
k_y (m/day)	1.2*10-3	6.05*10-4	4.5*10-4	3.02*10-4	6

The embankment base was 55 m wide and it was constructed in lifts of approximately 0.4 m in thickness. Each week a new lift was added to the embankment. Once the embankment was 2.5 m in height, the width was reduced on one side as the embankment was constructed to failure. At failure the embankment was 5.4 m in height and the crest was approximately 15 m wide. The analysis was as close to the field procedure as possible based on the limited data available. For the analysis the embankment height was increased 0.4 m each 7 days, and the height was increased or reduced as necessary to meet the total height of the base embankment and final embankment. The total analysis time was a little over 13 weeks. The embankment mesh and geometry are presented

in Figure 41, all measurements are in meters. The entire embankment was modeled due to the non-symmetric nature of the embankment.

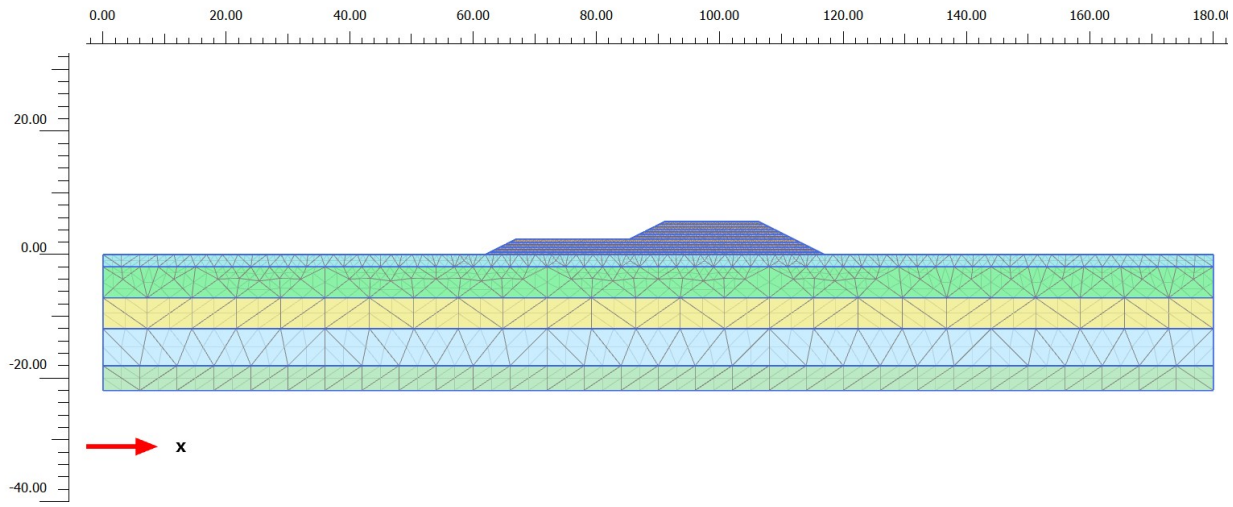

Figure 41. Muar Embankment Geometry and Mesh

The vertical deformation was recorded using settlement/heave plates along the ground surface beginning at the middle of the finished embankment and extending along the ground surface toward and beyond the slope of the embankment for approximately 40 m. The pore water pressure was recorded at 4 locations beneath the center of the embankment at depths of 0.5 m, 4.5 m, 9.0 m and 12.5 m. The lateral displacement of the subsurface soils was recorded using an inclinometer located at the toe of the embankment. The comparison graphs are presented in Figures 42 – 45 followed by a discussion.

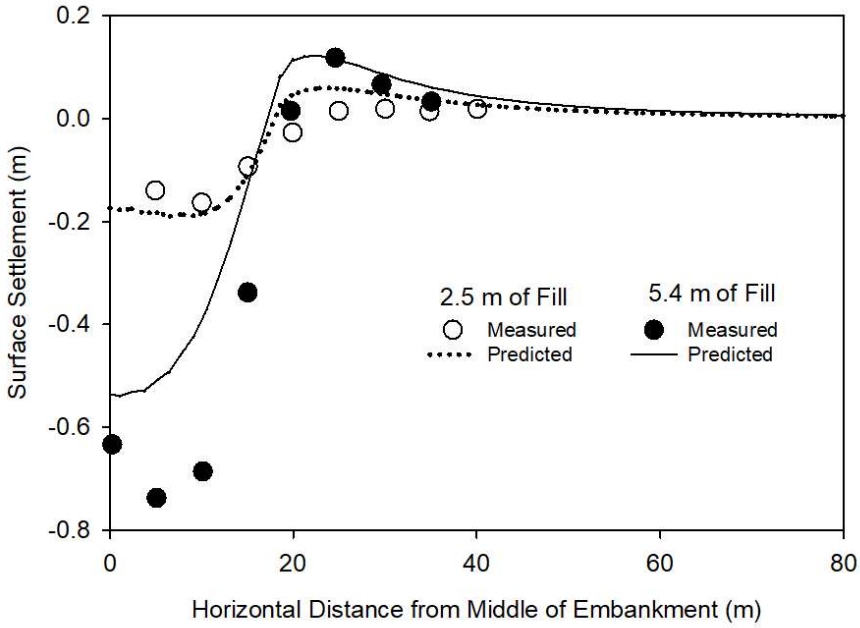

Figure 42. Muar Embankment Surface Settlement Comparison

The simulation was able to capture the profile of the surface settlement well. The magnitude of settlement under 2.5 m of fill was captured better than under 5.4 m of fill, though it should be noted that the embankment experienced slope failure shortly after reaching 5.4 m in height. The underpredicted settlement is likely the beginnings of slope failure for the embankment which is not captured as well in the simulation. The Bounding Surface Plasticity model includes the extension behavior of soil, which is similar to the loading along the slope failure surface for an embankment. Soil extension would manifest as heave along the ground surface beyond the toe of the embankment, as shown in Figure 42 the simulation was able to capture the heave behavior of the ground surface.

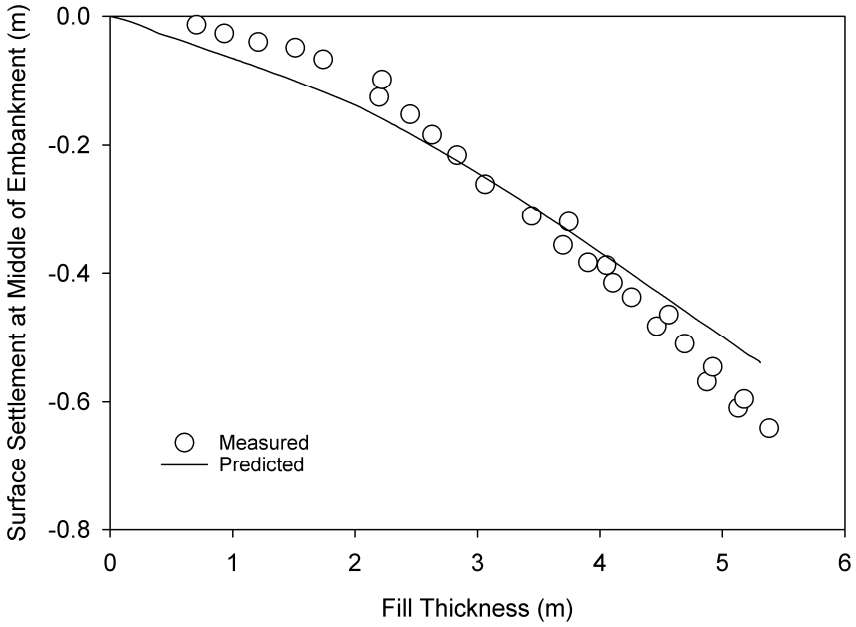

Figure 43. Muar Embankment Settlement Comparison

The magnitude of settlement at the center of the embankment was also measured with respect to fill thickness and compared. In general, the settlement behavior is captured with some deviations. As seen in Figure 43 under 3 m of fill thickness the settlement is over predicted and then beyond that it is under predicted.

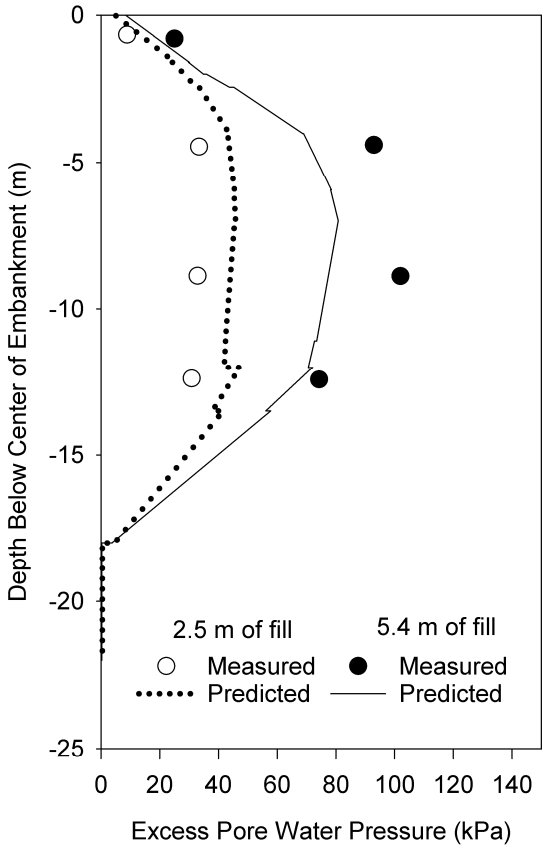

Figure 44. Muar Embankment Excess PWP with Depth Comparison

Since the embankment was rapidly loaded to failure excess pore water pressure dissipation readings are not available. Hence, the excess pore water pressure at discrete points and times is compared to the excess pore water pressure profiles from PLAXIS corresponding to the same times. The excess pore water pressure is overpredicted when the embankment is 2.5 m in height and underpredicted at 5.4 m of height.

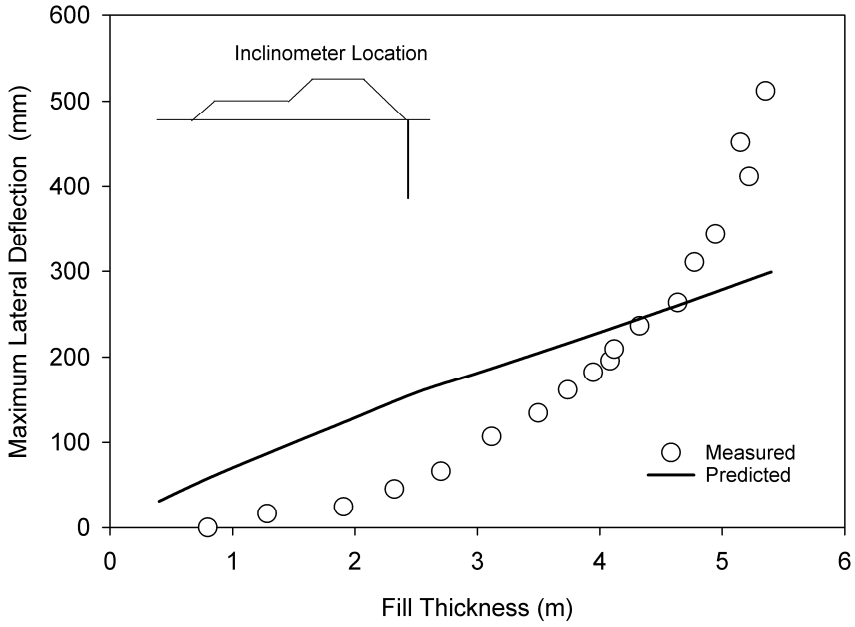

Figure 45. Muar Embankment Lateral Deformation Comparison

The maximum lateral deformation measured at the toe of the embankment is shown Figure 45. No indication of the location of the maximum deformation is mentioned so the comparison may be misleading. The lateral deformation measured in the field is exponentially increasing with fill height, suggesting the embankment is nearing failure. Failure was not achieved in the simulation, so a more linear behavior was calculated.

The Bounding Surface Plasticity model did reasonably well at capturing the settlement and excess pore water pressure development for the Muar test embankment. The lateral displacement behavior was not captured well. Other researchers, for example Chai et al. (1994) and Indraratna et al. (1992), encountered similar difficulties in capturing the lateral behavior of this embankment. If test results were available for a proper model calibration or back analysis of the lateral deformation were attempted better agreement could likely be found.

5.5 Conclusion and Discussion

In this chapter four instrumented test embankments from the literature were modeled using the Bounding Surface Model as implemented in PLAXIS 2D. The available information for calibration of the model ranged from triaxial and one-dimensional consolidation results to reported traditional model parameters in which case calibration was not possible and the additional parameters were taken as typical values. It's important to note that even for the Ballina Test embankment in which lab tests results were available there was insufficient results for a complete calibration of the model. Despite none of the test embankments having the necessary information for a complete calibration, the model was able to capture several aspects of the embankment behavior for all embankments modeled. More importantly the model was able to capture embankment behavior reasonably well even in the instances of very limited available model parameters, e.g.. The Murro and Muar embankments. The only embankment where acceptable results were not achieved was the Shaoxing embankment. The lateral displacement was captured in the Shaoxing embankment, but the settlement was largely underestimated. It is believed that the Shaoxing embankment was experiencing creep behavior and the implemented model is not equipped to handle creep behavior. Kaliakin (1985) extended the Bounding Surface Plasticity model to include creep behavior, but that is not the focus of this current research.

6.0 SH 3 OVER BNSF RAILROAD – ADA, OKLAHOMA

The test embankments presented in Chapter 5 were used to establish the abilities and shortcomings of the Bounding Surface Plasticity model. However, none of the instrumented embankments in the literature, to the authors knowledge, contained piles through the embankment supporting a bridge abutment. An additional piled embankment has been studied and is the focus of this chapter.

6.1 Description of the Site

The embankment is located in Ada, Oklahoma along SH-3 over the Burlington Northern Santa Fe (BNSF) railroad track. The embankment and adjacent twin bridges have been monitored by the University of Oklahoma since 2012. The north bridge has experienced more distress than the south bridge and therefore was more heavily instrumented. The bridge at this location was constructed in 1980 and began experiencing distress as early as 1983 (Muraleetharan et al. 2018). The anchor bolts for the bridge were rotated and pointing towards the abutment back wall, as shown in Figure 46, suggesting that the abutment and the bridge seats have moved underneath the girders away from the approach embankment. Following six years of monitoring it was hypothesized that a soft clay layer present below the embankment fill material was experiencing lateral deformation and pushing the embankment into the abutment (Muraleetharan et al. 2018). The concrete slope wall for the embankment also buckled, cracked, and is being pushed by the embankment into the first set of piers, as shown in Figure 47, further suggesting that the embankment was moving laterally; this movement caused the expansion joints on the bridge to close up (Muraleetharan et al. 2018).

Figure 46. SH-3 Ada, OK - Rotated Anchor Bolt

Figure 47. SH-3 Ada, OK - Buckled Slope Wall

The embankment on the east side is approximately 12.2 m in height and the embankment on the west side is 9.2 m in height. The bridges are 104.7 m in length divided over 5 spans and are skewed 23° 38’ from normal to roadway. The median between the bridges is approximately 9.2 m wide. Figure 48 shows the general elevation view for the north bridge made from the original construction plan set.

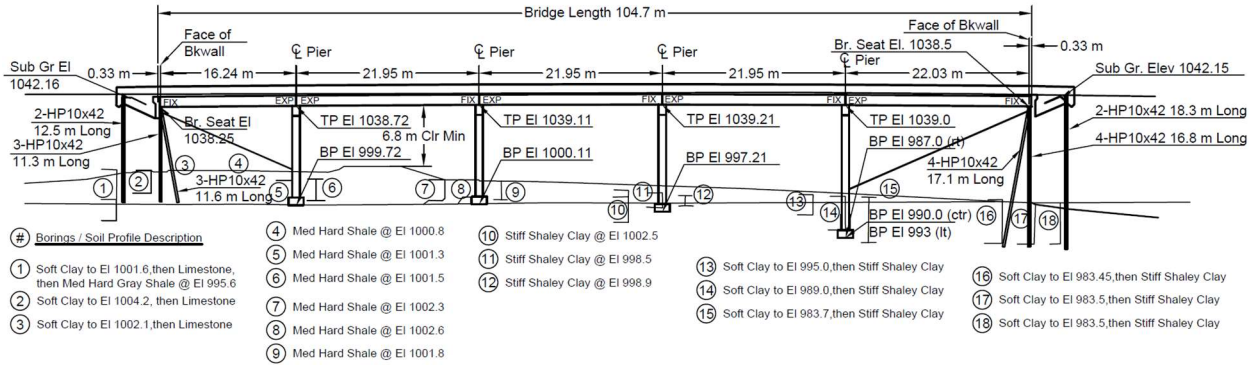

Figure 48. SH 3 over BNSF Elevation View

6.2 Site Investigation

A geotechnical site investigation was carried out on March 11, 2020. The purpose of the site investigation was to gather soil samples and log borings to characterize the site stratigraphy and soils. The investigation included three borings, one (B-1) on the west side and two (B-2 & B-3) on the east side. A boring location diagram is shown in Figure 49. The borings were extended to the top of bedrock resulting in termination depths of 11.7, 21.8, and 19.4 m for borings B-1, B-2, and B-3, respectively. In general, the foundation soils consisted of lean clay with cobbles underlain by sandstone and limestone. The embankment materials were an assortment of clay, sandstone, and sandy shale fill materials. The embankment and subsurface soils had a large amount of strength variability, as indicated by the Standard Penetration Test, due to the presence of

cobbles. The embankment was found to be very stiff likely due to the large amount of sandstone and shale used for the fill materials.

The borings were drilled using a CME 75 all-terrain mounted drill rig, with the drilling services provided by Drilling Services of Oklahoma. Wet rotary drilling methods were used to advance the borings. Sampling of the soil was completed using the Standard Penetration Tests (ASTM D1586) with a split spoon sampler and 76.2 mm thin wall tube sampling (ASTM D1587). Bedrock was determined by Standard Penetration Test refusal. Boring logs from the site investigation showing the in-situ testing that was conducted as well as the results of index tests completed on the samples can be found in Appendix A.

Figure 49. SH 3 over BNSF Boring Locations

6.3 Lab Testing

Following drilling activities, the samples were returned to the lab at the University of Oklahoma. The thin wall samples were extruded two days after the site investigation, wrapped in cellophane and stored in a humidity room.

Atterberg limits tests (ASTM D4318) and finer than 75 μm sieve by washing tests (ASTM D1140) were performed on select samples. Moisture content tests (ASTM D2216) were performed on all samples collected. The results of the Atterberg limits, sieve, and moisture content tests can be found on the boring logs in Appendix A.

In addition to the index testing, one dimensional consolidation tests (ASTM D2435) and consolidated undrained triaxial tests (ASTM D4767) were completed on selected thin wall tube samples. To perform the Bounding Surface Model calibration procedure for the soils, three triaxial compression and extension tests are typically needed. Ideally a normally consolidated, lightly overconsolidated (OCR $\approx$ 1.5), and heavily overconsolidated (OCR $\approx$ 6) sample for both compression and extension testing are needed. Since it is very difficult to get six, or even two, identical soil samples, multistage testing was done. When using the multistage technique one sample is saturated and consolidated in the triaxial device and then subjected to the first stress state, the sample is sheared just until the peak shear stress is reached and then shearing is stopped. The sample is then consolidated to the second stress state and sheared again until the peak shear stress is reached. Finally, the sample is consolidated to the third stress state and sheared to attain 10 to 15% axial strain. Since different OCRs were sought for the triaxial consolidation tests the first stress state represented the normally consolidated condition. Following the first stage shearing, the cell pressure was reduced causing the sample to become overconsolidated. When the cell pressure was reduced the samples generally expanded, and once the sample expansion was

completed the second shear stage began. The process was repeated again for the third shear stage. All the triaxial testing was completed using a GDS triaxial device. The end of consolidation/expansion was determined automatically from the GDS triaxial device, consolidation/expansion was considered completed when the volume changed less than 5 mm^3 in 5 minutes. The testing method while not ideal, provided reasonable results and sufficient information for the soil calibration.

For this project only one triaxial extension test was conducted. Due to the testing techniques required for the GDS extension device, multistage testing was not possible. Instead a single lightly overconsolidated extension loading test was completed. When conducting an extension test on the GDS triaxial device the sample is saturated and consolidated as normal, then prior to shearing the GDS extension top cap is seated on top of the sample top cap. The extension top cap allows the stress on the top of the sample to be reduced below the cell pressure. Once the extension top cap is seated a positive connection is made between the loading ram and the load frame cross arm, then the triaxial cell is secured to the load frame base platen. The load frame base platen is then moved downward at a constant rate in order to reduce the stress on the top of the sample. During the test the principle stress directions are flipped with the minor principle stress now occurring on the top and bottom of the sample and the major principle stress acts on the sides of the sample. The results of the one-dimensional consolidation and triaxial compression and extension tests can be found in Appendix B.

6.4 Soil Model Parameter Calibration

The soil model parameter calibration procedure followed the methods presented by Kaliakin et al. (1987). The traditional model parameters were determined from one dimensional consolidation and consolidated triaxial compression and extension tests. The remaining parameters

were determined using curve fitting techniques by systematically changing parameters and comparing the results of the actual and simulated triaxial results. Kaliakin et al. (1987) provides guidance on the impact of changing each parameter, which helps lessen the time needed for calibration. The soil profile at the site has been idealized as two layers characterized by two triaxial samples. The samples were taken at depths of 15.5 m and 17 m from the top of the embankment at boring B-2 (near the bridge on east side), these depths correspond to the foundation soils for the embankment. Some variability was noted between the soil test results for boring B-2 and B-3 for similar layers. Since boring B-2 was located in a critical location for lateral movement analysis, the results for boring B-2 were used. The calibrated parameters are shown in Table 9. Since only one triaxial extension test was completed, the one extension test results have been used for both soils.

Table 9. SH 3 over BNSF Adopted Model Parameters

Soil Layer	Top Clay Layer (B-2 15.5 m)	Bottom Clay Layer (B-2 17 m)
λ	0.076	0.056
κ	0.026	0.02
M_c	1.25	0.95
M_e/M_c	0.81	0.81
v	0.2	0.2
R_c	1.5	1.6
A_c	0.07	0.125
T	0.1	0.1
R_e/R_c	1.1	1.0
A_e/A_c	1.1	1.0
C	0.6	0.6
S	1.2	1.0
m	0.02	0.02
h_c	20	40
h_e/h_c	1	1
h_2	20	40
void ratio	0.616	0.802

The graphs utilized during the calibration procedure (p'-q, ε-q, and ε-excess PWP) are shown in Figures 50 through 56. These plots show the models ability to simulate the results with the adopted parameters.

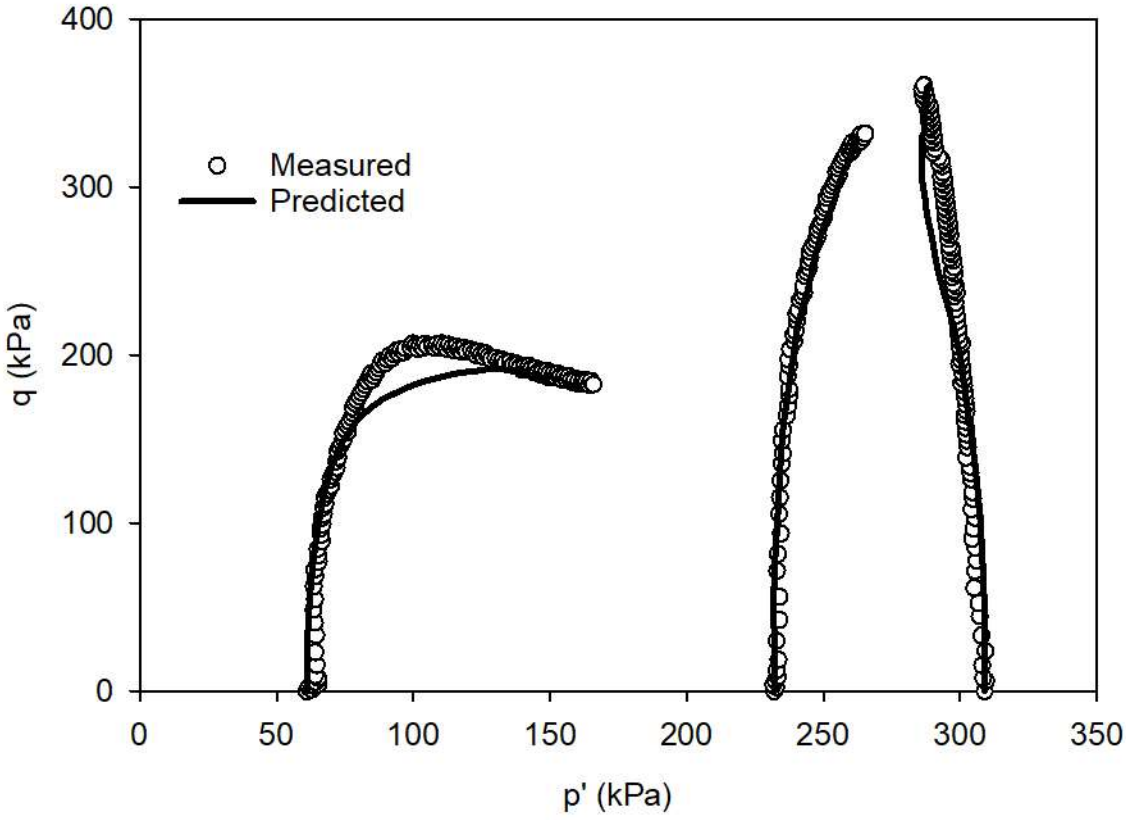

Figure 50. B-2 15.5 m p'-q Comparison

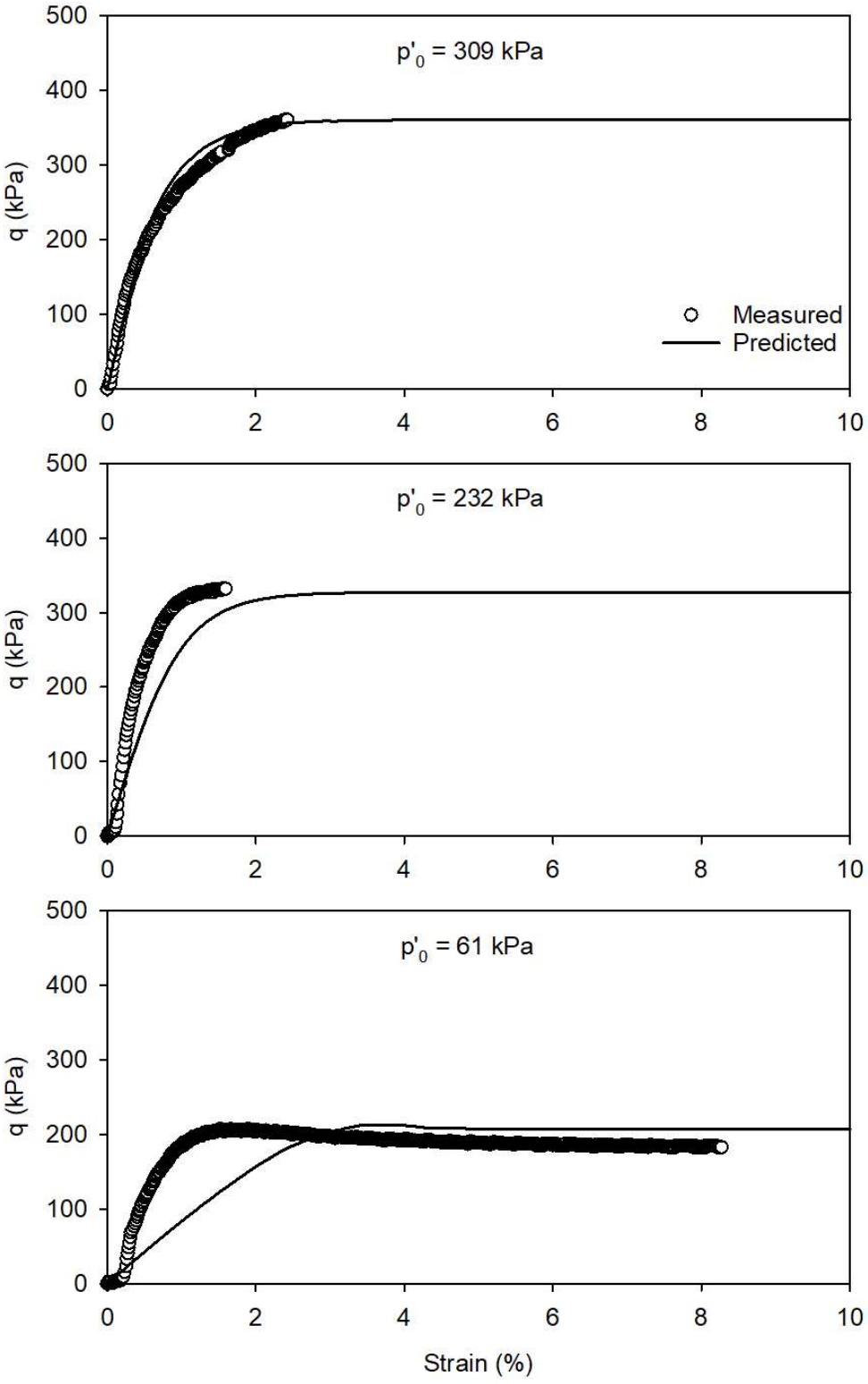

Figure 51. B-2 15.5 m Axial Strain-q Comparison

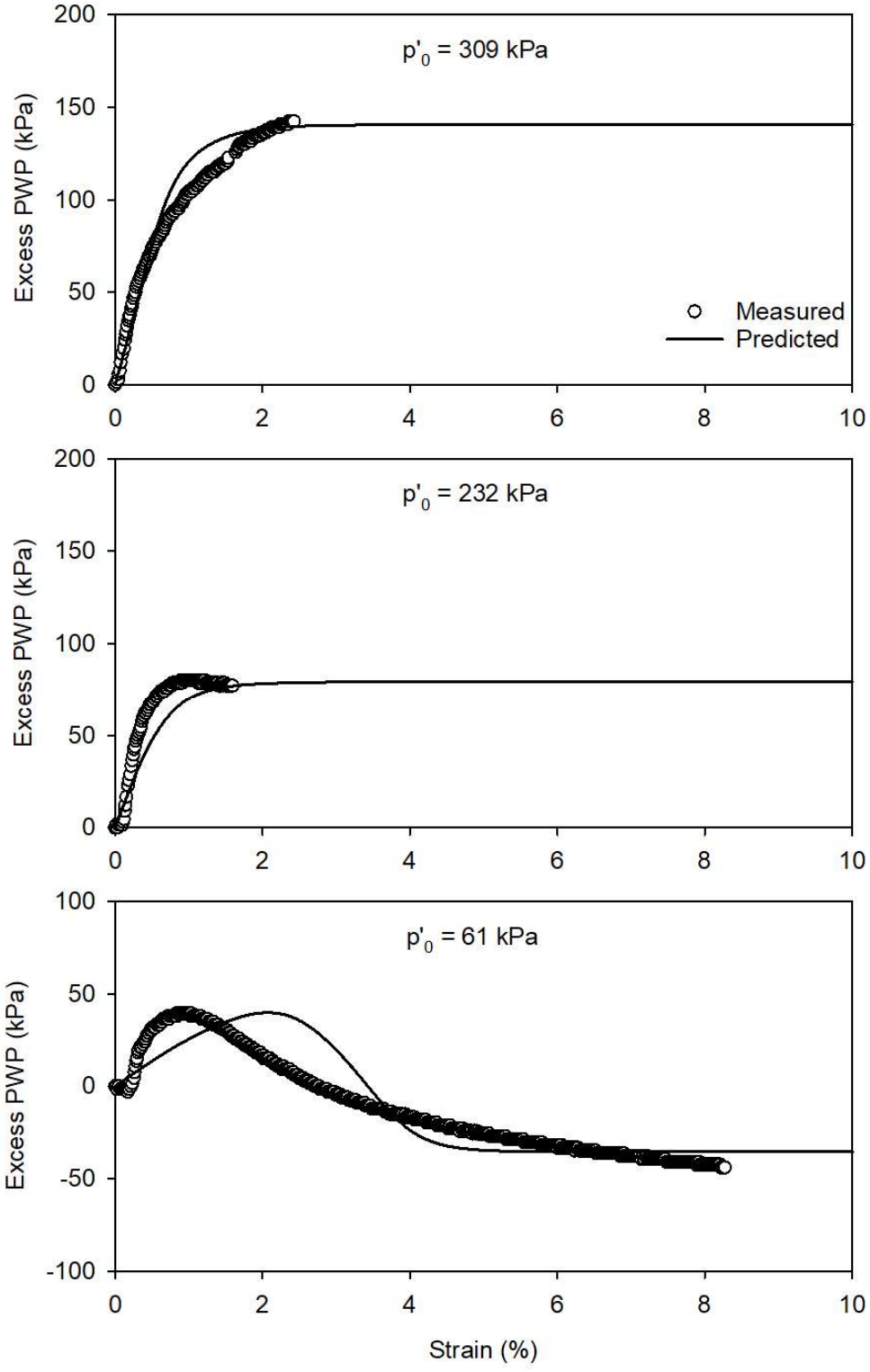

Figure 52. B-2 15.5 m Axial Strain-Excess PWP Comparison

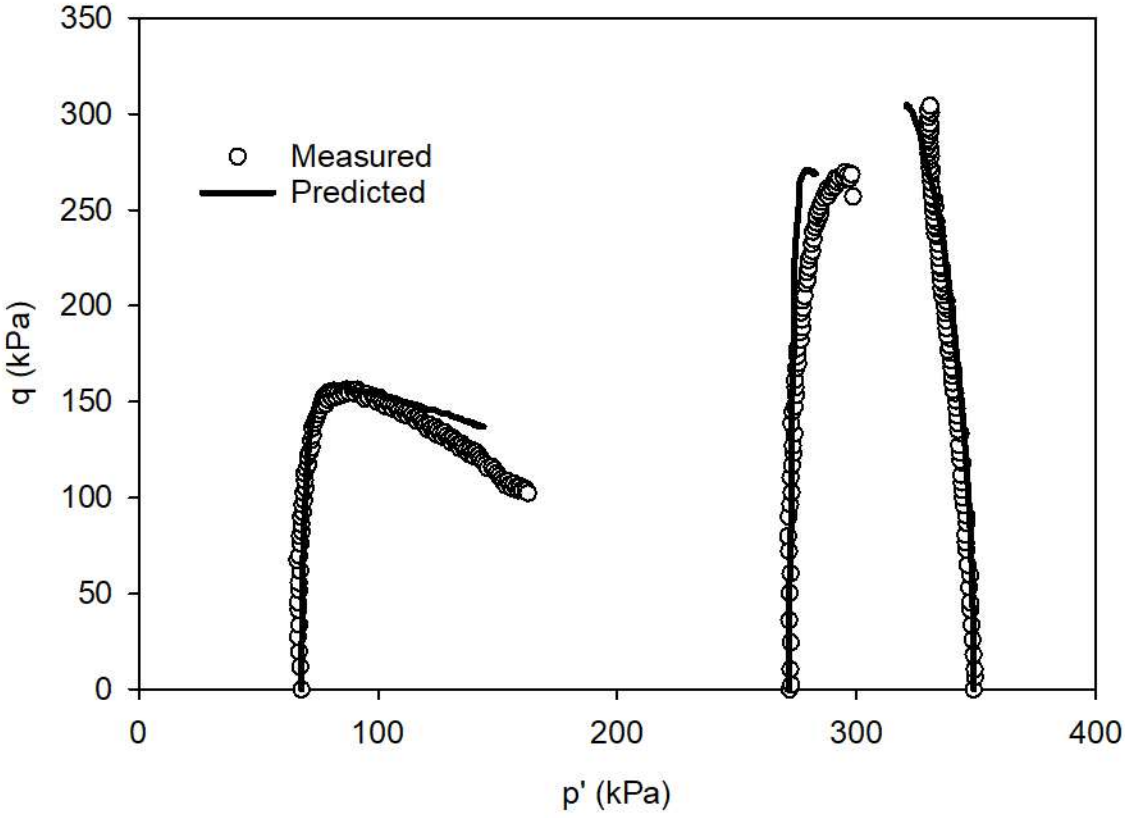

Figure 53. B-2 17 m p'-q Comparison

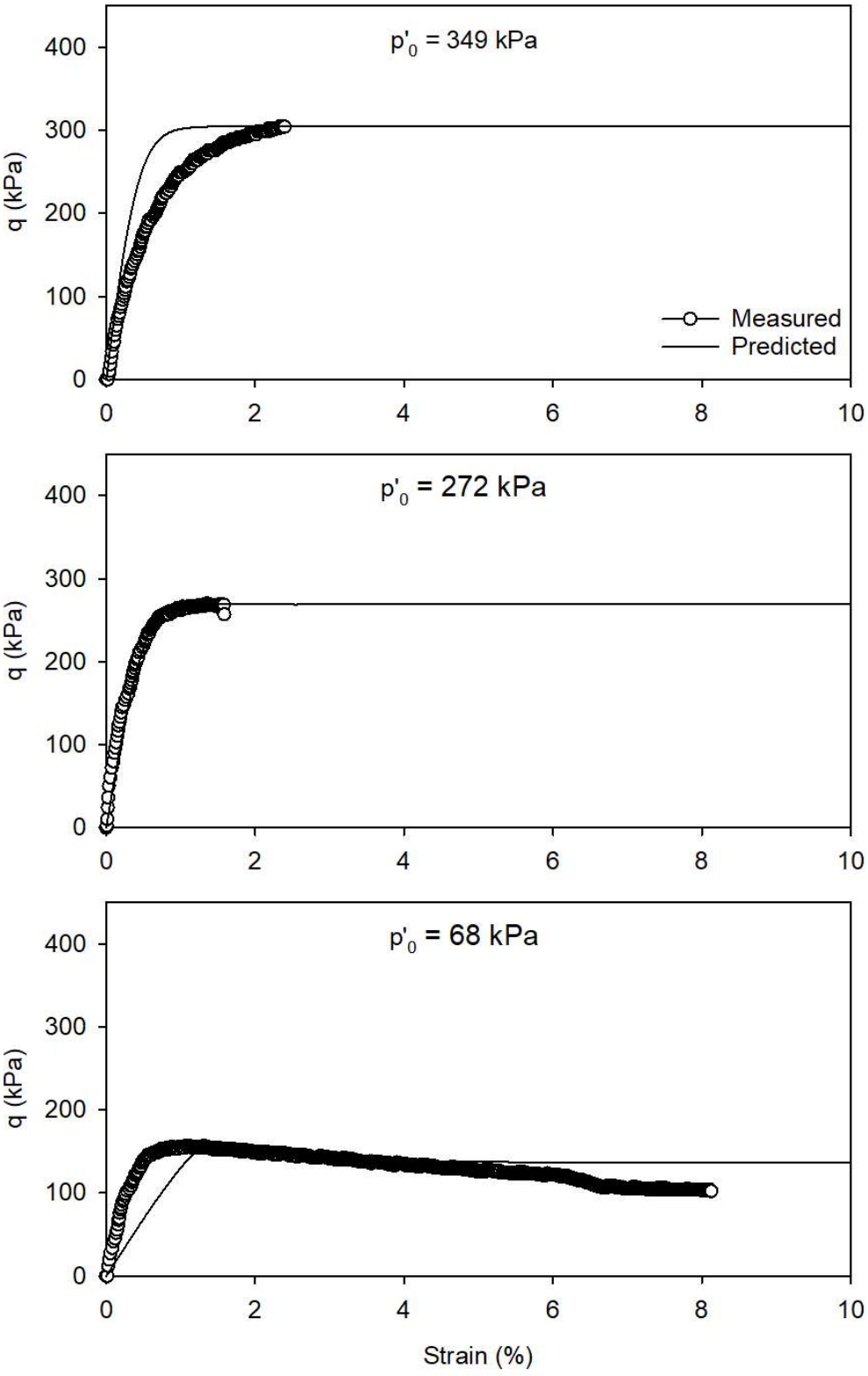

Figure 54 B-2 17 m Axial Strain-q Comparison

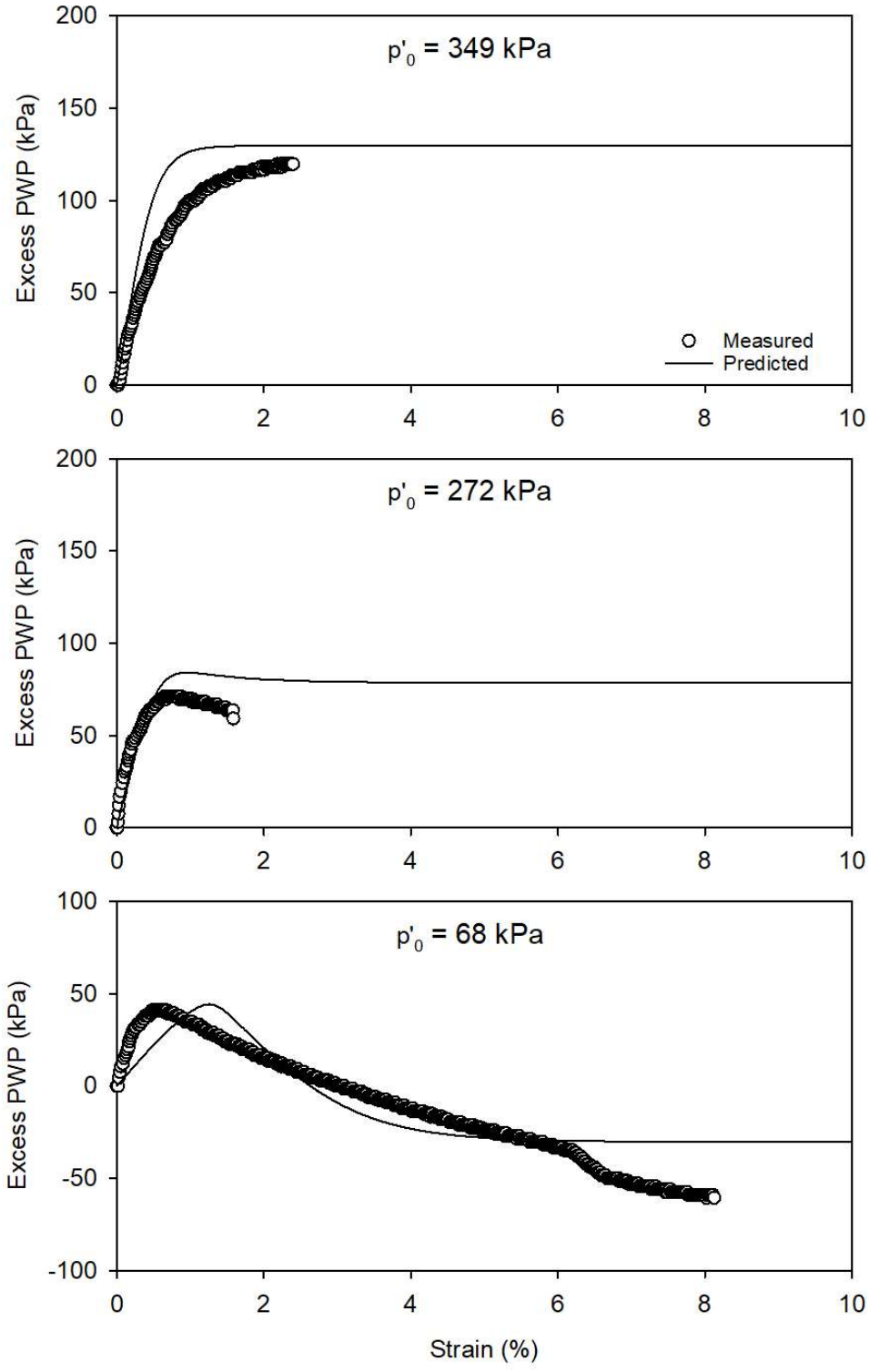

Figure 55 B-2 17 m Axial Strain-Excess PWP Comparison

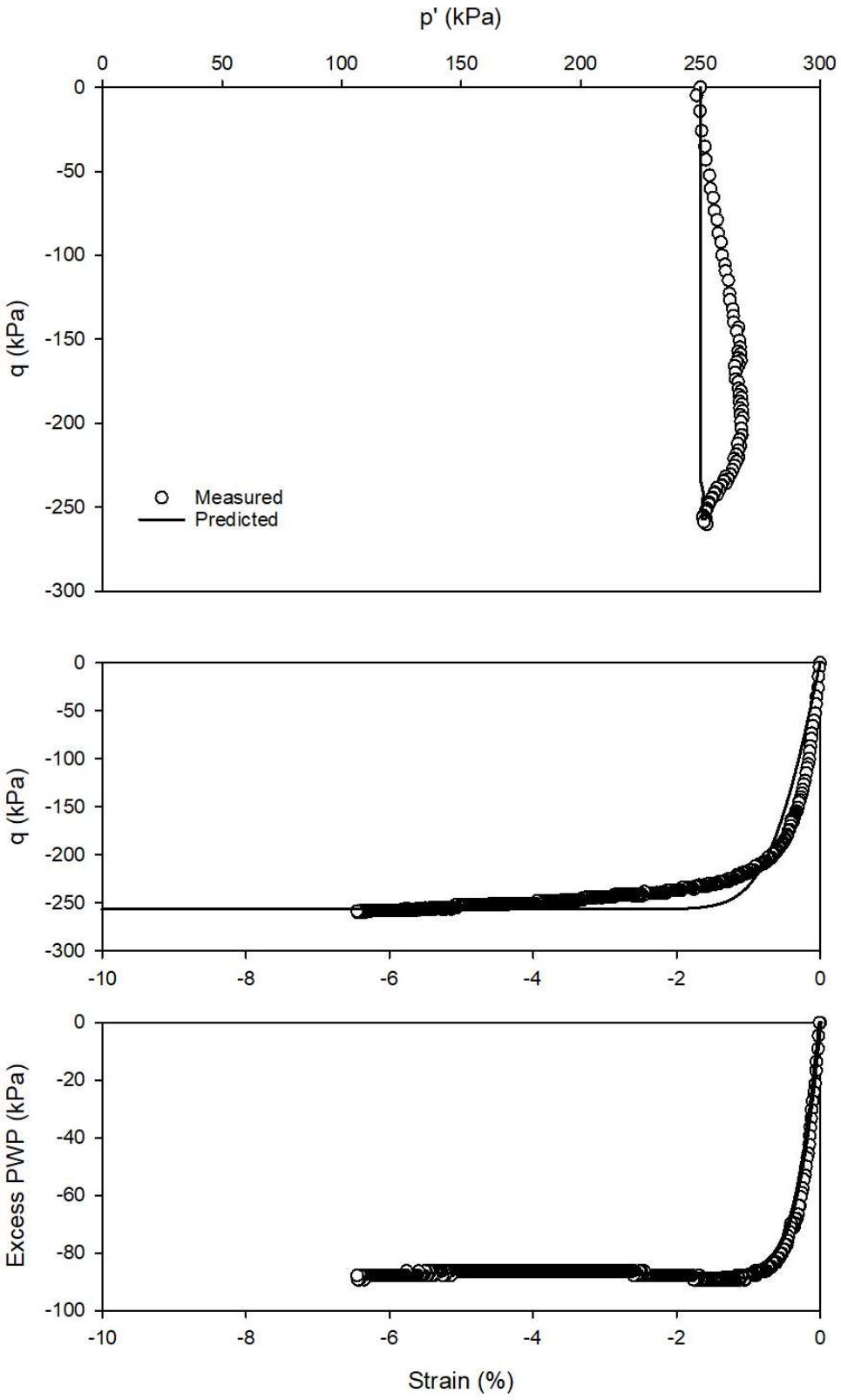

Figure 56 B-2 15.7 m Triaxial Extension Comparisons

The calibrated soil parameters are able to simulate the triaxial tests that were conducted on the soil samples reasonably well. There are some discrepancies most notably in the heavily overconsolidated samples, as shown in Figures 51 and 52. The soil model should have the ability to capture the behavior of overconsolidated soils based on results from past researchers, however for this sample it did not. The testing procedure may have induced too much disturbance on the samples leading to inaccurate predictions when modeling the heavily overconsolidated soils or the low confining pressure used during the heavily overconsolidated sample testing could be impacting the results.

The permeability of the soils used in the analyses were determined according to equations 23 through 26. The permeabilities used in the analyses are as follows: Top Clay Layer $K_x = K_y = 0.25 \times 10^{-3}$ m/day and Bottom Clay Layer $K_x = K_y = 0.35 \times 10^{-3}$ m/day. The permeability in the horizontal (K_x) and vertical (K_y) directions are likely different, however due to the lack of data on the ratio of horizontal to vertical permeabilities for the soils, they have been set equal.

6.5 Preliminaries on Pile Modeling in PLAXIS

PLAXIS 2D models the piles using an embedded beam row consisting of long slender structural elements. An out of plane spacing option is available for pile rows, as would be found under a bridge abutment, to create an equivalent stiffness per unit width. It should be noted that it is impossible to realistically model piles using a 2D model with a simplified approach (PLAXIS, 2019b) so what follows is a best attempt within the constraints of the 2D model. The simplified approach used in PLAXIS does not put the pile in the 2D mesh rather it is superimposed on the mesh and connected with special interface elements. The pile can then be described as rigid, hinged, or free at the top of the pile in reference to the soil. Descriptions of each connection type are summarized below (PLAXIS, 2019b):

- Rigid: displacement and rotation at the pile top are coupled with the element it is superimposed on
- Hinged: displacement is coupled with the element it is superimposed on, meaning the pile and the soil undergo the same displacement but the pile node will be free to rotate
- Free: not directly coupled to the soil element it is superimposed on. The interaction through the special interface elements is still present.

For the analysis describing piled bridge abutments the connection is specified as hinged since it is assumed that the soil is pushing the bridge piling and the pile is free to rotate as necessary.

The pile is described in PLAXIS using the following parameters:

- *E,* pile stiffness
- γ, unit weight of pile/soil combination ($\gamma_{pile} - \gamma_{soil}$)
- A, area of pile
- I, moment of inertia of pile
- $L_{spacing}$, out of plane spacing of piles
- Axial skin resistance, can be layer dependent based on input parameters or can be specified at the top and bottom of the pile and then linearly interpolated
- Lateral resistance, pile
    - $T_{lat,\ top}$, lateral resistance top
    - $T_{lat,\ bottom,}$ lateral resistance bottom
    - Can also be specified as “unlimited”
- $F_{max,}$ base resistance of pile

Once specified, the pile material can be assigned to pile structural elements in the model. The only parameter that is determined based on the soil properties is the axial skin resistance. The skin resistance is calculated from interface parameters for each layer which are entered within the soil material properties. For a user defined soil model the values of interface parameters are calculated using the interface oedometer modulus, E_{oed} defined below, and the interface cohesion; (C_{inter}), interface friction angle (φ_{inter}), and the interface dilation angle (ψ_{inter}) are all directly specified.

$$E_{oed}\left(\sigma' n\right) = E_{oed}^{ref}\left(\frac{\sigma' n}{UD - P^{ref}}\right)^{UD-Power} \tag{36}$$

where:

σ'n = effective normal stress at the interface stress point

UD-P^{ref} = reference stress level (usually 100 kN/m^2)

UD-Power = rate of stress dependency on the interface stiffness

The piles are modeled as line elements with three degrees of freedom per node, two translational (U_x and U_y) and one rotational (ϕ_z) in the x-y plane (PLAXIS, 2019b). When using the six node soil elements the pile is defined by a three node element with two pairs of Gaussian stress points. A 15 node soil element will have a five node pile element with four pairs of Gaussian stress points. Since the interaction between the pile and soil/rock can have a skin resistance and end resistance, special out of plane interface elements are used to connect the pile to the soil. The interface elements consist of springs in the longitudinal and transverse directions and a slider in the longitudinal direction as shown in the soil structure interaction schematic in Figure 57.

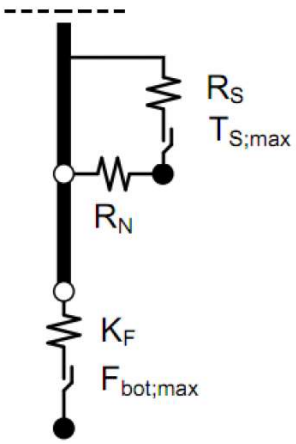

Figure 57. Modeling of Soil-Pile Interaction, from PLAXIS (2020)

where:

R_N = stiffness in the lateral direction

R_S = stiffness in the axial direction

K_F = base stiffness

$T_{s;max}$ = maximum force in the axial direction (directly entered as a pile parameter)

$F_{bot;max}$ = maximum base resistance (directly entered as a pile parameter)

$$R_N = ISF_{RN} \frac{G_{soil}}{L_{spacing}} \tag{37}$$

$$R_s = ISF_{RS} \frac{G_{soil}}{L_{spacing}} \tag{38}$$

$$K_F = ISF_{KF} \frac{G_{soil} R_{eq}}{L_{spacing}} \tag{39}$$

where:

ISF_{RS} = axial skin stiffness factor

ISF_{RN} = lateral stiffness factor

ISF_{KF} = pile base stiffness factor

$L_{spacing}$ = pile spacing in out of plane direction

G_{soil} = shear stiffness of surrounding soil

$$ISF_{RS,RN,KF} = 2.5\left(\frac{L_{spacing}}{D}\right)^{-0.75} \quad (40)$$

where:

D = pile diameter or equivalent width in the case of non-circular pile

For non-circular pile D = D_{eq}:

$$D_{eq} = \sqrt{\frac{12EI}{EA}} \quad (41)$$

6.5 PLAXIS Model and Analysis

The geometry for the bridge embankment was taken directly from the construction plan set provided by ODOT. The information taken from the plan set includes the embankment height, foreslope, pile location, pile termination depth, pile batter angle and pile end bearing capacity. The loading of the bridge on the pile tops was also estimated from the bridge plan set by considering the weight of the concrete beams, bridge deck, parapets, and abutment. It should be noted that the foreslope shown on the plan set was 2H:1V which is quite steep for a bridge embankment. Typically the foreslope is kept at 3H:1V or if economically feasible it is increased to 4H:1V, for this bridge there were geometric constraints posed by the location of the existing railroad track and conveyor belt which necessitated the 2H:1V foreslopes.

The soil stratigraphy was idealized from the boring logs developed following the site investigation and lab testing program as described previously. The only parameter necessary for the analysis that can be considered unknown for the foundation soils was the initial OCR. At the time of field investigation, the foundation soil had been compressed under the embankment for approximately 40 years causing the foundation soils to be normally consolidated. Since the OCR

of the foundation soils was unknown, a best estimate was made based on the available data and the results of the PLAXIS analysis. The OCR adopted for the Top Clay Layer was 2.0 while 6.0 was used for the Bottom Clay Layer. The reason 6.0 was chosen for the Bottom Clay Layer is during pile driving refusal was achieved near the interface of the two clay layers suggesting the bottom layer was much stiffer than the top layer, this is supported with the boring logs included in Appendix A. In Boring B-2 a hard layer was encountered near the interface of the two layers, following the hard layer a softer layer was encountered and an undisturbed sample was collected. This softer layer is where the calibrated soil parameters for the Bottom Clay Layer were derived. The Bottom Clay Layer was also interbedded with cobbles suggesting a stiffer response.

The embankment fill material was modeled using the Bounding Surface Model and modifying the parameters to achieve a very stiff soil. The embankment was found to have multiple layers of shale and sandstone fill material that was compacted very well. For this reason the embankment has been idealized as a very stiff material. The parameters adopted for the embankment material are presented below.

Table 10. SH 3 over BNSF Adopted Embankment Fill Parameters

λ	0.01
κ	0.001
M_c	2.0
M_e/M_c	1.0
v	0.2
R_c	2
A_c	0.2
T	0.1
R_e/R_c	1.0
A_e/A_c	1.0
C	0.5
S	1.75
m	0.02
h_c	500
h_e/h_c	1
h_2	500
void ratio	0.5

The pile properties used for this analysis were based on the HP 10x42 piles prescribed in the plan set. The battered and straight piles are alternated with a spacing of approximately 2.5 to 3 m depending on the pile orientation, battered or straight. It should be noted that there is not an option available to specify that the piles are in an alternating sequence in the out of plane direction. A summary of the pile parameters used in the analyses are presented below.

Table 11. SH 3 over BNSF Pile Parameters

Parameter	Value
E (kN/m^2)	200.0E6
γ (kN/m^3)*	55.0
Area (m^2)	8.00E-3
I (m^4)	0.0874E-3
$L_{spacing}$ (m)	3
Base Resistance (kN)	330

* Unit weight of pile soil combination ($\gamma_{pile} - \gamma_{soil}$)

Another key aspect in properly modeling the embankments is the construction sequence. Since the exact sequence is unknown and not available, an estimated construction schedule has been adopted. The construction schedule adopted is presented in Table 12. Following the construction schedule, the embankment behavior was analyzed for an additional 3000 days to observe the longtime behavior of the embankment.

Table 12. Adopted Construction Schedule for SH 3 over BNSF Railroad

Task	Time Frame
Embankment Construction	40 days
Pile driving	5 days
Bridge Construction	100 days

The bridge construction was modeled by adding a line load to the node at the intersection of the pile tops and embankment crest. The magnitude of the line load for the east side was 170 kN/m while the west side was 135 kN/m. The span adjacent to the west abutment was shorter than the span adjacent to the east abutment. The loading on the pile tops assumes that half of the adjacent span load is transferred to the abutment while the other half is transferred to the adjacent pier.

To refine the element size used in the mesh, the site was divided into two sides and the analysis for the east and west embankments were completed separately. The embankments are approximately 66 m apart when measured from the embankment toe. Due to the large distance between the embankments they are not anticipated to influence each other since the analysis does not include bridge elements excluding the piling. The boundary conditions utilized in both meshes are as follows: left and right sides are free to move in the vertical direction but restrained

horizontally and the bottom is fully fixed. The mesh used for the east and west sides are shown below.

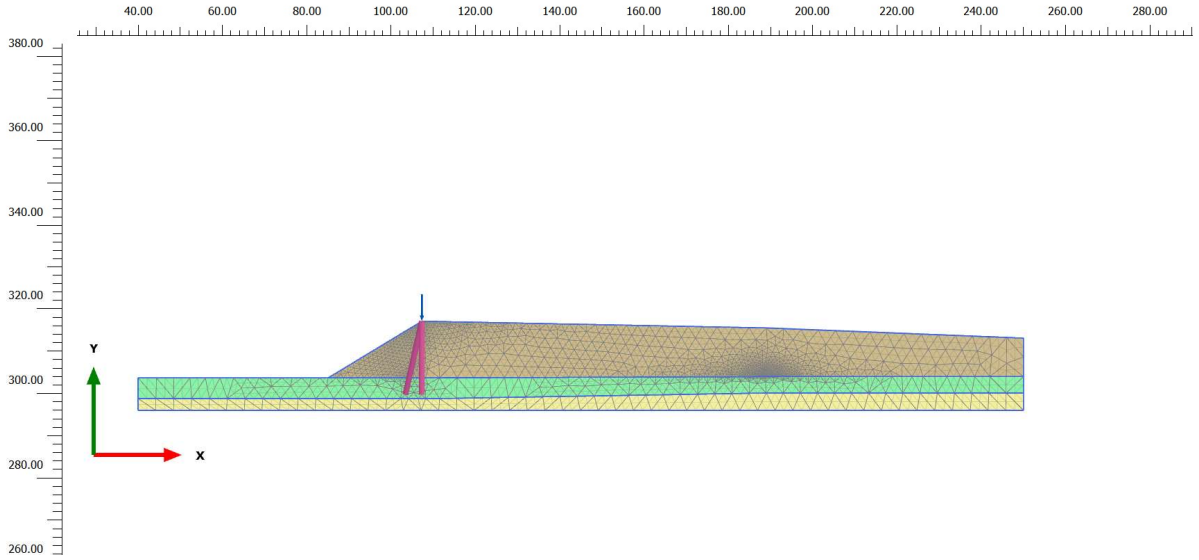

Figure 58. SH 3 over BNSF East Embankment Mesh

The east embankment was underlain by both the Top Clay layer and the Bottom Clay layer and the pile driving was terminated near the bottom of the Top Clay layer. The embankment was extended out approximately 150 m to ensure there would be no influence from the boundaries.

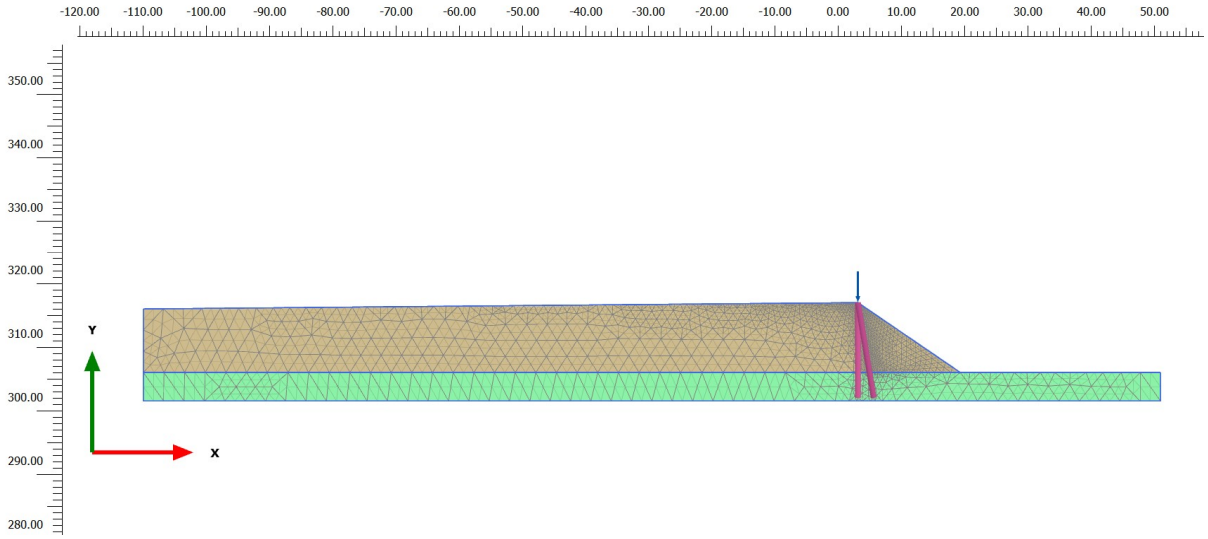

Figure 59. SH 3 over BNSF West Embankment Mesh

Only one clay layer was encountered beneath the west embankment, the clay layer was similar to what has previously been described as the Top Clay layer. Beneath the clay layer bedrock was encountered. This embankment was extended out approximately 100 m to ensure no influence from the boundaries.

6.6 Results and Discussion

Each embankment was analyzed for three scenarios. In the first scenario both the battered and straight piles were used, in the second scenario only straight piles were used, and in the third scenario no piles were used. The goal of this comparison was to determine the impact of the piles on the lateral movement of the embankments. A summary of the lateral movement each embankment experienced as measured from the embankment crest at the end of the analysis (3145 days) is presented in the table below.

Table 13. SH 3 over BNSF Influence of Bridge Piles

Scenario	East Embankment Crest Movement (mm)	West Embankment Crest Movement (mm)
Battered and straight piles	80.1	-18.3
Straight piles	81.2	-18.1
No piling*	95.8	-17.1

* did not include loading from bridge

The scenario without bridge piling had the bridge load omitted since there was not a structural element present to transfer the idealized line load to the bearing strata. Based on the analyses, the piling does appear to impact on the lateral deformation of the embankment; however, the addition of the battered pile does not appear to have much of an influence based on the analyses. It should be noted that the east embankment showed movement toward the bridge and the west embankment showed movement away from the bridge, the deformed mesh and lateral displacement contours for the east and west embankments including the battered and straight piles are shown below.

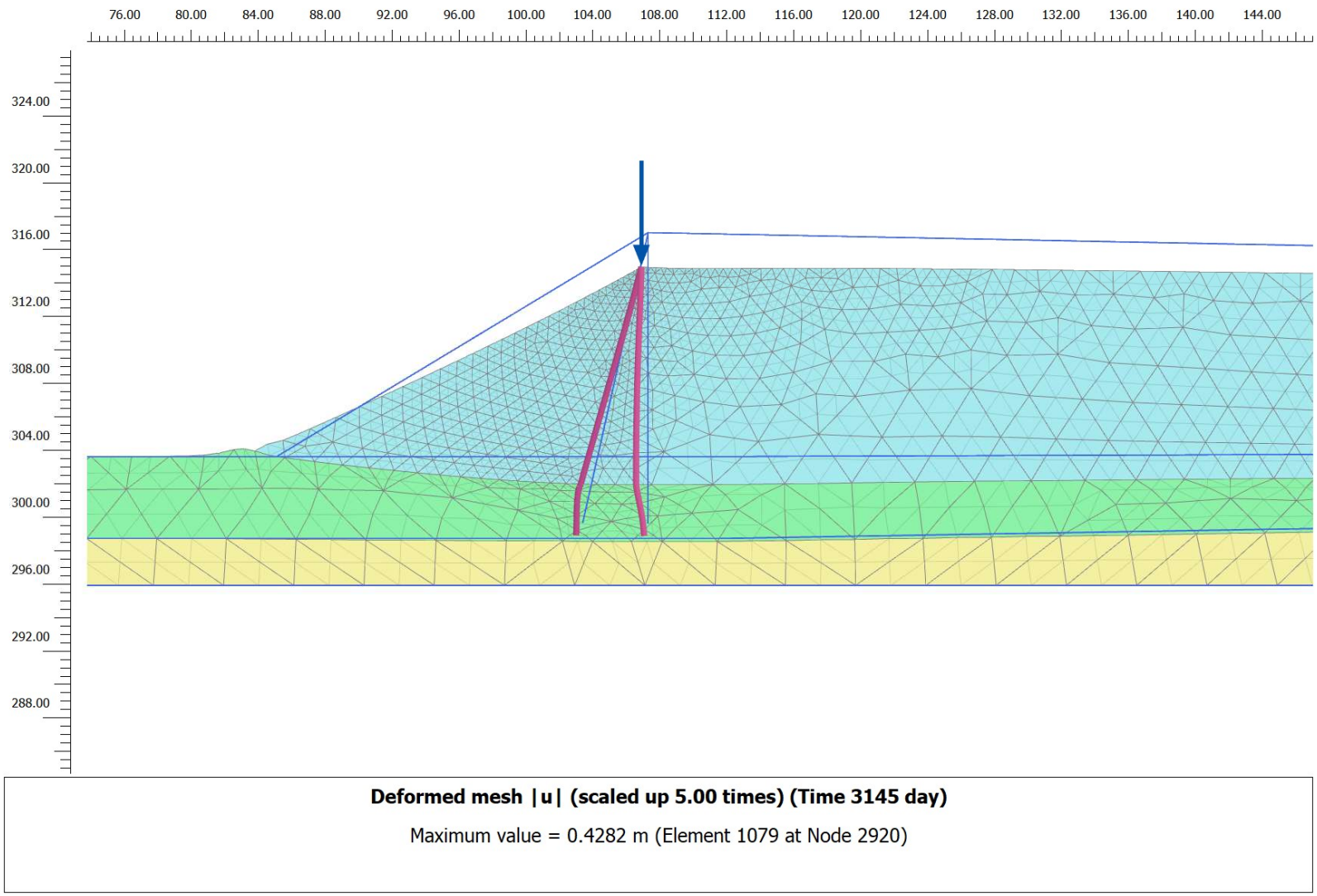

Figure 60. SH 3 over BNSF East Embankment Deformed Mesh

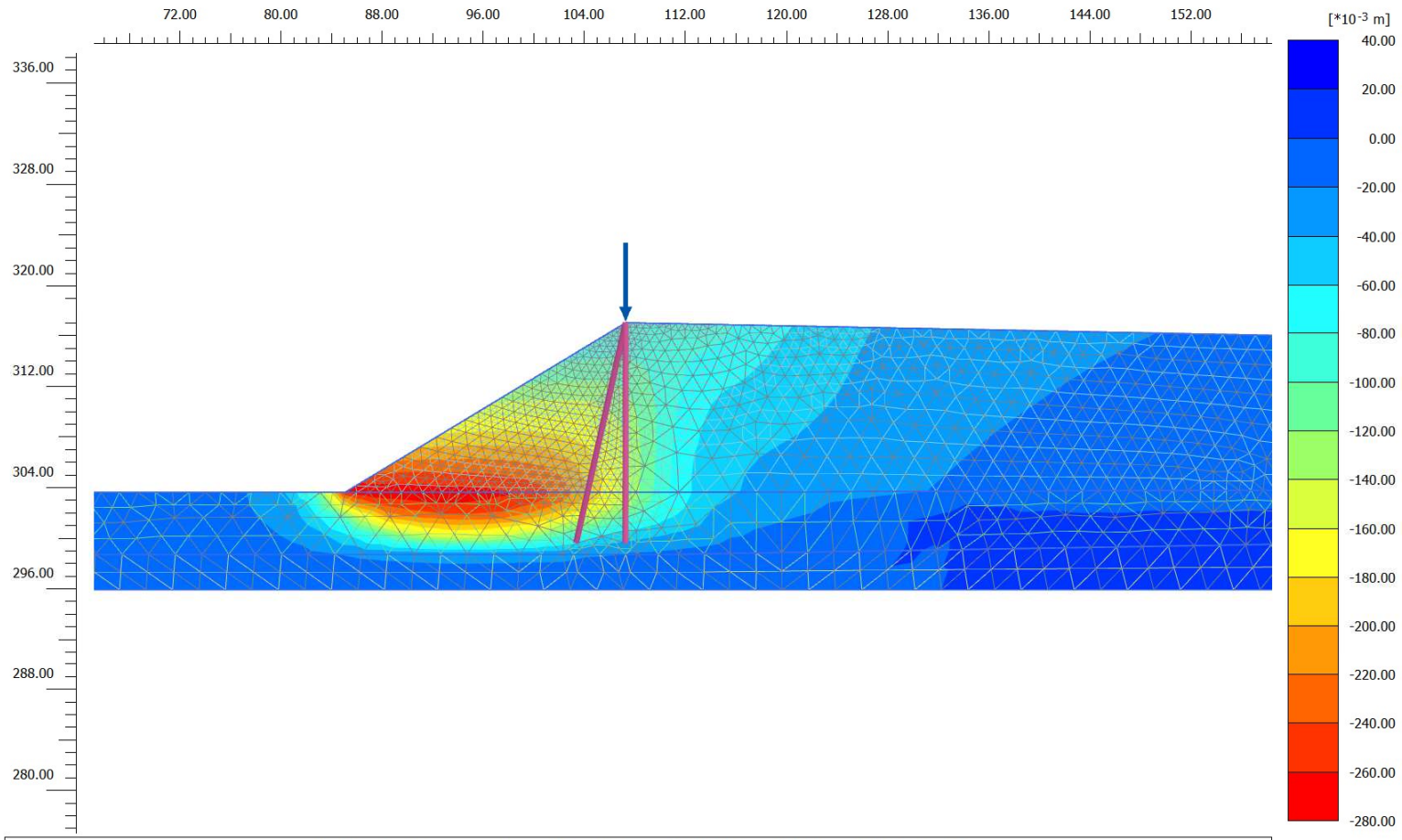

Total displacements u_x (scaled up 20.0 times) (Time 3145 day)

Maximum value = 0.02023 m (Element 2005 at Node 27)

Minimum value = -0.2758 m (Element 1463 at Node 4838)

Figure 61. SH 3 over BNSF East Embankment Lateral Displacement Contours

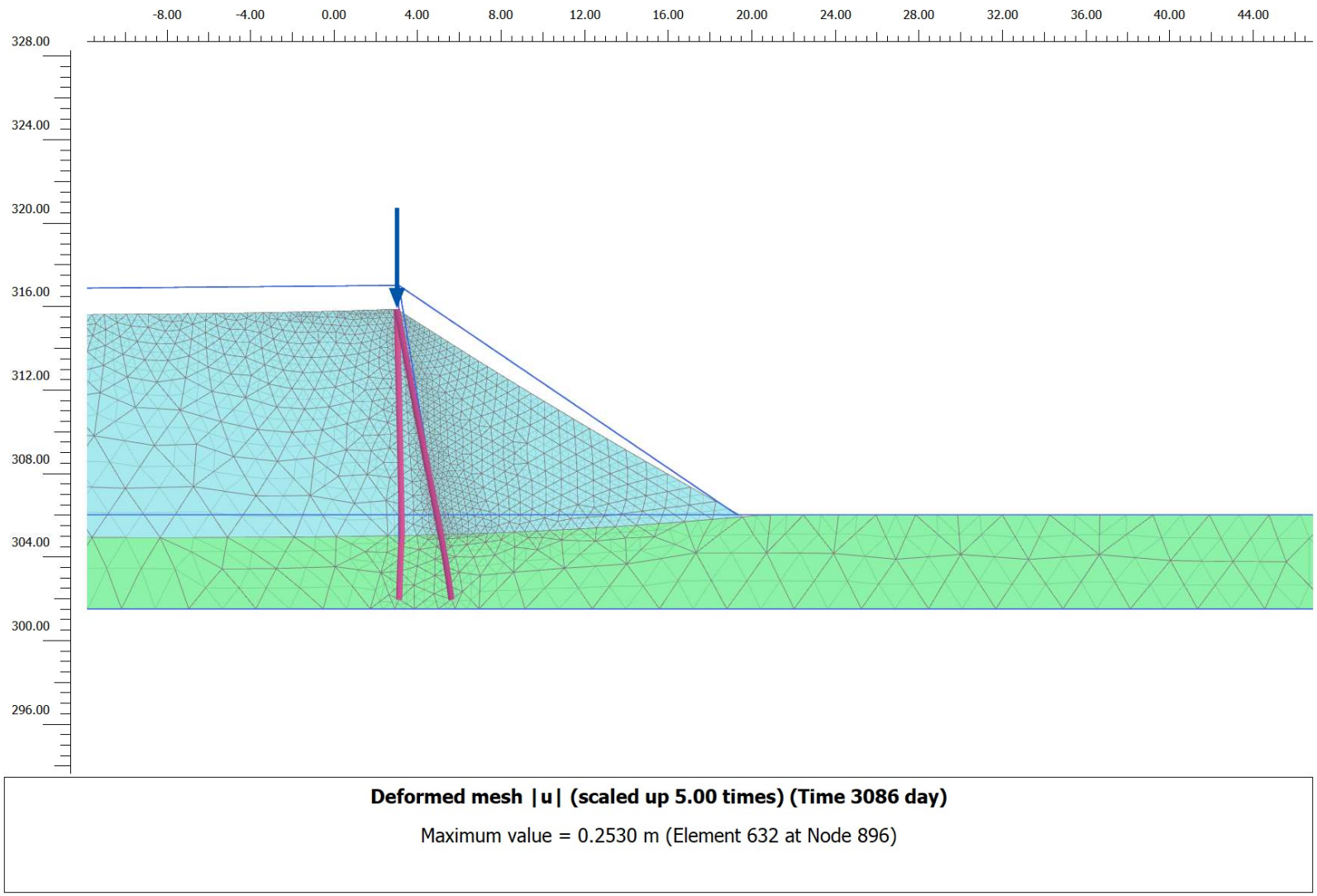

Figure 62. SH 3 over BNSF West Embankment Deformed Mesh

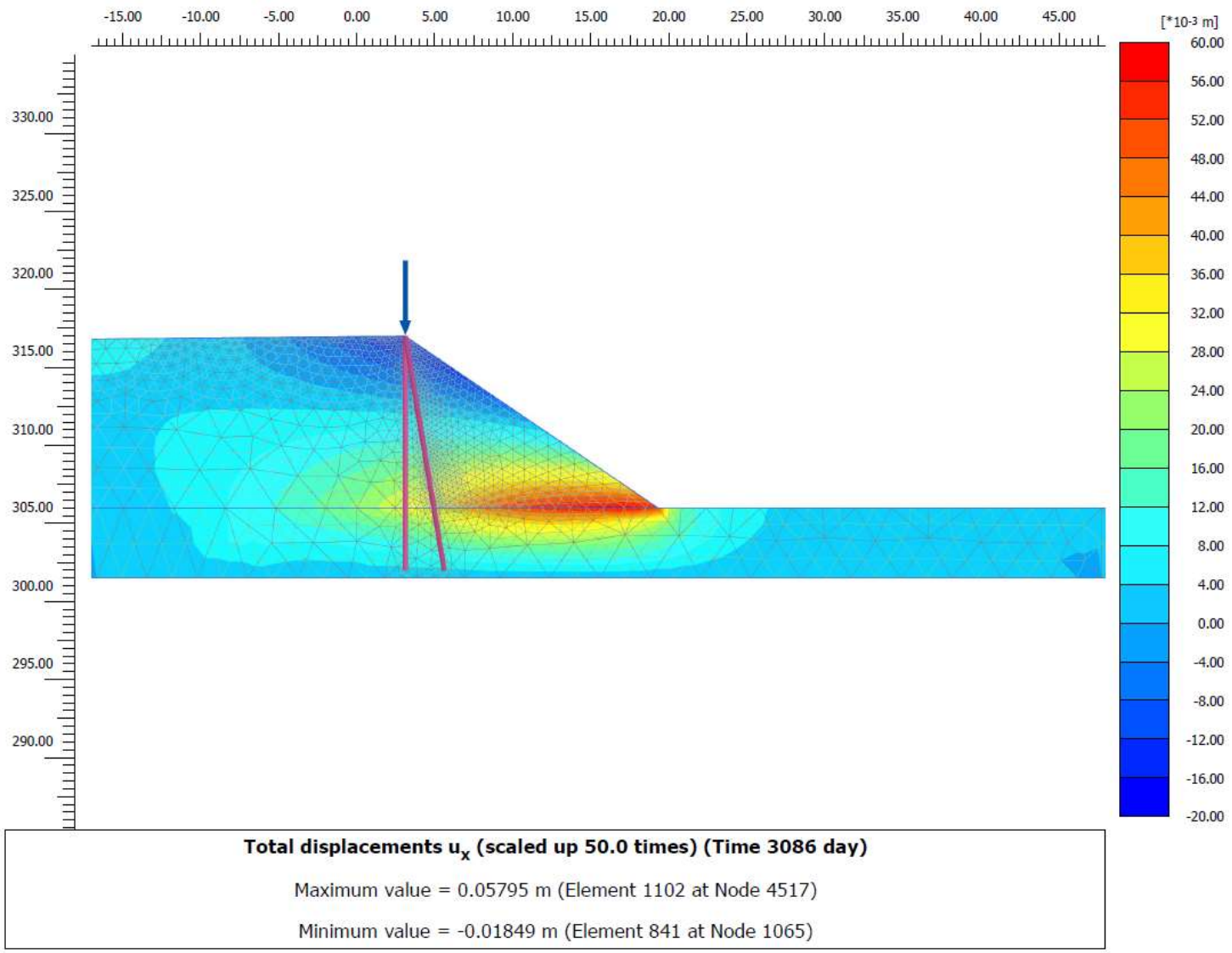

Figure 63. SH 3 over BNSF West Embankment Lateral Displacement Contours

Based on the conditions observed in the field a total movement of approximately 200 mm is expected to have occurred in order to fully close the bridge expansion joints. The actual amount of movement required to close the expansion joints could be less as a result of additional factors not accounted for in this analyses such as thermal expansion of bridge elements, the skew of the bridge, and debris present in the expansion joints. Furthermore, in both analyses excessive settlement is observed but there is not any indication the embankment underwent excessive settlement in the field other than some asphalt patching on the approach pavement. The asphalt patching appeared to have been placed in order to lessen the bump at the end of the bridge. Much of the settlement in the analyses occurred very early in the life of the bridge so it can reasonably be assumed that the height of the embankment would be adjusted as necessary to match the final grade before the pavement was placed.

During the analysis, the east embankment experienced approximately 80 mm of movement toward the bridge. The direction and magnitude of movement agrees well with observations in the field. The magnitude does not quite match up to 50% of the anticipated movement but based on the assumptions and the simplified analysis the results are more or less in agreement. Despite the magnitude of movement the piles did not yield, the maximum bending moment in the straight pile was 6.9 kN-m and the battered pile had a maximum bending moment of 1.6 kN-m.

The west embankment analysis showed movement away from the bridge. Based on observations in the field it is known that the west bridge abutment moved toward the bridge. The site investigation on the west side only included one boring so there is limited information on the foundation soil stratigraphy away from the bridge abutment. The movement away from the bridge is the result of excessive settlement under the full height of the embankment which causes the bottom of the embankment to be concave which then pulls the crest of the embankment back away

from the bridge. Due to the nature of the deformation the bridge piling had little impact on the lateral deformation, see Table 13. The piles for this bridge were terminated following refusal on top of a hard layer, additional reinforcement from the piles could have been gained if the piles were extended into the hard layer. This effect, the pile pinning effect, could help resist the lateral movement of the embankment.

Despite the lateral behavior not matching exactly to what was observed in the field the analysis provided some useful insights. The embankment material used for these bridges was a mix of clay, sand, shale and sandstone. Portions of the embankment were also very stiff due to the presence of shale and sandstone. The high stiffness of this embankment likely played a role in the lateral deformation experienced in the field. If the embankment had been constructed out of softer material a more concave behavior would have likely been observed for both sides resulting in the bridge abutment moving away from the bridge since the embankment wouldn't have resisted the tendency to deform in a concave shape. Based on the analysis, for the east side, it seems that the embankment is being carried laterally by the soft clay layer. Furthermore, the analysis verified the ability of the piles to reduce the lateral displacement the embankment experiences.

7.0 TRIAL EMBANKMENT ANALYSES

A trial embankment was systematically analyzed to find relationships between various parameters and the lateral movement the embankment experienced. Building on the knowledge gained in the previous chapters the embankment was analyzed using both straight and battered piles in accordance with ODOT's standard bridge specification. The trial embankment was analyzed 216 times allowing for a variety of lateral and vertical movements to be studied.

7.1 Embankment Geometry and Soil Properties

To gain a better understanding of the variables impacting the lateral movement of embankments the foreslope (slope facing the bridge), embankment height, foundation soil strength, foundation soil thickness and foundation soil permeability were systematically varied. Attempts were made to encompass a wide range for the variables while not analyzing unrealistic scenarios. One of the trial embankments is shown below.

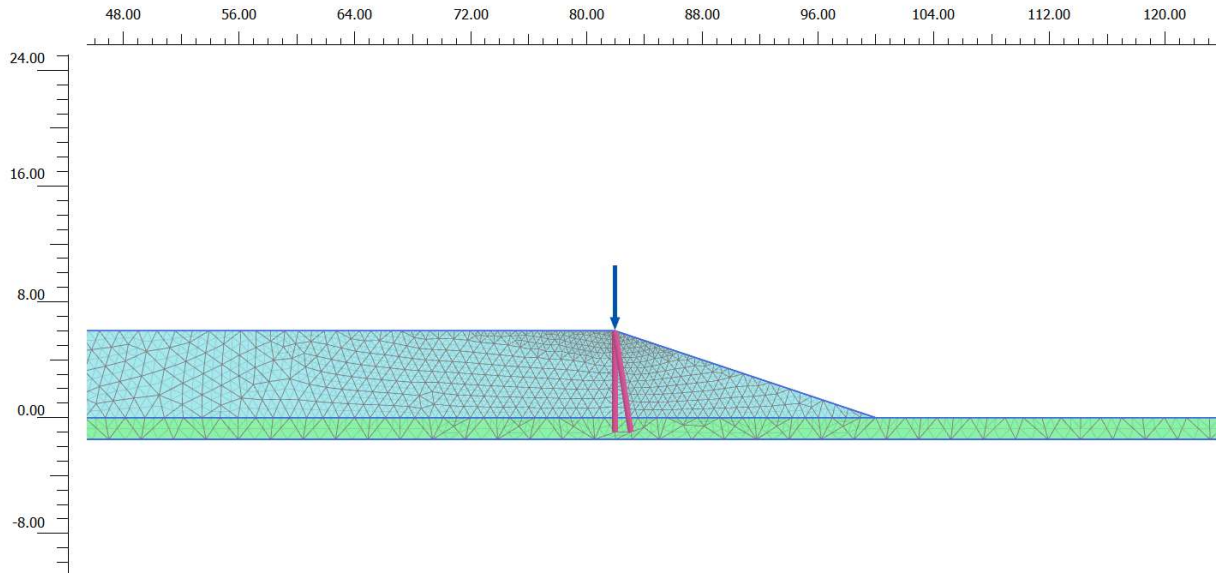

Figure 64. Trial Embankment: Height 6 m, Foundation thickness 1.5 m

Figure 64 is a zoomed in view, the boundaries extend from 0 to 150 m in the horizontal direction. Notice in the above figure that the piles do not extend to the bottom of the layer. When the piles were placed at the bottom boundary of the mesh numerical difficulties arose since the bottom boundary was defined as a fixed boundary and the piles will experience some vertical movement when the bridge loading is added. To avoid this issue the piles were placed 0.5 m above the minimum vertical boundary. The vertical displacements of the piles are impacted by the soil stiffness as shown in Equations 37 through 41, but are also controlled by a maximum end bearing which is directly entered into the program as part of the pile properties. The pile settlement is not anticipated to have a major impact on the outcomes of this research since it essentially matches the embankment settlement. The pile top conditions were treated as hinged to the mesh meaning they were allowed to rotate independently while the displacements were required to match that of the soil mesh. The boundary conditions of all embankments were kept constant and are as follows: left and right sides vertical displacements allowed but fixed in the horizontal direction bottom was fully fixed and top was free. Drainage was only allowed on the left and right sides and at the top.

A testing matrix displaying the variable combinations is shown in Table 14. Each of the scenarios shown in Table 14 were analyzed with three foundation soil permeabilities: 0.0025, 0.00025, and 0.000025 m/day. The geometry was similar to that shown in Figure 64 with the embankment height, foreslope and soil thickness changing as needed.

Table 14. Trial Embankment Test Matrix

Fore-slope	Embankment Height (m)	Soft soil strength	Soft Soil Thickness (m)
3H:1V	6	soft	1.5
			3
			4.5
			6
		medium	1.5
			3
			4.5
			6
		stiff	1.5
			3
			4.5
			6
	10	soft	1.5
			3
			4.5
			6
		medium	1.5
			3
			4.5
			6
		stiff	1.5
			3
			4.5
			6
	14	soft	1.5
			3
			4.5
			6
		medium	1.5
			3
			4.5
			6
		stiff	1.5
			3
			4.5
			6

Fore-slope	Embankment Height (m)	Soft soil strength	Soft Soil Thickness (m)
4H:1V	6	soft	1.5
			3
			4.5
			6
		medium	1.5
			3
			4.5
			6
		stiff	1.5
			3
			4.5
			6
	10	soft	1.5
			3
			4.5
			6
		medium	1.5
			3
			4.5
			6
		stiff	1.5
			3
			4.5
			6
	14	soft	1.5
			3
			4.5
			6
		medium	1.5
			3
			4.5
			6
		stiff	1.5
			3
			4.5
			6

Table 14 presents the three soil strengths used in the analyses as soft, medium, and stiff. Ultimately the soil used in each analysis had the same model parameters, excluding the OCR. To minimize the influence of model parameters on the lateral displacement the OCR was varied from 1.3, 2.5, and 4.0 to allow for three different soil strengths. Increasing the OCR increases the initial size of the bounding surface relative to the current stress state which allows for more elastic behavior. A normally consolidated condition was not included in the final series of analyses. An initial series of analyses found that when the foundation soil was normally consolidated, the analysis typically failed. In PLAXIS 2D the error received during the failed analysis was "soil body seems to collapse" meaning complete failure of the soil. The complete failure of the soil is likely indicative of slope stability failure and does not encompass the nature of this research. Hence a minimum OCR of 1.3 was chosen to provide a greater range of results.

The construction timing for each scenario was kept constant excluding the construction time for the embankment. However, the construction rate was kept the same. Following some preliminary analyses a rate of 0.2 m/day was chosen as the construction rate. A rate of construction is generally not specified for embankment construction. The rate utilized in this research was chosen to allow for most of the trial embankments to fully deform for the range of permeabilities proposed in the study.

Following the embankment construction, the piles were activated over a period of 5 days. The activation of the piles doesn't add any additional loading to the soils it merely makes the piled section stiffer. Once the piling was activated the bridge loading was added. The bridge loading was taken as 150 kN/m located on the top of the piles, the bridge loading was added over a period of 100 days. Finally, the embankments were allowed to consolidate for 3,000 days. Based on

preliminary analyses it was found that the 3,000 day time frame was adequate to allow for the lateral and vertical movements to come to an end.

The foundation and embankment soils used in the trial embankment analyses were the same as the soils adopted for the SH 3 over BNSF Railroad bridge analysis in Chapter 6. These soils were chosen since they are representative of the types of clayey soils found in Oklahoma. The foundation soil parameters are presented in Table 9 under the B-2 - 15.5 m heading and the embankment soil parameters are presented in Table 10. There is a desire to correlate the lateral displacement to information that would readily be available to a practicing engineer such as embankment geometry and a few representative soil parameters. To better assess the impact of soil strength on the lateral deformation, the maximum shear strength of the soils, when subjected to undrained in-situ stress conditions were estimated from simulated tests. The tests were simulated using triaxial loading and setting the cell pressure equal to the isotropic horizontal effective stress for the middle of the soil layer prior to placement of the embankment, that is $p'_0 = \sigma'_0$. Generally, triaxial tests are completed in triplicate by increasing the p'_0 value for each subsequent test. The range of p'_0 chosen are usually at the discretion of the engineer so the maximum shear strength when $p'_0 = \sigma'_0$ should be known or able to be estimated during routine embankment analysis. The maximum shear strength values are presented in the following table.

Table 15. Trial Embankment Analyses Estimated Shear Strength

Foundation Soil Thickness (m)	OCR	Shear Strength (kPa)
1.5	1.3	3.9
	2.5	6.5
	4.0	9.7
3	1.3	7.8
	2.5	13.1
	4.0	19.6
4.5	1.3	11.7
	2.5	19.2
	4.0	26.3
6	1.3	15.6
	2.5	25.1
	4.0	34.1

The maximum shear strength when subjected to effective in-situ stress was chosen as a strength parameter since it is fairly easily obtained using standard triaxial equipment and would only require one sample to obtain the results.

7.2 Analyses Results and Relationships

Following the completion of the analyses several resulting values were recorded. The lateral displacement at the toe of the embankment and at the crest of the embankment as well as the maximum vertical displacement of the embankment were recorded for each simulation. The complete set of results is included in Appendix C. Throughout the course of the simulations it was realized that the crest of the embankment generally moves less than the toe of the embankment

and often will tilt the opposite direction due to the concave nature of the settlement of the foundation layer.

After an inspection of the displacement with respect to time it was found that in general the crest of the embankment will move outward initially and then inward once the vertical displacement starts to dominate the behavior. The concave behavior is likely dependent on the stiffness of the embankment which was not a variable for this study. For this reason, the comparisons and relationships are all based on the movement at the toe rather than the movement at the crest with the acknowledgement that the movement may not be as severe at the crest.

7.2.1 Influence of Embankment Height on Lateral Displacement

The influence of the embankment height on the lateral displacement at the toe has been compared. Comparison graphs are shown in Figures 65 through 72 for the soft, medium, and stiff soils with a 3H:1V slope and permeabilities of 0.0025, 0.00025, and 0.000025 m/d. The graphs are further broken up by the foundation layer thickness. For brevity only the 3H:1V graphs are included.

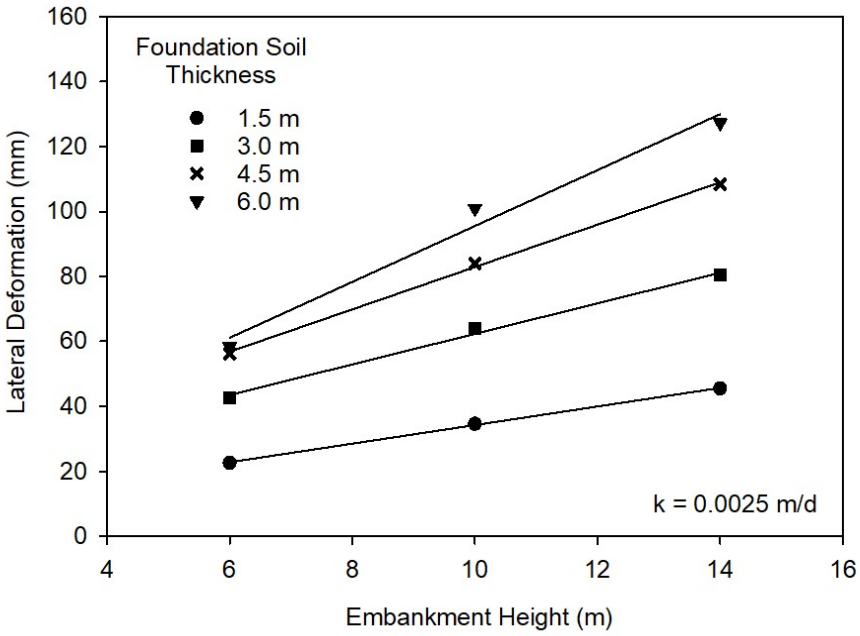

Figure 65. Embankment Height vs. Lateral Deformation of the Toe: Soft Soil and High Permeability

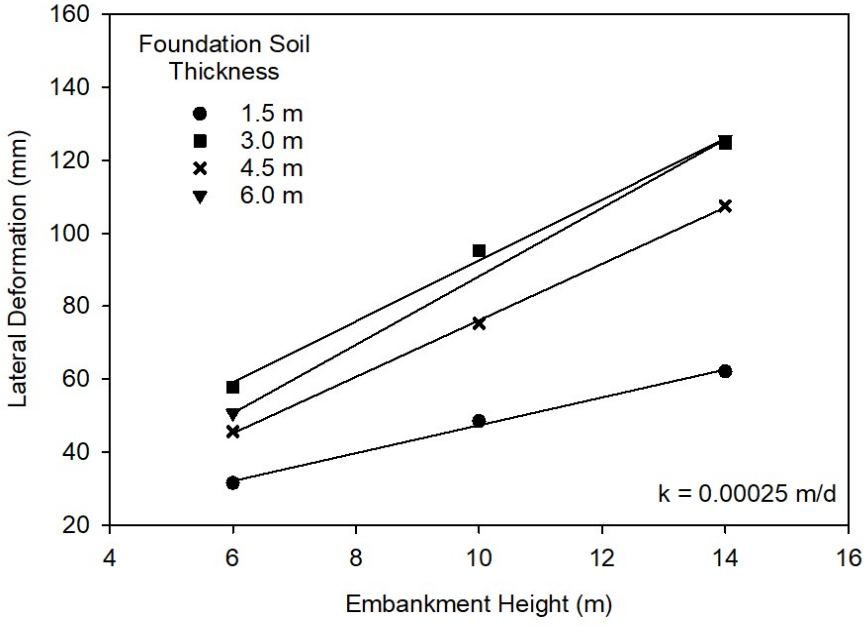

Figure 66. Embankment Height vs. Lateral Deformation of the Toe: Soft Soil and Medium Permeability

Figure 66 is missing a data point for the 10 m embankment height; the missing point is due to PLAXIS crashing for this scenario. The soft soil analyses was the most heavily influenced by the changing height of the embankment. The relationship between increasing the embankment height and the lateral displacement of the embankment is highly non-linear. A perfectly linear relationship would have roughly the same trendline slope for each layer thickness. However, for both Figures 65 and 66 the trendline slope is erratic and generally increases as the foundation layer thickness increases meaning the influence of the embankment height is more pronounced as the layer thickness increases. It is possible that this is from the soil nearly experiencing slope stability failure. If global slope stability failure is considered, then the thinner foundation layers underlain by a rigid boundary would effectively prevent the slip surface from being able to form.

The non-linear relationship is even more pronounced as the permeability of the foundation soil decreases. The influence of increasing the embankment height is greater for the lower permeable soil, see Figure 66. The lowest permeability included in the analyses, 0.000025 m/d resulted in failure messages for all scenarios including the soft soil, suggesting complete failure of the embankment.

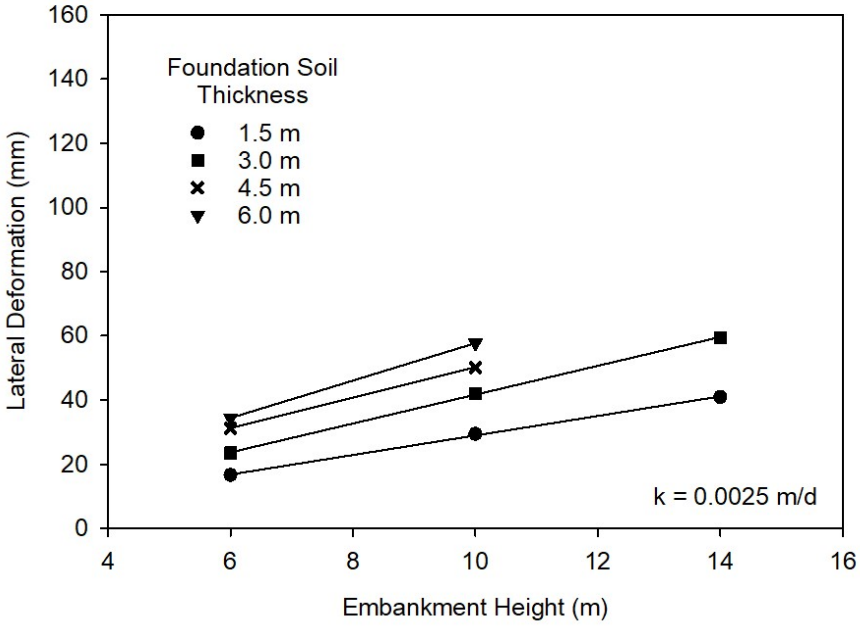

Figure 67. Embankment Height vs. Lateral Deformation of the Toe: Medium Soil and High Permeability

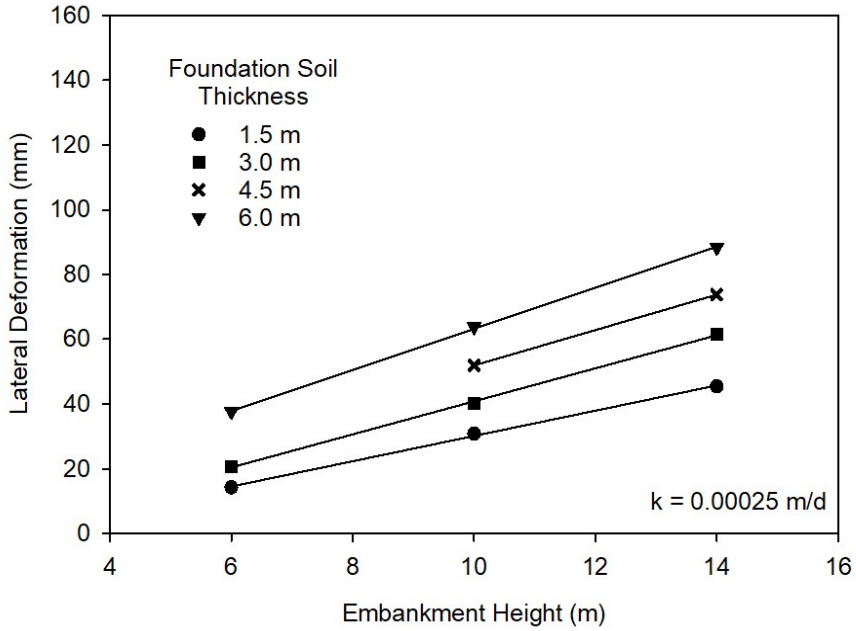

Figure 68. Embankment Height vs. Lateral Deformation of the Toe: Medium Soil and Medium Permeability

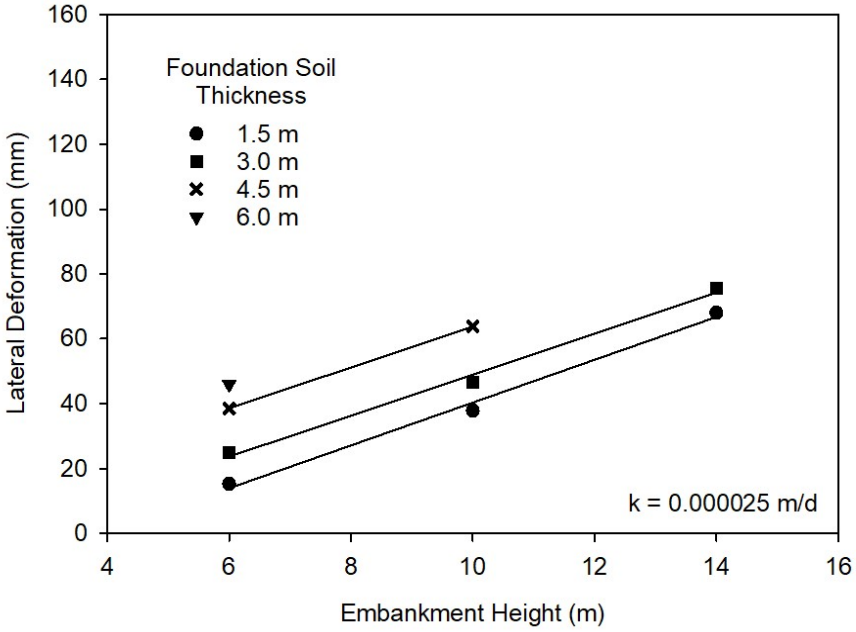

Figure 69. Embankment Height vs. Lateral Deformation of the Toe: Medium Soil and Low Permeability

A similar trend was found for the medium stiff soil (Figures 67 through 69), as the permeability decreases the influence of the embankment height on the lateral displacement becomes more pronounced. It is interesting to note that as the permeability decreases the relationship becomes more pronounced, but for a permeability of 0.000025 m/d it appears that the relationship between the embankment height and lateral displacement is fairly consistent with changes in the foundation layer thickness. This comparison can be somewhat misleading though since the thickest foundation layer, 6 m, was only successfully analyzed for one embankment height.

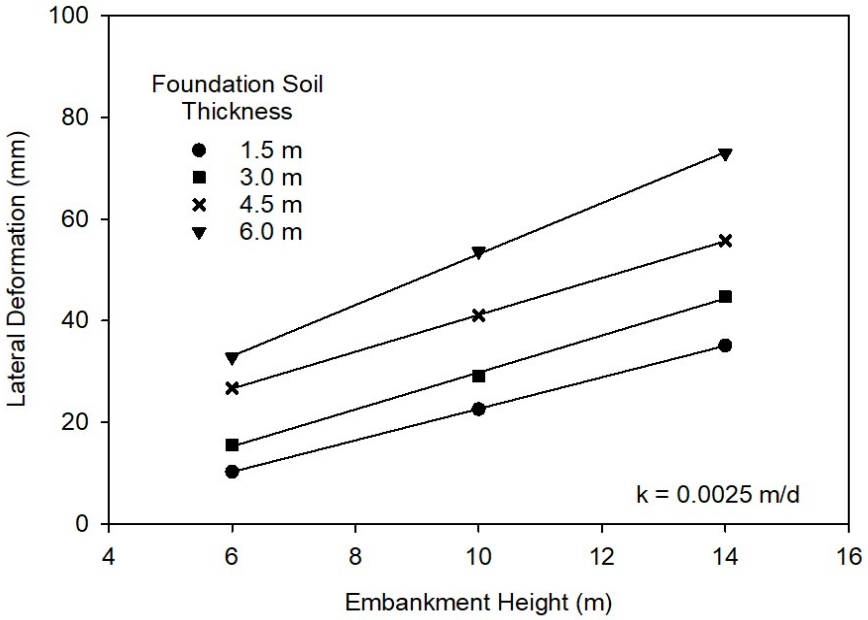

Figure 70. Embankment Height vs. Lateral Deformation of the Toe: Stiff Soil and High Permeability

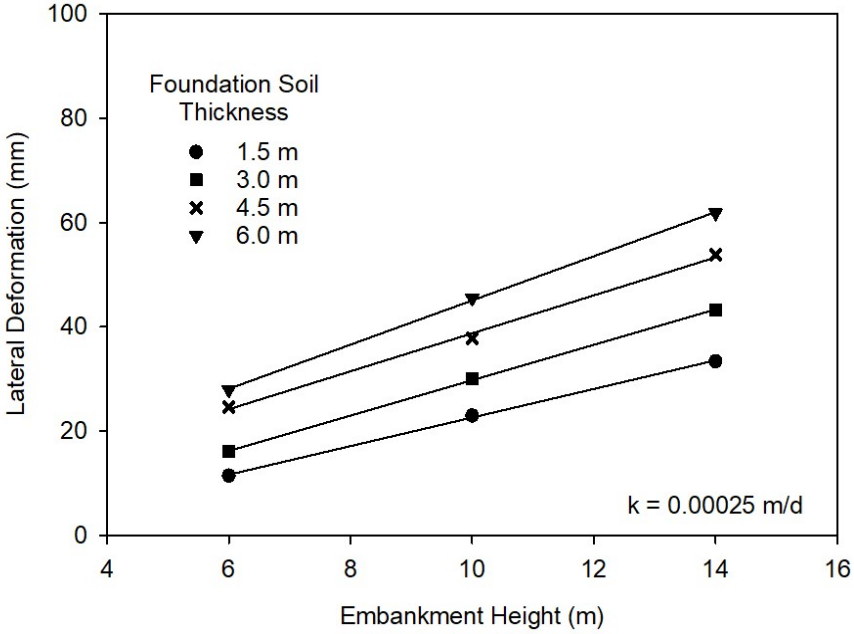

Figure 71. Embankment Height vs. Lateral Deformation of the Toe: Stiff Soil and Medium Permeability

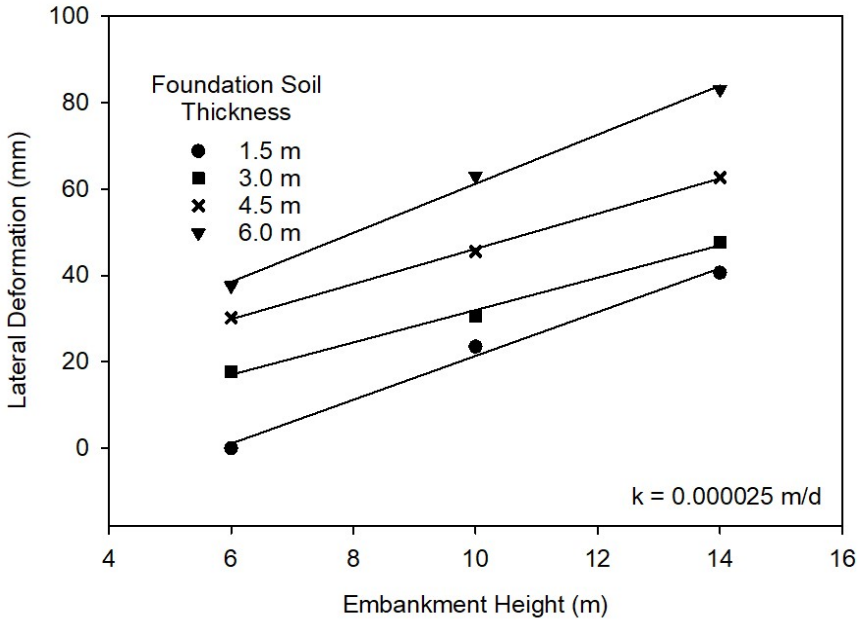

Figure 72. Embankment Height vs. Lateral Deformation of the Toe: Stiff Soil and Low Permeability

The stiff soil (Figures 70 through 72) was the only full set of analyses that every scenario was successfully calculated. Similar trends are found for the stiff soil, however, the stiff soil results tend to be less non-linear. The only graph for the stiff soil showing erratic behavior is when the permeability is 0.000025 m/d, this is similar to what was found with the other soil strengths considered.

As expected, the largest lateral movement was measured when the embankment height was the greatest and the foundation soil strength was the lowest. It is also important to notice that the largest vertical movements for each scenario occurred when the foundation soil layer was the thickest, 6 m for this study. The majority of lateral movement is believed to occur during undrained loading (Leroueil et.al, 1999; Ellis and Springman, 1999). When the soil is experiencing undrained one-dimensional loading any vertical displacement must have an equivalent lateral displacement since no water is allowed to escape and the water and soil particles are assumed incompressible.

The settlement would increase as the embankment height increased and as the foundation soil thickness increased with all other variables kept equal.

Visually the lateral movement as a function of embankment height appears to become more predictable as the soil strength increases. For example when comparing the soft foundation soil and the stiff foundation soil (Figures 65 and 70), the slopes of the trendlines for different foundation layer thickness is similar for the stiff soil, whereas the slopes of the trendlines for the soft soil are quite different. This is likely attributed to the increasing non-linearity when the soil is softer and is approaching a failure state. The trend line slopes calculated by the graphing software, SigmaPlot, have been tabulated and are presented in Table 16 to better understand the rate of change with respect to embankment height for the different heights and soils analyzed.

Table 16. Approximate Trendline Slope for Height-Lateral Displacement Comparison

Foundation Soil Thickness (m)	Soft Soil	Medium Soil	Stiff Soil
Permeability = 0.0025 m/d			
1.5	2.8	3.0	2.7
3	4.7	4.5	3.4
4.5	6.5	4.7	3.6
6	8.6	5.8	4.2
Permeability = 0.00025 m/d			
1.5	3.8	3.9	3.1
3	8.3	5.1	3.6
4.5	7.7	5.5	3.6
6	9.3	6.3	5
Permeability = 0.000025 m/d			
1.5	-	6.6	5.1
3	-	6.3	3.7
4.5	-	6.3	4.1
6	-	-	5.6

The table shows that as the soil strength increases the change in the slope with respect to foundation soil thickness reduces suggesting a more predictable behavior for stiffer soil. The slopes for the stiffer soils are also smaller than those for the softer soils suggesting that the height of the embankment has a larger impact on the deformation behavior when the foundation soils are softer. In addition, the soft soil appears to be influenced heavily by additional variables.

7.2.2 Influence of Foundation Soil Permeability on Lateral Displacement

The foundation soil permeability is believed to have a fairly significant impact on the lateral deformation behavior of the embankment. Based on the analyses comparing the influence of embankment height on the lateral deformation, it is apparent that the permeability does impact

the behavior as can be seen in Table 16. To get a comprehensive comparison it is necessary to compare changes in permeability with the displacement for a series of embankments. Unfortunately, the soft soil used in this analysis had calculation failure for many of the embankments when the permeability was the lowest value, 0.000025 m/d. While the softest soil would likely provide the most useful comparison such a comparison was not possible. As a compromise the medium stiff soil was instead compared since the majority of the analyses were successfully completed. Initially the permeability was plotted against the lateral deformation for each embankment height further divided by foundation soil thickness to isolate the effects of permeability. The following figure is how the typical graph turned out when compared in that manner.

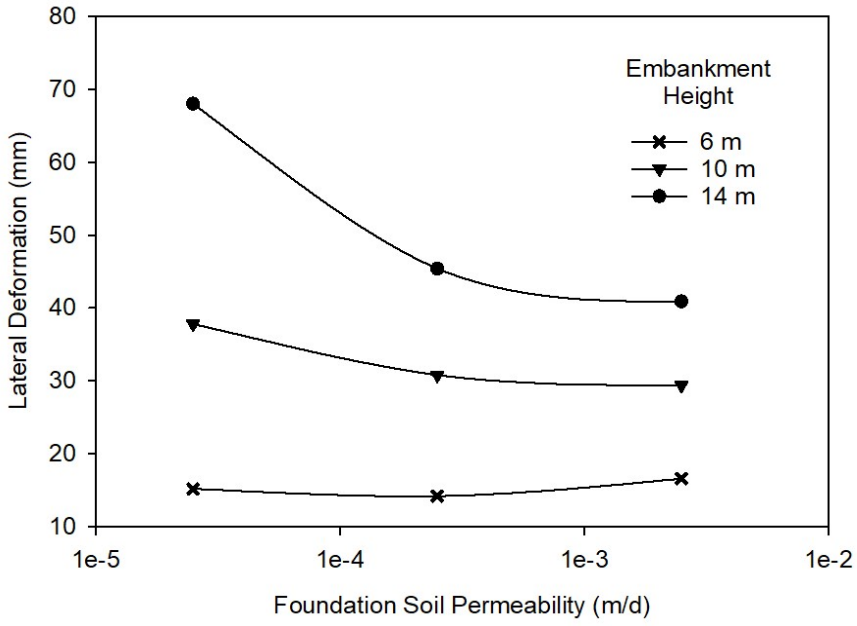

Figure 73. Permeability vs. Lateral Deformation of the Toe: Medium Soil and 3 m Foundation Thickness

The graph, plotted on a semi-log scale, shows that the permeability has a fairly significant impact on the lateral deformation of the embankment. The impact is most notable as the permeability decreases from 0.00025 to 0.000025 m/d.

To better visualize the influence of permeability, various parameters were explored to normalize the data so that more of the results could be compared. Unfortunately, no such parameter was found. Instead the average lateral deformation for a given embankment height was plotted for each permeability. A chart presenting the influence of foundation permeability for the medium strength soil is shown below.

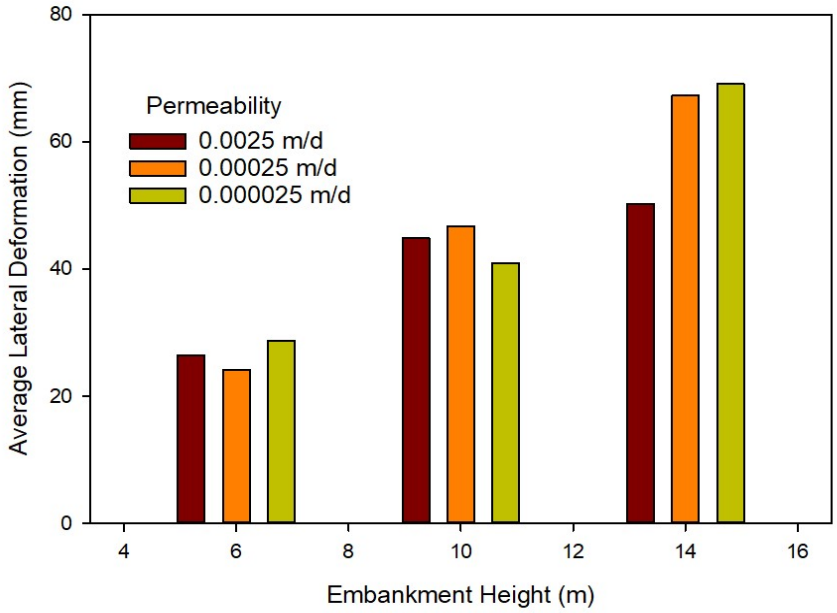

Figure 74. Influence of Permeability on Lateral Displacement – Medium Foundation Soil

According to the chart, while permeability does have some influence on the lateral displacement, the influence is not linear with respect to changing permeability. It can be seen that the lowest permeability foundation soil, on average, experienced less lateral displacement than the other two permeabilities when the embankment height was 10 m. Based on the bar graph above

there doesn't appear to be a direct linear relationship between permeability and lateral displacement.

7.2.3 Influence of on Embankment Foreslope on Lateral Displacement

The embankment foreslope is anticipated to influence the lateral displacement. The case study presented in this dissertation, SH 3 over BNSF Railroad, experienced substantial lateral displacement and had a very steep foreslope. The foreslope for the case study was approximately 2H:1V. The only foreslopes included in this study were 3H:1V and 4H:1V since those are the general foreslopes used for bridge embankments when obstacles such as railroads or other obstructions aren't an issue. Many efforts were made to find a sensible way to compare the two foreslopes in this study without depending on other output parameters. Unfortunately, such a relationship was not found. To provide a useful comparison, the lateral displacement has been plotted against the embankment settlement for each foreslope and one foundation soil permeability, 0.00025 m/d. The graph presenting the relationship is shown below.

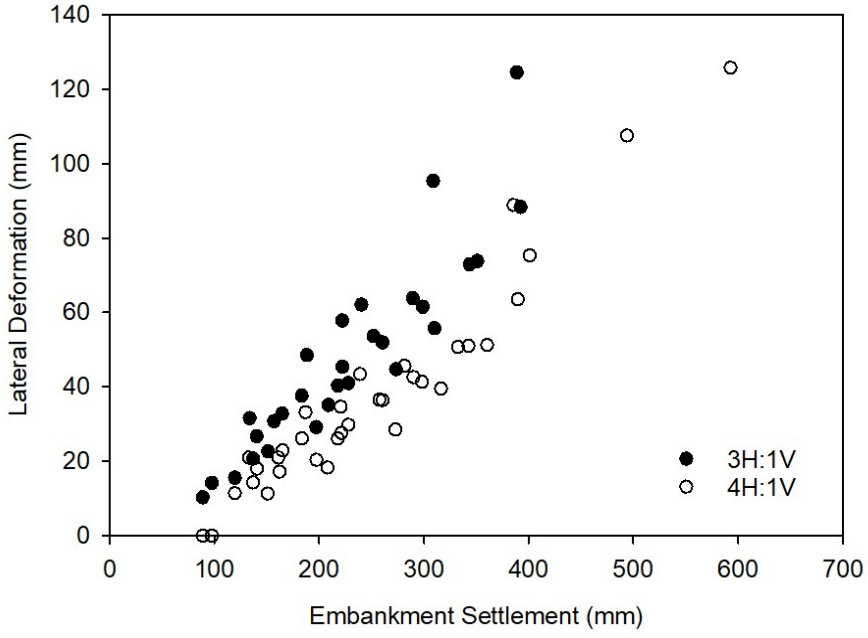

Figure 75. Influence of Foreslope on Lateral Displacement

Reducing the foreslope from a 3H:1V to a 4H:1V reduces the lateral deformation of the embankment. The results follow a similar trend, but in the majority of cases it appears that a reduction can be achieved by changing the foreslope. It should be noted that the reduction is not that large and the additional space and costs needed for a shallower foreslope likely wouldn't justify the benefit from the reduced lateral deformation. Figure 75 shows a strong relationship between the embankment settlement and the lateral deformation, this relationship will be explored in a subsequent section.

7.2.4 Influence of Soil Strength on Lateral Displacement

The soil strength will have an impact on the lateral displacement a piled bridge embankment experiences. Ideally one strength parameter would be used to indicate the strength of the entire soil layer. For this study the strength parameter used was the maximum shear strength determined using simulated triaxial compression tests when the soil was subjected to in-situ effective stress conditions. Due to the fairly large number of variables a straightforward meaningful comparison could not be done. Several of the variables had to be grouped along with the strength to better assess the impact of changing shear strength on the lateral deformation. The best fit group of variables were a ratio of the increase in vertical stress and the soil shear strength; the ratio is as follows:

$$\left(\frac{\Delta\sigma}{S}\right)t$$

$\Delta\sigma$ = increase in vertical stress from embankment loading (γ_{emb}*H)

H = embankment height

S = soil shear strength as determined from triaxial compression at in-situ effective stress

t = foundation soil thickness

The comparison graphs showing the impact of soil strength, presented below, are further separated by embankment foreslope and foundation soil permeability.

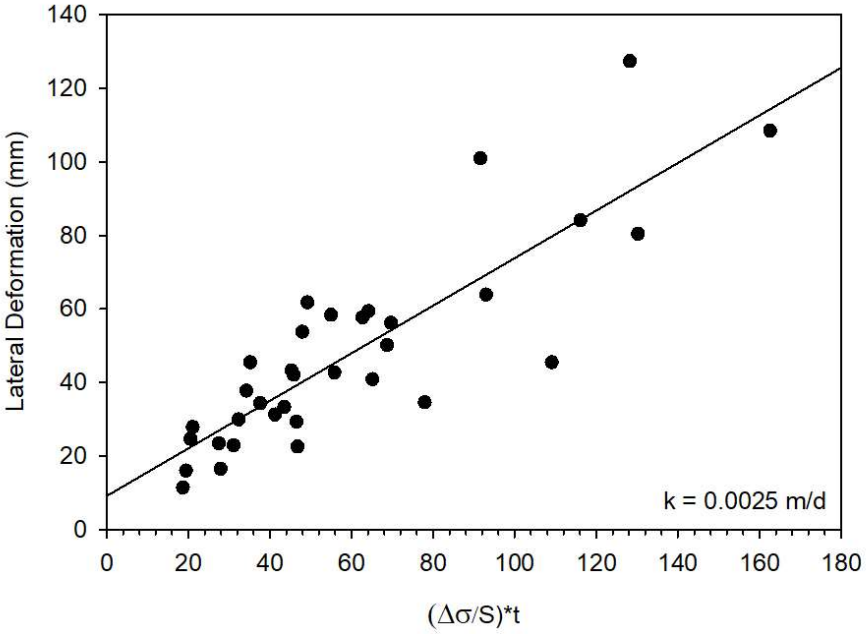

Figure 76. Soil Strength - 3:1 Foreslope High Permeability

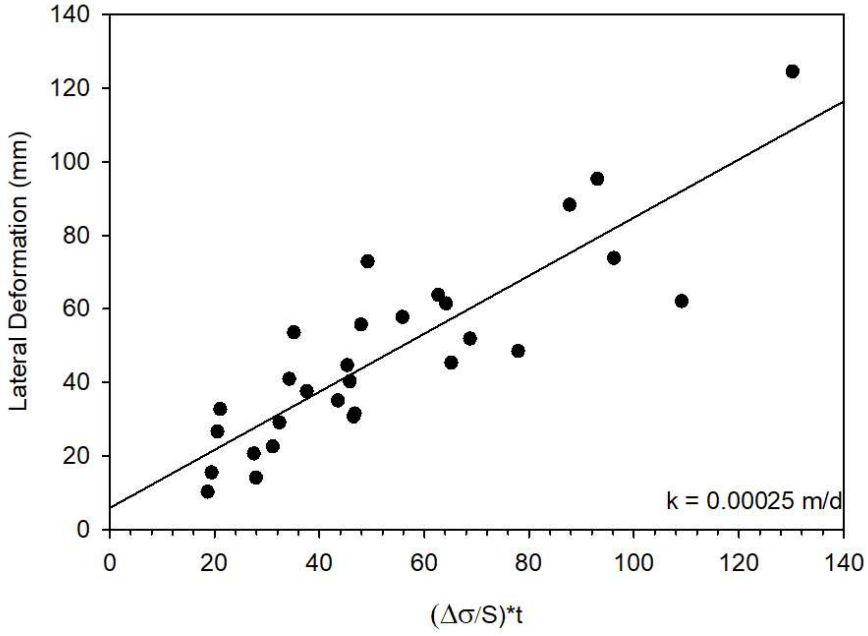

Figure 77. Soil Strength - 3:1 Foreslope Medium Permeability

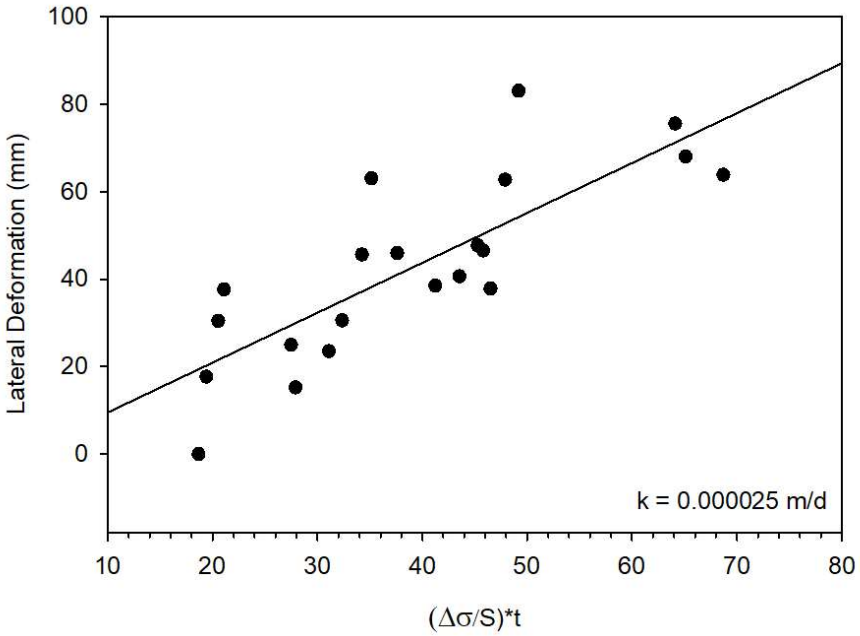

Figure 78. Soil Strength - 3:1 Foreslope Low Permeability

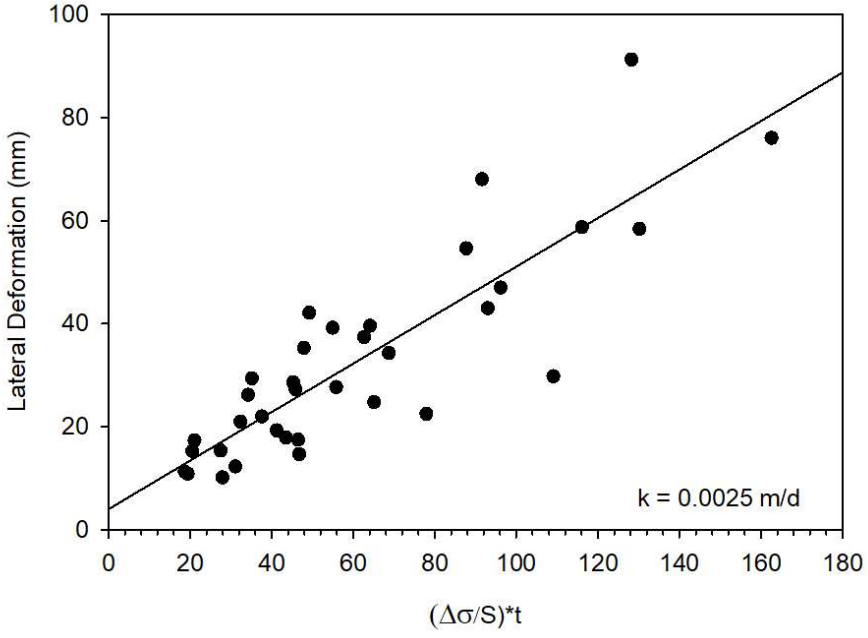

Figure 79. Soil Strength - 4:1 Foreslope High Permeability

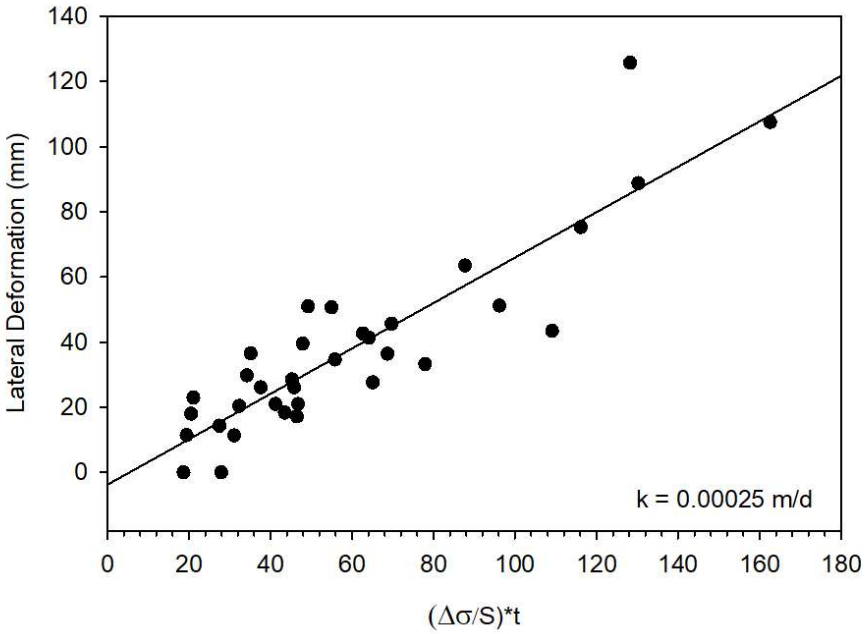

Figure 80. Soil Strength - 4:1 Foreslope Medium Permeability

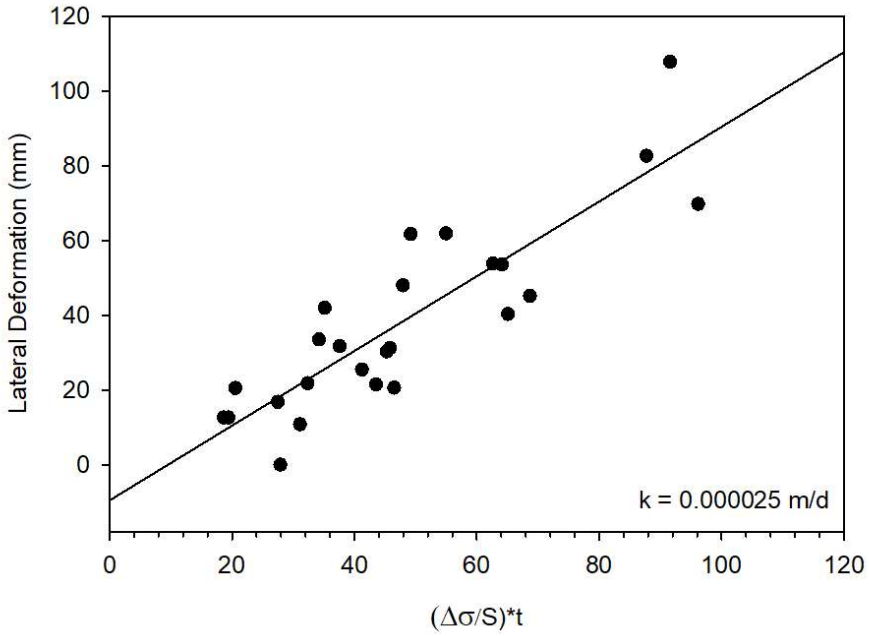

Figure 81. Soil Strength - 4:1 Foreslope Low Permeability

The relationship presented in Figures 76 through 81 show that as the ratio increases the lateral displacement also increases. Since the soil strength is in the denominator the ratio is inversely proportional to the soil strength, the behavior in the figures is what would be expected for the lateral displacement.

To better visualize the impact of soil strength on the lateral deformation with respect to changing permeability and foreslope, the slopes of the trendline and the coefficient of determination (R^2) values have been calculated by the graphing software and tabulated. The tabulated results are presented in Table 17.

Table 17. Soil Strength Trendline Slope and Coefficient of Determination

Permeability	Trendline Slope	R^2
Embankment Foreslope = 3H:1V		
0.0025	0.65	0.73
0.00025	0.78	0.75
0.000025	1.14	0.64
Embankment Foreslope = 4H:1V		
0.0025	0.47	0.74
0.00025	0.69	0.79
0.000025	1.0	0.75

The soil strength appears to play a larger role as the permeability decreases as indicated by the increasing trendline slopes. It should be noted that as the permeability decreases the coefficient of determination also decreases, likely due to increasing non-linearity in the analyses.

7.2.5 Influence of Embankment Settlement on Lateral Displacement

As shown previously in Figure 75 there appears to be a strong correlation between the settlement and lateral deformation an embankment experiences. This relationship was previously presented by Hannigan et al. (2016). They suggested that the lateral deformation was

approximately 25% of the vertical settlement. A composite graph including the settlements and lateral deformations of all analyses completed is shown below.

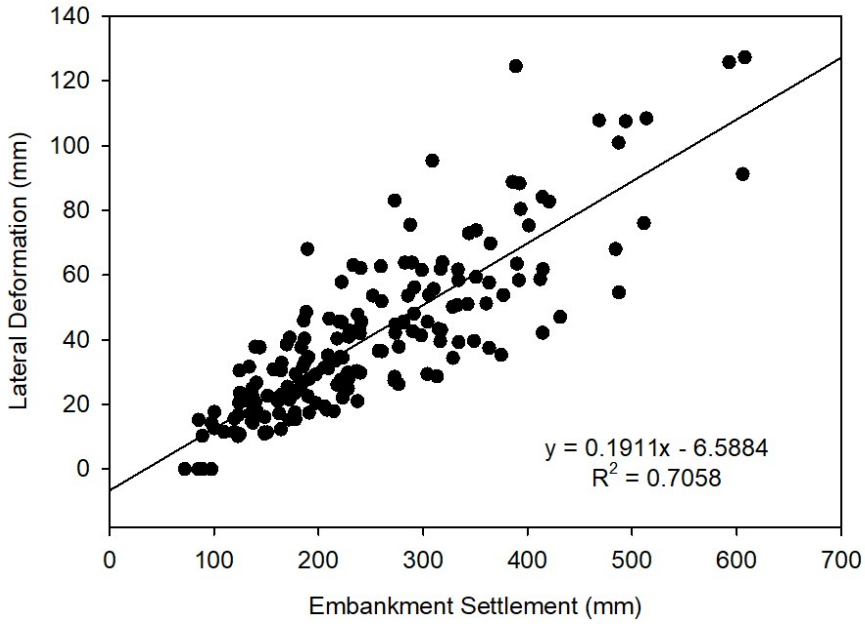

Figure 82. Influence of Settlement: Composite

The relationship has a fair amount of scatter, but it is also fairly close to the approximation suggested by Hannigan et al. (2016). In the composite analyses the lateral deformation is closer to 20% of the embankment settlement. It is suspected that the permeability will play a key role in this relationship since the magnitude of undrained loading will directly influence the ratio. To negate any effects introduced from changing permeability, plots for each permeability tested are shown below.

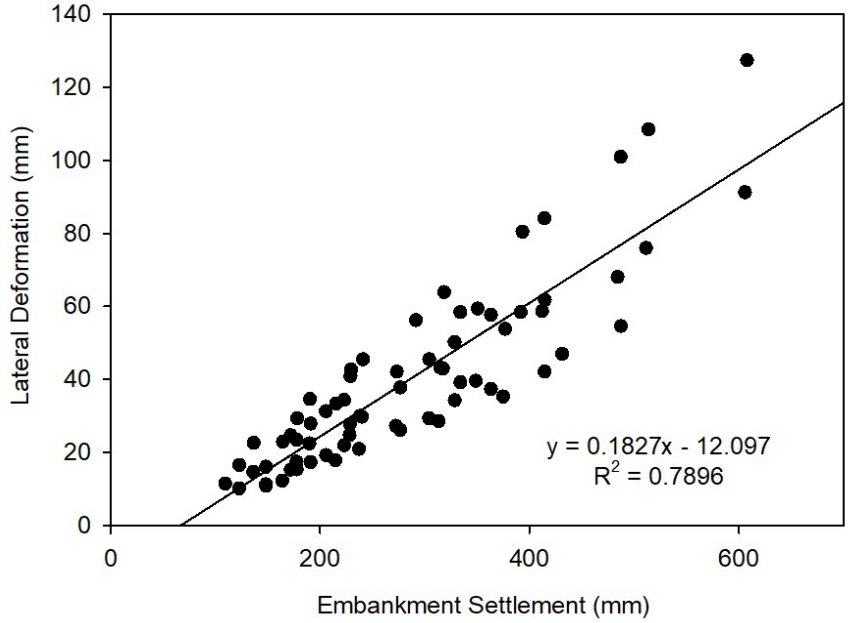

Figure 83. Influence of Settlement: High Permeability

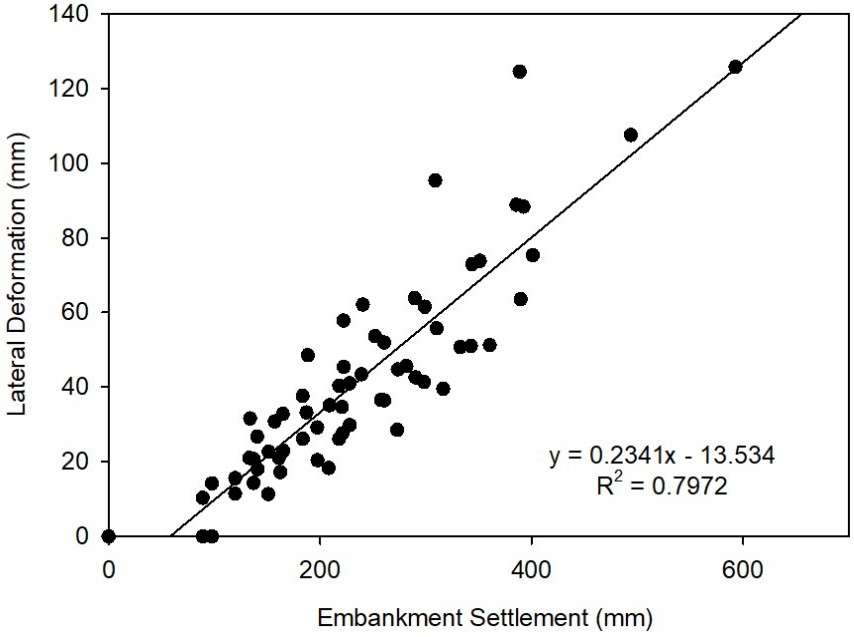

Figure 84. Influence of Settlement: Medium Permeability

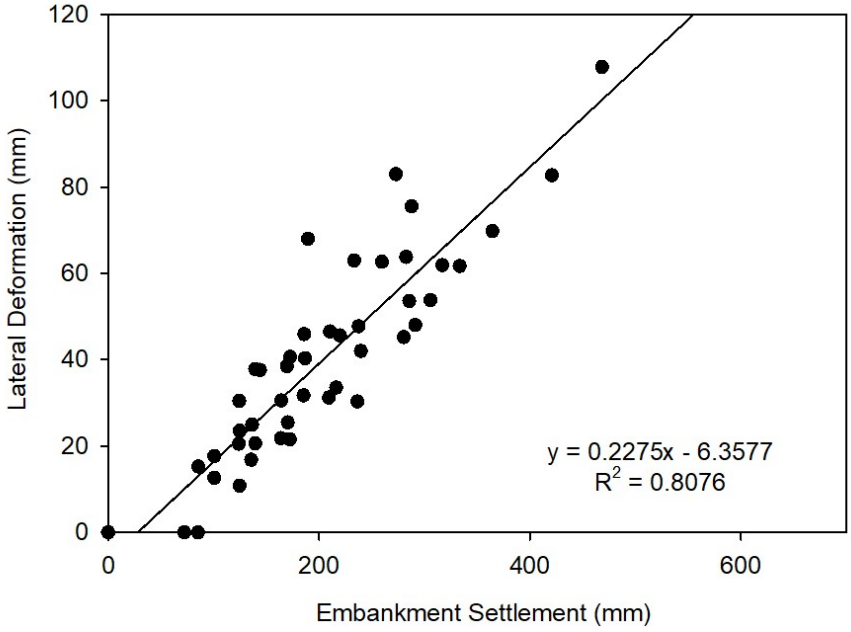

Figure 85. Influence of Settlement: Low Permeability

Better agreement was found when the effects of changing permeability were removed from the plots. It also appears that the correlation between lateral deformation and embankment settlement tends toward the relationship suggested by Hannigan et al. (2016), while never quite reaching the 25% relationship. In Figures 83, 84, and 85, a negative y-intercept was found cab be seen. A negative y-intercept implies that some settlement can occur without any lateral deformation and is a plausible scenario. Equating the lateral deformation to 25% of the embankment settlement may be a somewhat conservative approach although notice that the relationship was closer to 30% in some of the scenarios studied.

7.2.6 Proposed Empirical Relationship

One of the goals of this research was to develop an analytical method to evaluate the magnitude or potential for lateral spreading of piled bridge abutments. While the relationship in the previous section is fairly reasonable and the settlement is easily calculated and a routine part of the design process a procedure involving only the input variables to determine the lateral

displacement was desired. Use of traditional settlement parameters were not used in the development of the relationship since these values, included in the soil model as λ and κ, were not varied for the parametric study. Instead a relationship based on the absolute strength of the soil, geometry of the embankment, and soil stratigraphy was developed. The relationship is empirical in nature and is dependent on the input units. The empirical equation is as follows:

$$L_{disp} = \left(\frac{\Delta\sigma}{2S}\right)t^2 \times \tan(\beta) + \ln\left(\frac{H}{t}\right)t \quad (42)$$

L_{disp} = lateral displacement at toe of embankment (mm)

$\Delta\sigma$ = increase in vertical stress in the foundation soil from embankment loading (γ_{emb}*H) (kPa)

H = embankment height (m)

S = foundation soil shear strength as determined from triaxial compression at in-situ effective stress (kPa) prior to loading

t = foundation soil layer thickness (m)

β = angle between the foreslope and the ground surface

The equation has the following assumptions:

- Foundation soil permeability >0.000025 m/d
- Foundation layer thickness <6 m
- Foundation soil can be idealized as single layer
- Foundation soil layer is horizontal
- Embankment foreslope not steeper than 3H:1V
- Embankment top is horizontal (not slanted)
- Bridge piling is oriented in strong axis bending

The equation has been plotted against the lateral displacement predicted by PLAXIS 2D and is presented in Figure 86.

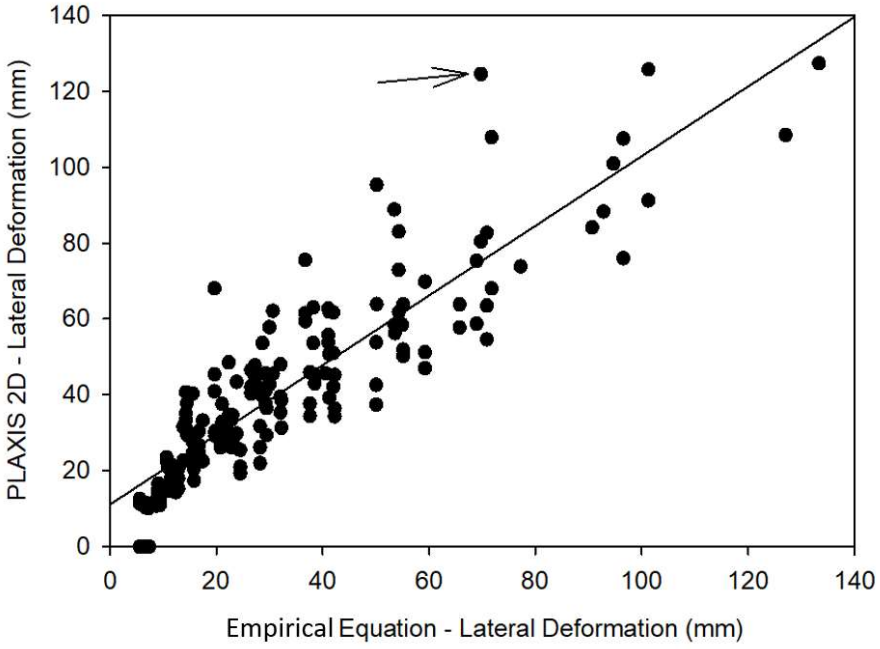

Figure 86. Empirical Equation Predictability

The equation reasonably predicts the lateral deformation of the embankment predicted by PLAXIS 2D. Ideally more data would be needed in the higher range to evaluate the equation's ability for predicting larger deformations. The equation serves as a good first step in estimating the lateral displacement a bridge embankment will experience. The relationship could be used as a check on lateral displacements to help determine if advanced analyses are necessary. It is important to note that in some instances the equation underpredicted the lateral deformation by a significant amount. For example, the data point near the arrow in Figure 86 is underpredicted by approximately 55 mm.

The empirical equation was also used to estimate the lateral deformation of the test embankments presented in Chapter 5. The test embankments did not contain piles and the maximum lateral deformation is taken in the foundation soils where inclinometer data is available.

Since the test embankments contained multiple foundation soil layers the lateral deformation was calculated using a weighted average of the foundation soil shear strength (S) for the soft soil layers, the stiffer layers (S > 30 kPa) were omitted from the calculation. The comparison is shown in Figure 87.

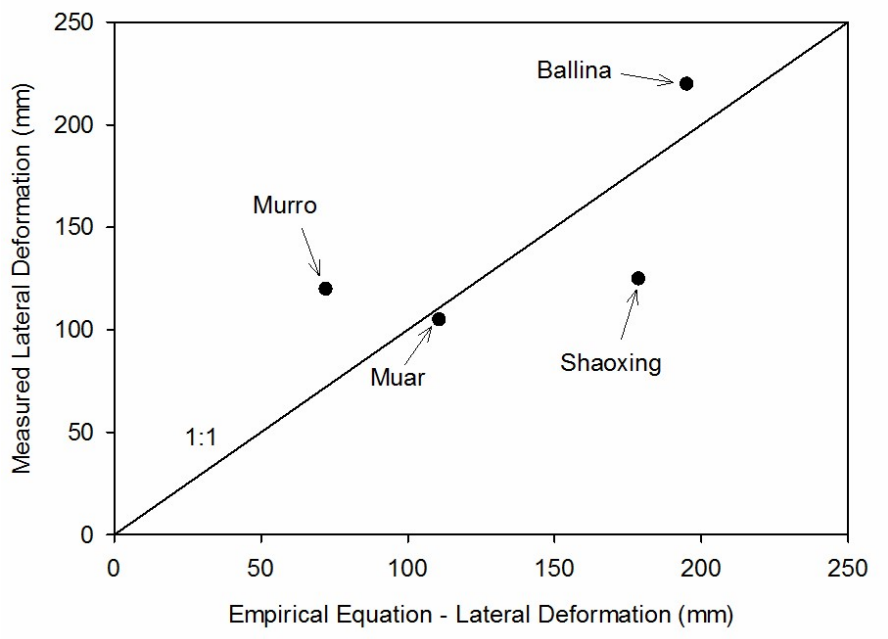

Figure 87. Test Embankment Empirical Equation Predictability

The empirical equation predicts the lateral deformation reasonably well, excluding in the case of the Murro test embankment. The Murro test embankment foundation soils had the lowest permeability of the test embankments shown which likely contributed to the discrepancy in the prediction. The Shaoxing test embankment deformation is overpredicted by approximately 50 mm. However, the lateral deformation profile for the Shaoxing test embankment was recorded 160 days after construction, thus the lateral deformation for the embankment was likely not completed at the time of the profile readings. This comparison further supports that the empirical equation could be used for estimating the lateral deformation of embankments.

7.3 Recommendations for Piled Bridge Embankments on Soft Soils

A parametric study was completed to better understand the lateral deformation behavior of piled bridge abutments. A better understanding of the lateral behavior would assist bridge designers and have the potential to mitigate bridge distress as a result of excessive lateral deformation of bridge embankments. By use of the present study it was found or verified that the following scenarios increase the potential for lateral deformations of piled bridge abutments:

- A steeper foreslope
- Softer foundation soil
- Thicker foundation soil layers
- Lower permeability soils
- Taller embankments

The influence of the above variables on the lateral displacement is not linear in nature and tend to become more dramatic as failure condition is approached.

Two methods have been proposed to estimate the magnitude of lateral deformation a piled bridge embankment will experience: equal to approximately 25% of the vertical settlement and the empirical equation, Equation 42. The empirical equation, while tentative, can provide a reasonable estimation of the lateral displacement an embankment will experience. For example, when the case study presented in Chapter 6 was analyzed using the empirical equation the lateral displacement calculated was 88.3 mm. During the finite element analysis 80.1 mm was observed. It should be noted that the empirical equation was developed based on movement at the toe while the case study measurement comes from the pile top, however an estimated displacement of that magnitude would have warranted advanced analysis. The following recommendations are made regarding when to pursue advanced analysis such as the finite element modeling:

- When the foundation soil permeability is <0.0005 m/d
- When the foreslope is steeper than 3H:1V
- When the foundation is anticipated to experience more than 80 mm of settlement
- When the lateral displacement, as calculated using Equation 42, exceeds 20 mm

8.0 CONCLUSIONS AND RECOMMENDATIONS

8.1 Major Contributions of Research

This research focused on studying the lateral deformation behavior of embankments, with and without piled bridge abutments. To support this research an advanced soil constitutive model, the Bounding Surface Plasticity Model for isotropic clayey soils, was implemented into the commercial finite element software PLAXIS 2D. Following the implementation, the ability of the Bounding Surface Plasticity model to estimate the deformation behavior of embankments was evaluated. The evaluation involved calibrating the soil model and modeling four heavily instrumented test embankments in locations spanning from Finland to Australia: the Ballina, Shaoxing, Murro, and Muar test embankments. Once the abilities of the model were validated, the influence of piles, such as those found under a bridge abutment, on the lateral displacement was evaluated. The influence of bridge piling was evaluated through the use of a case study: SH 3 over BNSF Railroad in Ada, Oklahoma. The SH 3 over BNSF Railroad bridge has been monitored by the University of Oklahoma since 2012 and experienced problems related to lateral movement of the embankment soon after its construction in 1983. To support the analysis a geotechnical site investigation was carried out and followed up by a fairly extensive laboratory testing program. Finally, a trial embankment was developed and a parametric study was carried out by systematically varying certain input parameters. The parametric study was completed to better understand the impact of various input parameters on the lateral deformation behavior of the embankment.

The following are considered the major contributions of this research:

1. The Bounding Surface Plasticity model was implemented into PLAXIS 2D. The implemented soil model is stored as a Dynamic Link Library and can be distributed for use by other practitioners.
2. The foundation soil for the four test embankments has been calibrated for the Bounding Surface Model. The calibrated soils can now be used by researchers to further study the behavior of the four test embankments.
3. The influence of bridge piling on the lateral deformation behavior was studied in a limited capacity.
4. Finite element modeling was completed on a case study, SH 3 over BNSF Railroad. The modeling further validates the original hypothesis regarding the initial source of the distress experienced by the bridge.
5. A parametric study was completed on a trial embankment. The results of the parametric study are included in Appendix C and can be used to find additional relationships regarding the lateral or vertical deformation behavior of piled bridge abutments.
6. Relationships from the parametric study were analyzed and summarized.
7. An empirical equation was developed to estimate the magnitude of lateral deformation of piled bridge abutments.
8. Recommendations for assessing the importance of lateral deformation of piled bridge abutments for the practicing engineer were developed.

8.2 Conclusions

1. The Bounding Surface Plasticity model for isotropic clayey soils is able to effectively capture the lateral and vertical deformation behavior of embankments.

2. The Bounding Surface Plasticity model for isotropic clayey soils is able to effectively capture the behavior in compression and extension when soil is subjected to triaxial stress states.
3. The addition of bridge piling does reduce the lateral deformation of bridge embankments. However, the reduction in lateral deformation is small thus the bridge piling should not be expected to eliminate the potential for lateral deformation of the embankment.
4. As permeability decreases the potential for lateral deformation increases.
5. As the embankment height increases the lateral deformation of the embankment will increase.
6. As the foundation soil layer thickness increases the potential for lateral deformation also increases.
7. A bridge embankment with a steeper foreslope will experience more lateral deformation than one with a shallow foreslope.
8. There is a strong relationship between the embankment vertical settlement and the lateral deformation the embankment experiences.
9. Due to the highly non-linear nature of lateral deformation it is unlikely that a comprehensive correlation equation can be developed. That is not to say that methods cannot be developed for different scenarios.

8.3 Recommendations for Future Research

1. Develop and construct a scaled centrifuge model with bridge piles and monitor the lateral deformation at the toe of the embankment, crest of the embankment, and the vertical settlement of the embankment. This would allow for the finite element implementation to

be further validated and would also assist with better understanding of the factors that cause lateral deformation to occur in piled bridge embankments.

2. Instrument a bridge abutment and adjacent embankment where lateral deformation is anticipated to occur. The deformation would not need to be of the magnitude to cause severe bridge distress in order to provide meaningful data.
3. Expand the parametric study to include a larger range of foundation thicknesses, embankment heights, foreslopes, soil strengths and permeabilities.
4. Expand the parametric study to include the presence of more than one foundation layer, consider including a harder layer over a softer layer.
5. Expand the parametric study to include slanted foundation layers.
6. Expand the parametric study to include bearing the piles in a harder layer below the soft foundation layer.
7. Expand the parametric study to include embankments that are not uniform thickness. This would cause the maximum height of the embankment to occur at the location of bridge abutment possibly leading to more lateral deformation of the embankment.
8. Develop a database of already constructed bridge embankment parameters and foundation soil information along with estimated or observed lateral deformation. Use the empirical equation, Equation 42, to evaluate the effectiveness of the equation and make further modifications as necessary to capture the behavior of full-scale embankments.
9. Perform a sensitivity study to investigate the effect of the with Bounding Surface Plasticity model parameters on bridge embankments.

REFRENCES

American Association of State Highway and Transportation Officials (AASHTO). (2014). AASHTO LRFD Bridge Design Specifications, US Customary Units, Seventh Edition, with 2015 Interim Revisions. American Association of State Highway and Transportation Officials, Washington, D.C., 1960 p.

Allen, David L.; Meade, Bobby W.; and Hopkins, Tommy C., (1985) "Analyses of Movements and Forces on Bridge Approaches: A Case Study (Bridge over Chesapeake Ave. on Interstate 471 in Campbell County, Kentucky)". *Kentucky Transportation Center Research Report*. 767.

Amirebrahimi, A. M., & Herrmann, L. R. (1993). "Continuum model and analyses of wick-drained systems". *International Journal for Numerical and Analytical Methods in Geomechanics*, *17*(12), 827-847.

Bourges, F., & Mieussens, C. (1979). Deplacements lateraux a proximite des remblais sur sols compressibles-methode de prevision. *BULL LIAISON LAB PONTS CHAUSS*, (101).

Bozozuk, M. (1978). "Bridge foundations move". *Transportation Research Record*, *678*, 17-21.

Chai J., Carter J.P. (2011) Vertical Drains. In: *Deformation Analyses in Soft Ground Improvement. Geotechnical, Geological, and Earthquake Engineering*, vol 18. Springer, Dordrecht. https://doi-org.ezproxy.lib.ou.edu/10.1007/978-94-007-1721-3_3

Chai, J. C., Sakajo, S., & Miura, N. (1994). "Stability analyses of embankment on soft ground: a case study". *Soils and foundations*, *34*(2), 107-114.

Chang, T. Y. (1980). A nonlinear finite element analyses program NFAP. *Civ. Engrg. Dept., Tech. Report Univ. of Akron*.

Crawford, Fannin, & Kern. (1995). "Embankment failures at Vernon, British Columbia". *Canadian Geotechnical Journal*, 32(2), 271-284.

Dafalias, Y. F., & Herrmann, L. R. (1986). "Bounding surface plasticity. II: Application to isotropic cohesive soils". *Journal of Engineering Mechanics*, *112*(12), 1263-1291.

De Beer, E. E. (1977). "The effects of horizontal loads on piles, due to surcharge or seismic effects". In *Proc. the 9th ICSMFE* (Vol. 558). Tokyo, Japan.

Doherty, J.P., Gourvenec, S., Gaone, F.M., Pineda, J.A., Kelly, R., O'Loughlin, C.D., Cassidy, M.J., Sloan, W. (2018). "A novel web based application for storing, managing and sharing geotechnical data, illustrated using the national soft soil field testing facility in Ballina, Australia", *Computers and Geotechnics,* Volume 93, Pages 3-8, ISSN 0266-352X, https://doi.org/10.1016/j.compgeo.2017.05.007.

Ellis, E. A., & Springman, S. M. (2001). “Full-height piled bridge abutments constructed on soft clay”. *Geotechnique*, *51*(1), 3-14.

Ensoft Inc. (2019). *LPILE v2019 user’s manual: a program for the analyses of deep foundations under lateral loading*.

Fredlund D.G., Rahardjo H., (1993) *Soil Mechanics for Unsaturated Soils*, John Wiley & Sons,

Goh, A. T. C., Teh, C. I., & Wong, K. S. (1997). “Analyses of piles subjected to embankment induced lateral soil movements”. *Journal of geotechnical and geoenvironmental engineering*, *123*(9), 792-801.

Hansbo, S. (1980). “Consolidation of fine-grained soils by prefabricated drains”. In *Proc. of. the. 10th ICSMFE* (Vol. 3, pp. 677-682).

Hannigan, P. J., Rausche, F., Garland, L. E., Robinson, B. R., Becker, M. L., & Shelsta, H. (2016). *Design and construction of driven pile foundations*. US Department of Transportation, Federal Highway Administration.

Herrmann, L. R., & Kaliakin, V. N. (1987). “User's manual for SAC-2, a two-dimensional nonlinear, time dependent, soil analyses code using the bounding surface elastoplasticity-viscoplasticity model”. *Volumes I and II, Department of Civil Engineering Report, University of California, Davis.*

Herrmann, L. R., & Mish, K. D. (1983). *User's Manual for SAC-2. A Two-Dimensional Nonlinear, Time Dependent Soil Analyses Code Using the Bounding Surface Plasticity Model*. CALIFORNIA UNIV DAVIS.

Hird, C. C., Pyrah, I. C., Russell, D., & Cinicioglu, F. (1995). “Modeling the effect of vertical drains in two-dimensional finite element analyses of embankments on soft ground”. *Canadian Geotechnical Journal*, *32*(5), 795-807.

Huang, W., Fityus, S., Bishop, D., Smith, D., & Sheng, D. (2006). “Finite-element parametric study of the consolidation behavior of a trial embankment on soft clay”. *International Journal of Geomechanics*, *6*(5), 328-341.

Indraratna, B, Balasubramaniam, A. S, & Balachandran, S. (1992). “Performance of Test Embankment Constructed to Failure on Soft Marine Clay”. *Journal of Geotechnical Engineering*, 118(1), 12-1.

Indraratna, B., Balasubramaniam, A. S., & Ratnayake, P. (1994). “Performance of embankment stabilized with vertical drains on soft clay”. *Journal of Geotechnical Engineering*, *120*(2), 257-273.

Indraratna, B, & Redana, I. W. (1997). "Plane-Strain Modeling of Smear Effects Associated with Vertical Drains". *Journal of Geotechnical and Geoenvironmental Engineering, 123*(5), 474-478.

Jones, C.A., Stewart, D.I. and Danilewicz, C.J. (2008) *Bridge distress caused by approach embankment settlement*. Geotechnical Engineering, 161 (2). pp. 63-74. ISSN 1353-2618

Kaliakin, V. (1985). *Bounding Surface Elastoplasticity-Viscoplasticity for Clays*. Ph. D. Thesis presented to the Univ. of California at Davis.

Kaliakin, V. N., Dafalias, Y. F., & Herrmann, L. R. (1987). "Time dependent bounding surface model for isotropic cohesive soils". *Notes for a short course. Tucson, Ariz*.

Kaliakin, V. N., & Herrmann, L. R. (1991). Guidelines for implementing the elastoplastic-viscoplastic bounding surface model. *Technical Rep., Department of Civil Engineering, Univ. of California, Davis, Calif*.

Karstunen, M., Krenn, H., Wheeler, S. J., Koskinen, M., & Zentar, R. (2005). "Effect of anisotropy and destructuration on the behavior of Murro test embankment". *International Journal of Geomechanics*, *5*(2), 87-97.

Karstunen, M., Wiltafsky, C., Krenn, H., Scharinger, F., & Schweiger, H. F. (2006). "Modeling the behaviour of an embankment on soft clay with different constitutive models". *International journal for numerical and analytical methods in geomechanics*, *30*(10), 953-982.

Karstunen, M, & Yin, Z.-Y. (2010). "Modeling time-dependent behaviour of Murro test embankment". *Géotechnique, 60*(10), 735-749.

Kelesoglu, M. K., & Cinicioglu, S. F. (2009). "Free-field measurements to disclose lateral reaction mechanism of piles subjected to soil movements". *Journal of geotechnical and geoenvironmental engineering*, *136*(2), 331-343.

Kelly, R. B., Sloan, S. W., Pineda, J. A., Kouretzis, G., & Huang, J. (2018). "Outcomes of the Newcastle symposium for the prediction of embankment behaviour on soft soil". *Computers and Geotechnics*, *93*, 9-41.

Koskinen, M., Vepsäläinen, P., and Lojander, M. (2002). "Modeling of anisotropic behavior of clays (Test embankment in Murro, Seinäjoki, Finland)." Finnra Rep. No. 16/2002, Finnish Road Administration, Helsinki, Finland.

Leroueil, S., Magnan, J. P., & Tavenas, F. (1990). *Embankments on soft clays*.

Leroueil, S., Tavenas, F., Mieussens, C., & Peignaud, M. (1978). “Construction pore pressures in clay foundations under embankments. Part II: Generalized behavior”. *Canadian Geotechnical Journal, 15*(1), 66-82.

Leroueil, S., & Vaughan, P. R. (1990). “The general and congruent effects of structure in natural soils and weak rocks”. *Géotechnique*, *40*(3), 467-488.

Martin, G. R., & Chen, C. Y. (2005). “Response of piles due to lateral slope movement”. *Computers & structures*, *83*(8-9), 588-598.

McCarron, W. and Chen W.F. (1987). “Application of a bounding surface model to Boston blue clay”. *Computers & Structures., 26*(6), 887.

Meade, B. W., & Allen, D. L. (1988). Soil-Bridge Abutment Interaction.

Miller, G. A., Hatami, K., Cerato, A. B., & Osborne, C. (2013). “Applied approach slab settlement research, design/construction” Technical Report (No. FHWA-OK-13-09). University of Oklahoma. School of Civil Engineering and Environmental Science.

Muraleetharan, K.K., Miller, G., Floyd, R., Zhang, B., Taghavi, A., Bounds, T., and Bright, Z. (2018). "Overturning forces at bridge abutments and the interaction of horizontal forces from adjacent roadways." Technical Report (No. FHWA-OK-17-03), Oklahoma Department of Transportation.

Oliveira, P. J. V., & Lemos, L. J. (2011). “Numerical predictions of the behavior of soft clay with two anisotropic elastoplastic models”. *Computers and Geotechnics*, *38*(5), 598-611.

Ozawa,Y., and Duncan, J.M. (1973). *A computer Program for Analyses of Static Stresses and Movements in Embankments*. Research Report No. TE-73-4, University of California, Berkeley, California.

Peck, R. B. (1969). “Deep excavations and tunneling in soft ground”. *Proc. 7th ICSMFE, 1969*, 225-290.

PLAXIS. (2019a). *Material Models Manual*, PLAXIS, Delft University of Technology, Delft, Netherlands

PLAXIS. (2019b). *Reference Manual,* PLAXIS, Delft University of Technology, Delft, Netherlands

PLAXIS. (2020). *Reference Manual,* PLAXIS, Delft University of Technology, Delft, Netherlands

Poulos, Harry. (1972). “Difficulties in prediction of horizontal deformations of foundations”. *Journal of the Soil Mechanics and Foundations Division*. 98. 843-848.

Poulos, H. G. (1973). “Analyses of piles in soil undergoing lateral movement”. *Journal of Soil Mechanics & Foundations Div*, *99*(Tech Rpt).

Qu, G., Hinchberger, S. D., & Lo, K. Y. (2009). “Case studies of three-dimensional effects on the behaviour of test embankments”. *Canadian Geotechnical Journal*, 46(11), 1356-1370.

Rezania, Mohammad, Bagheri, Meghdad, Mousavi Nezhad, Mohaddeseh, & Sivasithamparam, Nallathamby. (2017). “Creep analyses of an earth embankment on soft soil deposit with and without PVD improvement”. *Geotextiles and Geomembranes, 45*(5), 537-547.

Roscoe, K., & Burland, J. B. (1968). “On the generalized stress-strain behavior of wet clay”. *Engineering Plasticity*, Cambridge University

Roscoe, K. H., Schofield, A., & Thurairajah, A. (1963). “Yielding of clays in states wetter than critical”. *Geotechnique*, 13(3), 211-240.

Roscoe, K., Shofield, A., & Wroth, C. (1958). “On the yielding of soils”. *Geotechnique*, 9, 71-83

Samtani, N.C. and Nowatzki, E.A. (2006). *Soils and Foundations – Volume 1.* US Department of Transportation, Federal Highway Administration

Shen, S. L., Chai, J. C., Hong, Z. S., & Cai, F. X. (2005). “Analyses of field performance of embankments on soft clay deposit with and without PVD-improvement”. *Geotextiles and Geomembranes*, *23*(6), 463-485.

Silvestri, V. (1983). “The bearing capacity of dykes and fills founded on soft soils of limited thickness”. *Canadian Geotechnical Journal*, 20(3), 428-436.

Smadi, M. M. (2001). “Lateral deformation and associated settlement resulting from embankment loading of soft clay and silt deposits”. Ph.D. thesis, Univ. of Illinois at Urbana-Champaign, Urbana, IL.

Stewart, D. P., Jewell, R. J., & Randolph, M. F. (1993). “Numerical modeling of piled bridge abutments on soft ground”. *Computers and Geotechnics*, 15(1), 21-46.

Stewart, D. P., Jewell, R. J., & Randolph, M. F. (1994). “Design of piled bridge abutments on soft clay for loading from lateral soil movements”. *Geotechnique*, *44*(2), 277-296.

Tavenas, F., Mieussens, C., & Bourges, F. (1979). “Lateral displacements in clay foundations under embankments”. *Canadian Geotechnical Journal, 16*(3), 532-550.

Tschebotarioff, G. (1973). *Foundations: Retaining and earth structures; the art of design and construction and its scientific basis in soil mechanics [by] Gregory P. Tschebotarioff.* (2d ed.). New York: McGraw-Hill.

Turan, Alper; Sangiuliano, Tony; Alam, M. Shahria; and El Naggar, M. Hesham, "Lateral Movements of a Bridge Abutment Due to Compressible Foundation Soils" (2013). *International Conference on Case Histories in Geotechnical Engineering*. 83. http://scholarsmine.mst.edu/icchge/7icchge/session03/83

Wheeler, S. J., Näätänen, A., Karstunen, M., & Lojander, M. (2003). "An anisotropic elastoplastic model for soft clays". *Canadian Geotechnical Journal*, *40*(2), 403-418.

Whittle, A. J. (1987). *A constitutive model for overconsolidated clays with application to the cyclic loading of friction piles*. (Doctoral dissertation, Massachusetts Institute of Technology).

Whittle, A. J., DeGroot, D. J., Ladd, C. C., & Seah, T. H. (1994). "Model prediction of anisotropic behavior of Boston blue clay". *Journal of geotechnical Engineering*, *120*(1), 199-224.

Won-Pyo Hong & Kwang-Wu Lee (2009). "Evaluation of Lateral Movement of Piled Bridge Abutment Undergoing Lateral Soil Movement in Soft Ground". *Marine Georesources and Geotechnology*, 27:3, 177-189, DOI: 10.1080/10641190802625692

Yin, Zhen-Yu, Xu, Qiang, & Yu, Chuang. (2015). "Elastic-Viscoplastic Modeling for Natural Soft Clays Considering Nonlinear Creep". *International Journal of Geomechanics, 15*(5), 2015-10-01, Vol.15 (5).

APPENDIX A: SH 3 over BNSF Railroad Boring Logs

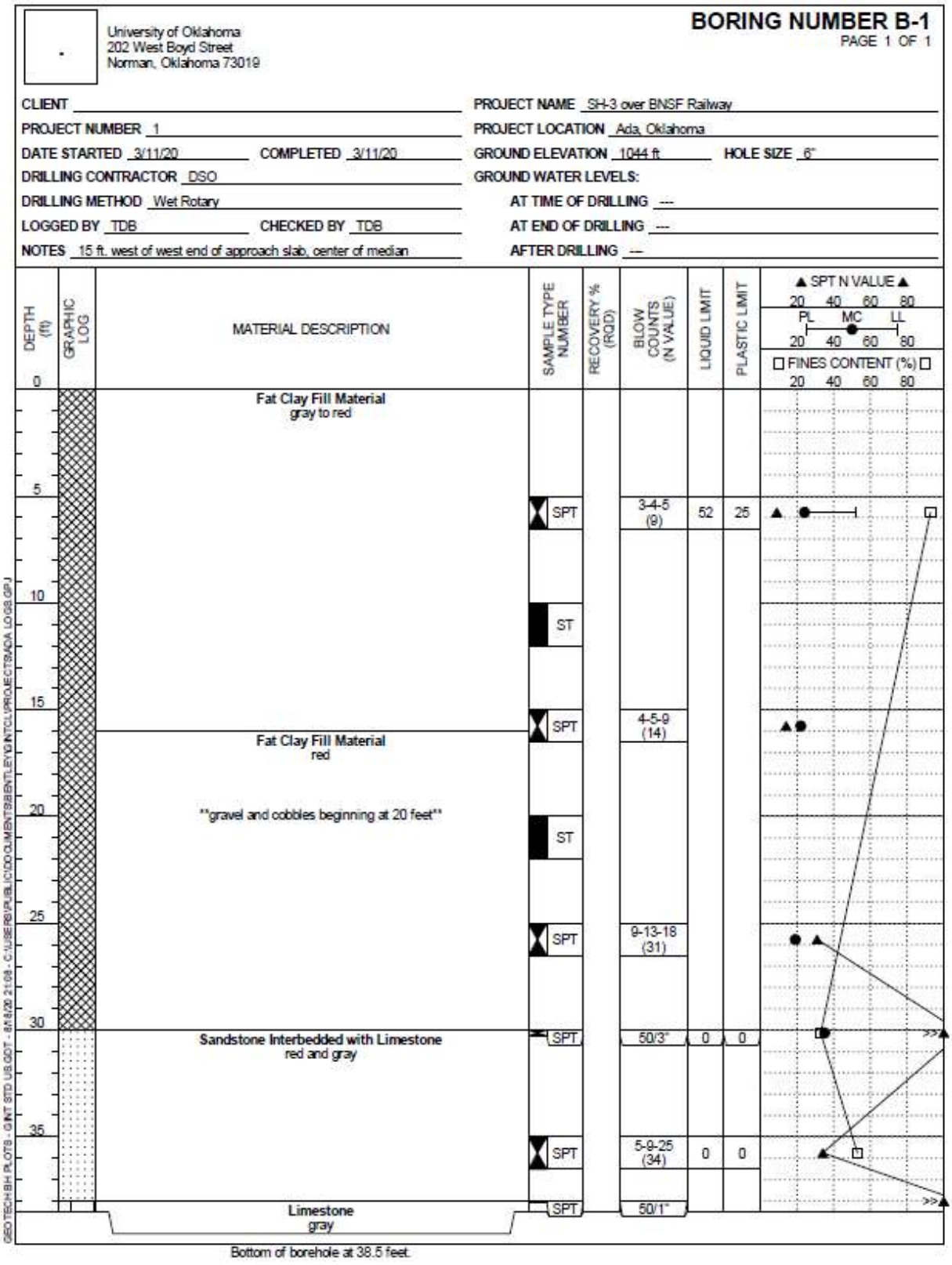

University of Oklahoma
202 West Boyd Street
Norman, Oklahoma 73019

BORING NUMBER B-2

CLIENT

PROJECT NAME SH-3 over BNSF Railway

PROJECT NUMBER 1

PROJECT LOCATION Ada, Oklahoma

DATE STARTED 3/11/20 COMPLETED 3/11/20

GROUND ELEVATION 1042 ft HOLE SIZE 6"

DRILLING CONTRACTOR DSO

GROUND WATER LEVELS:

DRILLING METHOD Wet Rotary

AT TIME OF DRILLING ---

LOGGED BY TDB CHECKED BY TDB

AT END OF DRILLING ---

NOTES 10 ft. east of east approach slab, center median

AFTER DRILLING ---

DEPTH (ft)	GRAPHIC LOG	MATERIAL DESCRIPTION	SAMPLE TYPE NUMBER	RECOVERY % (RQD)	BLOW COUNTS (N VALUE)	LIQUID LIMIT	PLASTIC LIMIT	▲ SPT N VALUE ▲ 20 40 60 80 / PL MC LL 20 40 60 80 / □ FINES CONTENT (%) □ 20 40 60 80
0		**Lean Clay Fill Material** greenish brown to reddish brown						
5			SPT		4-9-10 (19)			
10			ST					
15			SPT		5-5-8 (13)			
20		**Sandy Shale Fill Material** gray to black	SPT		34-13-14 (27)			
25			SPT		3-35-49 (84)			
30			SPT		19-50/6"	58	42	>>
35		**Silty Sandstone Fill Material** black to red	SPT		20-33-50/4"	0	0	>>
40								

(Continued Next Page)

GEOTECH BH PLOTS - GINT STD US.GDT - 8/18/20 21:08 - C:\USERS\PUBLIC\DOCUMENTS\BENTLEY\GINT\CLIVPROJECTS\ADA LOGS.GPJ

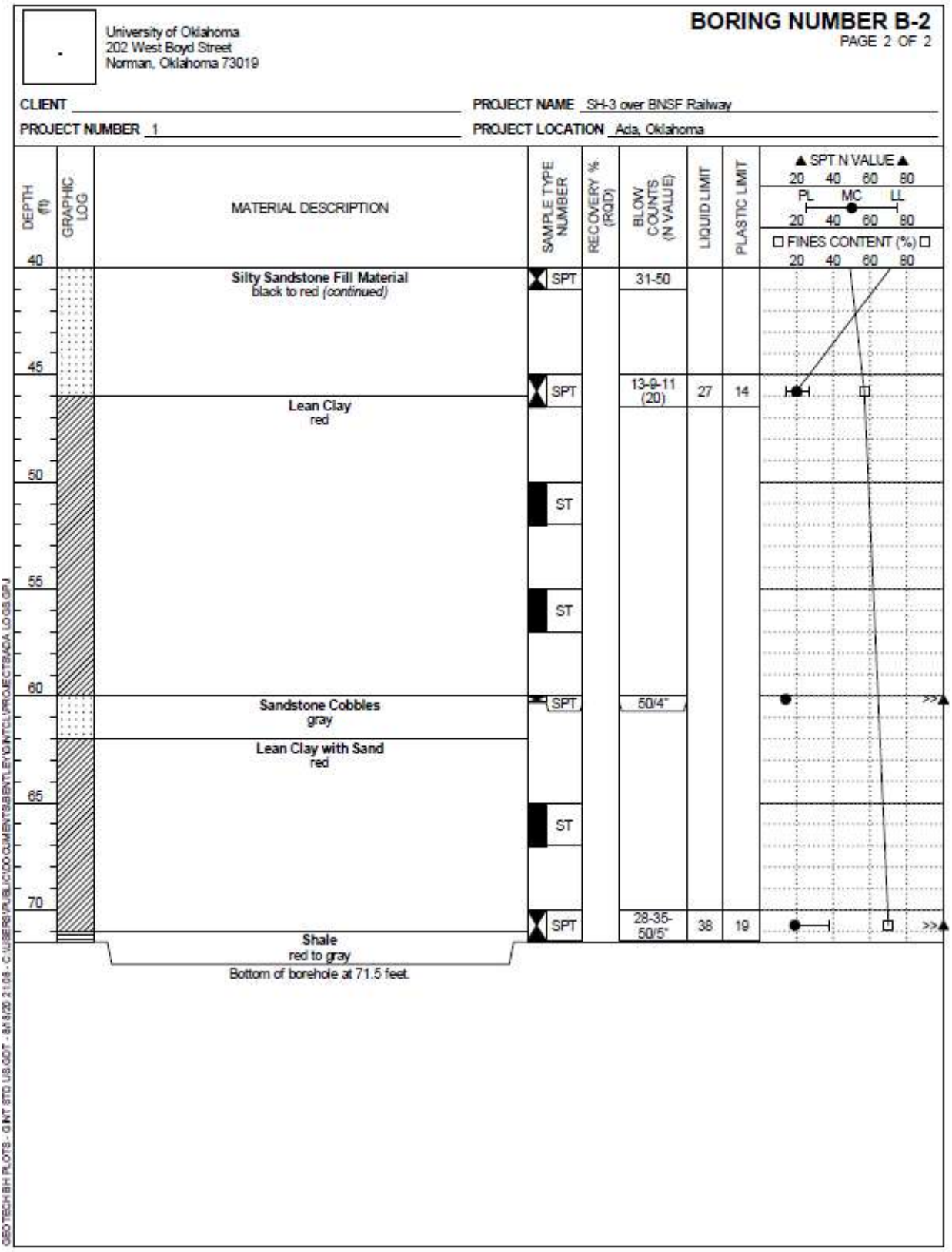
University of Oklahoma
202 West Boyd Street
Norman, Oklahoma 73019
BORING NUMBER B-2
PAGE 2 OF 2
CLIENT
PROJECT NAME SH-3 over BNSF Railway
PROJECT NUMBER 1
PROJECT LOCATION Ada, Oklahoma
DEPTH (ft)
GRAPHIC LOG
MATERIAL DESCRIPTION
SAMPLE TYPE NUMBER
RECOVERY % (RQD)
BLOW COUNTS (N VALUE)
LIQUID LIMIT
PLASTIC LIMIT
▲ SPT N VALUE ▲
20 40 60 80
PL MC LL
20 40 60 80
☐ FINES CONTENT (%) ☐
20 40 60 80
40
45
50
55
60
65
70
Silty Sandstone Fill Material
black to red (continued)
SPT
31-50
SPT
13-9-11 (20)
27
14
Lean Clay
red
ST
ST
Sandstone Cobbles
gray
SPT
50/4"
>>
Lean Clay with Sand
red
ST
Shale
red to gray
SPT
28-35-50/5"
38
19
>>
Bottom of borehole at 71.5 feet.
GEOTECH BH PLOTS - GINT STD US.GDT - 8/18/20 21:08 - C:\USERS\PUBLIC\DOCUMENTS\BENTLEY\DYNTCL\PROJECTS\ACA LOGS.GPJ

University of Oklahoma
202 West Boyd Street
Norman, Oklahoma 73019

BORING NUMBER B-3

CLIENT

PROJECT NAME SH-3 over BNSF Railway

PROJECT NUMBER 1

PROJECT LOCATION Ada, Oklahoma

DATE STARTED 3/11/20 COMPLETED 3/11/20

GROUND ELEVATION 1031 ft HOLE SIZE 6"

DRILLING CONTRACTOR DSO

GROUND WATER LEVELS:

DRILLING METHOD Wet Rotary

AT TIME OF DRILLING ---

LOGGED BY TDB CHECKED BY TDB

AT END OF DRILLING ---

NOTES 250 ft. eat of east approach slab, center median

AFTER DRILLING ---

DEPTH (ft)	GRAPHIC LOG	MATERIAL DESCRIPTION	SAMPLE TYPE NUMBER	RECOVERY % (RQD)	BLOW COUNTS (N VALUE)	LIQUID LIMIT	PLASTIC LIMIT
0		**Lean Clay Fill Material** **"Shale and Sandstone Cobbles Mixed in Fill Material"** greenish gray					
5			SPT		5-7-13 (20)		
		Silty Sand Fill Material **"Shale and Sandstone Cobbles Mixed in Fill Material"** greenish gray					
10			SPT		20-40-43 (83)	0	0
		Lean Clay Fill Material **"Shale and Sandstone Cobbles Mixed in Fill Material"** greenish gray					
15			SPT		9-22-25 (47)		
20		**Clayey Sand and Gravel Fill Material** Black to red to gray **"Strong Organic Odor"**	SPT		17-21-16 (37)	42	30
25			SPT		27-39-50/5"	0	0
30			SPT		50/3"		
35		**Lean Clay** greenish brown to red to dark brown	SPT		4-10-11 (21)		
40							

▲ SPT N VALUE ▲
20 40 60 80
PL MC LL
20 40 60 80
☐ FINES CONTENT (%) ☐
20 40 60 80

(Continued Next Page)

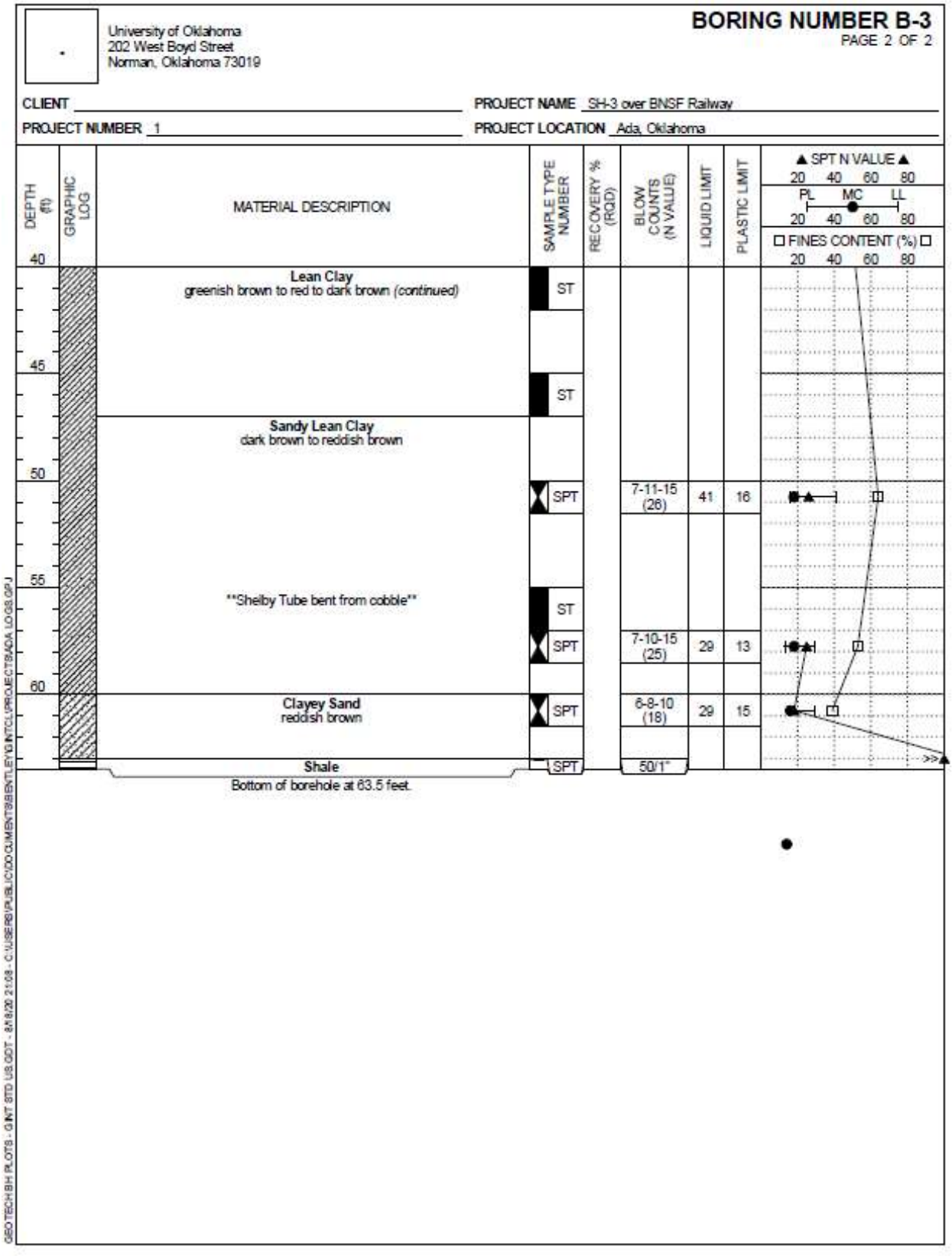
University of Oklahoma
202 West Boyd Street
Norman, Oklahoma 73019
BORING NUMBER B-3
PAGE 2 OF 2
CLIENT
PROJECT NAME SH-3 over BNSF Railway
PROJECT NUMBER 1
PROJECT LOCATION Ada, Oklahoma
DEPTH (ft)
GRAPHIC LOG
MATERIAL DESCRIPTION
SAMPLE TYPE NUMBER
RECOVERY % (RQD)
BLOW COUNTS (N VALUE)
LIQUID LIMIT
PLASTIC LIMIT
▲ SPT N VALUE ▲
20 40 60 80
PL MC LL
20 40 60 80
□ FINES CONTENT (%) □
20 40 60 80
40
Lean Clay
greenish brown to red to dark brown (continued)
ST
45
ST
Sandy Lean Clay
dark brown to reddish brown
50
SPT
7-11-15 (26)
41
16
55
Shelby Tube bent from cobble
ST
SPT
7-10-15 (25)
29
13
60
Clayey Sand
reddish brown
SPT
6-8-10 (18)
29
15
Shale
SPT
50/1"
Bottom of borehole at 63.5 feet.
GEOTECH BH PLOTS - GINT STD US.GDT - 8/18/20 21:08 - C:\USERS\PUBLIC\DOCUMENTS\BENTLEY\GINTCL\PROJECTS\ADA LOGS.GPJ

APPENDIX B: SH 3 over BNSF Railroad Lab Test Results

B.1 One Dimensional Consolidation Results

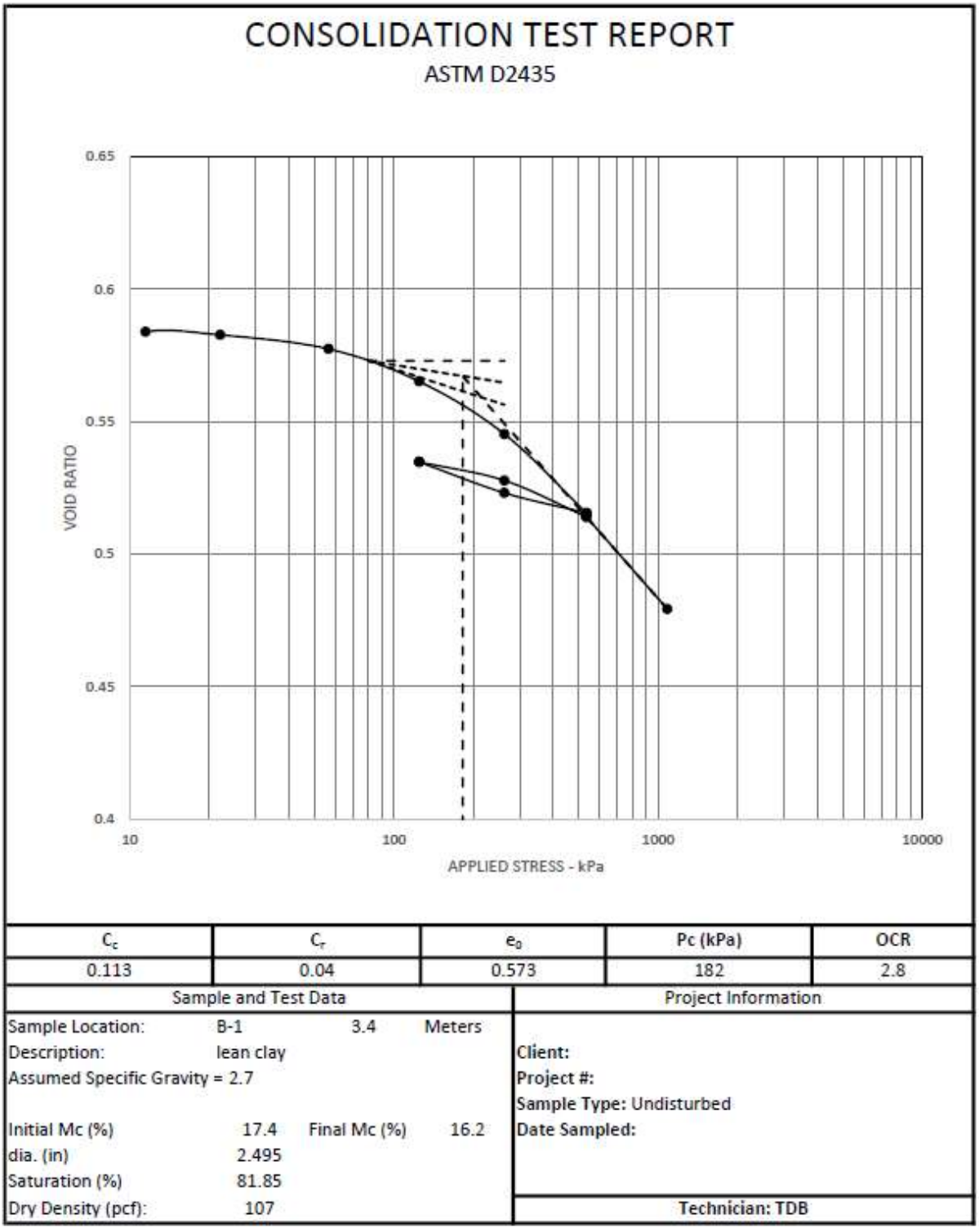

C_c	C_r	e_0	Pc (kPa)	OCR
0.113	0.04	0.573	182	2.8

Sample and Test Data				Project Information
Sample Location:	B-1	3.4	Meters	
Description:	lean clay			Client:
Assumed Specific Gravity = 2.7				Project #:
				Sample Type: Undisturbed
Initial Mc (%)	17.4	Final Mc (%)	16.2	Date Sampled:
dia. (in)	2.495			
Saturation (%)	81.85			
Dry Density (pcf):	107			Technician: TDB

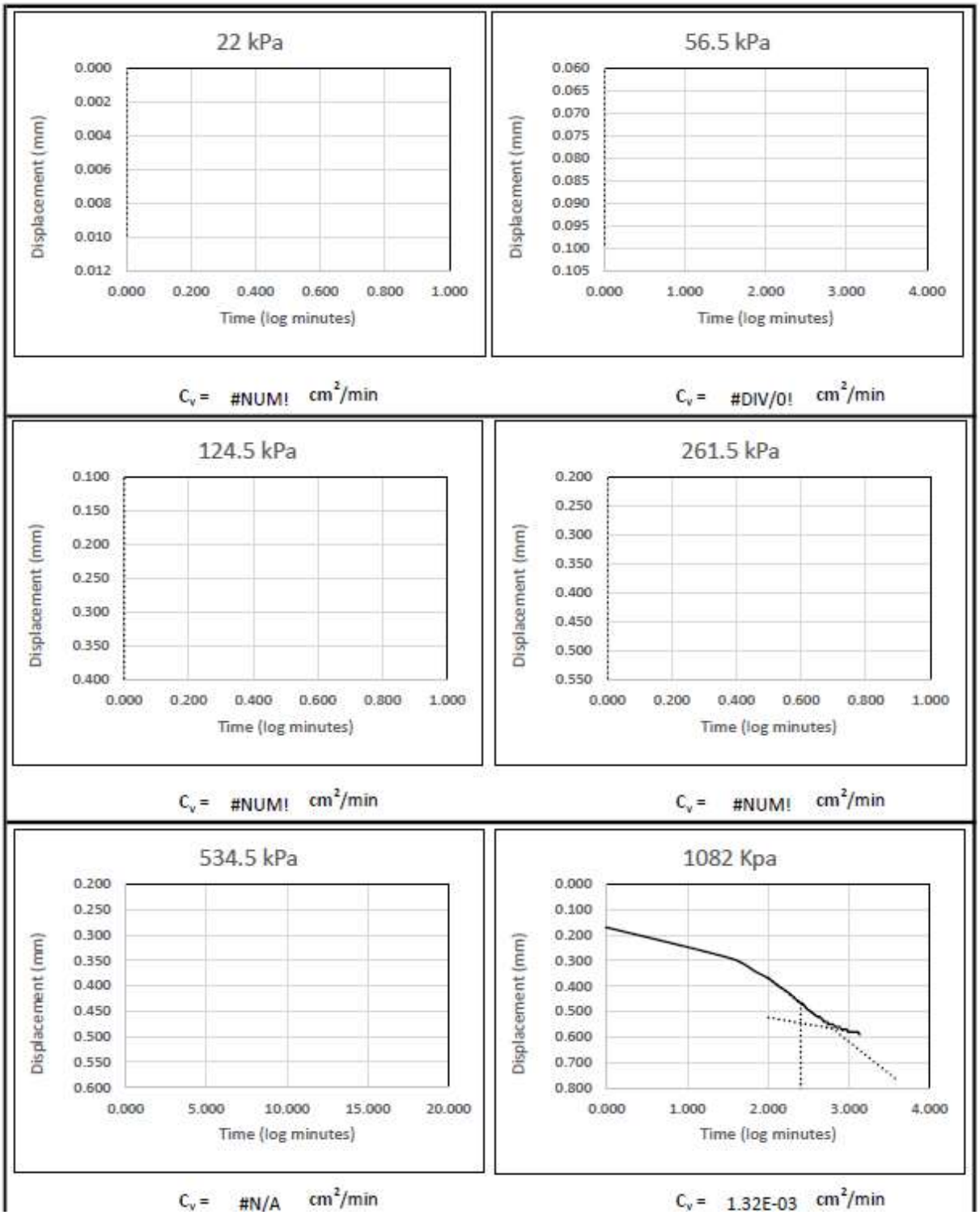
22 kPa
Displacement (mm)
0.000
0.002
0.004
0.006
0.008
0.010
0.012
0.000 0.200 0.400 0.600 0.800 1.000
Time (log minutes)
C_v = #NUM! cm^2/min
56.5 kPa
Displacement (mm)
0.060
0.065
0.070
0.075
0.080
0.085
0.090
0.095
0.100
0.105
0.000 1.000 2.000 3.000 4.000
Time (log minutes)
C_v = #DIV/0! cm^2/min
124.5 kPa
Displacement (mm)
0.100
0.150
0.200
0.250
0.300
0.350
0.400
0.000 0.200 0.400 0.600 0.800 1.000
Time (log minutes)
C_v = #NUM! cm^2/min
261.5 kPa
Displacement (mm)
0.200
0.250
0.300
0.350
0.400
0.450
0.500
0.550
0.000 0.200 0.400 0.600 0.800 1.000
Time (log minutes)
C_v = #NUM! cm^2/min
534.5 kPa
Displacement (mm)
0.200
0.250
0.300
0.350
0.400
0.450
0.500
0.550
0.600
0.000 5.000 10.000 15.000 20.000
Time (log minutes)
C_v = #N/A cm^2/min
1082 Kpa
Displacement (mm)
0.000
0.100
0.200
0.300
0.400
0.500
0.600
0.700
0.800
0.000 1.000 2.000 3.000 4.000
Time (log minutes)
C_v = 1.32E-03 cm^2/min

CONSOLIDATION TEST REPORT

ASTM D2435

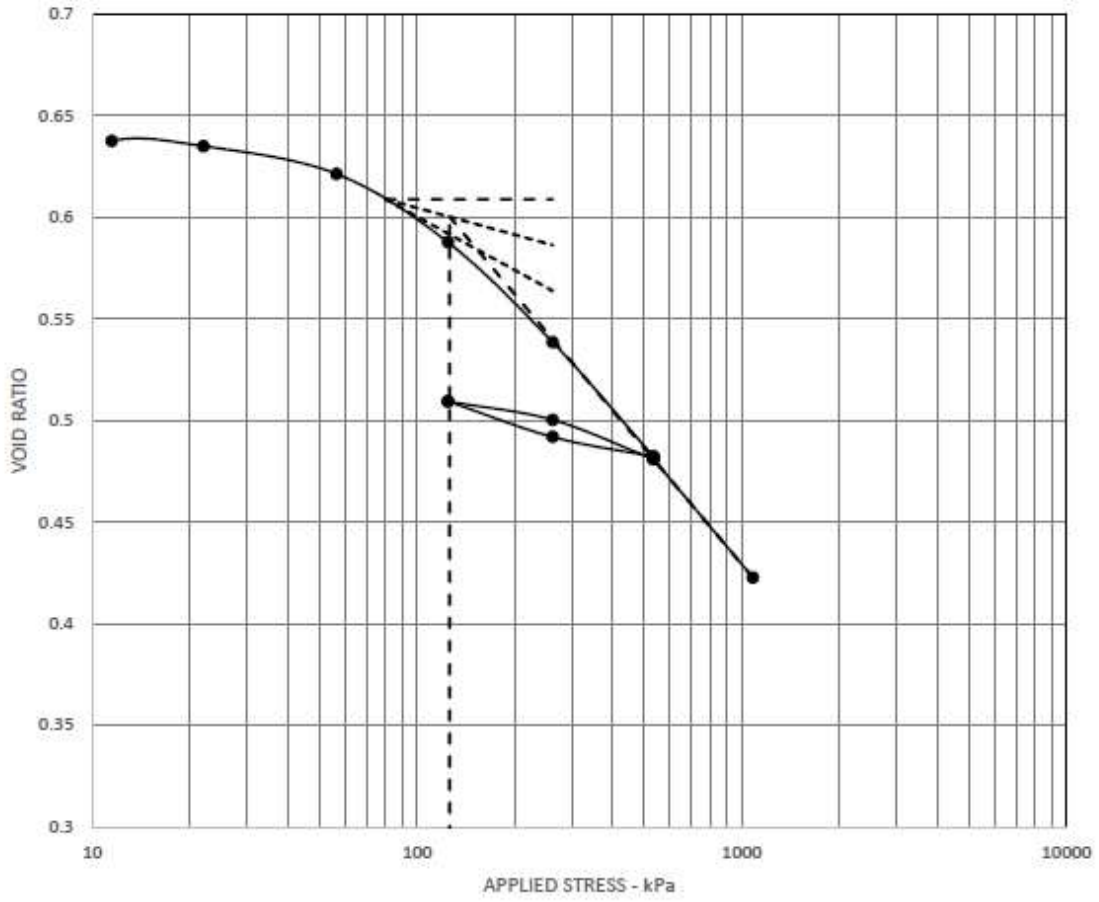

C_c	C_r	e_0	Pc (kPa)	OCR
0.19	0.11	0.616	126	1

Sample and Test Data				Project Information
Sample Location:	B-1	6.5	Meters	
Description:	lean clay			Client:
Assumed Specific Gravity = 2.7				Project #:
				Sample Type: Undisturbed
Initial Mc (%)	20.3	Final Mc (%)	18.5	Date Sampled:
dia. (in)	2.5			
Saturation (%)	88.93			
Dry Density (pcf):	104.2			Technician: TDB

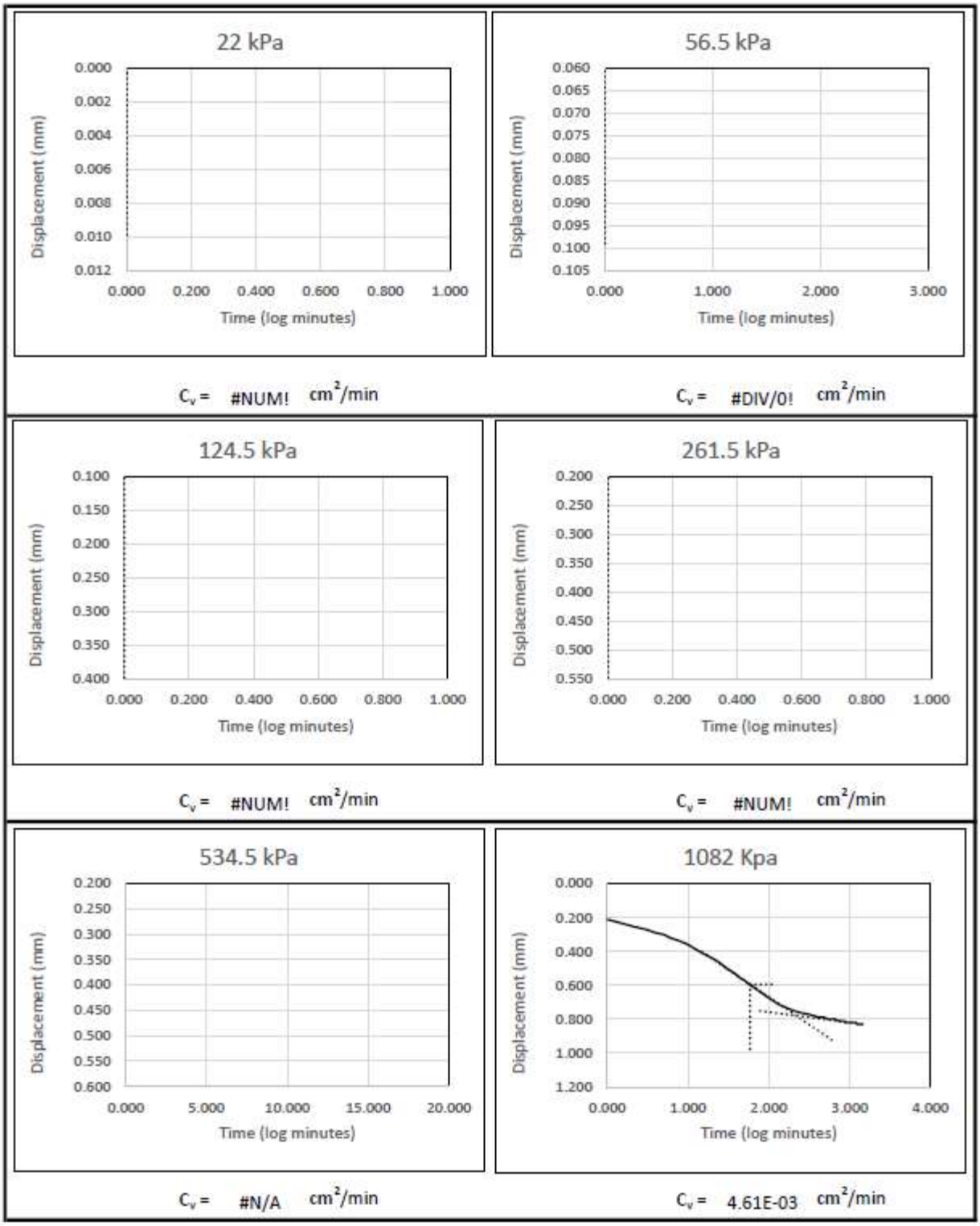
22 kPa
Displacement (mm)
0.000
0.002
0.004
0.006
0.008
0.010
0.012
0.000 0.200 0.400 0.600 0.800 1.000
Time (log minutes)
C_v = #NUM! cm^2/min
56.5 kPa
Displacement (mm)
0.060
0.065
0.070
0.075
0.080
0.085
0.090
0.095
0.100
0.105
0.000 1.000 2.000 3.000
Time (log minutes)
C_v = #DIV/0! cm^2/min
124.5 kPa
Displacement (mm)
0.100
0.150
0.200
0.250
0.300
0.350
0.400
0.000 0.200 0.400 0.600 0.800 1.000
Time (log minutes)
C_v = #NUM! cm^2/min
261.5 kPa
Displacement (mm)
0.200
0.250
0.300
0.350
0.400
0.450
0.500
0.550
0.000 0.200 0.400 0.600 0.800 1.000
Time (log minutes)
C_v = #NUM! cm^2/min
534.5 kPa
Displacement (mm)
0.200
0.250
0.300
0.350
0.400
0.450
0.500
0.550
0.600
0.000 5.000 10.000 15.000 20.000
Time (log minutes)
C_v = #N/A cm^2/min
1082 Kpa
Displacement (mm)
0.000
0.200
0.400
0.600
0.800
1.000
1.200
0.000 1.000 2.000 3.000 4.000
Time (log minutes)
C_v = 4.61E-03 cm^2/min

CONSOLIDATION TEST REPORT

ASTM D2435

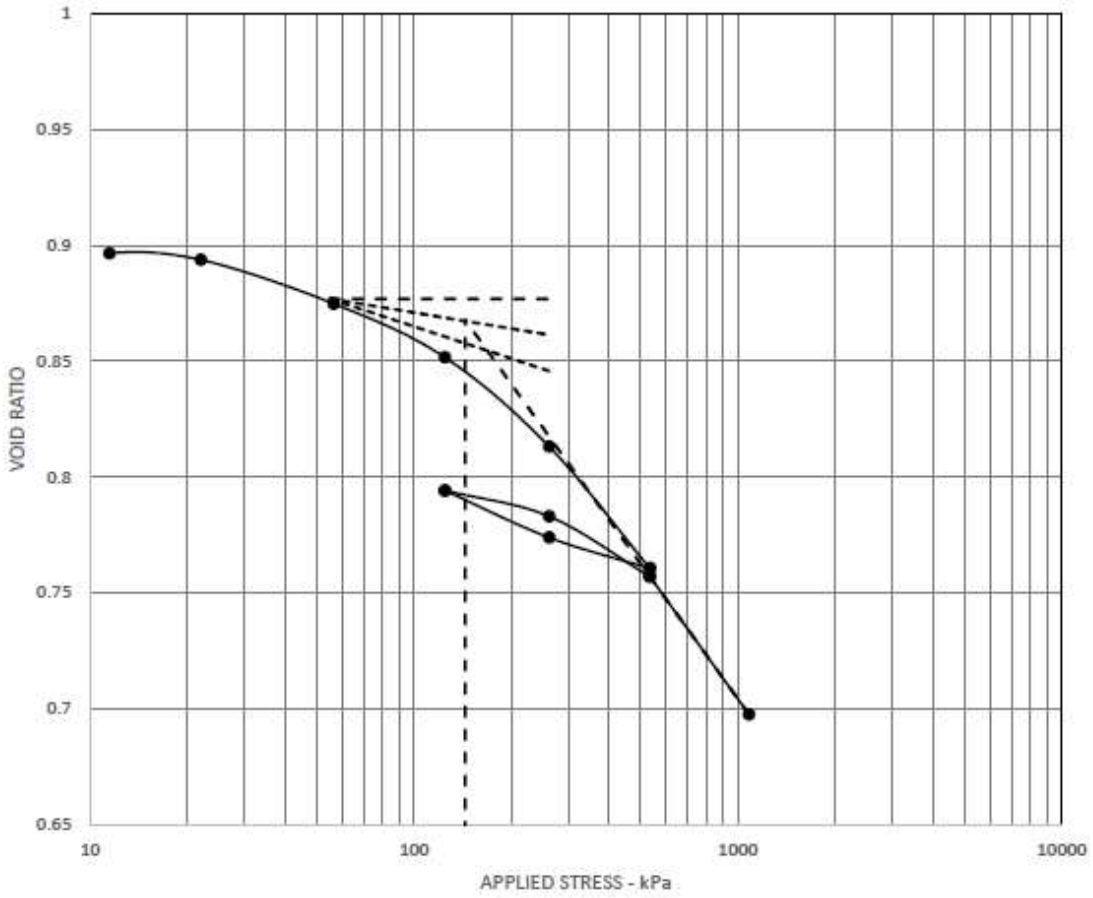

C_c	C_r	e_0	Pc (kPa)	OCR
0.194	0.071	0.887	144	2.3

Sample and Test Data				Project Information
Sample Location:	B-2	3.2	Meters	
Description:	lean clay			Client:
Assumed Specific Gravity = 2.7				Project #:
				Sample Type: Undisturbed
Initial Mc (%)	25.3	Final Mc (%)	21.6	Date Sampled:
dia. (in)	2.5			
Saturation (%)	76.97			
Dry Density (pcf):	89.3			Technician: TDB

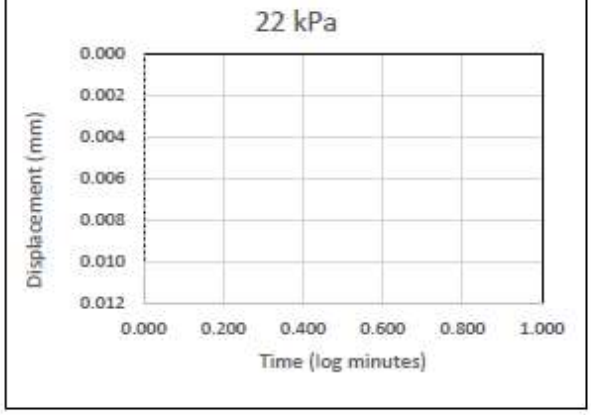

C_v = #NUM! cm^2/min

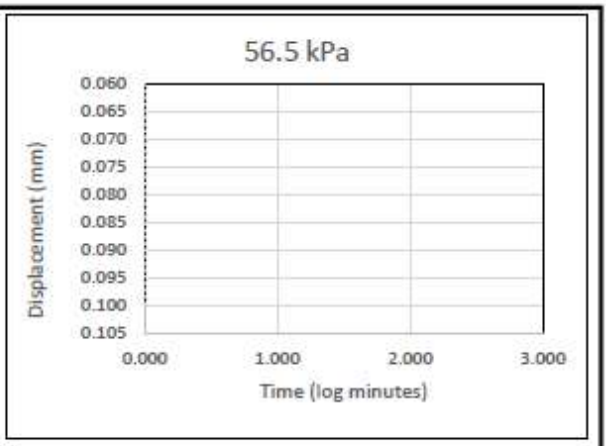

C_v = #DIV/0! cm^2/min

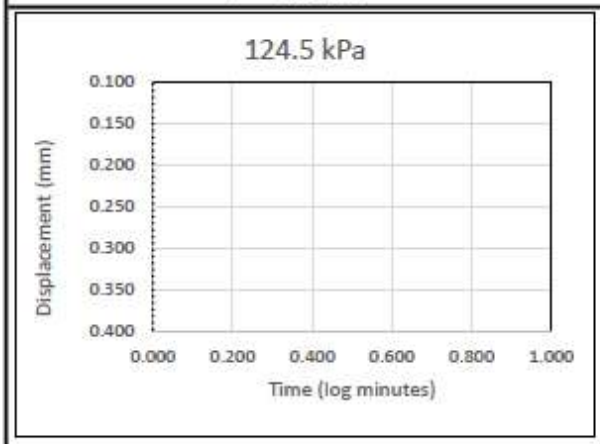

C_v = #NUM! cm^2/min

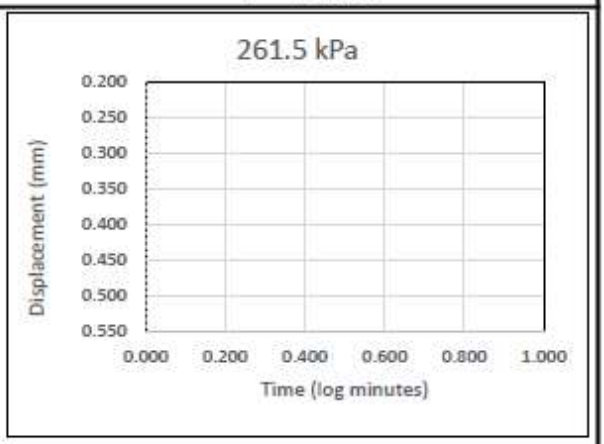

C_v = #NUM! cm^2/min

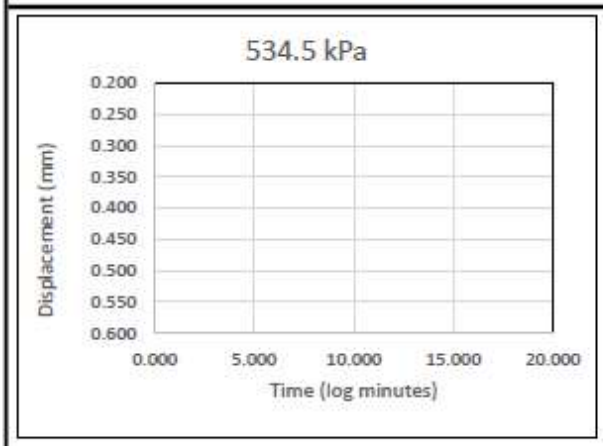

C_v = #N/A cm^2/min

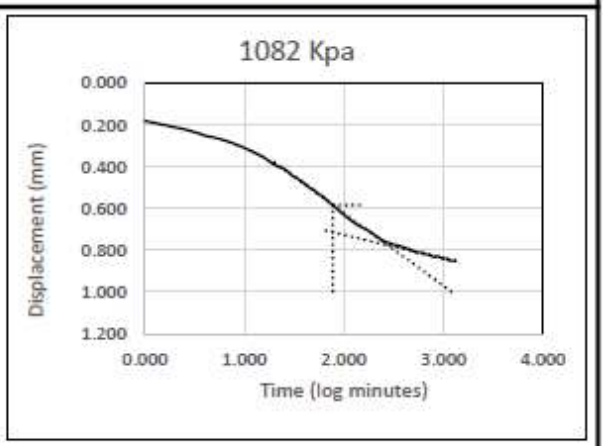

C_v = 4.06E-03 cm^2/min

CONSOLIDATION TEST REPORT

ASTM D2435

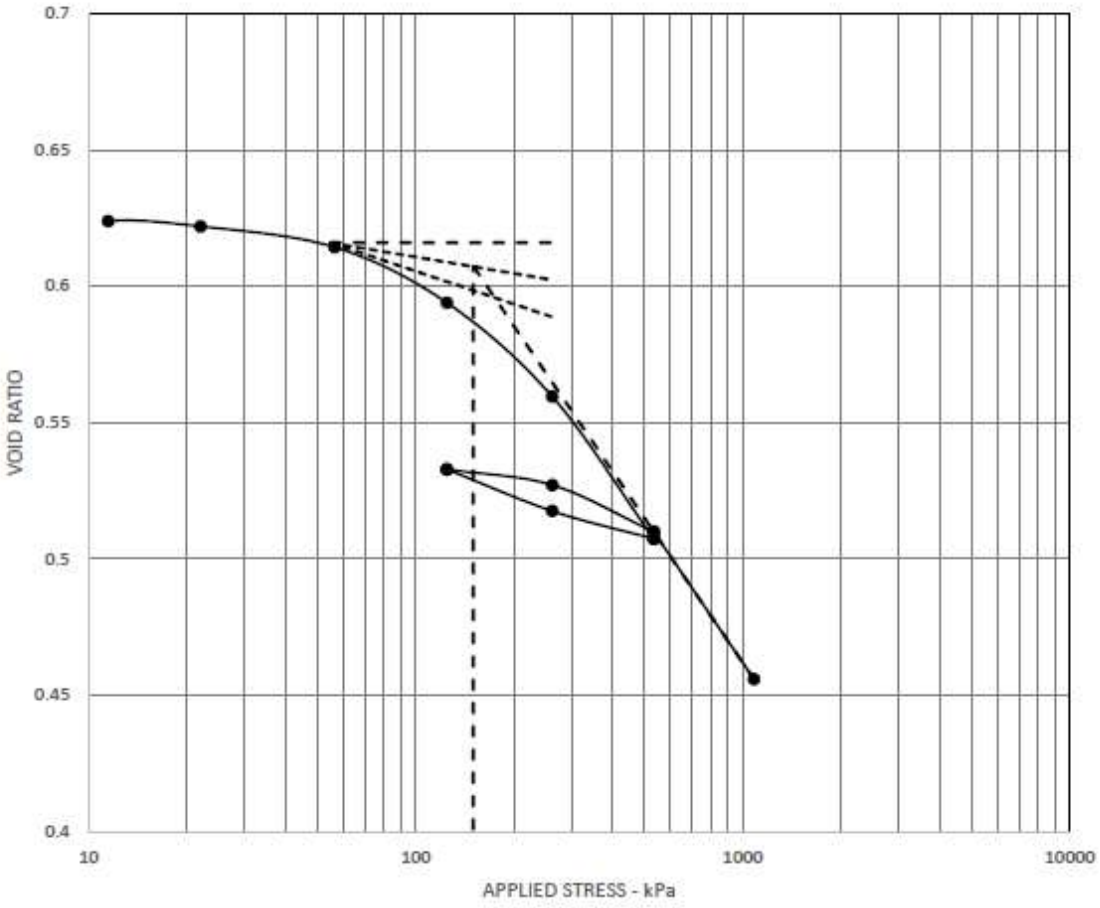

C_c	C_r	e_0	Pc (kPa)	OCR
0.176	0.062	0.616	150	0.4

Sample and Test Data				Project Information
Sample Location:	B-2	16.9	Meters	
Description:	lean clay			Client:
Assumed Specific Gravity = 2.7				Project #:
				Sample Type: Undisturbed
Initial Mc (%)	21	Final Mc (%)	19.1	Date Sampled:
dia. (in)	2.5			
Saturation (%)	91.9			
Dry Density (pcf):	104.2			Technician: TDB

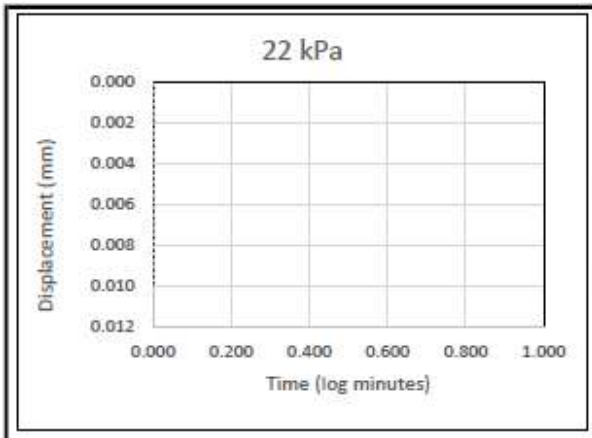

C_v = #NUM! cm^2/min

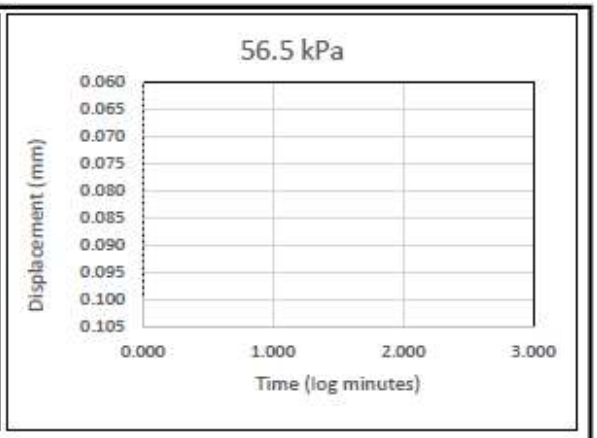

C_v = #DIV/0! cm^2/min

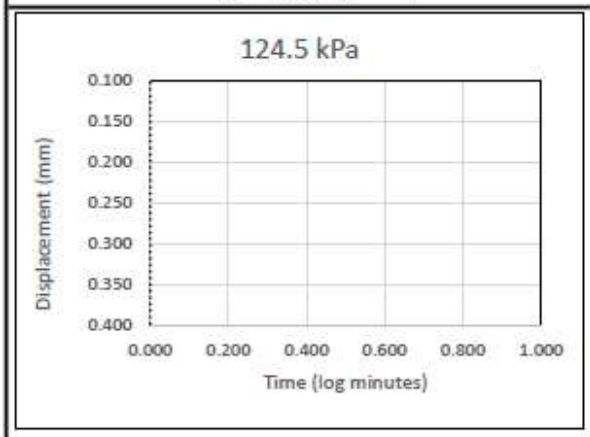

C_v = #NUM! cm^2/min

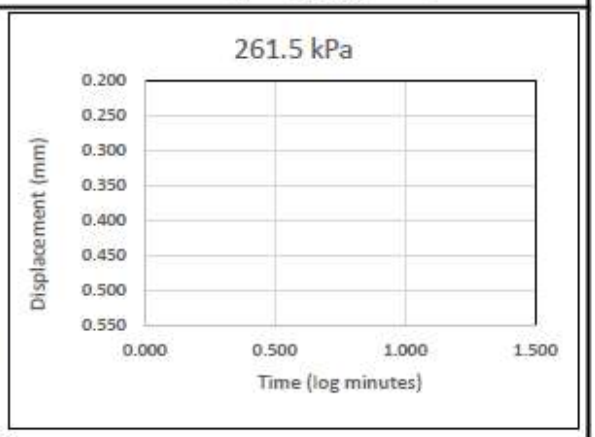

C_v = 4.44E-01 cm^2/min

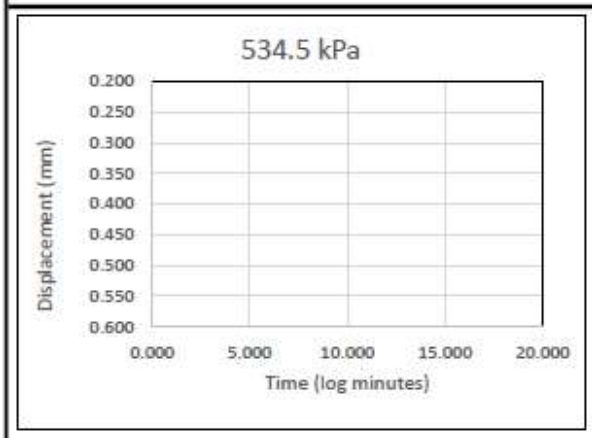

C_v = #N/A cm^2/min

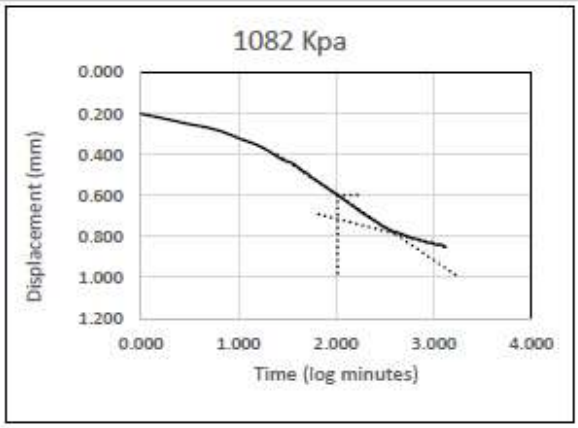

C_v = 2.69E-03 cm^2/min

CONSOLIDATION TEST REPORT

ASTM D2435

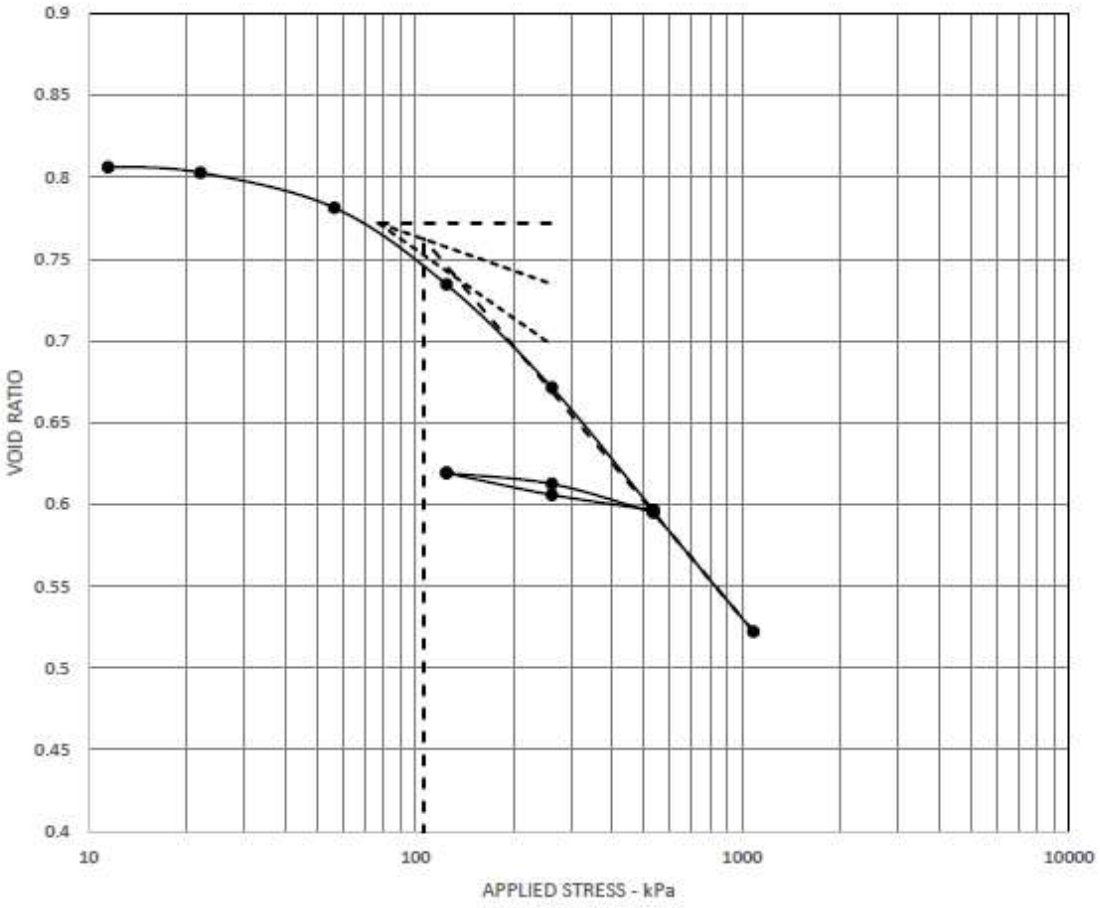

C_c	C_r	e_0	Pc (kPa)	OCR
0.238	0.179	0.802	106	0.3

Sample and Test Data				Project Information
Sample Location:	B-2	17	Meters	
Description:	lean clay			Client:
Assumed Specific Gravity = 2.7				Project #:
				Sample Type: Undisturbed
Initial Mc (%)	23.6	Final Mc (%)	17	Date Sampled:
dia. (in)	2.495			
Saturation (%)	79.37			
Dry Density (pcf):	93.4			Technician: TDB

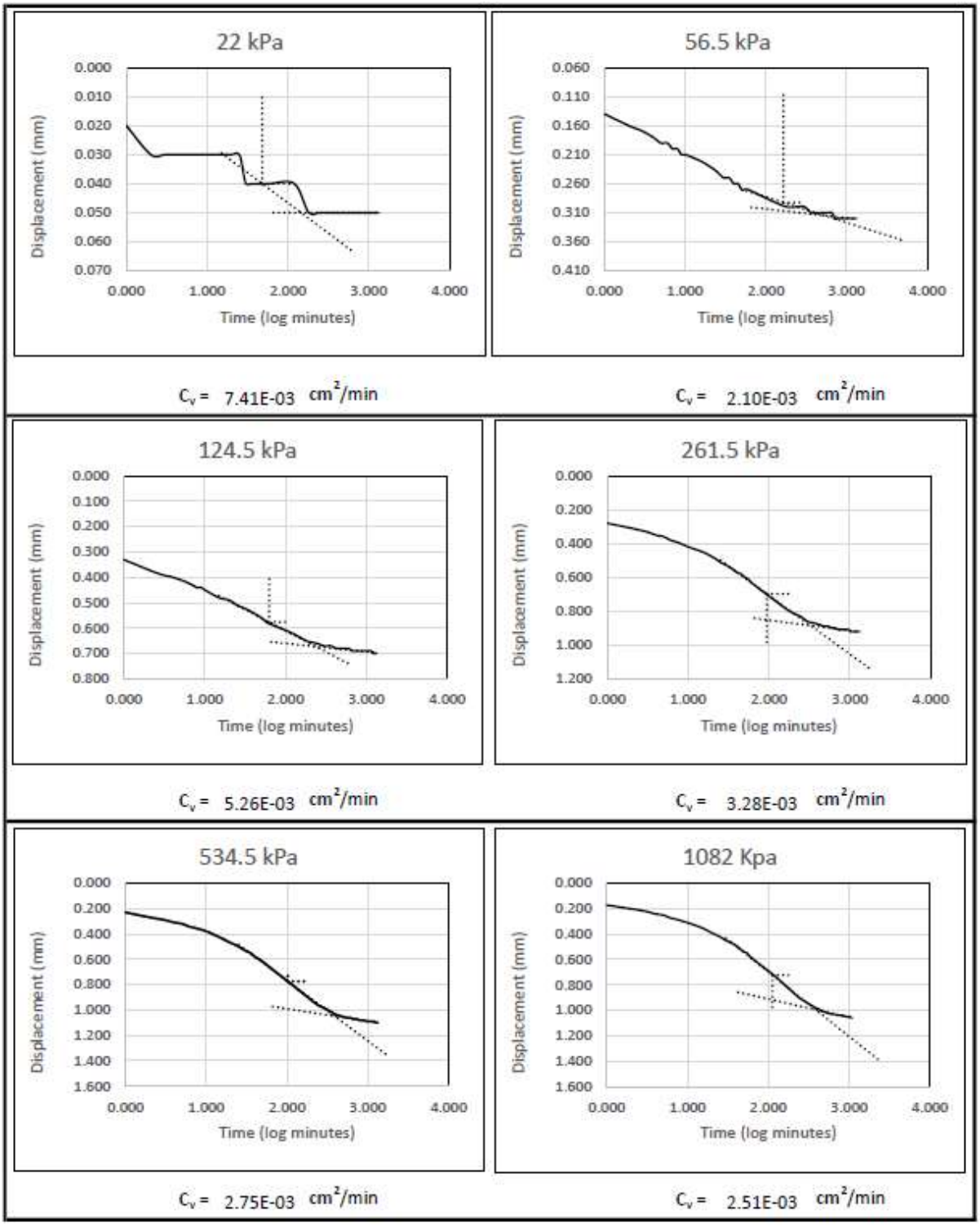
22 kPa
Displacement (mm)
0.000
0.010
0.020
0.030
0.040
0.050
0.060
0.070
0.000
1.000
2.000
3.000
4.000
Time (log minutes)
C_v = 7.41E-03 cm^2/min
56.5 kPa
Displacement (mm)
0.060
0.110
0.160
0.210
0.260
0.310
0.360
0.410
0.000
1.000
2.000
3.000
4.000
Time (log minutes)
C_v = 2.10E-03 cm^2/min
124.5 kPa
Displacement (mm)
0.000
0.100
0.200
0.300
0.400
0.500
0.600
0.700
0.800
0.000
1.000
2.000
3.000
4.000
Time (log minutes)
C_v = 5.26E-03 cm^2/min
261.5 kPa
Displacement (mm)
0.000
0.200
0.400
0.600
0.800
1.000
1.200
0.000
1.000
2.000
3.000
4.000
Time (log minutes)
C_v = 3.28E-03 cm^2/min
534.5 kPa
Displacement (mm)
0.000
0.200
0.400
0.600
0.800
1.000
1.200
1.400
1.600
0.000
1.000
2.000
3.000
4.000
Time (log minutes)
C_v = 2.75E-03 cm^2/min
1082 Kpa
Displacement (mm)
0.000
0.200
0.400
0.600
0.800
1.000
1.200
1.400
1.600
0.000
1.000
2.000
3.000
4.000
Time (log minutes)
C_v = 2.51E-03 cm^2/min

CONSOLIDATION TEST REPORT

ASTM D2435

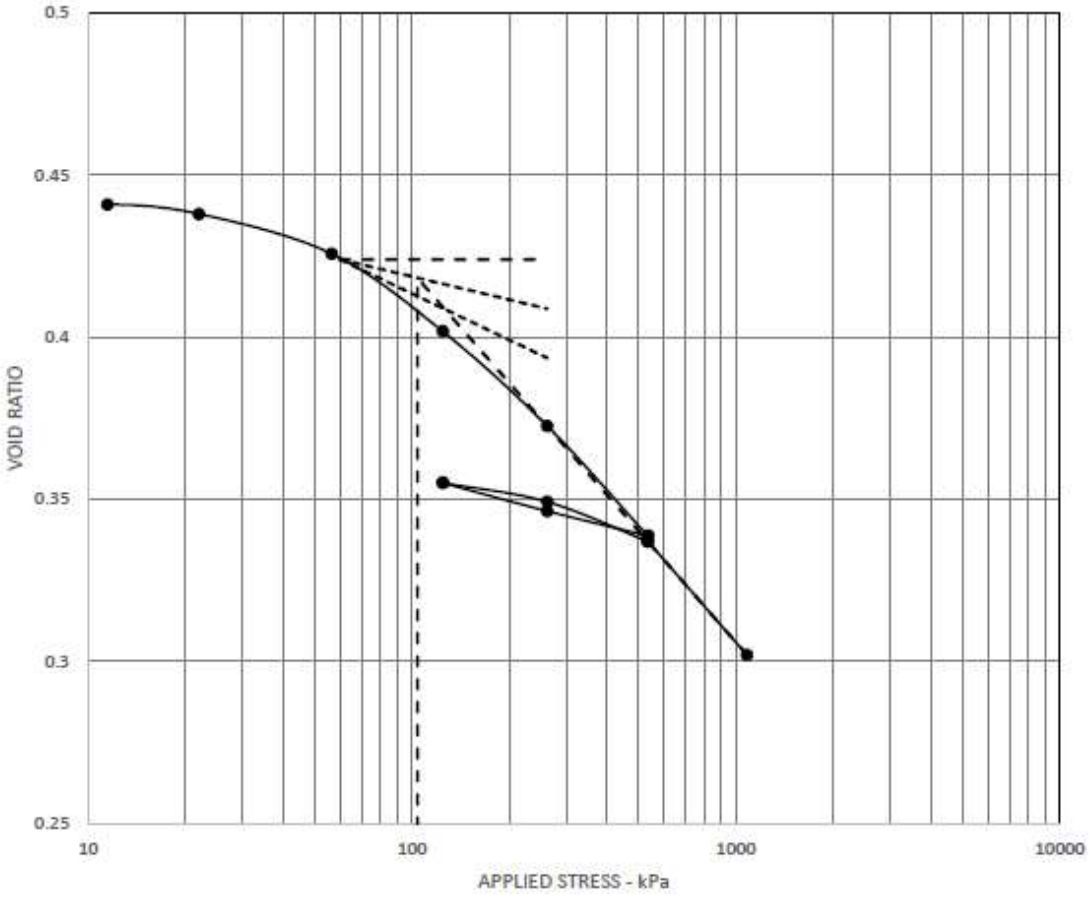

C_c	C_r	e_0	Pc (kPa)	OCR
0.114	0.07	0.438	104	0.4

Sample and Test Data				Project Information
Sample Location:	B-3	12.3	Meters	
Description:	lean clay			Client:
Assumed Specific Gravity = 2.7				Project #:
				Sample Type: Undisturbed
Initial Mc (%)	16.4	Final Mc (%)	14.9	Date Sampled:
dia. (in)	2.5			
Saturation (%)	100.95			
Dry Density (pcf):	117.1			Technician: TDB

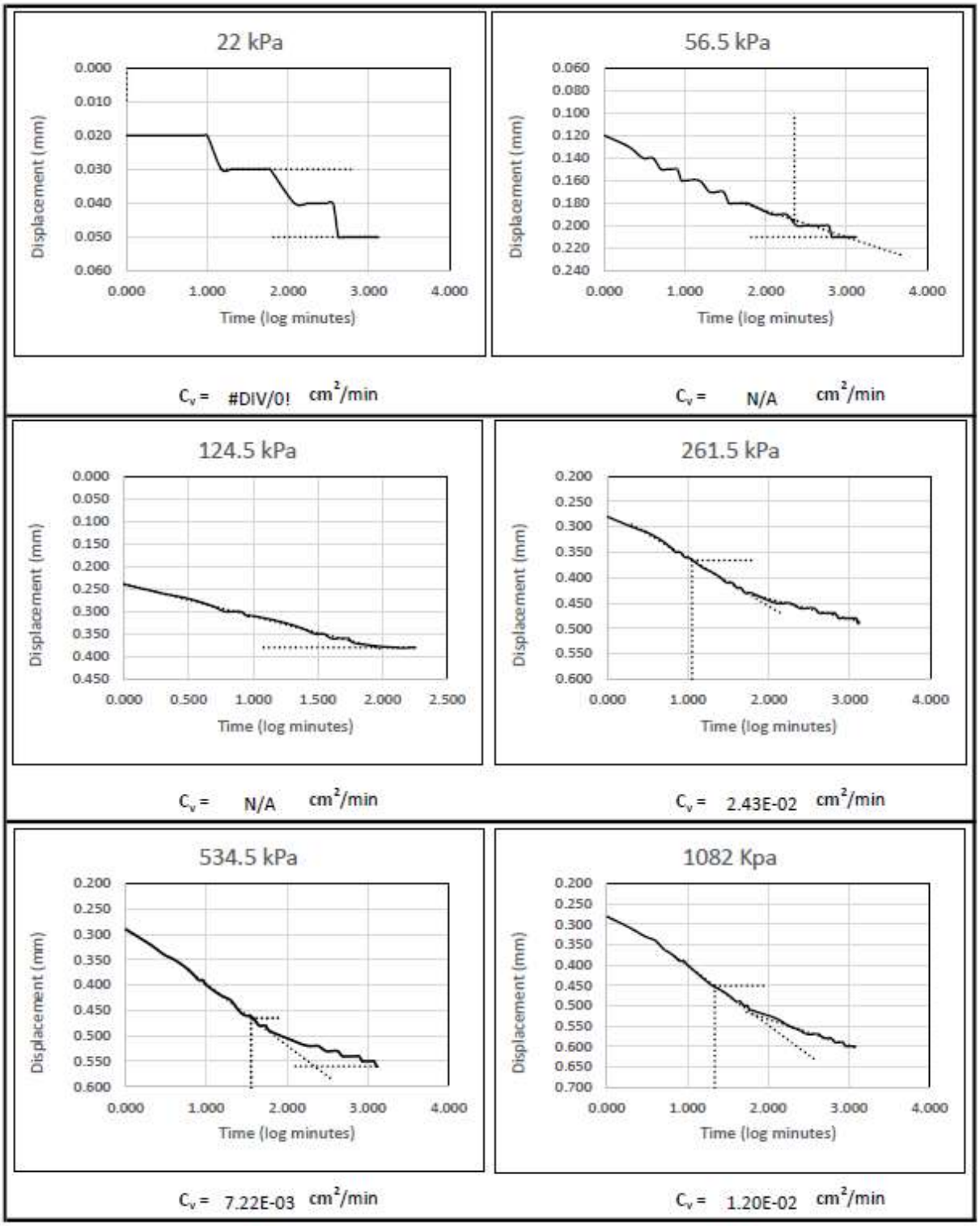
22 kPa
Displacement (mm)
0.000
0.010
0.020
0.030
0.040
0.050
0.060
0.000
1.000
2.000
3.000
4.000
Time (log minutes)
C_v = #DIV/0! cm^2/min
56.5 kPa
Displacement (mm)
0.060
0.080
0.100
0.120
0.140
0.160
0.180
0.200
0.220
0.240
0.000
1.000
2.000
3.000
4.000
Time (log minutes)
C_v = N/A cm^2/min
124.5 kPa
Displacement (mm)
0.000
0.050
0.100
0.150
0.200
0.250
0.300
0.350
0.400
0.450
0.000
0.500
1.000
1.500
2.000
2.500
Time (log minutes)
C_v = N/A cm^2/min
261.5 kPa
Displacement (mm)
0.200
0.250
0.300
0.350
0.400
0.450
0.500
0.550
0.600
0.000
1.000
2.000
3.000
4.000
Time (log minutes)
C_v = 2.43E-02 cm^2/min
534.5 kPa
Displacement (mm)
0.200
0.250
0.300
0.350
0.400
0.450
0.500
0.550
0.600
0.000
1.000
2.000
3.000
4.000
Time (log minutes)
C_v = 7.22E-03 cm^2/min
1082 Kpa
Displacement (mm)
0.200
0.250
0.300
0.350
0.400
0.450
0.500
0.550
0.600
0.650
0.700
0.000
1.000
2.000
3.000
4.000
Time (log minutes)
C_v = 1.20E-02 cm^2/min

CONSOLIDATION TEST REPORT

ASTM D2435

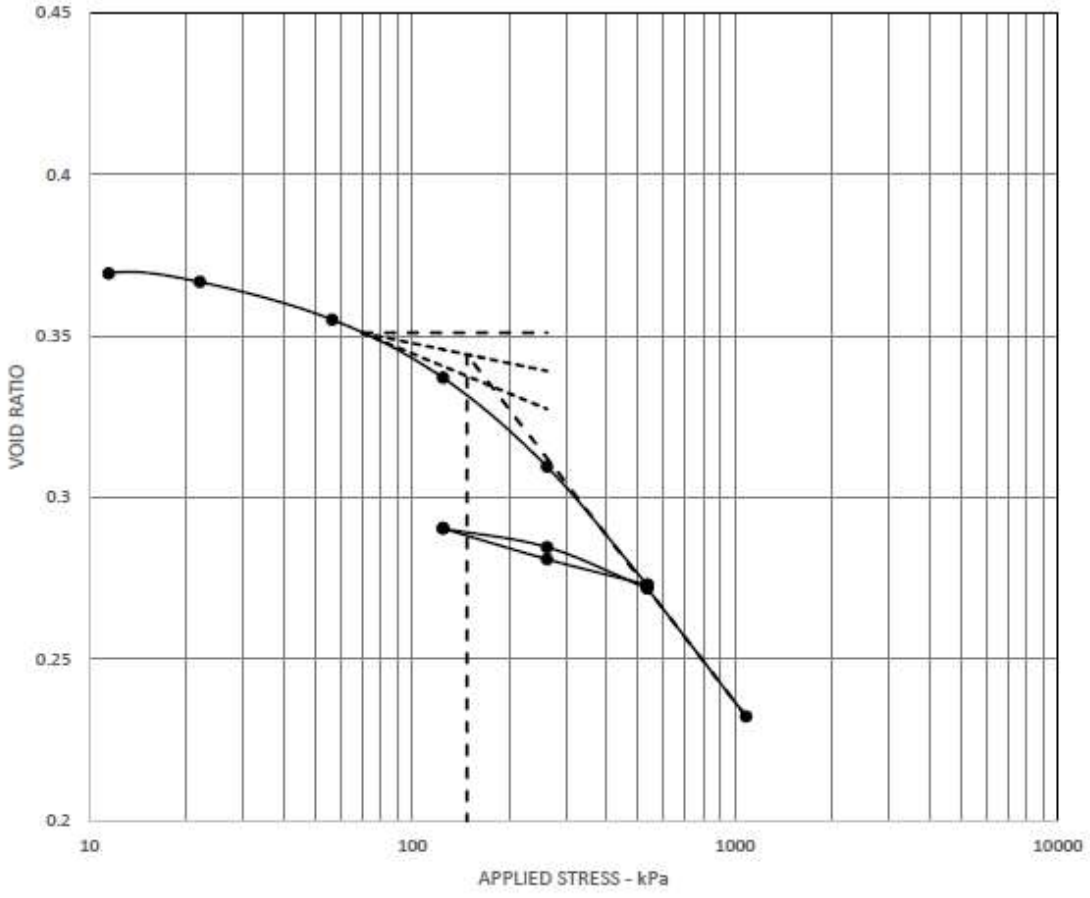

C_c	C_r	e_0	Pc (kPa)	OCR
0.129	0.055	0.358	148	0.5

Sample and Test Data				Project Information
Sample Location:	B-3	14.2	Meters	
Description:	lean clay			Client:
Assumed Specific Gravity = 2.7				Project #:
				Sample Type: Undisturbed
Initial Mc (%)	3.7	Final Mc (%)	16.9	Date Sampled:
dia. (in)	2.495			
Saturation (%)	27.84			
Dry Density (pcf):	124			Technician: TDB

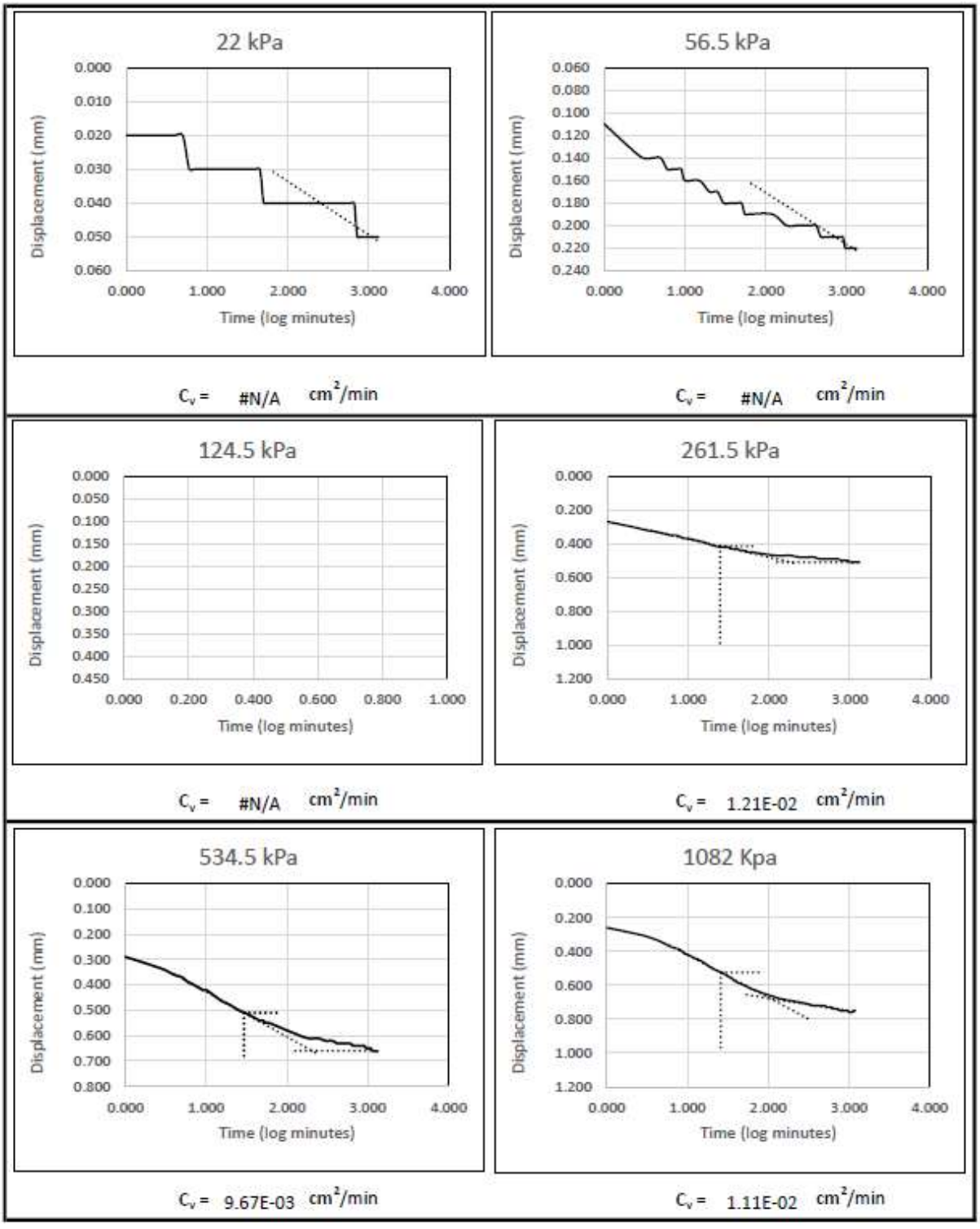
22 kPa
Displacement (mm)
0.000
0.010
0.020
0.030
0.040
0.050
0.060
0.000
1.000
2.000
3.000
4.000
Time (log minutes)
C_v = #N/A cm²/min
56.5 kPa
Displacement (mm)
0.060
0.080
0.100
0.120
0.140
0.160
0.180
0.200
0.220
0.240
0.000
1.000
2.000
3.000
4.000
Time (log minutes)
C_v = #N/A cm²/min
124.5 kPa
Displacement (mm)
0.000
0.050
0.100
0.150
0.200
0.250
0.300
0.350
0.400
0.450
0.000
0.200
0.400
0.600
0.800
1.000
Time (log minutes)
C_v = #N/A cm²/min
261.5 kPa
Displacement (mm)
0.000
0.200
0.400
0.600
0.800
1.000
1.200
0.000
1.000
2.000
3.000
4.000
Time (log minutes)
C_v = 1.21E-02 cm²/min
534.5 kPa
Displacement (mm)
0.000
0.100
0.200
0.300
0.400
0.500
0.600
0.700
0.800
0.000
1.000
2.000
3.000
4.000
Time (log minutes)
C_v = 9.67E-03 cm²/min
1082 Kpa
Displacement (mm)
0.000
0.200
0.400
0.600
0.800
1.000
1.200
0.000
1.000
2.000
3.000
4.000
Time (log minutes)
C_v = 1.11E-02 cm²/min

B.2 Triaxial Compression Results

TRIAXIAL SHEAR TEST REPORT

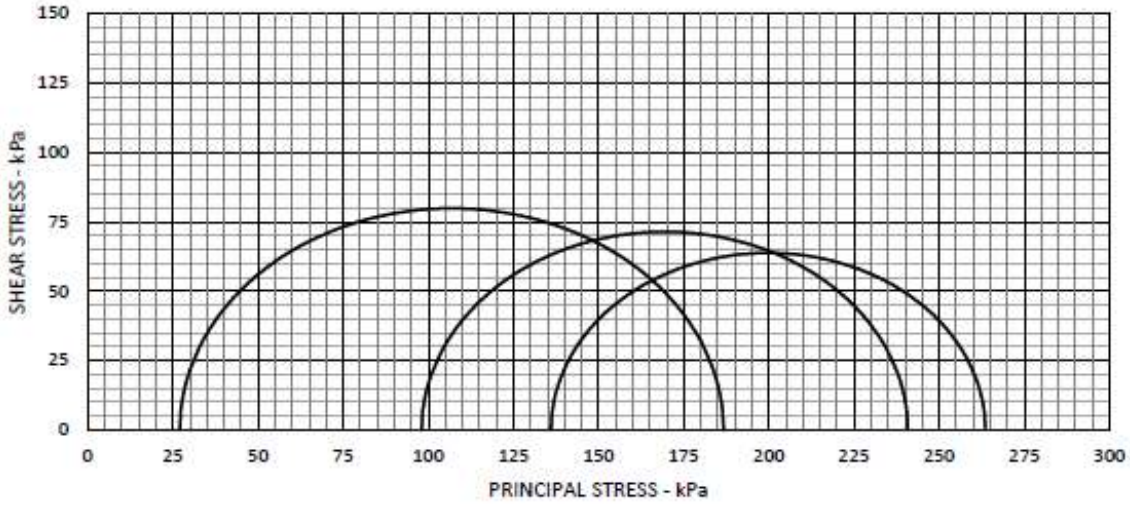

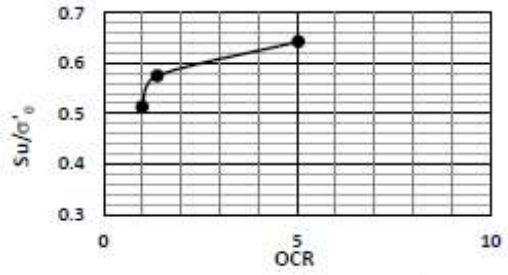

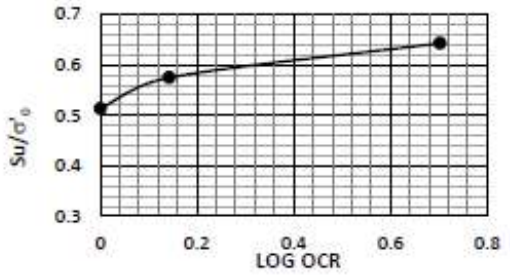

EFFECTIVE STRESS PARAMETERS	c' =	kPa	ϕ' =	deg.

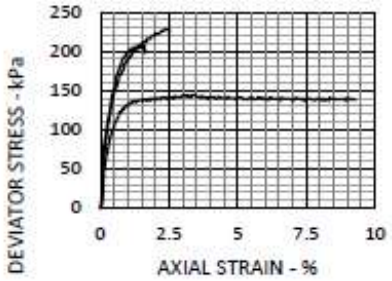

SAMPLE NO.	1	2	3
Initial Moisture Content - %	0.19	0.19	0.19
Final Moisture Content - %	0.23	0.23	0.23
Dry Density - kN/m^3	16.45	16.45	16.45
Diameter - mm	73.16	73.16	73.16
Height - mm	146.00	146.00	146.00
Effect. Cell Pressure - kPa	136	98	27
Strain Rate - mm/min	0.02	0.02	0.02
σ_1' at Failure - kPa	263.545	240.761	186.6575
σ_3' at Failure - kPa	136	98	27

TEST METHOD:	Consolidated Undrained
SAMPLE TYPE:	Undisturbed
DESCRIPTION:	Reddish Brown Lean Clay
BORING:	B-1
DEPTH:	21' 5" to 21' 11"

PROJECT INFORMATION

PROJECT:	SH 3 over BNSF
LOCATION:	Ada, Oklahoma
DATE:	7/15/2020
COMMENT:	Multistage test, loaded to NC condition and then unloaded to mimic overconsolidated soil
TESTED BY:	Tommy D. Bounds, PE

SAMPLE 1

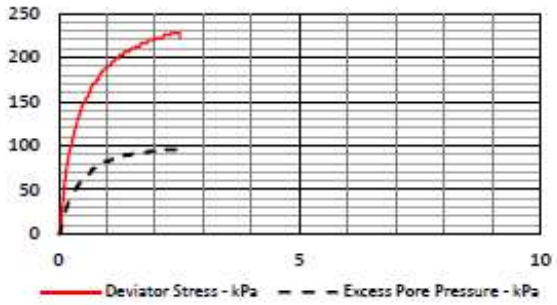

SAMPLE 2

SAMPLE 3

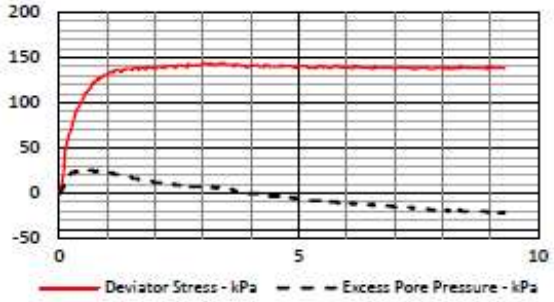

NOTE:

p' and q calculated based on Cambridge definition under triaxial stress conditions

$$p' = \frac{(\sigma_1' + 2\sigma_3')}{3}$$

$$q = (\sigma_1 - \sigma_3)$$

p'-q Diagram

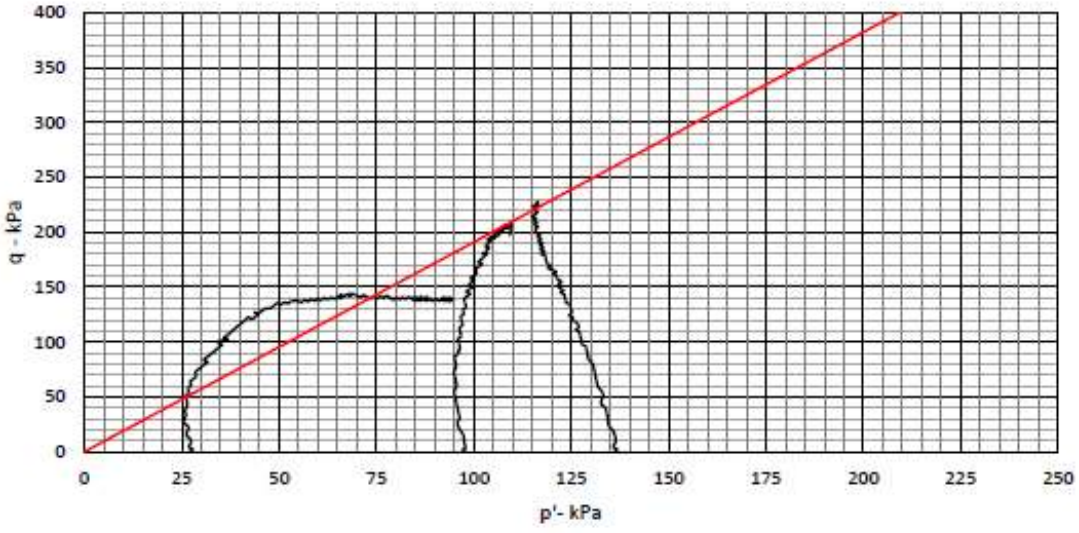

PROJECT:	SH 3 over BNSF	BORING:	B-1
LOCATION:	Ada, Oklahoma	DEPTH:	21' 5" to 21' 11"
DATE:	7/15/2020	TESTED BY:	Tommy D. Bounds, PE

TRIAXIAL SHEAR TEST REPORT

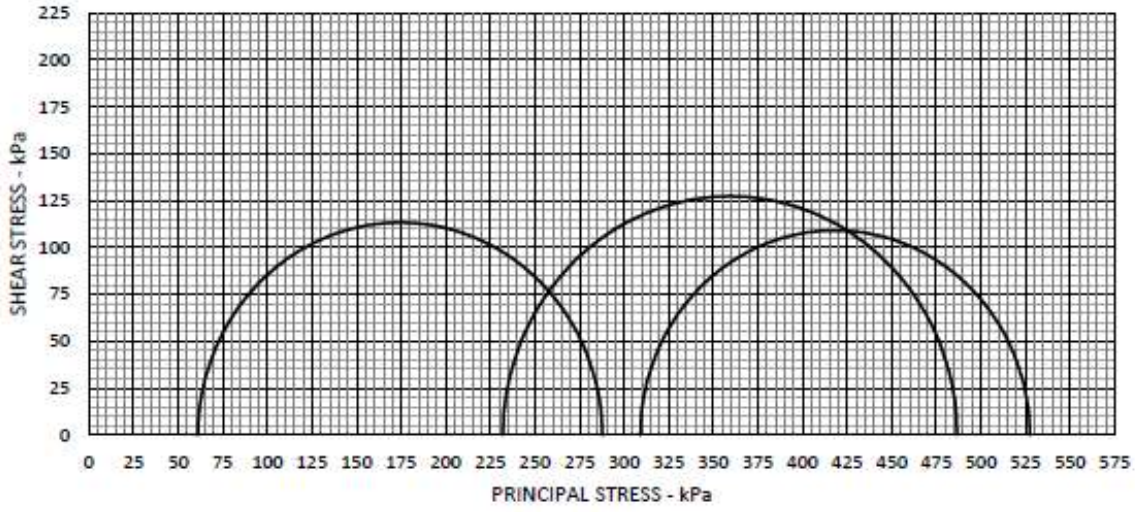

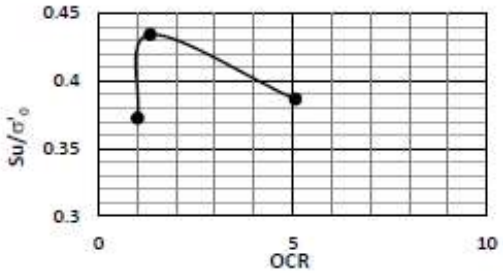

EFFECTIVE STRESS PARAMETERS | c' = kPa | φ' = deg.

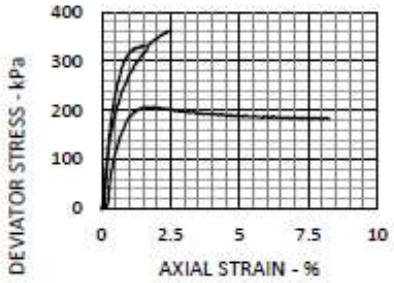

SAMPLE NO.	1	2	3
Initial Moisture Content - %	0.19	0.19	0.19
Final Moisture Content - %	0.22	0.22	0.22
Dry Density - kN/m^3	16.05	16.05	16.05
Diameter - mm	73.91	73.91	73.91
Height - mm	145.90	145.90	145.90
Effect. Cell Pressure - kPa	309	232	61
Strain Rate - mm/min	0.02	0.02	0.02
σ_1' at Failure - kPa	527.3034	486.5765	287.6001
σ_3' at Failure - kPa	309	232	61

TEST METHOD:	Consolidated Undrained
SAMPLE TYPE:	Undisturbed
DESCRIPTION:	Reddish Brown Lean Clay
BORING:	B-2
DEPTH:	50'-10" to 51'-4"

PROJECT INFORMATION

PROJECT:	SH 3 over BNSF
LOCATION:	Ada, Oklahoma
DATE:	7/15/2020
COMMENT:	Multistage test, loaded to NC condition and then unloaded to mimic overconsolidated soil
TESTED BY:	Tommy D. Bounds, PE

SAMPLE 1

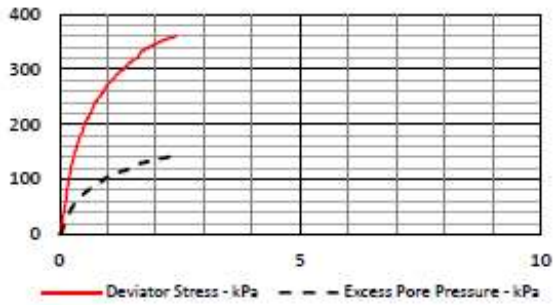

SAMPLE 2

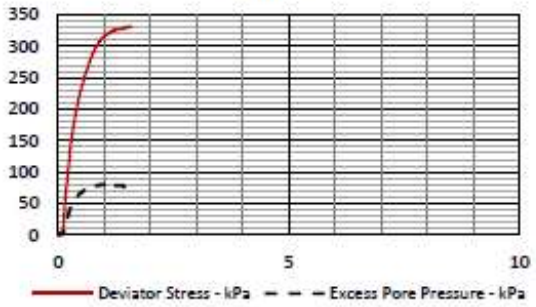

SAMPLE 3

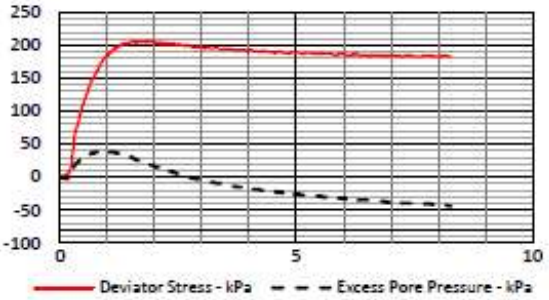

NOTE:

p' and q calculated based on Cambridge definition for triaxial stress conditions

$$p' = \frac{(\sigma_1' + 2\sigma_3')}{3}$$

$$q = (\sigma_1 - \sigma_3)$$

p'-q Diagram

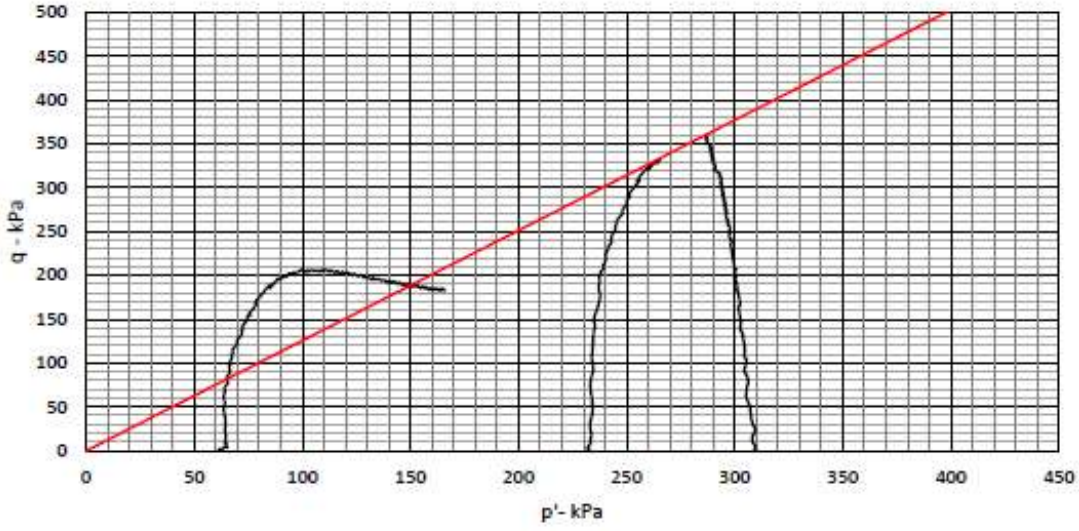

PROJECT:	SH 3 over BNSF	BORING:	B-2
LOCATION:	Ada, Oklahoma	DEPTH:	50'-10" to 51'-4"
DATE:	7/15/2020	TESTED BY:	Tommy D. Bounds, PE

TRIAXIAL SHEAR TEST REPORT

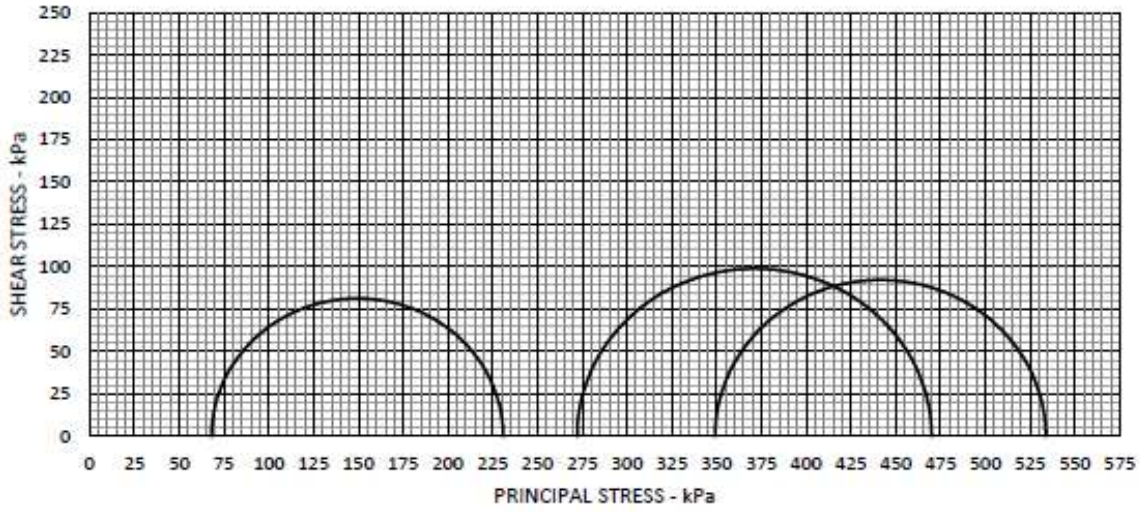

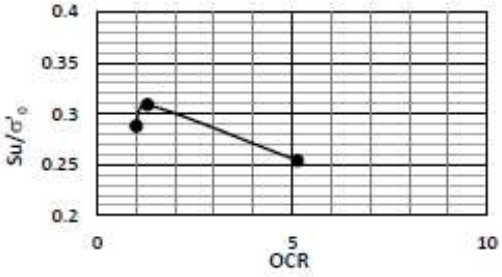

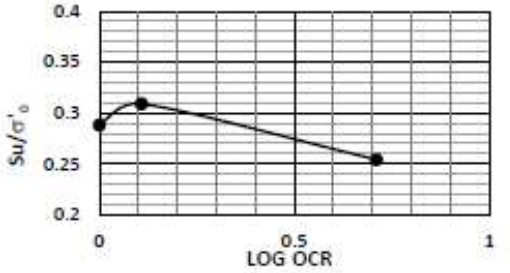

EFFECTIVE STRESS PARAMETERS | c' = kPa | φ' = deg.

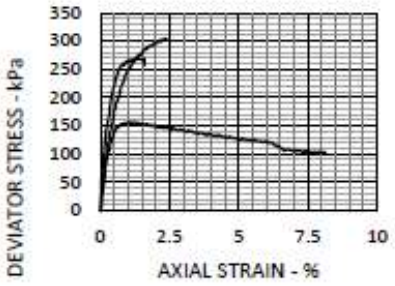

SAMPLE NO.	1	2	3
Initial Moisture Content - %	#DIV/0!	#DIV/0!	#DIV/0!
Final Moisture Content - %	0.21	0.21	0.21
Dry Density - kN/m^3	#DIV/0!	#DIV/0!	#DIV/0!
Diameter - mm	72.92	72.92	72.92
Height - mm	145.16	145.16	145.16
Effect. Cell Pressure - kPa	349	272	68
Strain Rate - mm/min	0.02	0.02	0.02
σ_1' at Failure - kPa	533.6142	469.9335	230.7747
σ_3' at Failure - kPa	349	272	68

TEST METHOD:	Consolidated Undrained
SAMPLE TYPE:	Undisturbed
DESCRIPTION:	Reddish Brown Lean Clay
BORING:	B-2
DEPTH:	55'-8" to 56'-2"

PROJECT INFORMATION

PROJECT:	SH 3 over BNSF
LOCATION:	Ada, Oklahoma
DATE:	7/15/2020
COMMENT:	Multistage test, loaded to NC condition and then unloaded to mimic overconsolidated soil
TESTED BY:	Tommy D. Bounds, PE

SAMPLE 1

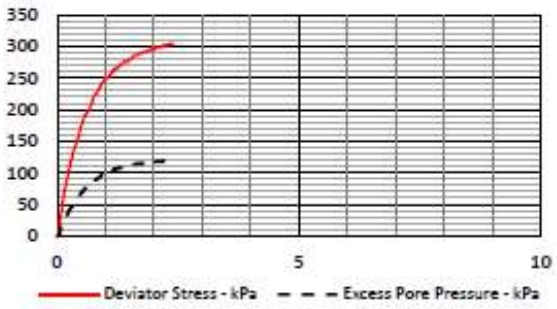

SAMPLE 2

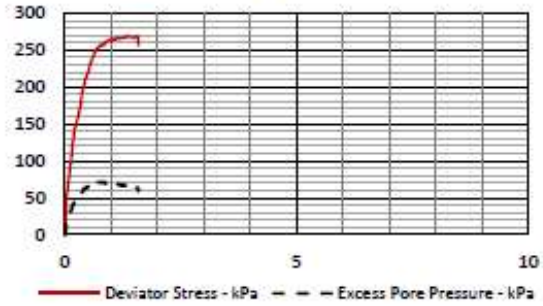

SAMPLE 3

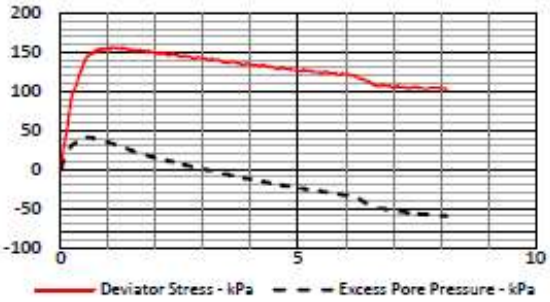

NOTE:

p' and q calculated based on Cambridge definition under triaxial stress conditions

$$p' = \frac{(\sigma_1' + 2\sigma_3')}{3}$$

$$q = (\sigma_1 - \sigma_3)$$

p'-q Diagram

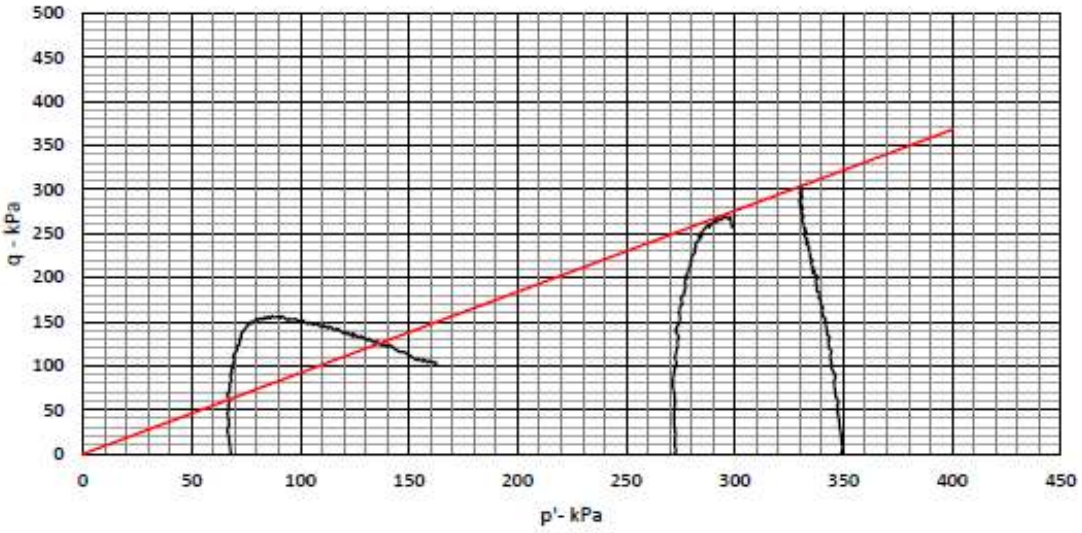

PROJECT:	SH 3 over BNSF	BORING:	B-2
LOCATION:	Ada, Oklahoma	DEPTH:	55'-8" to 56'-2"
DATE:	7/15/2020	TESTED BY:	Tommy D. Bounds, PE

TRIAXIAL SHEAR TEST REPORT

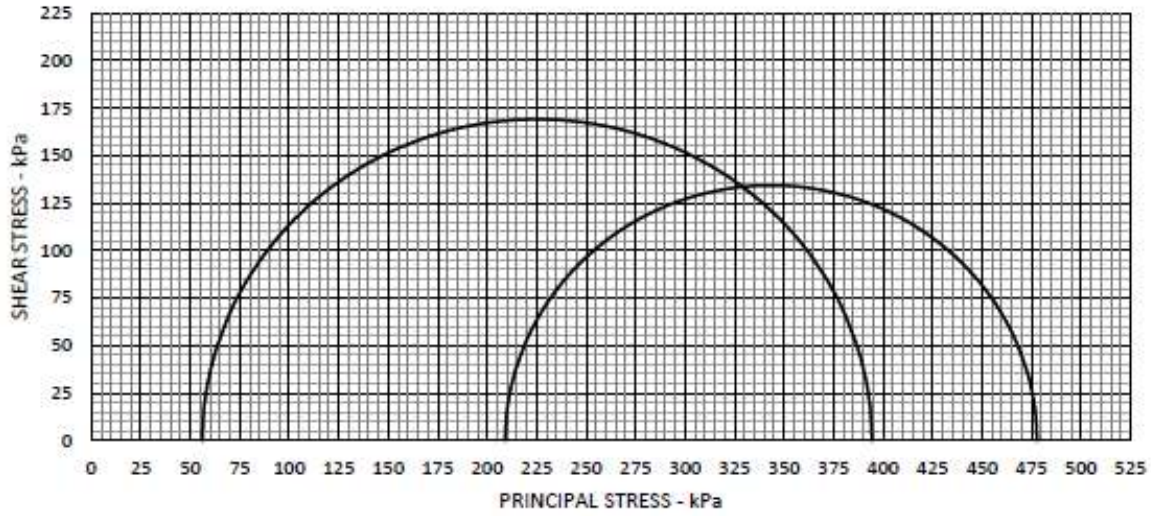

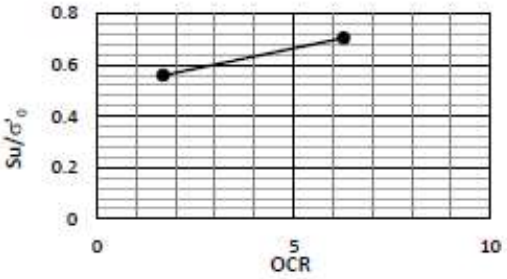

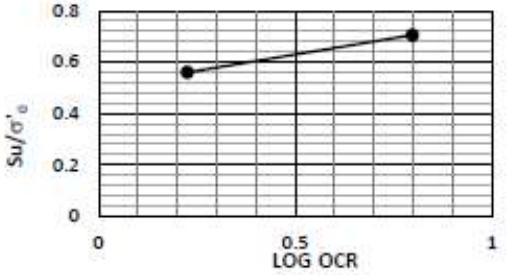

EFFECTIVE STRESS PARAMETERS | c' = kPa | φ' = deg.

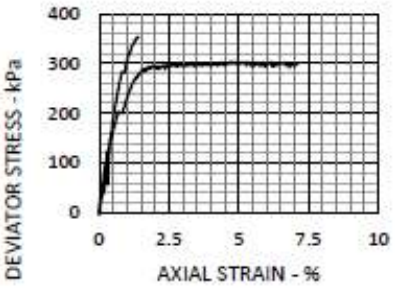

SAMPLE NO.	1	2	3
Initial Moisture Content - %	0.17	0.17	0.17
Final Moisture Content - %	0.16	0.16	0.16
Dry Density - kN/m^3	17.94	17.94	17.94
Diameter - mm	71.69	71.69	71.69
Height - mm	147.17	147.17	147.17
Effect. Cell Pressure - kPa		209	56
Strain Rate - mm/min		0.02	0.02
σ_1' at Failure - kPa		477.718	394.3418
σ_3' at Failure - kPa		209	56

TEST METHOD:	Consolidated Undrained
SAMPLE TYPE:	Undisturbed
DESCRIPTION:	Reddish Brown Lean Clay
BORING:	B-3
DEPTH:	41'-6" to 42'-0"

PROJECT INFORMATION

PROJECT:	SH 3 over BNSF
LOCATION:	Ada, Oklahoma
DATE:	7/15/2020
COMMENT:	Issue with loading during Normally Consolidated Sample
TESTED BY:	Tommy D. Bounds, PE

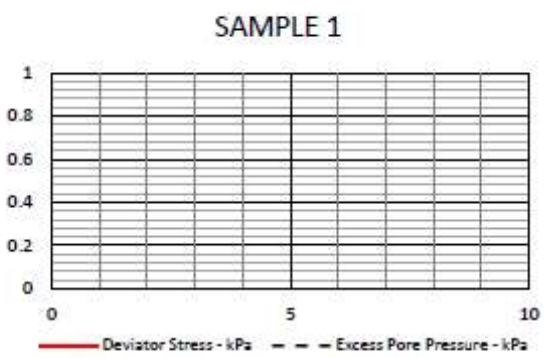

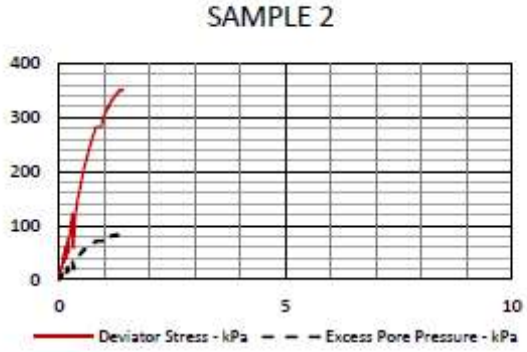

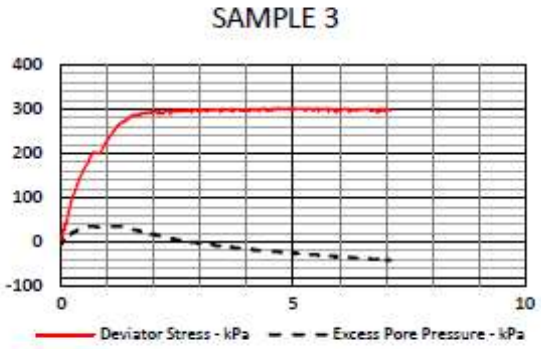

NOTE:

p' and q calculated based on Cambridge definition for triaxial stress conditions

$$p' = \frac{(\sigma_1' + 2\sigma_3')}{3}$$

$$q = (\sigma_1 - \sigma_3)$$

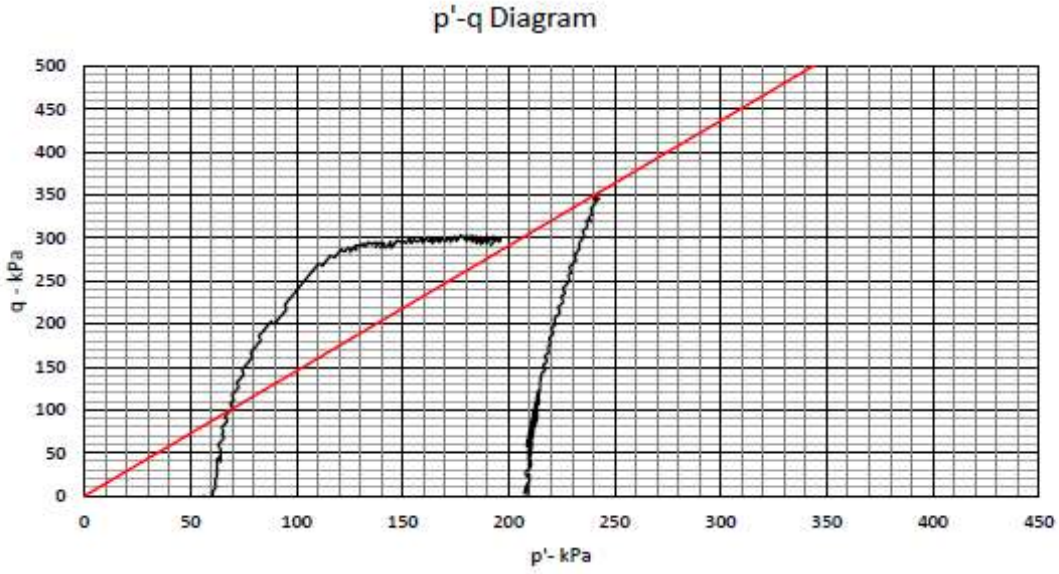

PROJECT:	SH 3 over BNSF	BORING:	B-3
LOCATION:	Ada, Oklahoma	DEPTH:	41'-6" to 42'-0"
DATE:	7/15/2020	TESTED BY:	Tommy D. Bounds, PE

TRIAXIAL SHEAR TEST REPORT

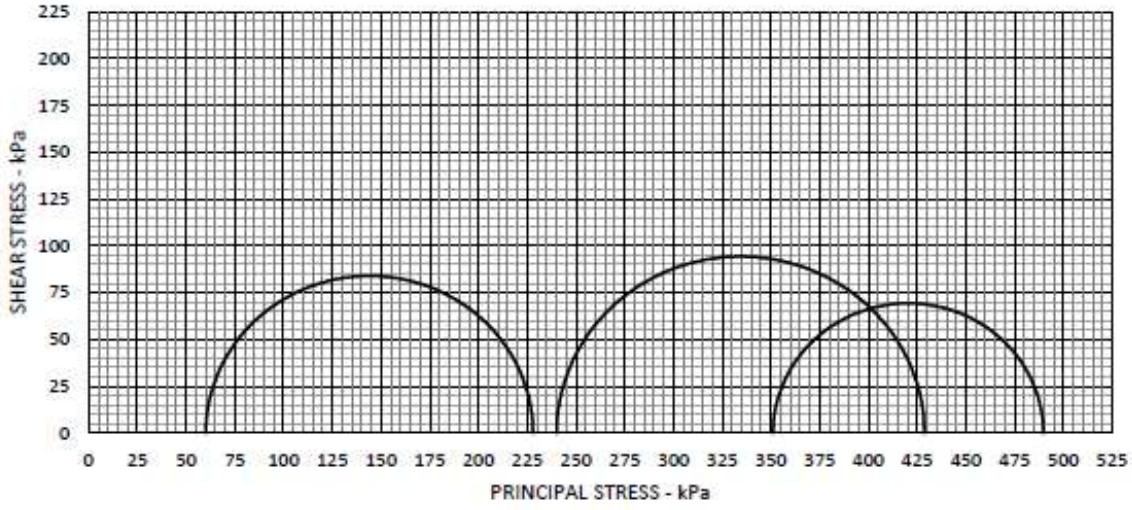

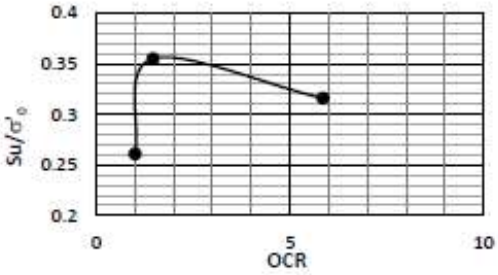

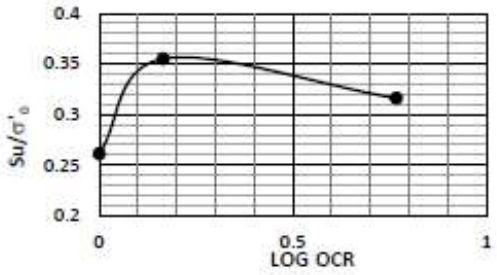

EFFECTIVE STRESS PARAMETERS | c' = kPa | φ' = deg.

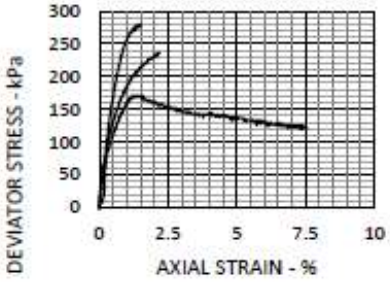

SAMPLE NO.	1	2	3
Initial Moisture Content - %	0.18	0.18	0.18
Final Moisture Content - %	0.17	0.17	0.17
Dry Density - kN/m^3	17.57	17.57	17.57
Diameter - mm	71.53	71.53	71.53
Height - mm	143.89	143.89	143.89
Effect. Cell Pressure - kPa	351	240	60
Strain Rate - mm/min	0.02	0.02	0.02
σ_1' at Failure - kPa	489.729	428.7107	227.9381
σ_3' at Failure - kPa	351	240	60

TEST METHOD:	Consolidated Undrained
SAMPLE TYPE:	Undisturbed
DESCRIPTION:	Reddish Brown Lean Clay
BORING:	B-3
DEPTH:	46'-0" to 46'-6"

PROJECT INFORMATION

PROJECT:	SH 3 over BNSF
LOCATION:	Ada, Oklahoma
DATE:	7/15/2020
COMMENT:	Multistage test, loaded to NC condition and then unloaded to mimic overconsolidated soil
TESTED BY:	Tommy D. Bounds, PE

SAMPLE 1

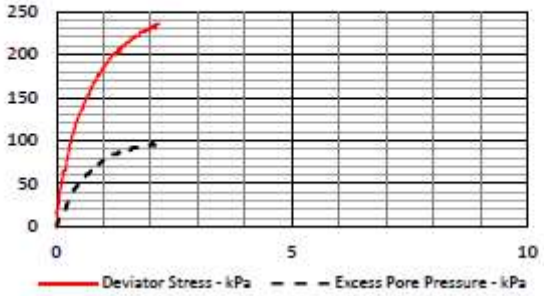

SAMPLE 2

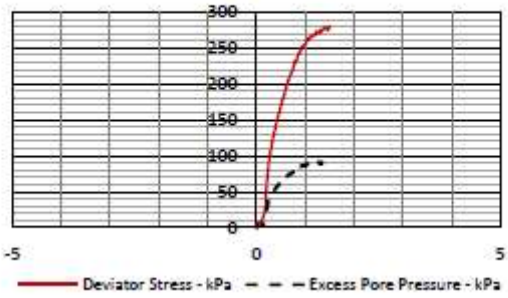

SAMPLE 3

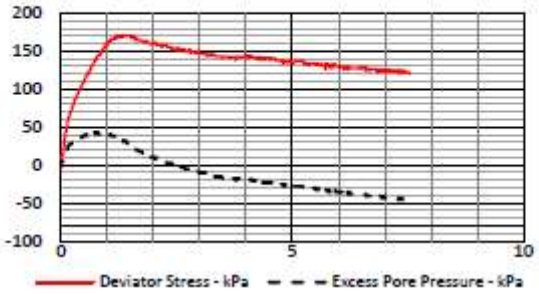

NOTE:

p' and q calculated based on Cambridge definition for triaxial stress conditions

$$p' = \frac{(\sigma_1' + 2\sigma_3')}{3}$$

$$q = (\sigma_1 - \sigma_3)$$

p'-q Diagram

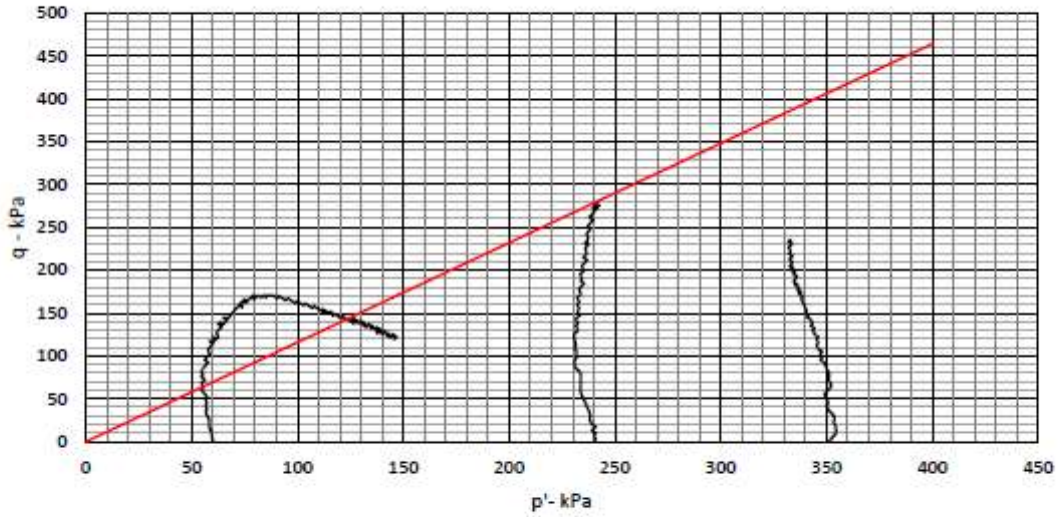

PROJECT:	SH 3 over BNSF	BORING:	B-3
LOCATION:	Ada, Oklahoma	DEPTH:	46'-0" to 46'-6"
DATE:	7/15/2020	TESTED BY:	Tommy D. Bounds, PE

B.3 Triaxial Extension Results

TRIAXIAL SHEAR TEST REPORT

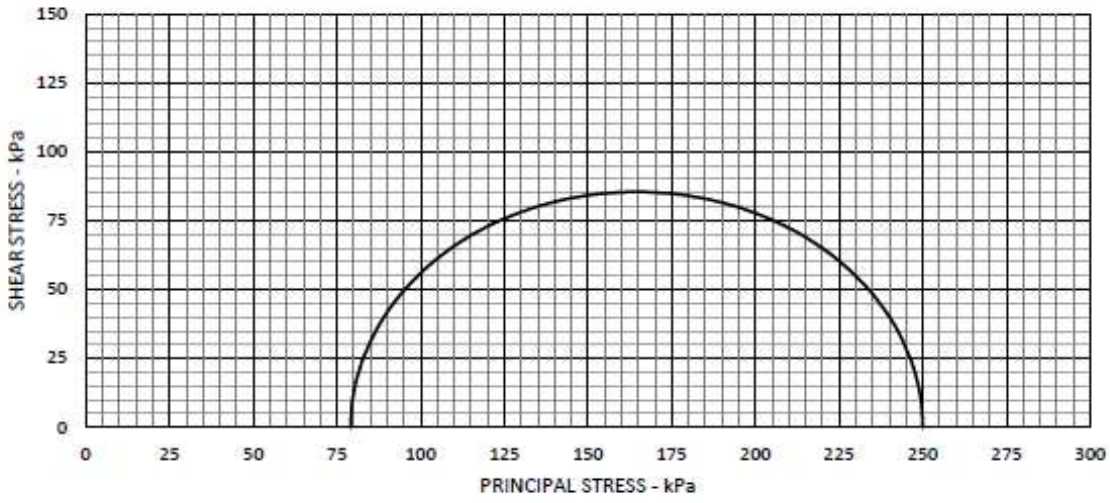

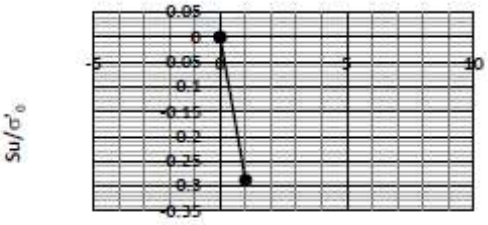

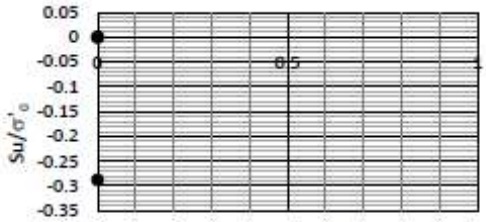

EFFECTIVE STRESS PARAMETERS	c' =	kPa	ϕ' =	deg.

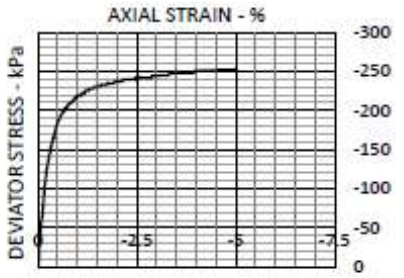

SAMPLE NO.	1	2	3
Initial Moisture Content - %	0.22		
Final Moisture Content - %	0.21		
Dry Density - kN/m^3	15.76		
Diameter - mm	72.88		
Height - mm	145.42		
Effect. Cell Pressure - kPa	250		
Strain Rate - mm/min	0.02		
σ_1' at Failure - kPa	79.03658		
σ_3' at Failure - kPa	250		

TEST METHOD:	Consolidated Undrained
SAMPLE TYPE:	Undisturbed
DESCRIPTION:	Reddish Brown Lean Clay
BORING:	B-2
DEPTH:	51'-6" to 52'-0"

PROJECT INFORMATION

PROJECT:	SH 3 over BNSF
LOCATION:	Ada, Oklahoma
DATE:	8/26/2020
COMMENT:	Multistage test, loaded to NC condition and then unloaded to mimic overconsolidated soil
TESTED BY:	Tommy D. Bounds, PE

SAMPLE 1

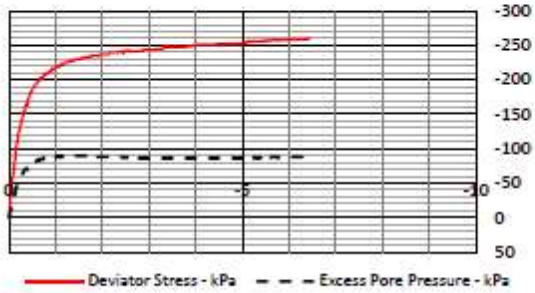

SAMPLE 2

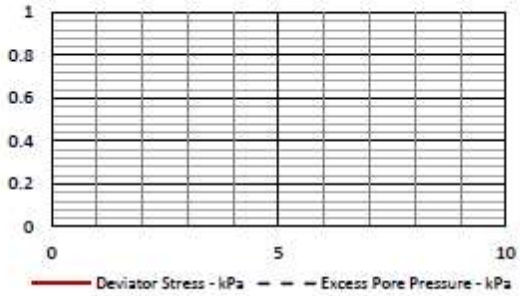

SAMPLE 3

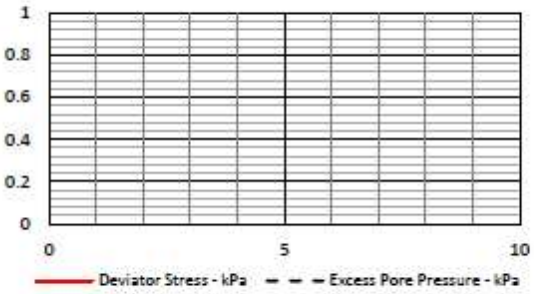

NOTE:

p' and q calculated based on Cambridge definition for triaxial stress conditions

$$p' = \frac{(\sigma_1' + 2\sigma_3')}{3}$$

$$q = (\sigma_1 - \sigma_3)$$

p'-q Diagram

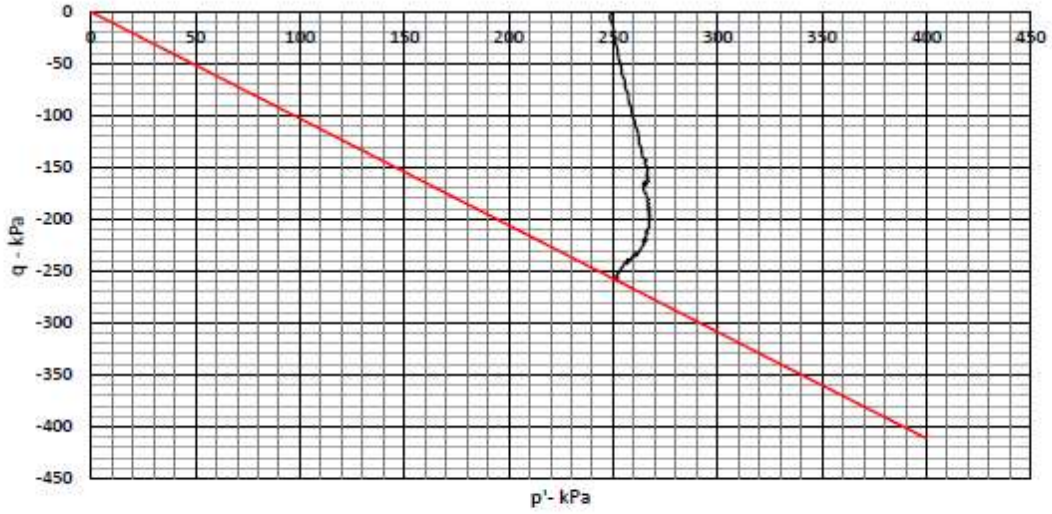

PROJECT:	SH 3 over BNSF	BORING:	B-2
LOCATION:	Ada, Oklahoma	DEPTH:	51'-6" to 52'-0"
DATE:	8/26/2020	TESTED BY:	Tommy D. Bounds, PE

APPENDIX C: Parametric Study Results

fore-slope	Emb. Height (m)	soil strength (ocr)	Soil Thickness (m)	soil Perm. (m/s)	Soil Strength (kPa)	Ux at toe (mm)	Ux at crest (mm)	Sett. (mm)
3	6	1.3	1.5	0.00025	3.85	31.6	0	133.7
3	6	1.3	3	0.00025	6.45	57.8	10.5	222
3	6	2.5	1.5	0.00025	6.45	14.2	0	97.5
3	6	2.5	3	0.00025	13.1	20.7	0	137
3	6	2.5	6	0.00025	19.15	37.61	0	183.4
3	6	4	1.5	0.00025	9.65	10.3	0	88.9
3	6	4	3	0.00025	18.55	15.6	0	119.5
3	6	4	4.5	0.00025	26.3	26.7	0	140.3
3	6	4	6	0.00025	34.15	32.8	0	164.6
3	10	1.3	1.5	0.00025	3.85	48.5	11.9	188.2
3	10	1.3	3	0.00025	6.45	95.3	26.3	308.8
3	10	2.5	1.5	0.00025	6.45	30.8	0	156.9
3	10	2.5	3	0.00025	13.1	40.3	0	217.8
3	10	2.5	4.5	0.00025	13.1	51.9	0	260.3
3	10	2.5	6	0.00025	19.15	63.8	0	289.3
3	10	4	1.5	0.00025	9.65	22.6	0	151.2
3	10	4	3	0.00025	18.55	29.2	0	197.2
3	10	4	4.5	0.00025	26.3	41	0	227.9
3	10	4	6	0.00025	34.15	53.6	0	251.8
3	14	1.3	1.5	0.00025	3.85	62.1	15.4	240.3
3	14	1.3	3	0.00025	6.45	124.5	34.5	388.7
3	14	2.5	1.5	0.00025	6.45	45.4	0	222.3
3	14	2.5	3	0.00025	13.1	61.5	11.3	298.8
3	14	2.5	4.5	0.00025	13.1	73.8	13.6	351.1
3	14	2.5	6	0.00025	19.15	88.3	16.8	392.4
3	14	4	1.5	0.00025	9.65	35.1	0	208.8
3	14	4	3	0.00025	18.55	44.7	0	273.4
3	14	4	4.5	0.00025	26.3	55.7	0	310
3	14	4	6	0.00025	34.15	72.9	14	343.7
4	6	1.3	1.5	0.00025	3.85	21	0	133
4	6	1.3	3	0.00025	6.45	34.6	0	220.4
4	6	1.3	4.5	0.00025	7.75	45.6	0	281.5
4	6	1.3	6	0.00025	13.1	50.7	0	332.5
4	6	2.5	1.5	0.00025	6.45	0	0	97.5
4	6	2.5	3	0.00025	13.1	14.3	0	137
4	6	2.5	4.5	0.00025	13.1	21	0	161

fore-slope	Emb. Height (m)	soil strength (ocr)	Soil Thickness (m)	soil Perm. (m/s)	Soil Strength (kPa)	Ux at toe (mm)	Ux at crest (mm)	Sett. (mm)
4	6	2.5	6	0.00025	19.15	26.1	0	183.5
4	6	4	1.5	0.00025	9.65	0	0	88.93
4	6	4	3	0.00025	18.55	11.4	0	119.5
4	6	4	4.5	0.00025	26.3	18	0	140.8
4	6	4	6	0.00025	34.15	22.9	0	165
4	10	1.3	1.5	0.00025	3.85	33.2	0	187
4	10	1.3	4.5	0.00025	7.75	75.3	17.3	401.1
4	10	2.5	1.5	0.00025	6.45	17.2	0	162.4
4	10	2.5	3	0.00025	13.1	26.1	0	217.8
4	10	2.5	4.5	0.00025	13.1	36.4	0	260.6
4	10	2.5	6	0.00025	19.15	42.6	0	290
4	10	4	1.5	0.00025	9.65	11.3	0	150.7
4	10	4	3	0.00025	18.55	20.4	0	197.3
4	10	4	4.5	0.00025	26.3	29.8	0	228
4	10	4	6	0.00025	34.15	36.5	0	257.4
4	14	1.3	1.5	0.00025	3.85	43.4	14.6	238.9
4	14	1.3	3	0.00025	6.45	88.8	29.6	385.7
4	14	1.3	4.5	0.00025	7.75	107.5	35.9	493.8
4	14	1.3	6	0.00025	13.1	125.7	36.3	592.8
4	14	2.5	1.5	0.00025	6.45	27.6	0	221.2
4	14	2.5	3	0.00025	13.1	41.3	11.7	298.2
4	14	2.5	4.5	0.00025	13.1	51.2	13.4	360.4
4	14	2.5	6	0.00025	19.15	63.5	16.6	389.7
4	14	4	1.5	0.00025	9.65	18.3	0	207.9
4	14	4	3	0.00025	18.55	28.5	0	272.8
4	14	4	4.5	0.00025	26.3	39.5	10.4	316.4
4	14	4	6	0.00025	34.15	51	14.3	342.5
3	6	1.3	1.5	0.0025	3.85	22.6	0	136.6
3	6	1.3	3	0.0025	6.45	42.7	0	229.6
3	6	1.3	4.5	0.0025	7.75	56.2	0	291.5
3	6	1.3	6	0.0025	13.1	58.4	0	333.8
3	6	2	1.5	0.000025	6.45	15.2	0	85.3
3	6	2	1.5	0.0025	6.45	16.6	0	122.9
3	6	2	3	0.000025	13.1	24.91	0	136.4
3	6	2	3	0.0025	13.1	23.51	0	177.6
3	6	2	4.5	0.000025	13.1	38.5	0	169.3
3	6	2	4.5	0.0025	13.1	31.3	0	205.5
3	6	2	6	0.000025	19.15	45.9	0	185.8
3	6	2	6	0.0025	19.15	34.4	0	223

fore-slope	Emb. Height (m)	soil strength (ocr)	Soil Thickness (m)	soil Perm. (m/s)	Soil Strength (kPa)	Ux at toe (mm)	Ux at crest (mm)	Sett. (mm)
3	6	3	1.5	0.000025	9.65	0	0	72
3	6	3	1.5	0.0025	9.65	11.5	0	109.4
3	6	3	3	0.000025	18.55	17.65	0	100.4
3	6	3	3	0.0025	18.55	16.1	0	148.3
3	6	3	4.5	0.000025	26.3	30.4	0	124.3
3	6	3	4.5	0.0025	26.3	24.7	0	171.9
3	6	3	6	0.000025	34.15	37.6	0	143.8
3	6	3	6	0.0025	34.15	27.9	0	190.9
3	10	1.3	1.5	0.0025	3.85	34.6	0	190.4
3	10	1.3	3	0.0025	6.45	63.9	0	318.5
3	10	1.3	4.5	0.0025	7.75	84.1	0	414.3
3	10	1.3	6	0.0025	13.1	100.9	0	487.2
3	10	2	1.5	0.000025	6.45	37.8	0	139.2
3	10	2	1.5	0.0025	6.45	29.4	0	178.1
3	10	2	3	0.000025	13.1	46.5	0	210.2
3	10	2	3	0.0025	13.1	42.1	0	273.2
3	10	2	4.5	0.000025	13.1	63.8	0	282.4
3	10	2	4.5	0.0025	13.1	50.2	0	328.4
3	10	2	6	0.0025	19.15	57.7	0	363.2
3	10	3	1.5	0.000025	9.65	23.5	0	124.7
3	10	3	1.5	0.0025	9.65	23	0	164.5
3	10	3	3	0.000025	18.55	30.5	0	164
3	10	3	3	0.0025	18.55	30	0	237.9
3	10	3	4.5	0.000025	26.3	45.6	0	219.7
3	10	3	4.5	0.0025	26.3	37.8	0	276.7
3	10	3	6	0.000025	34.15	63	14.1	233.2
3	10	3	6	0.0025	34.15	45.5	0	304.1
3	14	1.3	1.5	0.0025	3.85	45.5	0	241
3	14	1.3	3	0.0025	6.45	80.4	11.2	393.4
3	14	1.3	4.5	0.0025	7.75	108.4	13.9	513.7
3	14	1.3	6	0.0025	13.1	127.3	13.9	607.8
3	14	2	1.5	0.000025	6.45	68	22.9	189.4
3	14	2	1.5	0.0025	6.45	40.9	0	229
3	14	2	3	0.000025	13.1	75.5	16.7	287.6
3	14	2	3	0.0025	13.1	59.4	0	350.6
3	14	3	1.5	0.000025	9.65	40.6	0	172.4
3	14	3	1.5	0.0025	9.65	33.4	0	215.3
3	14	3	3	0.000025	18.55	47.7	0	237.4
3	14	3	3	0.0025	18.55	43.3	0	314.6

fore-slope	Emb. Height (m)	soil strength (ocr)	Soil Thickness (m)	soil Perm. (m/s)	Soil Strength (kPa)	Ux at toe (mm)	Ux at crest (mm)	Sett. (mm)
3	14	3	4.5	0.000025	26.3	62.7	16	259.5
3	14	3	4.5	0.0025	26.3	53.8	0	376.8
3	14	3	6	0.000025	34.15	83	25.02	272.8
3	14	3	6	0.0025	34.15	61.8	0	414.7
4	6	1.3	1.5	0.0025	3.85	14.7	0	136.2
4	6	1.3	3	0.0025	6.45	27.7	0	228.4
4	6	1.3	6	0.000025	13.1	61.9	10.7	316.8
4	6	1.3	6	0.0025	13.1	39.2	0	334
4	6	2	1.5	0.000025	6.45	0	0	85.1
4	6	2	1.5	0.0025	6.45	10.2	0	122.7
4	6	2	3	0.000025	13.1	16.8	0	135.5
4	6	2	3	0.0025	13.1	15.4	0	177.8
4	6	2	4.5	0.000025	13.1	25.46	0	170.2
4	6	2	4.5	0.0025	13.1	19.3	0	205.7
4	6	2	6	0.000025	19.15	31.7	0	185.1
4	6	2	6	0.0025	19.15	22	0	223
4	6	3	1.5	0.000025	9.65	12.6	0	100.4
4	6	3	1.5	0.0025	9.65	11.3	0	148.3
4	6	3	3	0.000025	18.55	12.6	0	100.4
4	6	3	3	0.0025	18.55	10.9	0	148.3
4	6	3	4.5	0.000025	26.3	20.5	3	123.8
4	6	3	4.5	0.0025	26.3	15.3	0	171.9
4	6	3	6	0.0025	34.15	17.4	0	190.9
4	10	1.3	1.5	0.0025	3.85	22.5	0	189.8
4	10	1.3	3	0.0025	6.45	43	0	317.3
4	10	1.3	4.5	0.0025	7.75	58.7	0	412.1
4	10	1.3	6	0.000025	13.1	107.8	26.7	468.4
4	10	1.3	6	0.0025	13.1	68	0	484.2
4	10	2	1.5	0.000025	6.45	20.6	0	139.4
4	10	2	1.5	0.0025	6.45	17.5	0	177.5
4	10	2	3	0.000025	13.1	31.2	0	209.2
4	10	2	3	0.0025	13.1	27.3	0	272.4
4	10	2	4.5	0.000025	13.1	45.2	0	280.2
4	10	2	4.5	0.0025	13.1	34.3	0	328.5
4	10	2	6	0.000025	19.15	53.8	0	305.5
4	10	2	6	0.0025	19.15	37.4	0	363.2
4	10	3	1.5	0.000025	9.65	10.8	0	124.5
4	10	3	1.5	0.0025	9.65	12.3	0	163.9
4	10	3	3	0.000025	18.55	21.8	4	163.7

fore-slope	Emb. Height (m)	soil strength (ocr)	Soil Thickness (m)	soil Perm. (m/s)	Soil Strength (kPa)	Ux at toe (mm)	Ux at crest (mm)	Sett. (mm)
4	10	3	3	0.0025	18.55	21	0	237.2
4	10	3	4.5	0.000025	26.3	33.5	5	216.1
4	10	3	4.5	0.0025	26.3	26.2	0	276.5
4	10	3	6	0.000025	34.15	42	9	239.5
4	10	3	6	0.0025	34.15	29.4	0	304
4	14	1.3	1.5	0.0025	3.85	29.8	5	240.1
4	14	1.3	3	0.0025	6.45	58.4	11.4	391.7
4	14	1.3	4.5	0.0025	7.75	76	14.5	511.3
4	14	1.3	6	0.0025	13.1	91.2	15.3	605.8
4	14	2	1.5	0.000025	6.45	40.3	17.2	186.6
4	14	2	1.5	0.0025	6.45	24.8	0	228.2
4	14	2	3	0.000025	13.1	53.6	15.4	285.4
4	14	2	3	0.0025	13.1	39.6	5	348.7
4	14	2	4.5	0.000025	13.1	69.8	17.5	364.5
4	14	2	4.5	0.0025	13.1	47	3	431.3
4	14	2	6	0.000025	19.15	82.7	18.3	420.7
4	14	2	6	0.0025	19.15	54.6	0	487.4
4	14	3	1.5	0.000025	9.65	21.5	8	172.1
4	14	3	1.5	0.0025	9.65	17.9	3	214.6
4	14	3	3	0.000025	18.55	30.3	8	236.2
4	14	3	3	0.0025	18.55	28.6	0	313.2
4	14	3	4.5	0.000025	26.3	48	12.9	291.2
4	14	3	4.5	0.0025	26.3	35.3	0	374.8
4	14	3	6	0.000025	34.15	61.7	16.2	333.3
4	14	3	6	0.0025	34.15	42.1	0	414.5